universität wien

# DISSERTATION

Titel der Dissertation

„Site preferences of the substitutional solid solutions in the systems Hf-Nb-As, Hf-Nb-Ge and Hf-Nb-Ga“

Verfasser

Dipl.-Ing. Piotr Warczok

angestrebter akademischer Grad

Doktor der Naturwissenschaften (Dr. rer. nat.)

Wien, 2008

| | |
|---|---|
| Studienkennzahl lt. Studienblatt: | A 091 419 |
| Dissertationsgebiet lt. Studienblatt: | 419 Chemie |
| Betreuerin / Betreuer: | O. Univ.-Prof. Dr. Herbert Ipser |

***Mojej Rodzinie***

*(An meiner Familie)*

*(To my family)*

## ZUSAMMENFASSUNG

Es wurde die Rolle der bevorzugten Besetzung von Punktlagen für die Substitution in den festen Lösungen, die in den Systemen Hf-Nb-As, Hf-Nb-Ge und Hf-Nb-Ga existieren untersucht. Nach einer gründlichen Literaturrecherche wurden die Ziele für jedes dieser Systeme formuliert.

Im System Hf-Nb-Ge wurden die Grundzustandsenergien der festen Lösung $Hf_{5-x}Nb_xGe_4$ ($Sm_5Ge_4$-typ) mit DFT (Dichtefunktionalstheorie) modelliert; mit diesen Ergebnissen wurde die Phase mit dem CEM (Compound Energy Model) thermodynamisch modelliert. Die berechneten Ergebnisse wurden mit der in der Literatur vorhandenen Strukturdaten verglichen. Die DFT-Rechnungen erlaubten die Vorhersage sowohl der bevorzugte Besetzung von Punktlagen als auch - in einem gewissen Ausmaß - die Änderung der Gitterparameter mit der Zusammensetzung der feste Lösung. Es wurde eine gute Übereinstimmung zwischen den berechneten und den in der Literatur gegebenen Werten der Besetzungszahlen festgestellt.

Im System Hf-Nb-Ga wurden die Besetzungszahlen in der festen Lösung $Hf_{1-x}Nb_xGa$ (ThTl-type) mit Röntgenbeugung an gepulverten Proben (getempert bei 1200°C) untersucht. Die Besetzungszahlen wurden mittels Rietveld-Verfeinerung bestimmt. Die Grundzustandsenergien dieser Phase wurden mit DFT-Rechnungen modelliert, wobei die Besetzung von Punktlagen gut vorhersagbar war. Auch hier stimmt die experimentell gefundene Änderung der Gitterparameter als Funktion der Phasenzusammensetzung mit den berechneten Strukturdaten im Grundzustand überein. Die thermodynamische Modellierung (CEM) ergab eine gute Übereinstimmung zwischen den theoretischen und den experimentellen Daten.

Im System Hf-Nb-As System wurde eine Serie von metallreichen Proben (<50 at.% As) hergestellt. Das Vorliegen der in der Literatur beschriebenen binären Phasen wurde bei 1400°C bestätigt. Zusätzlich wurden die neue Phasen $Nb_2As$ ($Nb_2P$-Typ), $Hf_{3+x}Nb_{1-x}As_2$ ($0.29<x<0.61$; $Zr_2P$-Typ), $Hf_{1+x}Nb_{1-x}As$ ($-0.06<x<0.42$; $Co_2Si$-Typ), $Hf_{4-x}Nb_{3+x}As_3$ ($-0.08<x<1.62$; neuer Strukturtyp), $Hf_{2+x}Nb_{1-x}As$ ($0.12<x<0.65$; $Ti_3P$-Typ) and $Hf_{3+x}Nb_{3-x}As_2$ ($0.09<x<0.25$; neuer Strukturtyp) gefunden. Die Phase $Hf_{7.22}Nb_{3.78}As_4$ ($Zr_{6.45}Nb_{4.55}As_4$-Typ) wurden bei dieser Temperatur als metastabil identifiziert. Aufgrund der Röntgenbeugung an Einkristall- und Pulverproben wurden die Besetzungszahlen in den Phasen $(Hf,Nb)_5As_3$ ($Nb_5As_3$-Typ), $Hf_{4-x}Nb_{3+x}As_3$, $Hf_{2+x}Nb_{1-x}As$, $Hf_{3+x}Nb_{3-x}As_2$ und $Hf_{7.22}Nb_{3.78}As_4$ bestimmt. Die kristallographisch unterschiedliche Metallpositionen wurden bezüglich ihres Volumens (mit Voronoi Polyedern beschrieben) und der Bildungsstärke der Metall-Metall Bindung (mit der

Pauling Bindungsordnung berechnet) analysiert. Die bevorzugte Besetzung kann unter der Annahme, dass Niobatome Gitterplätze bevorzugen, an denen mehr Elektronen an der Metall-Metall Bindung teilnehmen können, und dass die Hafniumatome Gitterplätze grösseren Volumens bevorzugen, als Kompromiss zwischen diesen beiden Faktoren qualitativ erklärt werden. Die DFT-Rechnungen zeigen die Stabilität der meisten der binären Hafnium- und Niobarseniden bei 0 K. Die Rechnungen deuten auch auf die Stabilität der binären $Nb_3As$ Phase mit dem neu gefundenen $Hf_{3+x}Nb_{3-x}As_2$ Strukturtyp bei 0 K, anstatt des bei höheren Temperaturen gefundenen $Ti_3P$-Typs. Die experimentell bestimmten Besetzungszahlen in $Hf_{3+x}Nb_{3-x}As_2$ und $Hf_{2+x}Nb_{1-x}As$ stimmen mit der Vorhersage der DFT Rechnung überein und die thermodynamische Modellierung ergibt Besetzungszahlen, welche mit den verfeinerten Werten gut zusammenpasst.

## ABSTRACT

The role of the site preferences for the substitution in the solid solutions found in the systems Hf-Nb-As, Hf-Nb-Ge and Hf-Nb-Ga were examined. After a thorough literature review, the aims for every system were formulated.

In the Hf-Nb-Ge system, the ground state energy of the $Hf_{5-x}Nb_xGe_4$ phase ($Sm_5Ge_4$-type) was modelled with DFT (density functional method) calculations and, based on these results, the thermodynamic modelling with CEM (Compound Energy Model) was done. The calculated results were compared with the reported site preferences. The DFT calculations allowed predicting qualitatively the site preferences and, to some extent, the variation of the lattice parameter with the composition of the solid solution. A good agreement between the calculated site fractions with the ones reported in the literature for this solid solution was found.

In the Hf-Nb-Ga system, the site occupancies in the $Hf_{1-x}Nb_xGa$ (ThTl-type) solid solution was investigated by X-ray diffraction of powdered samples within the phase field and annealed at 1200°C (1473 K). The site fractions were found by the Rietveld refinement method. The ground state energies of this phase were modelled with DFT calculations and the site preferences could be well predicted. Also here, the experimentally found variation of the lattice parameters with the composition agrees reasonably with the calculated ground state structures of the ordered compounds. The thermodynamic modelling (CEM) showed a good agreement between the modelled and refined site fractions.

In Hf-Nb-As system, a series of samples was prepared, covering the metal-rich (<50 at.% As) part. The existence of all reported binary phases was confirmed at 1400°C (1673 K). Additionally, new phases with the stoichiometries $Nb_2As$ ($Nb_2P$-type), $Hf_{3+x}Nb_{1-x}As_2$ ($0.29<x<0.61$; $Zr_2P$-type), $Hf_{1+x}Nb_{1-x}As$ ($-0.06<x<0.42$; $Co_2Si$-type), $Hf_{4-x}Nb_{3+x}As_3$ ($-0.08<x<1.62$; new structure type), $Hf_{2+x}Nb_{1-x}As$ ($0.12<x<0.65$; $Ti_3P$-type) and $Hf_{3+x}Nb_{3-x}As_2$ ($0.09<x<0.25$; new structure type) were found. Furthermore, $Hf_{7.22}Nb_{3.78}As_4$ ($Zr_{6.45}Nb_{4.55}As_4$-type) was found, but this is believed to be metastable at this temperature. Based on single crystal or powder diffraction experiments, the site occupancies were determined in $(Hf,Nb)_5As_3$ ($Nb_5As_3$-type), $Hf_{4-x}Nb_{3+x}As_3$, $Hf_{2+x}Nb_{1-x}As$, $Hf_{3+x}Nb_{3-x}As_2$ and $Hf_{7.22}Nb_{3.78}As_4$. The metal sites in these phases were examined with regard to the metal site volume (Voronoi polyhedra volume) and the capability of forming metal-metal bonding on a given site (based on Pauling bond order calculation). The site preferences can be quantitatively rationalised as a result of the compromise between these factors, with the assumption that niobium tends to occupy sites where more electrons are involved in the

metal-metal bonding, while hafnium prefers the sites with a larger volume. The DFT calculations show the stability of the majority of the binary arsenides at 0 K. It suggests also the existence of the binary $Nb_3As$ phase with the new found $Hf_{3+x}Nb_{3-x}As_2$ structure type at 0 K instead of the $Ti_3P$ structure type found at the elevated temperatures. The site preferences found in $Hf_{2+x}Nb_{1-x}As$ and $Hf_{3+x}Nb_{3-x}As_2$ are in a good agreement with the DFT calculations. The thermodynamic modelling yields site fractions which are also in satisfying agreement with the ones found in the experiment. In the concluding remarks the influence of the metal-metal bonding and site volumes on the site preferences is summarised and the usefulness of the DFT calculations as a basis for thermodynamic modelling is stressed.

# CONTENTS

# 1. Introduction

## 1.1 General remarks

"Materials science is the study of the properties of solid materials and how those properties are determined by a material's composition and structure" - this quote taken from "Encyclopaedia Britannica"[1] suggests already the existence of the influence of the material's structure on its properties. The structure is a result of the interaction of the constituent's molecules or atoms and is dependent on the material's chemical composition (both qualitative and quantitative). However, it is possible that two different materials with identical chemical composition occur with different structures. A classical illustration are graphite and diamond which consist of carbon atoms but their different structure causes that their properties are not even similar to each other. Investigation of the way the matter is built and organized in nature along with the use of this knowledge to design new materials with the desired properties is what (among others) makes this science field very exciting. Speaking about the material's structure, one can consider it on two different levels. The first level describes the ordering of the single atoms in a pure phase. On this level the crystalline (ordered) and amorphous (disordered) materials are distinguishable. The second level describes the form, size and distribution of the pure phases in the material – this is information is usually referred to "material's microstructure". In this work, the description on the crystal structure level (the first level mentioned) is of primary interest.

The crystalline materials are substances in which the constituent atoms are placed in a characteristic order. It means that one can always find a specific atom arrangement (motif) which is repeated by translation in three dimensions in the whole crystal's volume. In order to describe the crystal structure, one needs to give details about the atom arrangement in the motif and the way it is translated. The usual way of doing that is by describing the unit cell of the crystal, i.e. the smallest repeating cell which has the full symmetry of the crystal structure [2]. The information includes the dimensions and shape of the cell and the set of coordinates of the atom positions placed in it. Not all positions of the atoms in the cell must be given, as many of them can be derived from the "minimal" set of atom positions and the symmetry elements present. There are 230 possible combinations of the symmetry elements within the unit cell and the information about the one present in the given structure is an important information. The atom positions related to each other by the symmetry operations ("crystallographically dependent positions") have the same number and distances to the

neighbour atom positions, i.e. they have the same coordination sphere. The unit cell data are obtained mostly by X-ray diffraction experiments and collected in databases for many classes of substances (intermetallic phases, minerals, etc.; for example [3]). As many of the crystal structures were found similar, they were grouped into structure type families of which databases were also created [4]. About 25000 different intermetallic compounds (and also crystal structures) classified in about 2500 structure types were described in literature till 1989 [3] and this number still rises.

The next important information about the occurrence of the phases (and their crystal structures) for different chemical compositions, temperatures and pressures are gathered in the phase diagrams. These are based mostly on experimental results (X-ray investigation, thermal analysis) and are of fundamental interest for material designing. In literature, there are over 4000 phase diagrams of binary alloys [5] and over 15000 diagrams (isothermal sections) describing over 8800 ternary systems [6]. Unfortunately, with increasing number of elements, more experimental work and time is needed, as more samples must be prepared to cover the representative field of the given system. This can be illustrated by the fact that for the possible 4950 binary and 161700 ternary phase diagrams (the numbers of possible combinations of 100 elements), we have a good knowledge of over 80% binary systems and of only about 5% of the ternary ones. Suffice to say, in order to save the experimental resources during the investigation of the multi-component systems, as well as just for the satisfaction of our desire for understanding and shaping the world around us, the theoretical work which describes, explains and (if possible) predicts the existence and the homogeneity range of a given crystal structure deserves a lot of attention.

The basic theoretical assumption states that the most stable structures (or the mixture of these) under the given conditions possess a minimal Gibbs energy. If one knew the Gibbs energy (later referred to as structure energy) of all possible crystal structures in the whole range of compositions in the given system, one could always find the most stable structure (or the mixture of these) and construct the phase diagram easily. This is a foundation of the theory of the phase diagram calculations which is known as *Calphad* (**CAL**culation of **PHA**se **D**iagrams). Usually, the structure energy is determined by calorimetric or electromotive force measurements of the pure phase and the few obtained experimental values are fitted to a polynomial of an arbitrary chosen form and extrapolated. Such polynomials describing the dependence of the structure energy on the temperature (with fixed phase composition and pressure) can be found in thermodynamic databases [7, 8]. By using these data in the existing models for the solutions, the solubility ranges of the phases can be also described. This

approach gives a good description of a given system, but it still requires a considerable amount of experimental work needed to find the coefficients used in the model. A very promising alternative is to relate the structure energy with the atoms included in the structure. Their properties such as atomic radius, number of valence electrons or electronegativity determine the mutual interactions between them and must obviously influence the order in their spatial distribution. Many semi-empirical models were proposed (e.g. Miedema's model for formation enthalpy, Pettifor's structure maps) [9], but their application is usually limited to binary systems. The more theoretical approach are the first-principles (*ab initio*) methods, in which the atoms are represented by their wave functions describing the interactions on the atomistic level (between the atom cores and the valence electrons). From the proper combination of the constituent wave functions, an approximation of the potential describing the interaction between the charged particles and an iterative solving of the Schrödinger equation, the structure energy in the ground state (the lowest structure energy) can be obtained. This value can be used directly for a comparison with the ground state energies of the other structures to check its stability and be an input for the modelling of the structure energy as a function of the other parameters (temperature, pressure, composition). However, no matter how sophisticated the modelling method is, its results must be confirmed by an experiment which will always judge the usefulness of the theory.

## 1.2 What is so interesting in the chemistry of the ternary metal-nonmetal compounds?

Among many multicomponent systems, the ones combining metals with non-metals are of much interest, due to an abundance of compounds occurring with unusual stoichiometries (e.g. $Cs_7O$, $Ta_6S$, $Nb_7P_4$, $NaN_3$, $K_2S_5$ [3]). The classic valence rule presented in the introductory chemistry courses assumes that the sum of the valence electrons taken from the constituent atoms in the stoichiometric ratio should allow the non-metal atoms the creation of a filled octet electron configuration. Unfortunately, this rule is not applicable in many of those compounds, as can be seen from the cited examples, even if the lower oxidation states for the metal or the higher for the non-metal atoms are assumed. Their explanation is only possible if bonding between two metal or non-metal atoms is taken into account. Hence, the interatomic interactions in these phases are not only of ionic character, as would be the case in the “classic valence rule obedient” compounds, but also have the metallic and covalent contributions.

**Table 1. A list of reported binary metal-rich phosphides, sulphides and selenides [10] (Compounds marked with "*" are taken from [11]).**

| | P | S | Se |
|---|---|---|---|
| Ti | TiP, $Ti_5P_3$, $Ti_2P$, $Ti_3P$ | TiS, $Ti_2S$, $Ti_8S_3$ | $Ti_2Se$, $Ti_5Se_4$, $Ti_8Se_3$, $Ti_{11}Se_4$, $Ti_{45}Se_{16}$, $Ti_9Se_2$ |
| Zr | ZrP, $Zr_{14}P_9$, $Zr_7P_4$, $Zr_2P$ $Zr_3P$ | ZrS, $Zr_2S$, $Zr_{21}S_8$*, $Zr_9S_2$ | $Zr_2Se$ |
| Hf | HfP, $Hf_3P_2$, $Hf_{27}P_{16}$, $Hf_7P_4$, $Hf_2P$, $Hf_3P$ | HfS*, $Hf_2S$ | $Hf_2Se$* |
| V | VP, $V_2P$, $V_3P$ | VS, $V_5S_4$, $V_3S$ | VS, $V_5Se_4$* |
| Nb | NbP, $Nb_5P_3$, $Nb_7P_4$, $Nb_2P$, $Nb_3P$ | NbS, $Nb_{14}S_5$, $Nb_{21}S_8$* | $Nb_5Se_4$, $Nb_2Se$ |
| Ta | TaP, $Ta_5P_3$, $Ta_2P$, $Ta_3P$ | TaS, $Ta_3S_2$ $Ta_2S$, $Ta_6S$ | $Ta_2Se$ |

This makes these substances a very interesting and large subject for research. An example with a long list of substances is the metal-rich phosphides, sulfides and selenides of the early transition metals $[M]_xN$ (M - metal(s) of the groups 4 and/or 5, N – phosphor, sulfur, selenium, $x \geq 1$). An analysis of the bonding in the crystal structures of these binary compounds (see Table 1) based on the interatomic distances, supported by the „point-charge" calculations, showed that there are virtually no bonds between the non-metal atoms in these phases [11]. Moreover, the present incompletely filled d-bands are involved in the bonding between metal atoms in addition to the s-band and also contribute to the metal-nonmetal bonding. Another interesting feature is, that the coordination spheres of the metal atoms often resemble the ordering of the body centred cubic structure.

Investigation of the ternary systems, with a second metal introduced, delivers some more interesting observations. As the early transition metals have similar chemical properties, especially the ones within the same group, a ternary phase diagram is expected to consist mainly of the extended solid solutions based on the structures of the binary compounds. Quite surprisingly, an occurrence of many ternary phases with structure types not present in the corresponding binary systems was found. As an example, the system Nb-Ta-S may be given, in which this behaviour was observed for the first time. The following ternary phases were found in this system: $Nb_{2.73}Ta_{4.27}S_2$ [12], $Nb_{6.74}Ta_{5.26}S_4$ [13], $Nb_{4.92}Ta_{6.08}S_4$ [14], $Nb_{1.72}Ta_{3.28}S_2$

**Table 2. Structure data of $Nb_{2.73}Ta_{4.27}S_2$ [12]. Positions "M1", "M2", …etc., are occupied by both metal atoms. "$y_{Ta}$" describes the site fraction of tantalum atoms on the given position, i.e. the probability of finding a tantalum atom on the given site. The sum of site fractions of niobium and tantalum equals unity.**

| Formula: | $Nb_{2.73}Ta_{4.27}S_2$ | | | | |
|---|---|---|---|---|---|
| Pearson symbol: | *oP*36 | | | | |
| Space group: | *Pnma* (no. 62) | | | | |
| Lattice parameters [Å]: | a = 5.4708(5)<br>b = 10.7133(9)<br>c = 10.3025(7) | | | | |
| Atom positions | Wyckoff position | x | y | z | $y_{Ta}$ |
| Ta | 4*c* | 0.3383(1) | 1/4 | 0.25624(6) | 1 |
| M1 | 8*d* | 0.09885(8) | 0.11438(5) | 0.05315(5) | 0.71(1) |
| M2 | *4c* | 0.0576(1) | 1/4 | 0.50300(7) | 0.74(1) |
| M3 | *8d* | 0.0817(1) | 0.01078(6) | 0.33985(6) | 0.43(1) |
| M4 | 4*c* | 0.1407(2) | 1/4 | 0.7992(1) | 0.23(1) |
| S | 8*d* | 0.3184(4) | 0.0965(2) | 0.6312(2) | - |

[15], $Nb_{0.95}Ta_{1.05}S$ [16]. The first four ternary phases have the $M_7N_2$, $M_3N$, $M_{11}N_4$, and $M_5N_2$ stoichiometry respectively, which were not found in the binary system. The last ternary phase has the $M_2N$ stoichiometry found in the binary system ($Ta_2S$), but the structure type is not related to the binary one. An analysis of their structures revealed that all (or nearly all in case of $Nb_{2.73}Ta_{4.27}S_2$) metal sites were occupied by both niobium and tantalum atoms, whereas the Nb:Ta ratio for the various crystallographically independent positions were different. This means that these two metals are not equally distributed on the available sites and site preferences are observed (example - see Table 2). Again, no bonding between the non-metal atoms was present.

These observations led to the formulation of the *differential fractional site occupancy* (DFSO) concept [17, 18]. According to this concept, the new ternary phase is stabilised primarily by the interaction between the metal atoms. Of the two component metals, one establishes a metallic bonding with higher energy – it can be recognized by comparison of the sublimation enthalpy (in case of Nb-Ta-S system it is tantalum which has a sublimation enthalpy of 782 kJ/mol compared to 733 kJ/mol for niobium [7]). The atoms of this metal tend to occupy the positions with the largest number of nearest neighbour metal atoms and the smallest distance to them at the same time. However, if only this factor was present, one would expect the ternary phases to exhibit completely ordered structures, i.e the metal sites

would be occupied by only one kind of atoms. Therefore, it is concluded that the full ordering of the structure is prevented by the entropy which reaches a maximal value when atoms of both metals are randomly - and in effect equally - distributed among all the metal sites. As a result of the compromise between the desire of creating strong metallic bonds and the tendency of the uniform mixing of the metal atoms, new ternary phases with often complex structures are formed.

Some confusion arises about the "degree of ordering" which is allowed for a phase considered to be DFSO-stabilised. The original concept was formulated for compounds in which mixed occupancies were observed on all metal sites and the site fractions were "rather narrowly fixed" [18]. The more general definition [19] allows some of the metal sites to be occupied only by one metal which seems to be inevitable if the phase should have a broader range of existence. This is the case of $Nb_{2.73}Ta_{4.27}S_2$ in which one of the metal sites is occupied only by tantalum atoms (Table 2). However, if a ternary phase becomes a completely ordered structure for any composition then it is not considered to be a DFSO phase anymore, as in the case of $Zr_{1-x}Ti_{1+x}As$ ($0 \leq x \leq 0.42$) which has a completely ordered structure for $x = 0$ [20]. Also, if the ternary structure is present in the corresponding binary systems (e.g. $Zr_{2.7}Hf_{11.3}P_9$ [21] isostructural with $Zr_{14}P_9$) then it is classified as "partly ordered substitutional solid solution" but not as a DFSO phase [19], even if it is obviously stabilised for the same reasons. This definition restriction seems to be quite confusing for the author of this work.

Further investigation showed that the presence of this mechanism is not only limited to the ternary phases of two early transition metals and a non-metal. The DFSO-stabilisation was also found in the following systems:

- Systems of one early transition metal and two non-metals or metalloids. In these ternary phases, the mixing of the p-block elements on the non-metal sites is observed. Such phases are known as *anionic* DFSO phases, while the previous ones with the mixing of two metals are called *cationic* DFSO phases
- Systems in which the metalloids of the other groups (Si, Ge, As, Sb) are included. These may include both cationic and anionic DFSO phases
- Systems in which a transition metal with more d-orbital electrons (e.g. Mo, Ni) is one of the components in the cationic DFSO phases.

**Table 3. List of the ternary DFSO-stabilised ternary phases [19]**

| | | |
|---|---|---|
| Cationic DFSO phases | S | $Nb_{2.73}Ta_{4.27}S_2$, $Nb_{6.74}Ta_{5.26}S_4$, $Nb_{4.92}Ta_{6.08}S_4$, $Nb_{1.72}Ta_{3.28}S_2$, $Nb_{0.95}Ta_{1.05}S$, $Hf_{7.5}Ti_{13.5}S_8$, $Ta_{4.75}V_{1.25}S$ |
| | P | $Zr_{6.45}Nb_{4.55}P_4$, $Hf_{9.29}Mo_{3.71}P$, $Hf_{5.08}Mo_{0.92}P_3$, $Hf_{1.06}Mo_{0.94}P$ |
| | As [22] | $Hf_{1-x}Ti_{1+x}As$, $Hf_{1-y}V_{1+y}As$ |
| | Sb | $Zr_{7.5}V_{5.5}Sb_{10}$, $Zr_{7.5}V_{3.5}Sb_8$, $Zr_{4.32}Ti_{2.68}Sb_7$, $Hf_{5.95}Ti_{1.05}Sb_4$ |
| | Ge [23] | $Zr_{4-x}Ta_{1+x}Ge_4$, $Zr_{2+y}Ta_{3-y}Ge_4$ |
| Anionic DFSO phases | Ti | $Ti_5Si_{1.32}Sb_{1.68}$ |
| | Zr | $Zr_2Sb_{0.5}Se_{0.5}$, $Zr_7Sb_{1.6}Se_{2.4}$, $ZrSi_{0.74}Sb_{1.26}$ |
| | Hf | $Hf_{27}Si_{6.0}P_{10.0}$ |
| | Ta | $Ta_5S_{1.5}Se_{0.5}$, $Ta_9S_{3.1}Se_{0.9}$, $Ta_5S_{1.12}Te_{0.88}$, $Ta_6S_{1.0}Te_{3.0}$, $Ta_5Se_{1.2}Te_{0.8}$ |

A summary of the ternary "legal" DFSO phases is given in Table 3. The abundance of these phases together with a number of those which do not fulfil the DFSO definition requirements may suggest that many of the still unknown compounds could be explained in terms of the mechanism lying under the "DFSO-stabilisation" concept.

### 1.3 Aim of this work

The basic goal of this work is to gain as much knowledge as possible about the ternary compounds present in the metal rich part (i.e. <50%at As) of the Hf-Nb-As system. While this system is not technologically significant, there are a few factors which make it interesting from the structure-chemical point of view:

- Both metals are early transition metals and they form a variety of binary metal-rich arsenides, as will be presented later.
- Niobium has a larger value of the vaporisation enthalpy (733.0 kJ/mol) than hafnium (619.2 kJ/mol) [7] and as such it will probably prefer the crystal sites which allow creating a stronger metal-metal bonding.
- Hafnium has a larger atomic radius than niobium and as such would probably prefer to occupy the crystal sites with a larger coordination sphere.

The above mentioned features seem promising for the formation of DFSO-stabilised phases. Even if this would not be the case, one would expect the existence of structures which would be stabilised by partial ordering.

An additional goal would be the analysis of the systems Hf-Nb-Ge and Hf-Nb-Ga. As it was mentioned before, the DFSO-stabilisation was reported in ternary germanides (Ta-Zr-Ge) [23]. It may be interesting to revisit both ternary systems and investigate the influence of the mixed site occupancies in the known ternary phases. As arsenic, germanium and gallium are neighbours in the same period of the periodic table, showing decreasing electronegativity and increasing metallic character, it might be expected that the covalent bonds will be replaced by the metallic ones and that site preferences of the transition metals should play a more and more marginal role.

The work will consist of the literature report on the data of all elements and their binary and ternary system descriptions (systems of As-Ga, As-Ge, Ga-Ge and As-Ga-Ge will not be included). On this basis the range and conditions of the experimental work will be defined which will consist of the sample preparation and their structural analysis. Also some modelling based on the *Density Functional Theory* (DFT) and *Calphad* approach will be done. The literature, experimental and modelling results will be compared and discussed. The author hopes that this work will contribute to a better understanding of the formation of multicomponent compounds.

# 2. Literature review

## 2.1 The elements [24], [25], [26]

As no arsenides, germanides and gallides of hafnium or niobium are commercially available, the synthesis of the samples must start from the pure elements. Therefore, it is important to have some information on their physical and chemical properties. Some parameters describing the physical properties of the constituents are given in Table 4 and 5.

**Table 4. Some physical properties of Hf and Nb.**

| Symbol | Hf | Nb |
|---|---|---|
| Atomic number | 72 | 41 |
| Ground state electron configuration | $[Xe]4f^{14}5d^{2}6s^{2}$ | $[Kr]4d^{4}5s^{1}$ |
| Relative atomic mass ($^{12}C$=12.0000) | 178.49 | 92.906 |
| Atomic radius (Pauling) [pm] | 144.2 | 134.2 |
| Electronegativity (Pauling) | 1.3 | 1.6 |
| Density [$g*cm^{-3}$] | 13.31 | 8.57 |
| Melting point [°C] | 2230 | 2468 |
| Boiling point [°C] | ~5200 | ~4750 |
| Electrical resistivity [Ω*m] | $35.1*10^{-8}$ | $12.5*10^{-8}$ |
| Thermal conductivity [$W*m^{-1}*K^{-1}$] | 23.0 | 53.7 |

Hafnium is a lustrous, silvery, ductile metal. At room temperature, it reacts with oxygen from the air so that a hafnium powder may burn, but in case of the bulk material, an oxide film on the surface prevents the further corrosion. At room temperature the metal does not react with alkalis or acids except of HF. The hafnium minerals occur in nature together with the ones of zirconium. The similar chemical properties of both metals make their separation difficult. The crystal structure of hafnium is hexagonal closed packed (Mg-type structure, Fig. 1) in which each atom has twelve neighbours in almost equal distance – six atoms in the same plane at 3.12 Å and six others on the two adjacent planes (three atoms in each plane) at 3.20 Å. This structure is stable only to about 1760°C (2033 K), above this temperature the body centred cubic structure (W-type structure, later referred to as *bcc*) appears in which every

atom has eight nearest neighbours in the equal distance of 3.13 Å. The bcc structure is stable up to the melting point of hafnium.

Niobium (old name: columbium) is a soft, ductile, silvery metal. Similar to hafnium, at room temperature it forms an oxide layer on the surface and is resistant to alkalis and acids, with the exclusion of HF. Niobium minerals are usually accompanied by tantalum compounds and, similar to the mentioned case of Zr and Hf, their separation is a difficult task. The crystal structure of niobium is body centred cubic (W-type structure, Fig. 2) which is stable up to the melting point. The distance to the eight nearest neighbours is 2.86 Å.

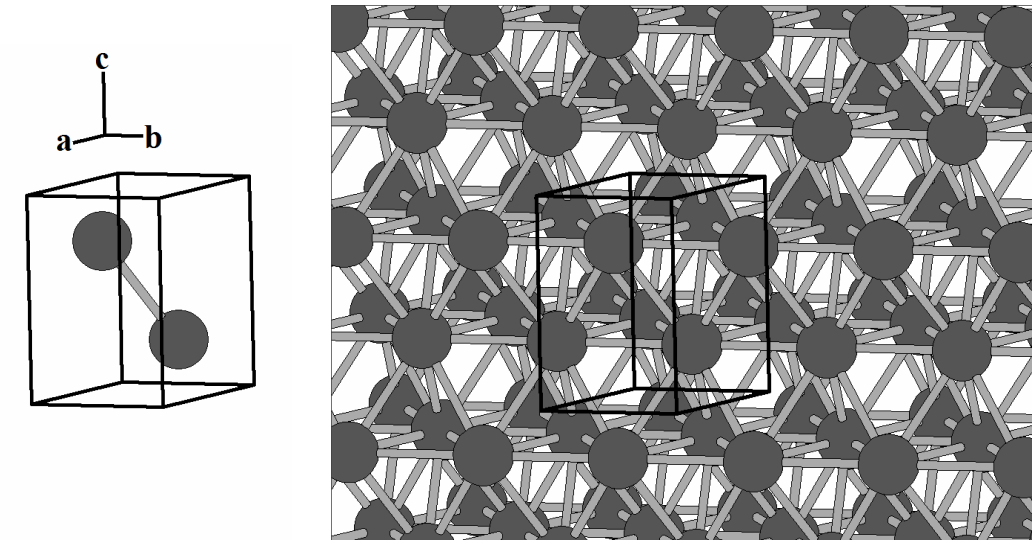


**Fig. 1. The unit cell of hafnium hcp phase (left) and a view at a larger section of the crystal structure (right). The nearest neighbours are connected by sticks.**

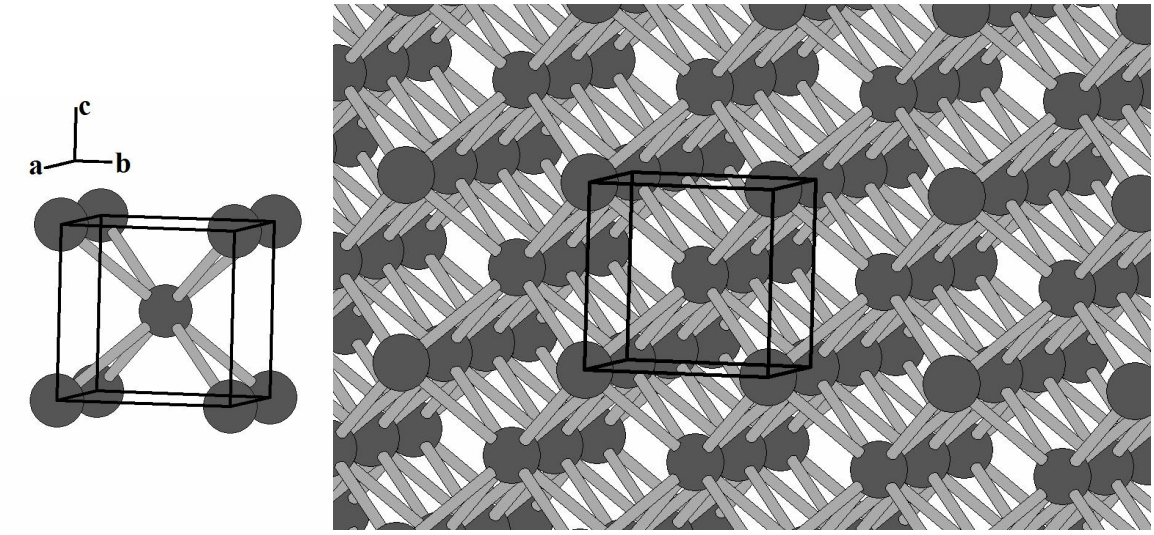


**Fig. 2. The unit cell of niobium bcc phase (left) and a view at a larger section of the crystal structure (right). The nearest neighbours are connected by sticks. Hafnium also crystallises in this structure above 1760°C**

**Table 5. Some physical properties of grey As, Ge and Ga**

| Symbol | As (grey) | Ge | Ga |
|---|---|---|---|
| Atomic number | 33 | 32 | 31 |
| Ground state electron configuration | $[Ar]3d^{10}4s^24p^3$ | $[Ar]3d^{10}4s^24p^2$ | $[Ar]3d^{10}4s^24p^1$ |
| Relative atomic mass ($^{12}C$=12.0000) | 74.92 | 72.61 | 69.72 |
| Atomic radius (Pauling) [pm] | 121.0 | 124.2 | 124.6 |
| Electronegativity (Pauling) | 2.18 | 2.01 | 1.81 |
| Density [$g*cm^{-3}$] | 5.78 | 5.32 | 5.91 |
| Melting point [°C] | 817 (high pressure) | 937 | 29.8 |
| Boiling point [°C] | 616 (sublimes) | 2830 | 2403 |
| Electrical resistivity [Ω*m] | $26*10^{-8}$ | 0.46 | $27*10^{-8}$ |
| Thermal conductivity [$W*m^{-1}*K^{-1}$] | 50.0 | 59.9 | 40.6 |

Arsenic is an element of which three different allotropic forms are known. The most stable one is "grey" arsenic – a steel-grey, brittle semimetal with a rhombohedral structure, isostructural with antimony and bismuth. "Black" arsenic appears by condensation of arsenic vapour as an amorphous mirror reverting to the grey form after heating. "Yellow" non-metallic arsenic may be obtained by a rapid cooling of the arsenic vapour but it reverts slowly to the grey form when exposed to light. At room temperature, grey arsenic does not react with dry air, while in the moist air the surface will oxidise. It reacts with nitric acid to form arsenous acids ($H_3AsO_3$, $H_3AsO_4$). Besides, it reacts with hot concentrated $H_2SO_4$ ($\rightarrow As_2O_3$) and fused NaOH ($\rightarrow Na_3AsO_3$). The structure of the most stable form ("grey") consists of layers (Fig. 3). Within each layer every atom has three nearest neighbours (2.52 Å), the next three neighbours being in the adjacent layer (3.10 Å). The unit cell can be described in the hexagonal system.

Germanium is a grey-white, brittle, lustrous crystalline semiconductor. At room temperature it does not react with air, diluted acids or alkalis, unless an oxidant (like $H_2O_2$) is present. In concentrated oxidant acids ($HNO_3$, hot $H_2SO_4$), it slowly reacts to $GeO_2$. It crystallises in the diamond structure in which each atom has four neighbours at the equal distance of 2.45 Å (Fig. 4). Two other metastable allotropic structures are reported.

Gallium is a soft, bright silvery metal (some sources still count it as a metalloid [26]). At room temperature, it does not react with air. Gallium reacts with acids and alkalis, building

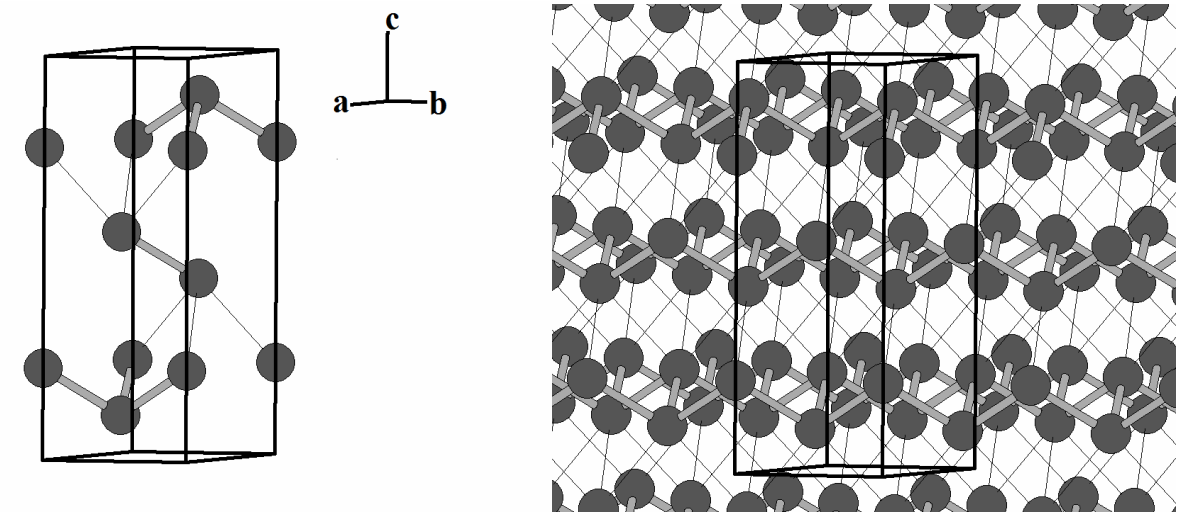


**Fig. 3. The unit cell of grey arsenic (left) and a view at a larger section of the crystal structure (right). The nearest neighbours are connected by sticks (within the layer) and lines (contacts to the next layer)**

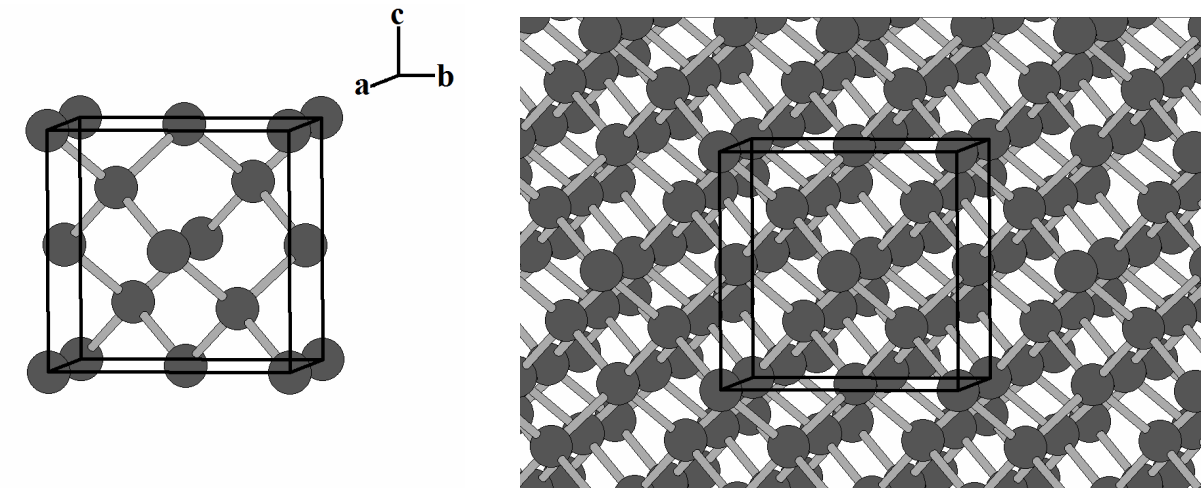


**Fig. 4. The unit cell of germanium structure (left) and a view at a larger section of the crystal structure (right). The nearest neighbours are connected by sticks**

soluble products (containing $Ga^{3+}$ or $GaO_3^{3-}$), unless the acid is oxidising which causes the formation of the oxide layer on the surface. It crystallises in a unique crystal structure type in which every atom has one nearest neighbour (2.48 Å) and six others slightly further away (2.7-2.8 Å). The presence of one nearest neighbour and also the results of investigation of liquid gallium suggest the existence of $Ga_2$ units. In the solid state these units build a face centred orthorhombic unit cell containing eight atoms (Pearson symbol: *oF*8). An alternative illustration of the structure describes it with layers, where each atom has six next nearest neighbours within the same layer and the nearest neighbour in the neighbouring one. Fig. 5 depicts the two descriptions.

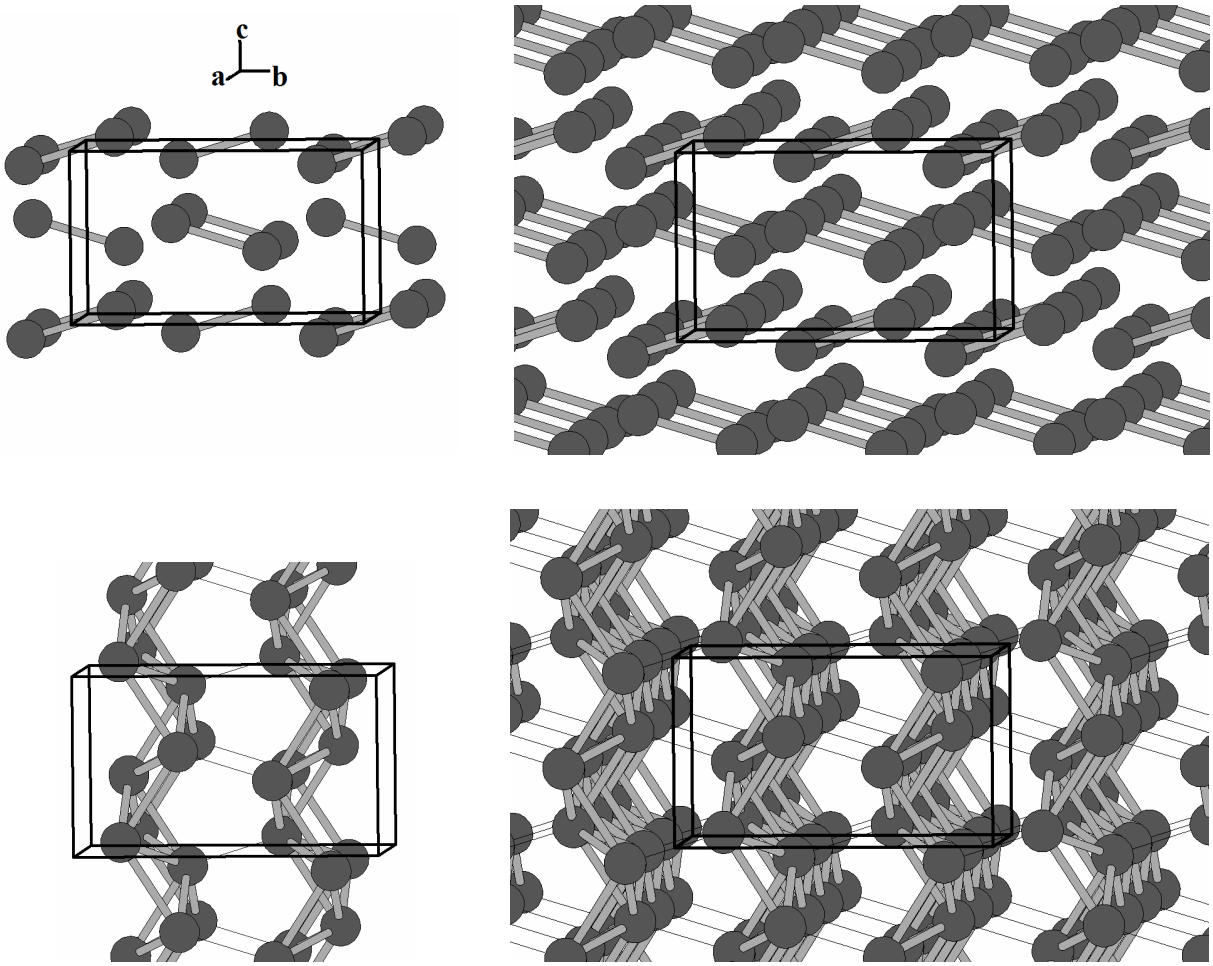


**Fig. 5. The unit cell of gallium with two nearest neighbours connected (top left) and a view at a larger section of the crystal structure (top right). An alternative description with infinite gallium layers is shown below (thin lines connect the nearest neighbours).**

### 2.2 Binary systems

For the investigation of any ternary system, a previous knowledge of the binary terminating systems is very helpful. The binary phase diagrams give information about the existence of the binary phases which may extend to the ternary region. Additionally, they give information about the temperature range which should be used for the experiments in the ternaries. Attention will also be paid to the reported descriptions of the sample preparation. In all phase diagrams presented below, dashed lines represent the assumed or only modelled equilibrium compositions, while solid lines represent the ones for which the experimental evidence can be found.

### 2.2.1 Hf-Nb binary system

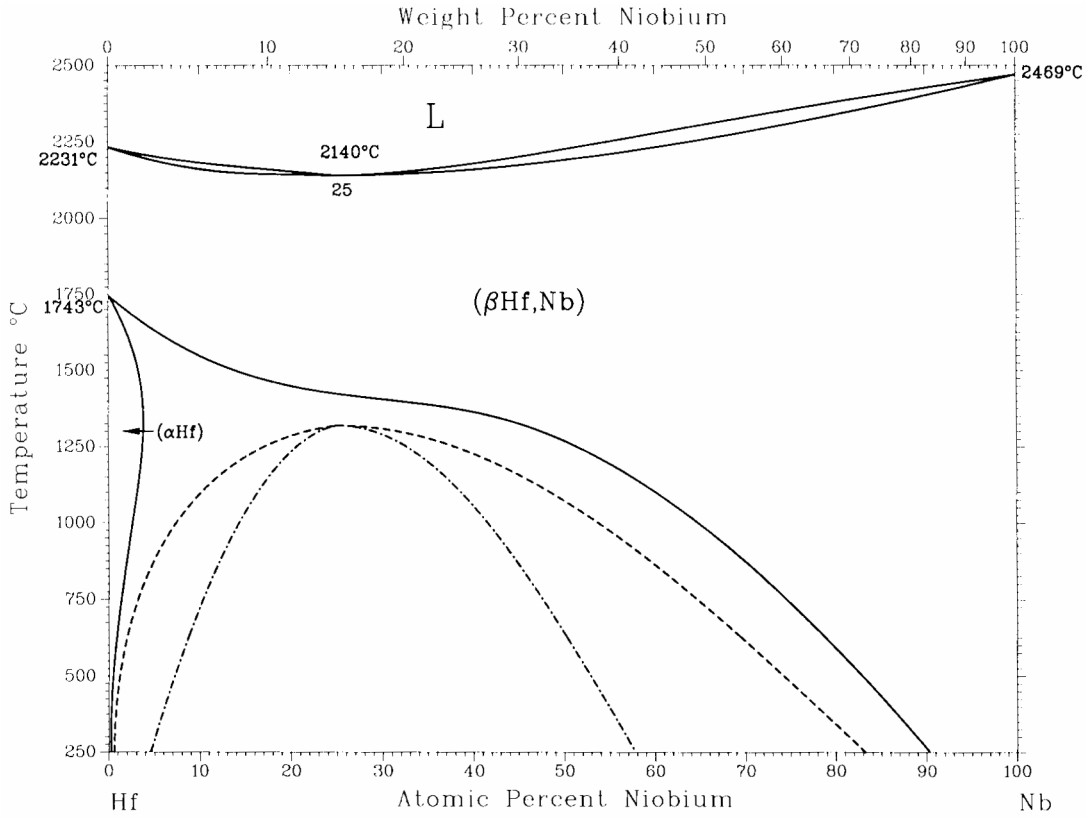


**Fig. 6. Phase diagram of Hf-Nb binary system [5].**

The assessed phase diagram published in Massalski's compilation [5] is shown in Fig. 6. It consists of two phases:

- αHf terminal solid solution of Nb in Hf with hexagonal close packed structure of low temperature hafnium. The maximum solid solubility of Nb is about 5 at.% at 1300-1400°C.
- β(Hf,Nb) continuous solid solution with body centred cubic structure of niobium and high temperature hafnium.

The minimum of the liquidus is predicted to be at 2140°C for about 25 at.% of Nb. The dashed lines represent the range of the metastable miscibility gap between two phases with bcc structure reported by some authors [27]. However, it is intended to be only a rough orientation mark, as the area of this miscibility gap depends strongly on the applied modelling parameters.

### 2.2.2 Hf-As binary system

There is no phase diagram available for this system, but eight binary phases were reported till now. The first literature record of research in this system is from 1962, when Jeitschko and Nowotny prepared mixtures of the element powders with the composition range 20-66.6 at.% As in evacuated silica tubes and raised the temperature to 600°C in 70 hours and subsequently to 1000°C in 50 hours, keeping the samples at this temperature for the next 50-70 hours [28]. In these samples, the occurrence of three binary phases was observed, from which HfAs and $HfAs_2$ could be identified and have their structures solved, while the third phase was presumed to have the stoichiometry of $Hf_4As$ and posses the superstructure related to Mg-type. Further experiments in this system were done by Rundqvist and Carlsson who prepared the samples in the similar way (annealing at 900°C for 3 days) and additionally arc-melted them afterwards [29]. In result, more phases were observed which were found isostructural with $Hf_3P_2$, $Nb_5P_3$, $Nb_7P_4$, $Ta_2P$ and $Fe_3P$, suggesting the stoichiometries of the new phases $Hf_3As_2$, $Hf_5As_3$, $Hf_7As_4$, $Hf_2As$ and $Hf_3As$, but the achievement of the equilibrium state was not claimed by the authors. Finally, the structure of $Hf_3As$ was solved and found to represent the $Ta_3As$ structure type [30]. The summary of the reported phases is given in Table 6.

**Table 6. Reported binary compounds in Hf-As system**

| Phase | As content [at.%] | Pearson symbol | Space group | Prototype | Structure refined | Ref. |
|---|---|---|---|---|---|---|
| $Hf_3As$ | 25 | *mC*64 | *C*2/*c* | $AsTa_3$ | Yes | [30] |
| $Hf_2As$ | 33.3 | *oP*36 | *Pnnm* | $PTa_2$ | No | [29] |
| $Hf_7As_4$ | 36.4 | *mC*44 | *C*2/*m* | $Nb_7P_4$ | No | [29, 31] |
| $Hf_5As_3$ | 37.5 | *oP64* | *Pnma* | $As_3Nb_5$ | No | [29, 32] |
| $Hf_3As_2$ | 40 | *oP*20 | *Pnma* | $S_3Sb_2$ | No | [29] |
| HfAs | 50 | *hP*8 | $P6_3/mmc$ | AsTi | Yes | [28] |
| $HfAs_2$ | 66.7 | *oP*12 | *Pnma* | $Co_2Si$ | Yes | [28] |

### 2.2.3 Nb-As binary system

Similarly to the Hf-As system, no phase diagram is available for the Nb-As system, only the existence of six binary phases was reported. In 1931, Heinerth and Biltz heated niobium and arsenic in an evacuted silica tube at 600°C for two days and, based on the mass balance, they described the obtained product as $NbAs_{1.8}$ [33]. Boller and Parthé reported the NbAs phase crystallising in a unique structure type [34]. The samples were prepared in a similar way as for the hafnium arsenides, i.e. the elements were sealed in silica tubes, heated slowly to 1200°C, kept for 24-48 hours at this temperature and slowly cooled. Furuseth and Kjekshus presented a series of papers about the arsenides and antimonides of niobium in which $NbAs_2$ and NbAs (independently from [34]) phases were reported [35, 36, 37, 38]. The structure of NbAs was confirmed and the structure of $NbAs_2$ was established. Again, the samples were prepared by sealing the mixture of the elements in silica tubes (covered range: 20-75 at.% As), heated at 1000°C for two days, then at 720°C for 14 days and quenched in ice water. As reaction between niobium and silica glass was observed for the mixtures with a Nb content greater than 50 at.%, an alternative way of obtaining the NbAs phase was given by the decomposition of $NbAs_2$ at 1100°C. The third report comes from Saini et al. who obtained both phases in a similar way (annealing the mixture of elements at 1000°C) [39]. The existence of the $Nb_3As$ phase was also suggested. Moreover, they were able to produce single crystals of the NbAs and $NbAs_2$ phases by halide vapour transport with chlorine and bromine, with the polycrystalline diarsenide as an input substance held at 1000°C and the sink held at 600-700°C. The halide vapour transport with iodine was also done by Schäfer and Fuhr who conducted a series of experiments in which both NbAs and $NbAs_2$ were synthesized, this time the stable NbAs was obtained in the hotter end of the silica tube (e.g.: source – 940°C, sink – 1065°C) [40]. They also observed the formation of NbO as a result of the reaction of niobium with silica glass for the substrate mixtures containing more than 50 at.% Nb, but believed that this can be avoided when the cold end of the tube is kept at ~450°C (the source with substrates still kept at ~900°C and the sink at ~1000°C). Ganglberger prepared the mixtures by direct synthesis in silica tubes annealed at 1000°C and afterwards applied a temperature of ~2000°C for 30 seconds on them. This allowed to confirm the existence of the $Nb_3As$ phase crystallising in the $Ti_3P$ structure type [41, 42]. Rundqvist et al. prepared the monoarsenide mixtures by the same way and subsequently mixed them with metal, arc-melted them, and some of them were additionally annealed in an induction furnace at temperatures up to 1700°C [32]. In the samples covering the range 0-45 at.%As, they identified phases

isostructural with $Ti_3P$ ($Nb_3As$), $Nb_7P_4$ ($Nb_7As_4$), $Nb_5P_3$ ($Nb_5As_3$) and a unique one with $Nb_4As_3$ stoichiometry. Similarly to their work in the Hf-As system [29], no equilibrium state was believed to have been achieved and "considerable losses of arsenic" by arc-melting and annealing were mentioned. Later on, Carlsson and Rundqvist were able to determine the crystal structure of $Nb_4As_3$ [43], Waterstrat et al. determined the structure of $Nb_3As$ [44] and Laohavanich et al. determined the structure of $Nb_5As_3$ [45]. Noteworthy, the single crystal used in ref. [44] was prepared by melting an ingot of $Nb_3As$ composition in a high pressure furnace under argon pressure of 40 atm., in a beryllium oxide crucible, kept for 6 hours "at a temperature somewhat below the solidus" and cooled by switching the furnace off. The structure of $NbAs_2$ was reinvestigated by Bensch and Heid who proposed the $OsGe_2$ structure type instead of the previously assumed $NbSb_2$ [46]. A summary of the reported phases is given in Table 7.

**Table 7. Reported binary compounds in Nb-As system**

| Phase | As content [at.%] | Pearson symbol | Space group | Prototype | Structure refined | Ref. |
|---|---|---|---|---|---|---|
| $Nb_3As$ | 25 | *tP*32 | $P4_2/n$ | $PTi_3$ | Yes | [44] |
| $Nb_7As_4$ | 36.4 | *mC*44 | $C2/m$ | $Nb_7P_4$ | No | [32] |
| $Nb_5As_3$ | 37.5 | *oP*64 | *Pnma* | $As_3Nb_5$ | Yes | [45] |
| $Nb_4As_3$ | 42.9 | *oC*56 | *Cmcm* | $As_3Nb_4$ | Yes | [43] |
| NbAs | 50 | *tI*8 | $I4_1md$ | AsNb | Yes | [37] |
| $NbAs_2$ | 66.7 | *mC*12 | *C*2 | $OsGe_2$ | Yes | [46] |

### 2.2.4 Hf-Ge binary system

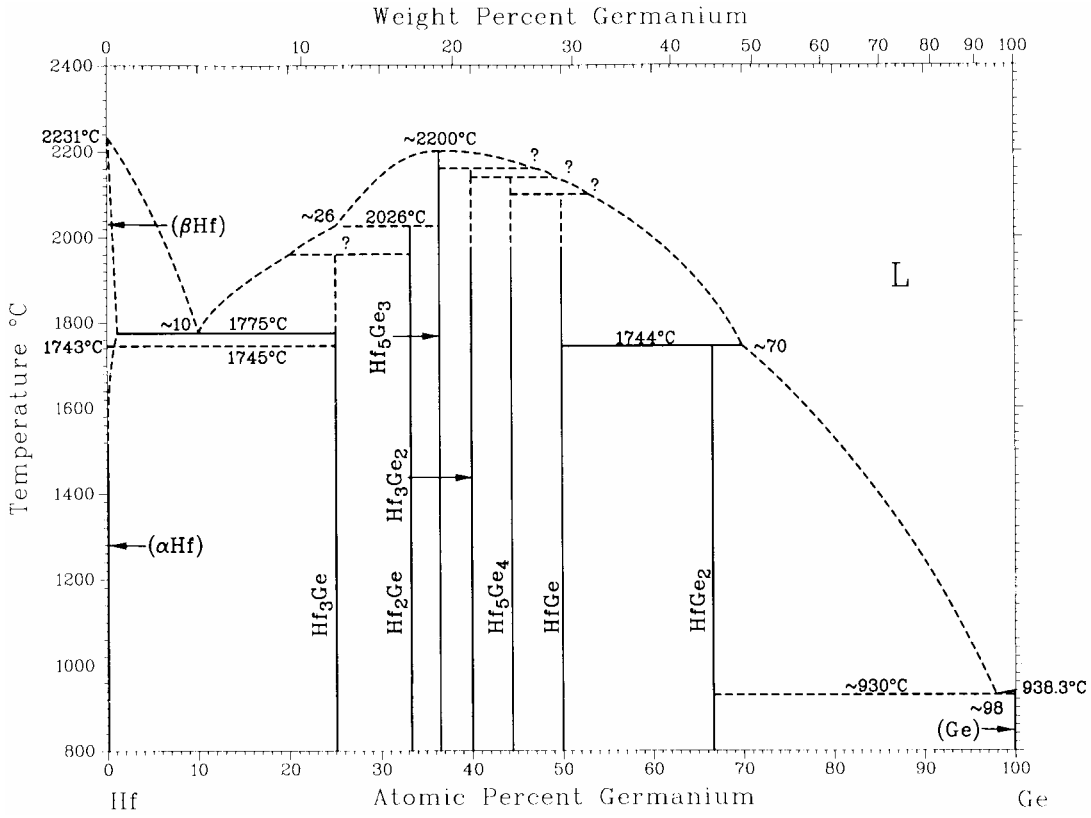


**Fig. 7. Phase diagram of Hf-Ge binary system [5].**

The phase diagram published in Massalski's compilation [5] is shown in Fig. 7. It is based on the work of Nowotny et al. [47]. They prepared a series of samples covering the range 5–67 at.% Ge. The temperatures of the solidus were estimated by finding the point on which the sample changed its shape when heated in a tungsten tubular furnace. This diagram was supplemented later by Schubert et al. [48], Rossteutscher and Schubert [49] and Zhao and Parthe [50] who found binary phases not reported earlier, but no data on the melting points were given, and the newly reported phases were just fitted into the diagram proposed in ref. [47]. In Massalski's compilation, it is assumed that the phase with the stoichiometry $Hf_6Ge_5$ reported in ref. [49] corresponds to HfGe. A summary of the intermetallic phases in the system Hf-Ge is given in Table 8, but it must be stressed that the author is not aware of any paper in which the phases HfGe and $Hf_5Ge_4$ were coexisting in the binary system. No homogeneity range was found for any of the binary phases. The maximal Ge solubility is about 1 at.% at 1775°C in bcc Hf and less than this in hcp Hf. The Hf solubility in Ge is negligible. Based on the metallographic pictures, the existence of the reactions presented in Table 9 is presumed to occur in this system. The samples in this system were prepared either by hot pressing of the powdered elements at 1000°C or by arc-melting. The annealing was

done either in silica tubes with the samples wrapped in tantalum sheet (under 1200°C) or in the tubular furnace under vacuum or argon atmosphere (over 1200°C).

**Table 8. Binary compounds reported in Hf-Ge system**

| Phase | Ge content [at.%] | Pearson symbol | Space group | Prototype | Structure refined | Ref. |
|---|---|---|---|---|---|---|
| $Hf_3Ge$ | 25 | *tP*32 | $P4_2/n$ | $PTi_3$ | no | [48] |
| $Hf_2Ge$ | 33.3 | *tI*12 | $I4/mcm$ | $Al_2Cu$ | yes | [51] |
| $Hf_5Ge_3$ | 37.5 | *hP*16 | $P6_3/mcm$ | $Mn_5Si_3$ | yes | [52] |
| $Hf_3Ge_2$ | 40 | *tP*10 | $P4/mbm$ | $Si_2U_3$ | no | [49] |
| $Hf_5Ge_4$ | 44.4 | *oP*36 | *Pnma* | $Ge_4Sm_5$ | yes | [50] |
| HfGe | 50 | *oP*8 | *Pnma* | BFe | no | [53] |
| $HfGe_2$ | 66.7 | *oC*12 | *Cmcm* | $Si_2Zr$ | yes | [54] |

**Table 9. Reactions in Hf-Ge binary system**

| Reaction type | Reaction equation | Temperature [°C] |
|---|---|---|
| Eutectic | L → βHf + $Hf_3Ge$ | 1775 |
| | L → $HfGe_2$ + Ge | ~930 |
| Peritectic | L + $Hf_2Ge$ → $Hf_3Ge$ | ? |
| | L + $Hf_5Ge_3$ → $Hf_2Ge$ | 2026(?) |
| | L + $Hf_5Ge_3$ → $Hf_3Ge_2$ | ? |
| | L + $Hf_3Ge_2$ → $Hf_5Ge_4$ | ? |
| | L + $Hf_5Ge_4$ → HfGe | ? |
| | L + HfGe → $HfGe_2$ | 1744 |
| Peritectoidal | βHf + $Hf_3Ge$ → αHf | ~1745 |

### 2.2.5 Nb-Ge binary system

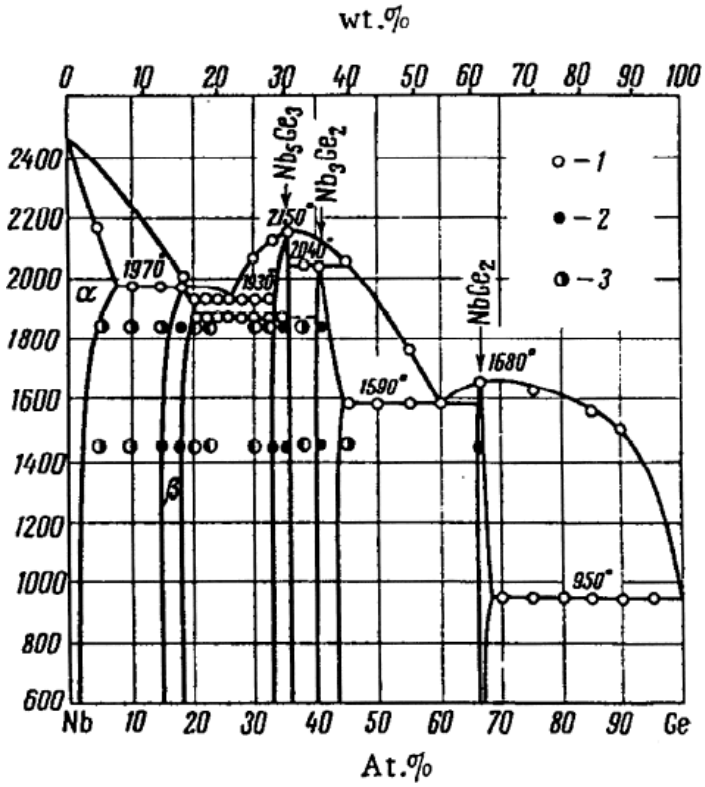


**Fig. 8 Phase diagram of Nb-Ge binary system proposed by Pan et al. [55] (taken from [56]).**

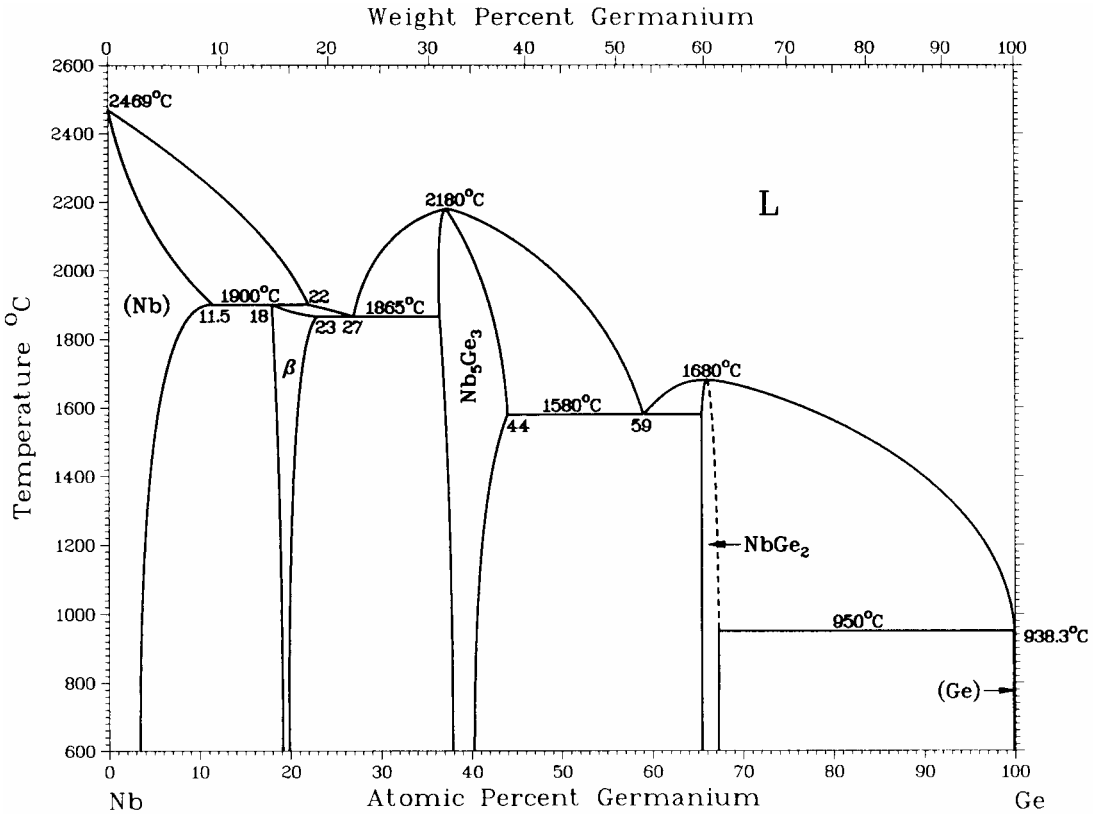


**Fig. 9. Phase diagram of Nb-Ge binary system presented in Massalski's compilation [5].**

The phase diagram proposed by Pan et al. [55] is shown in Fig. 8 (taken from [56]). Although it is an older work than the diagram published in Massalski's compilation [5] (Fig. 9), it is more accurate, as it includes the binary compound with 40-44 at.% Ge omitted in the one given in Massalski's database. Unfortunately, the original paper of Pan et al. was not available to the author so that nothing more can be written on the experimental techniques and results. The diagram in ref. [5] is based mostly on the work of Jorda et al. [57]. In this paper, a series of samples covering the range 0–70 at.% Ge was prepared and annealed at temperatures up to 1900°C, and DTA measurements were done up to the melting of the levitated sample. But, this diagram does not include the $Nb_{10}Ge_7$ phase (described as $Nb_3Ge_2$ in ref. [55]) which was believed to be impurity stabilised. Yet, the stability of this phase was confirmed later by Horyń and Kubiak [58] and Richter et al. [56]. Additionaly, during thin film experiments, the $Nb_3Ge$ phase was reported to exist with the structure of $AuCu_3$ [59], the $Nb_5Ge_3$ phase was obtained with the $B_3Cr_5$ structure type [60] and the $Nb_{10}Ge_7$ phase was found to crystallise in the own unique structure [61]. A summary of the intermetallic phases in the system Nb-Ge is given in Table 10. The homogeneity ranges are reported for the phases $Nb_3Ge$ (18-23 at.% Ge at 1865°C [5]), $Nb_5Ge_3$ (33-35 at.% Ge up to ~1700°C [55]), $Nb_{10}Ge_7$ (40-44 at.% Ge at 1590°C [55]) and $NbGe_2$ (66-68at.% Ge up to ~1500°C [5]) with the accuracy of 1 at.%. The maximal Ge solubility in Nb is about 11 at.% at 1900°C [5]. The Nb solubility in Ge is negligible. Based on the DTA measurements [57] and the data visible on the diagram given in ref. [55], the reactions presented in Table 11 are presumed to occur in this system.

**Table 10. Binary compounds reported in Nb-Ge system**

| Phase | Ge content [at.%] | Pearson symbol | Space group | Prototype | Structure refined | Ref. |
|---|---|---|---|---|---|---|
| $Nb_3Ge$ | 18-23 | *cP*8 | $Pm\bar{3}n$ | $Cr_3Si$ | Yes | [55] |
| $Nb_5Ge_3$ | 33-35 | *tI*32 | $I4/mcm$ | $Si_3W_5$ | Yes | [57] |
| $Nb_{10}Ge_7$ | 40-44 | *hP*18 | $P6_3/mcm$ | $Ga_4Ti_5$ | yes | [56] |
| $NbGe_2$ | 66-68 | *hP*9 | $P6_222$ | $CrSi_2$ | yes | [62] |

**Table 11. Reactions in Nb-Ge binary system**

| Reaction type | Reaction equation | Temperature [°C] |
|---|---|---|
| Eutectic | L → $Nb_3Ge$ + $Nb_5Ge_3$ | 1865 |
| | L → $Nb_{10}Ge_7$ + $NbGe_2$ | 1580 |
| Peritectic | L + Nb → $Nb_3Ge$ | 1900 |
| | L + $Nb_5Ge_3$ → $Nb_{10}Ge_7$ | 2040 |
| | L + $NbGe_2$ → Ge | 950 |

### 2.2.6 Hf-Ga binary system

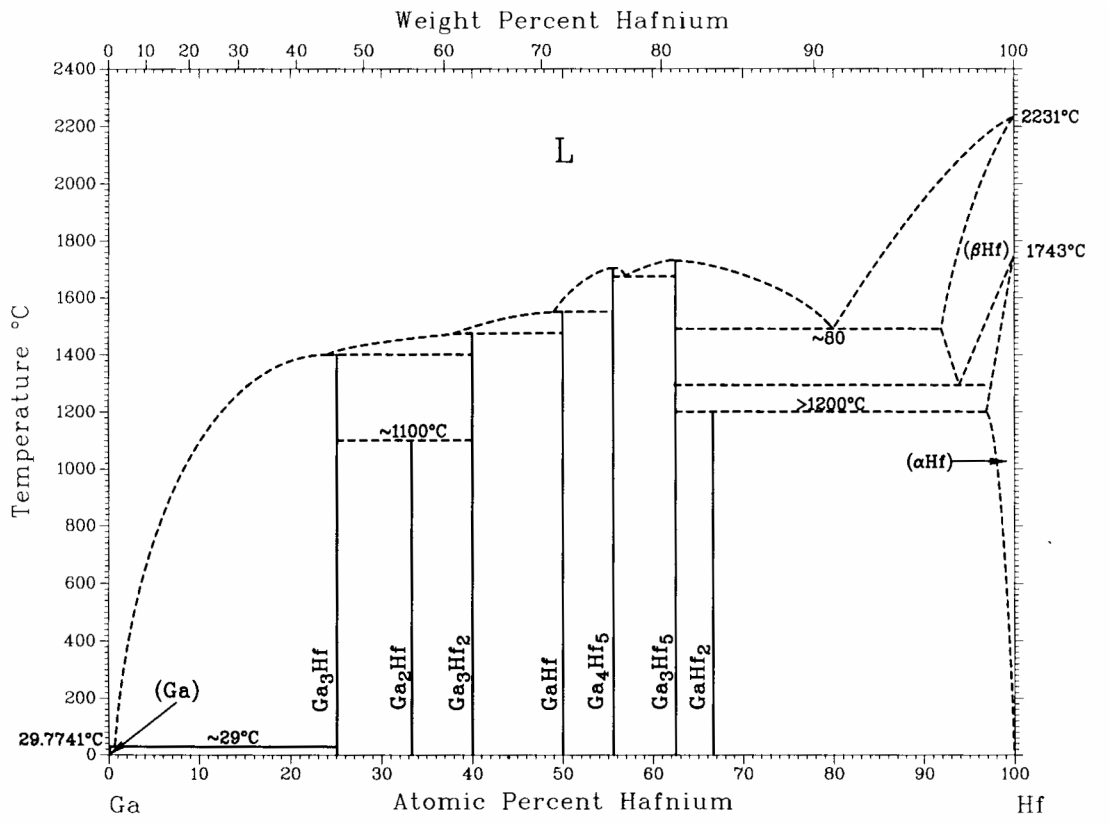


**Fig. 10. Phase diagram of Hf-Ga binary system [5].**

The phase diagram published in Massalski's compilation [5] is shown in Fig. 10. It is based on the work of Pötzschke and Schubert [63]. They prepared a series of samples covering the range 20 – 80 at.% Ga annealed at different temperatures (up to 1200°C). Due to the high melting points, no thermal analysis was performed and the liquidus lines are just roughly estimated. This diagram needs to be modified, as Markiv et al. reported later the existence of $Hf_{11}Ga_{10}$ instead of $Hf_5Ga_4$ phase [64]. A summary of the intermetallic phases in

the system is given in Table 12. No homogeneity range was found for any of these. The maximal Ga solubility in Hf is estimated to be about 3 at.% at about 1200°C (for hcp Hf) and 8 at.% at about 1500°C (in bcc Hf). The Hf solubility in Ga is negligible. Based on micrographs, the existence of the reactions presented in Table 13 is presumed to occur in this system. The samples were prepared by multiple arc-melting of the elements, annealing in silica tubes and quenching in cold water. In case of gallium-rich samples, master alloys were used instead of pure hafnium. In both cases, the observed gallium losses (8-10% of the initial gallium weight) were replenished after the melting.

**Table 12. Binary compounds reported in Hf-Ga system**

| Phase | Ga content [at.%] | Pearson symbol | Space group | Prototype | Structure refined | Ref. |
|---|---|---|---|---|---|---|
| $Hf_2Ga$ | 33.3 | *tI*12 | $I4/mcm$ | $Al_2Cu$ | ab-initio* | [65] |
| $Hf_5Ga_3$ | 37.5 | *hP*16 | $P6_3/mcm$ | $Mn_5Si_3$ | yes | [66] |
| $Hf_{11}Ga_{10}$ | 47.6 | *tI*84 | $I4/mmm$ | $Ge_{10}Ho_{11}$ | yes | [64] |
| HfGa | 50 | *o*P24 | *Pbcm* | ThTl | yes | [67] |
| $Hf_2Ga_3$ | 60 | *oF*40 | *Fdd*2 | $Al_3Zr_2$ | yes | [63] |
| $HfGa_2$ | 66.7 | *tI*24 | $I4_1/amd$ | $Ga_2Hf$ | yes | [63] |
| $HfGa_3$ | 75 | *tI*8 | $I4/mmm$ | $Al_3Ti$ | yes | [63] |

* - atom positions taken from quantum mechanical calculations

**Table 13. Reactions in Hf-Ga binary system**

| Reaction type | Reaction equation | Temperature [°C] |
|---|---|---|
| Eutectic | L → βHf + $Hf_5Ga_3$ | ~1500°C |
| | L → $Hf_5Ga_3$ + $Hf_{11}Ga_{10}$ | ~1680°C |
| | L → $HfGa_3$ + Ga | ~29°C |
| Eutectoidal | βHf → αHf + $Hf_5Ga_3$ | ~1300°C |
| Peritectic | L + $Hf_{11}Ga_{10}$ → HfGa | ~1540°C |
| | L + HfGa → $Hf_2Ga_3$ | ~1480°C |
| | L + $Hf_2Ga_3$ → $HfGa_3$ | ~1400°C |
| Peritectoidal | αHf + $Hf_5Ga_3$ → $Hf_2Ga$ | >1200°C |
| | $Hf_2Ga_3$ + $HfGa_3$ → $HfGa_2$ | ~1100°C |

### 2.2.7 Nb-Ga binary system

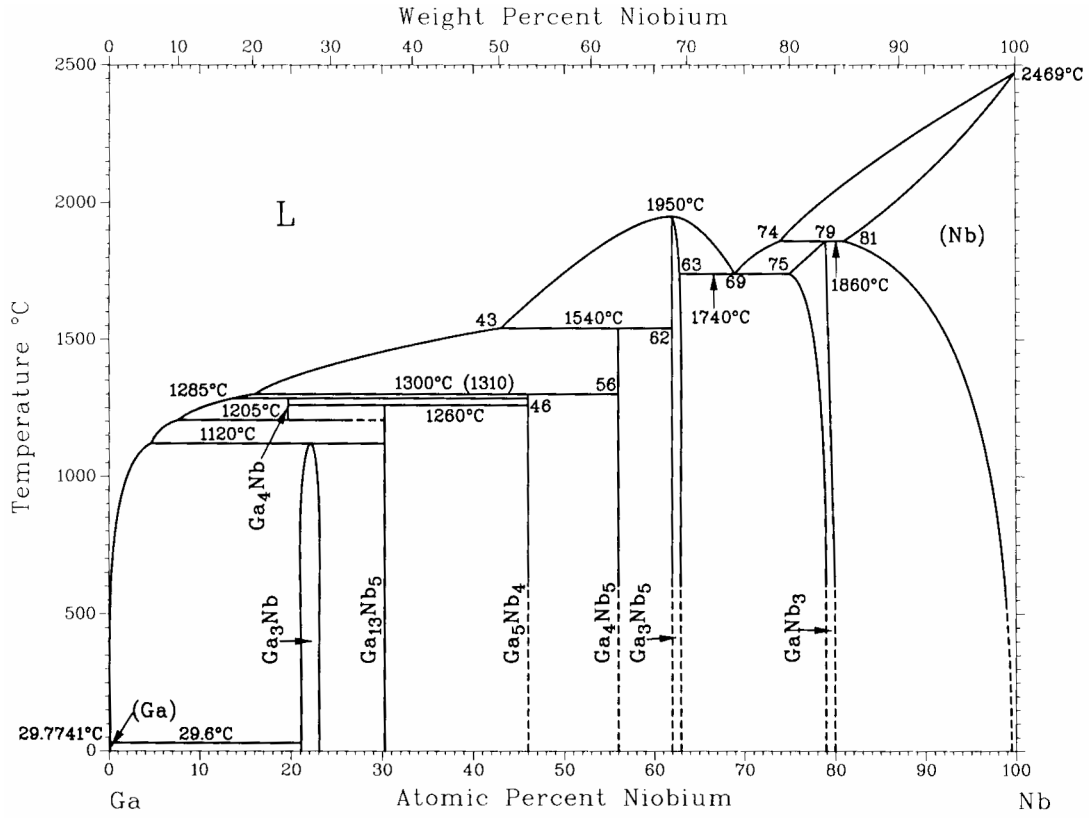


**Fig. 11. Phase diagram of Nb-Ga binary system [5].**

The phase diagram published in Massalski's compilation [5] is shown in Fig. 11. It is based on the works of Jorda et al. [68] and Pan and Latysheva [69]. The diagram was prepared on the basis of an investigation of samples covering the range 10-80 at.% Ga and annealed up to 2000°C. In both works, DTA experiments were done up to the melting of the sample. A summary of the intermetallic phases in the systems is given in Table 14. Additionally, the oxygen containing phases $Nb_5Ga_3O_x$ [70] and $NbGa_2O_x$ [71] were reported. No information on the structure of $NbGa_4$ is given (this phase is reported only in ref. [69]). $Nb_4Ga_5$ was indexed but it does not match any known structure type [72]. The phase $Nb_3Ga_2$ ($Si_2U_3$ structure type) reported by Holleck et al. [73], was not confirmed by the other authors. A homogeneity range was found for the phases $Nb_3Ga$ (20-24 at.% Ga at 1740°C), $Nb_5Ga_3$ (37-38 at.% Ga up to 1740°C) and $NbGa_3$ (75-78 at.% Ga up to 1000°C) with the accuracy of 1 at.%. The maximal Ga solubility in Nb is 19 at.% at 1860°C. Similarly to the Hf-Ga system, the Nb solubility in Ga is negligible. Based on DTA measurements, the existence of the reactions presented in Table 15 was established. The samples were prepared by multiple arc-melting of the elements, annealing in silica tubes (below 1200°C) or in an induction furnace and quenching in water or by splat cooling.

**Table 14. Binary compounds reported in Nb-Ga system**

| Phase | Ga content [at.%] | Pearson symbol | Space group | Prototype | Structure refined | Ref. |
|---|---|---|---|---|---|---|
| $Nb_3Ga$ | 20-24 | *cP*8 | $Pm\bar{3}n$ | $Cr_3Si$ | Yes | [74] |
| $Nb_5Ga_3$ | 37-38 | *tI*32 | $I4/mcm$ | $Si_3W_5$ | Yes | [75] |
| $Nb_5Ga_4$ | 44.4 | *hP*18 | $P6_3/mcm$ | $Ga_4Ti_5$ | Yes | [76] |
| $Nb_4Ga_5$ | 55.6 | *t*? | ? | ? | No | [72] |
| $Nb_5Ga_{13}$ | 72.2 | *oC*36 | *Cmmm* | $Ga_{13}Nb_5$ | Yes | [77] |
| $NbGa_3$ | 75 | *tI*8 | $I4/mmm$ | $Al_3Ti$ | Yes | [75] |
| $NbGa_4$ | 80 | ? | ? | ? | No | [69] |

**Table 15. Reactions in Nb-Ga binary system**

| Reaction type | Reaction equation | Temperature [°C] |
|---|---|---|
| Eutectic | L → $Nb_3Ga$ + $Nb_5Ga_3$ | 1740°C |
| | L → $NbGa_3$ + Ga | 29.6°C |
| Peritectic | L + Nb → $Nb_3Ga$ | 1860°C |
| | L + $Nb_5Ga_3$ → $Nb_5Ga_4$ | 1540°C |
| | L + $Nb_5Ga_4$ → $Nb_4Ga_5$ | 1300-1310°C |
| | L + $Nb_4Ga_5$ → $NbGa_4$ | 1285°C |
| | L + $Nb_5Ga_{13}$ → $NbGa_3$ | 1120°C |
| Peritectoidal | $NbGa_4$ + $Nb_4Ga_5$ → $Nb_5Ga_{13}$ | 1260°C |
| Catatectic | $NbGa_4$ → L + $Nb_5Ga_{13}$ | 1205°C |

## 2.3 Ternary systems

Similarly to the binary systems, a review of the ternary systems should yield the knowledge of the existing phases, the range of their occurrence and the experimental procedure used to obtain them.

### 2.3.1 Hf-Nb-As ternary system

As no binary phase diagram of both metal-arsenic systems are known, the ternary one is also not reported. Neither any ternary phases, nor the solubility ranges of the binary phases are given in the literature. Comparing the binary arsenides $M_5As_3$ and $M_7As_4$ which are isostructural in both systems, one can speculate about a continuous solid solubility range in the ternary system. However, the two phases are very close to each other (37.5 and 36.3 at.% As respectively) and a coexistent solubility range across the whole ternary field would seem unusual. According to the published structure maps for the pnictides and chalcogenides with $M_2Q$ stoichiometry (M – metal, Q – non-metal) [78, 79], some prediction could be made about the structure types for a possible ternary phase with this stoichiometry in the Hf-Nb-As system. This map was built by calculating a quantity *f* defined by:

$$f = \frac{vec_M * n_M^2 * (r_M / r_Q)}{(8 - e_Q)^2}$$

Where:

$vec_M$ – an average number of valence electrons available for M-M bonding per M atom

$n_M$ – an average of the maximal principial quantum number of valence shell for the M atom

$r_M$ – an average for Slater radii for M atoms

$r_Q$ – an average for Slater radii for Q atom

$e_Q$ – number of valence electrons for Q atom

Calculating *f* for binary $Hf_2As$ and $Nb_2As$, the following values are obtained:

$$f_{Hf2As} = \frac{2.5 * 6^2 * (155/115)}{(8-5)^2} \approx 13.48$$

$$f_{Nb2As} = \frac{3.5 * 5^2 * (145/115)}{(8-5)^2} \approx 12.26$$

Comparing these values with data gathered in the mentioned map (Fig. 12), the structure of possible new ternary phases would be of the $Nb_2P$, $Zr_2P$ or $Co_2Si$ type ($Ta_2P$-type is represented by $Hf_2As$).

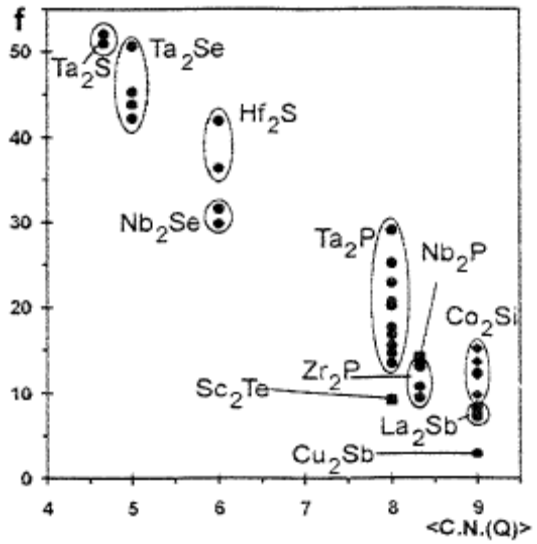


**Fig. 12. Structure map for $M_2Q$ pnictides and chalcogenides [79]. <C.N.(Q)> describes the coordination number of atom Q.**

A similar map prepared for $M_5Q_3$ compounds does not assume the existence of a ternary phase on the $Hf_5As_3$-$Nb_5As_3$ line with the structure type other than $Nb_5As_3$ [79].

Considering the doubts about the equilibrium conditions which emerged during the experiments with the binaries and which were expressed in the literature, it is clear that the construction of the ternary phase diagram will be a very difficult task.

### 2.3.2 Hf-Nb-Ge ternary system

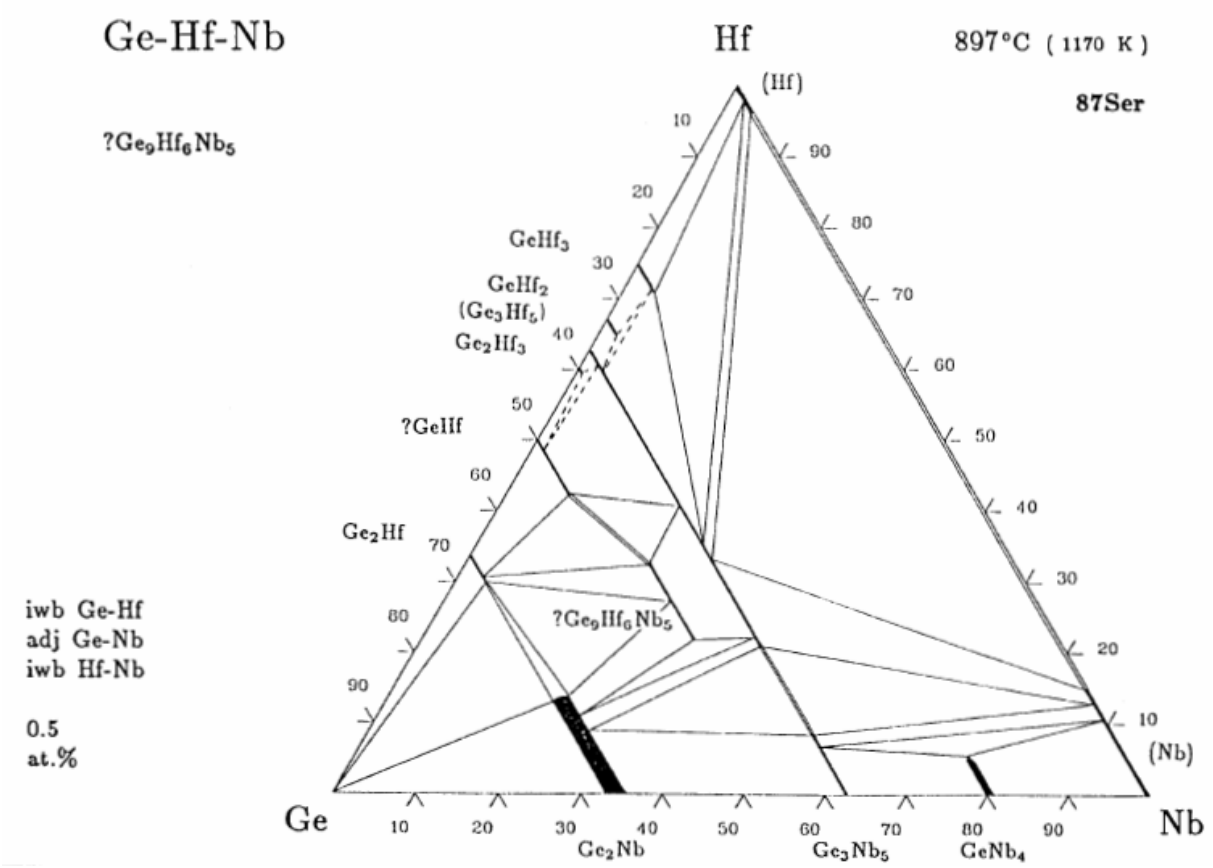


**Fig. 13. Phase diagram of the Ge-Hf-Nb ternary system [6].**

The phase diagram published in the *"Handbook of Ternary Alloy Phase Diagrams"* [6] is shown in Fig. 13. It is taken from the paper of Seropegin and Rudometkina [80] who presented the isothermal section of the diagram at 897°C. The samples were prepared by multiple arc-melting of the elements and annealed in silica ampoules with a titanium getter. The existence of the ternary phase described as $Hf_2Nb_3Ge_4$ (interpreted in ref. [6] as $Hf_6Nb_5Ge_9$, see Fig. 13) was reported within the niobium content of 22-33 at.% and a homogeneity range between 44-46 at.% Ge (which was not considered in ref. [6] and thus, it is not represented on Fig. 13). This compound was found to be isostructural with $Zr_2Nb_3Ge_4$ [81] which itself is related to the $Sm_5Ge_4$ structure type. A list of the intermetallic phases found in the system and their solubility ranges is given in Table 16. The diagram is not consistent with the binary diagram of the Nb-Ge system (Fig. 8), as it does not include the binary $Nb_{10}Ge_7$ phase. It is not consistent with the binary diagram of the Hf-Ge system (Fig. 7), either, as it does not include the binary $Hf_5Ge_4$ phase, and the solubility ranges of Hf in Nb are different than in the binary Hf-Nb diagram. Richter et al. showed later that the binary

$Hf_5Ge_4$ extends indeed into the ternary field up to $Hf_{1.2}Nb_{3.8}Ge_4$ (42.2 at.% Nb) at 1400°C, thus covering also the composition range of the reported $Hf_2Nb_3Ge_4$ [82].

**Table 16. Ternary solubilities reported in the Hf-Nb-Ge system. The homogeneity range for $Hf_5Ge_4$ phase is given for 1400°C [82]. The homogeneity ranges for other phases are given for 897°C [80].**

| Phase | Ge content [at.%] | Second metal solubility [at.%] | Prototype |
|---|---|---|---|
| $Nb_3Ge$ | 18-23 | 0-5 (Hf) | $Cr_3Si$ |
| $Nb_5Ge_3$ | 38-44 | 0-8(Hf) | $Si_3W_5$ |
| $NbGe_2$ | 66-68 | 0-12 (Hf) | $CrSi_2$ |
| $Hf_3Ge$ | 25 | 0-4 (Nb) | $PTi_3$ |
| $Hf_2Ge$ | 33.3 | 0-2 (Nb) | $Al_2Cu$ |
| $Hf_5Ge_3$ | 37.5 | 0-42 (Nb) | $Mn_5Si_3$ |
| $Hf_3Ge_2$ | 40 | 0-2 (Nb) | $Si_2U_3$ |
| HfGe | 50 | 0-8 (Nb) | BFe |
| $HfGe_2$ | 66.7 | 0-3 (Nb) | $Si_2Zr$ |
| $Hf_5Ge_4$ | 44-46 | 0-42(Nb) | $Ge_4Sm_5$ |

### 2.3.3 Hf-Nb-Ga ternary system

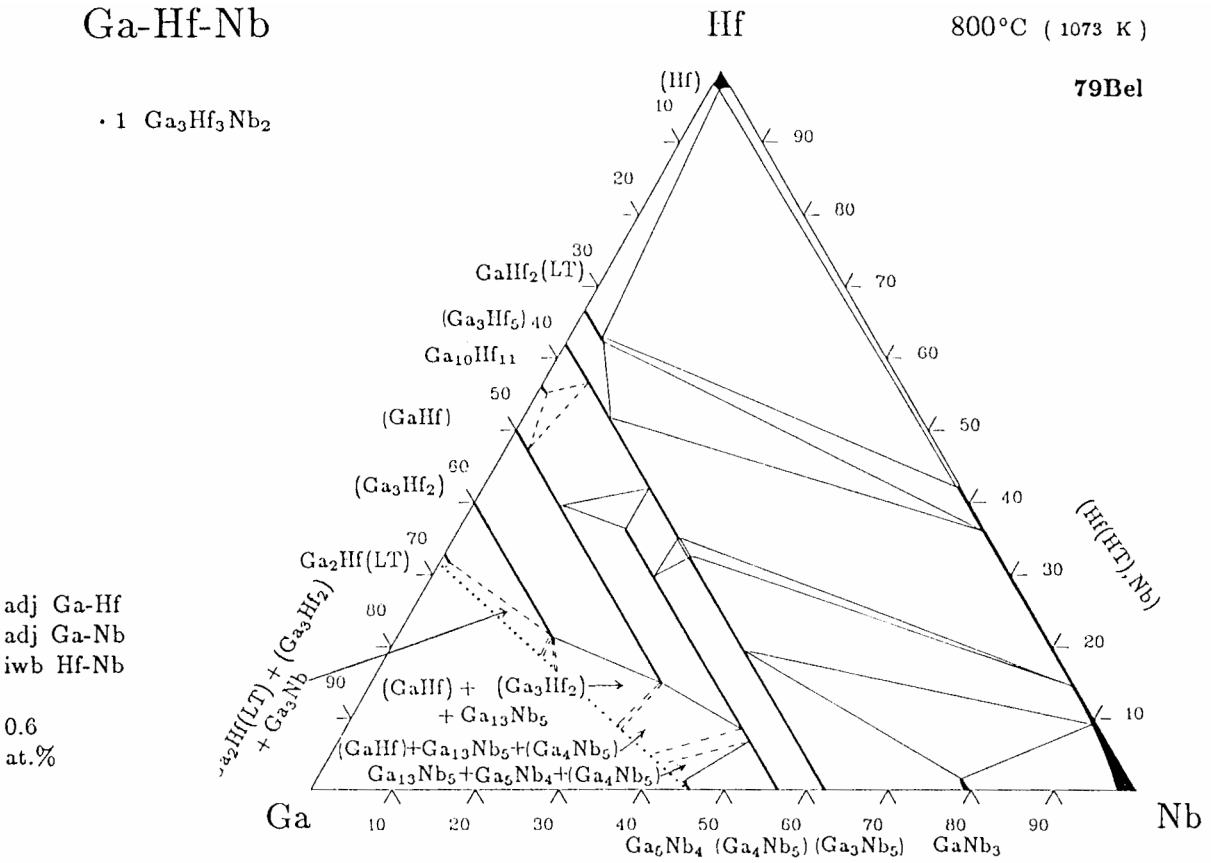


**Fig. 14. Phase diagram of the Ga-Hf-Nb ternary system [6].**

The phase diagram published in the *"Handbook of Ternary Alloy Phase Diagrams"* [6] is shown in Fig. 14. It is taken from the paper of Belyavina and Markiv [83] who presented the isothermal section of the diagram at 800°C excluding the gallium-rich corner (the isopleth connecting 70 at.% Ga in Ga-Hf and 55% at Ga in Ga-Nb). No ternary phase was detected. A list of the intermetallic phases found in the system and their solubility ranges is given in Table 17. The samples were prepared by multiple arc-melting of gallium, niobium and hafnium, annealed subsequently in silica ampoules. There are some differences in the Hf solubility in Nb as compared to the binary Hf-Nb phase diagram (Fig. 6).

A measurement of niobium solubility in the HfGa phase at 1200°C was performed by Oberseider [84]. The samples were prepared by melting the metals in the arc-furnace and annealing the samples in tantalum crucibles in an argon atmosphere under 0.5 bar for three days. The maximal niobium solubility found by EPMA analysis was about 36 at.% Nb, which corresponds to the stoichiometry of $Hf_{0.28}Nb_{0.72}Ga$.

**Table 17. Ternary solubilities reported in the Hf-Nb-Ga system. The homogeneity range for HfGa phase is given for 1200°C [84]. The homogeneity ranges for other phases are given for 800°C [83].**

| Phase | Ga content [at.%] | Second metal solubility [at.%] | Prototype |
|---|---|---|---|
| $Hf_2Ga$ | 33.3 | 0- ~5(Nb) | $Al_2Cu$ |
| $Hf_5Ga_3$ | 37.5 | 0-25 (Nb) | $Mn_5Si_3$ |
| $Hf_{11}Ga_{10}$ | 47.6 | 0- ~3(Nb) | $Ge_{10}Ho_{11}$ |
| HfGa | 50 | 0-35 (Nb) | ThTl |
| $Hf_2Ga_3$ | 60 | 0-20 (Nb) | $Al_3Zr_2$ |
| $HfGa_2$ | 66.7 | 0- ~3(Nb) | $Ga_2Hf$ |
| $Nb_3Ga$ | 20-24 | 0- ~2(Hf) | $Cr_3Si$ |
| $Nb_5Ga_3$ | 37-38 | 0-27 (Hf) | $Si_3W_5$ |
| $Nb_5Ga_4$ | 44.4 | 0-35 (Hf) | $Ga_4Ti_5$ |

### 2.4 The crystal structures described in terms of the coordination polyhedra

The knowledge of the binary structures can support the understanding of the substitution mechanisms. The comparison of the binary structures with the potentially new ternary structures can also yield some conclusions about the stabilisation of the ternary structures. In this section, the crystal structures of the known binary metal-rich arsenides of hafnium and niobium, as well as of the phases $Hf_5Ge_4$ and HfGa will be described shortly. The last two structures are chosen for further investigation, due to the reported large niobium solubility (with the Nb/Hf ratio exceeding over 1) and three metal sites on which the metal atom exchange can take place – this creates an opportunity to analyse the possible site preferences. It will be shown that in most of these structures the transition metal atoms form trigonal prisms around the main group elements.

The detailed structure data for all phases are given in the appendices A, B and C.

### 2.4.1 Arsenides

#### 2.4.1.1 HfAs and NbAs (50 at.% As, Appendix A.1)

The two structures are depicted in Fig. 15 and 17. Although both compounds are described with unit cells having different symmetry, they are both related to each other, as it was demonstrated by Boller and Parthé [34] who derived them from the simpler structure types of WC and NaCl.

In HfAs (*hP*8, [28]), hafnium atoms surround arsenic atoms in two ways - Octahedra are formed around As1 atoms and trigonal prisms are formed around As2 atoms. Both kinds of polyhedra are linked by sharing a common edge and form layers in (001) plane. The layers are stacked consecutive in ABA'B'ABA'B'… sequence (A – octahedral layer, B – trigonal prism layer) - X and X' layers are related by a rotation around a twofold axis parallel to the *c* axis (Fig. 16).

NbAs (*tI*8, [37]), niobium atoms surround arsenic atoms forming trigonal prisms only. The prisms are stacked parallel to (001) plane, and all layers of prisms are aligned in [100] and [010] directions. Also in this case, the prisms form layers, whereby within the layer each prism is linked with two prisms by sharing a common face (a base) and with another two by sharing a common edge. The layers are stacked, so that each next layer is rotated and shifted by a fourfold screw axis parallel to *c* axis (Fig. 18).

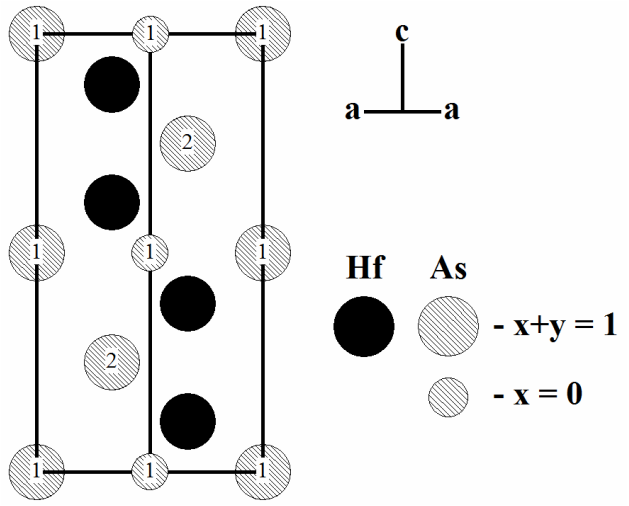


**Fig. 15. The unit cell of HfAs – view in [$\bar{1}\,\bar{1}$0]) direction. The numbers describe the atoms on the given atom position (see Appendix A.1).**

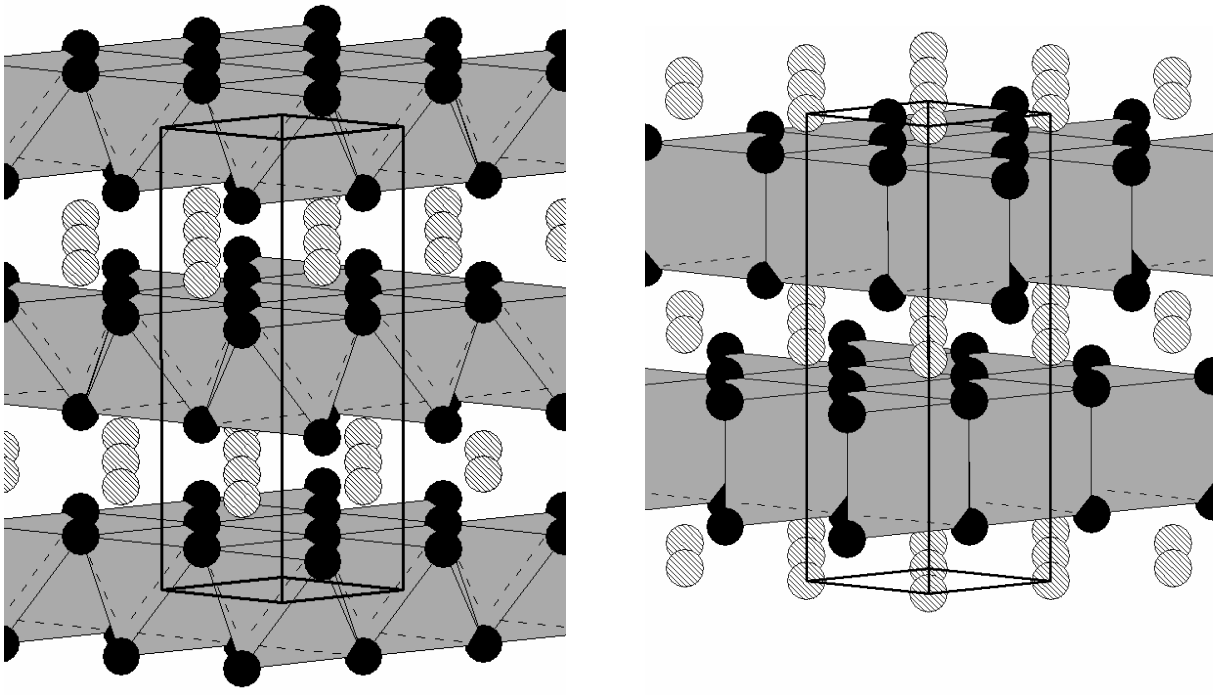

**Fig. 16. The stacking of octahedra centred on As1 (left) and trigonal prisms centred on As2 (right) in HfAs structure – view parallel to ($\bar{1}10$) plane**

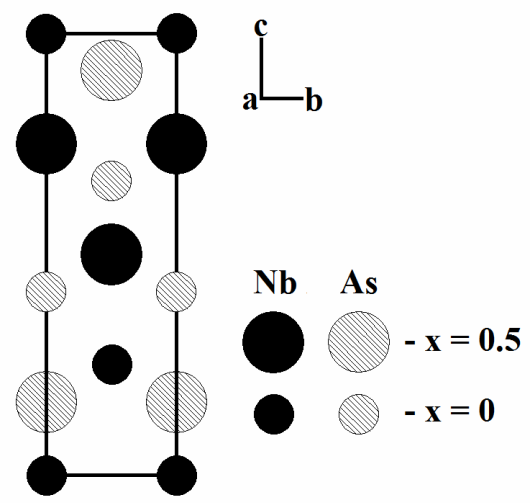


**Fig. 17. The unit cell of NbAs compound – view in [$\bar{1}10$]) direction.**

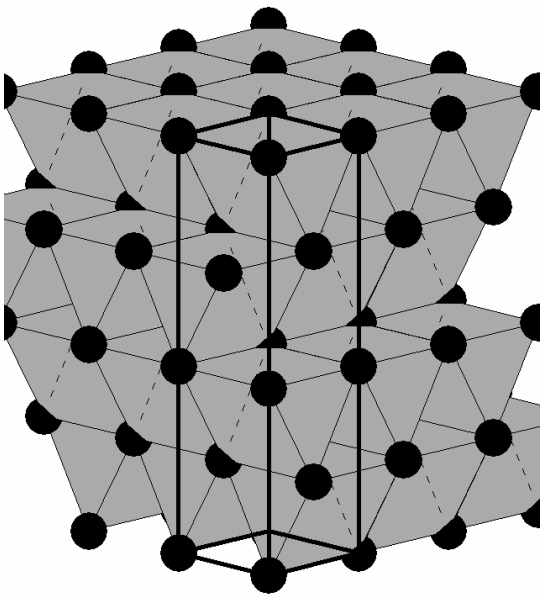

**Fig. 18. The stacking of trigonal prisms centred on As (right) in NbAs structure – view parallel to ($\bar{1}$10) plane**

### 2.4.1.2 Metal-rich arsenides with As content in range 30-50 at.%

A common feature of the following structures is one lattice parameter in range 3.3-3.6 Å, which is notably shorter than the other ones. In all these structures, the metal atoms form trigonal prisms around the arsenic metals. Generally, the prisms are aligned either parallel or perpendicular to the short axis direction (i.e. this direction either intersects the base plane perpendicularly or is laying in the plane, respectively). The prisms parallel to the short axis direction are linked with each other by a common face along this direction. Otherwise, all prisms are linked by a common edge. In all but one structure, some of the metal atoms are arranged in bcc fragments which is a feature observed in many DFSO-compounds reported in literature.

- $Nb_4As_3$ (42.9 at.% As, Appendix A.2, [43])

The structure of $Nb_4As_3$ (*oC*56) is depicted in Fig. 19 and the arrangement of the trigonal prisms is shown in Fig. 20. The prisms centred on As1 and As4 are aligned parallel to the short axis (*a*) direction, while the ones centred on As3 are perpendicular to it. One niobium (Nb1) and one arsenic atom (As2) are not included in the prism construction. The Nb1 atom is surrounded by eight other niobium atoms (4xNb4, 4xNb5) lying in the distance of 2.91-3.08

Å, forming a slightly distorted cube, resembling the body centred cubic structure of the metal. As2 atom is surrounded by six niobium atoms (2xNb2, 2xNb3, 2xNb4), whereby four of them are lying in the same plane (i.e. parallel to (001)) as the As atom and the two remaining ones are shifted by a/2, one above and the other one below the plane.

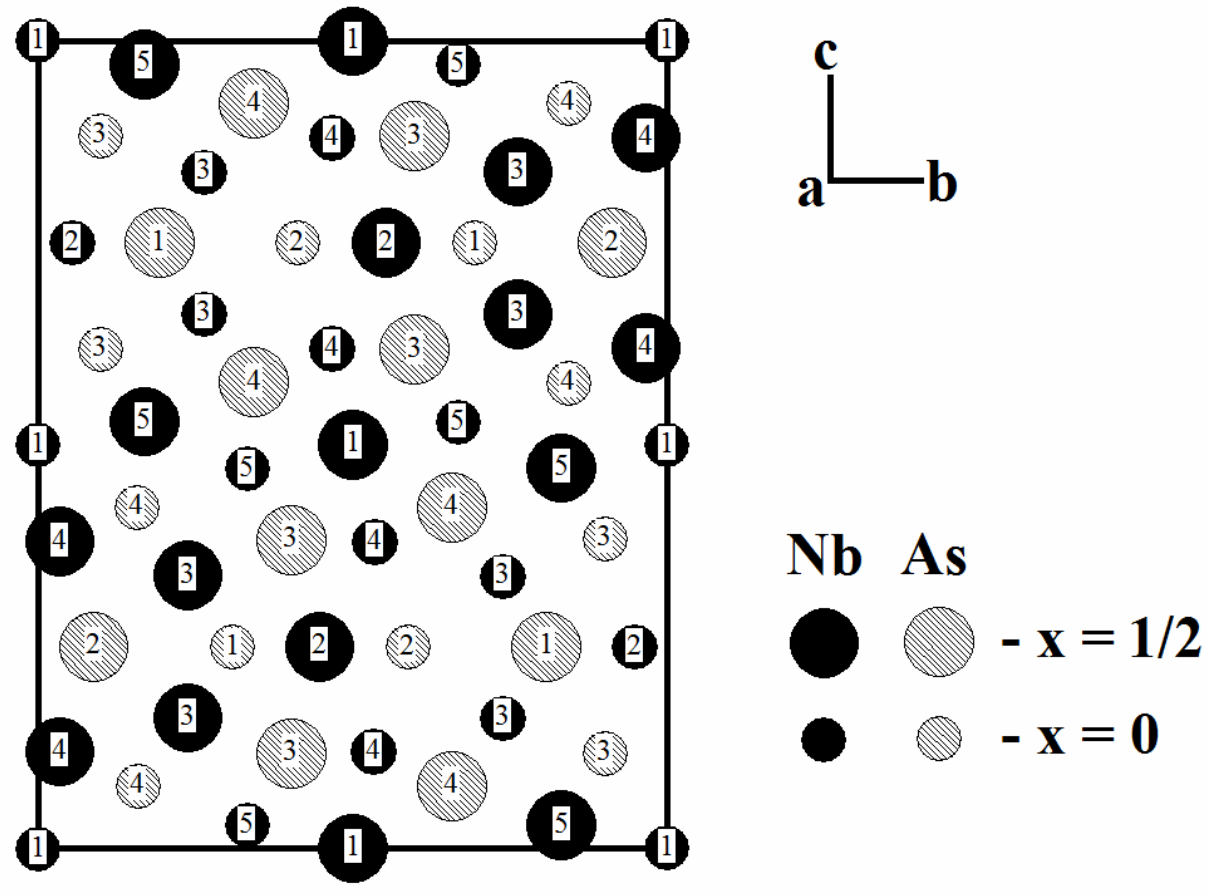


**Fig. 19. The unit cell of $Nb_4As_3$ – view in [$\bar{1}$00]) direction. The numbers describe the atoms on the given atom position (see Appendix A.2).**

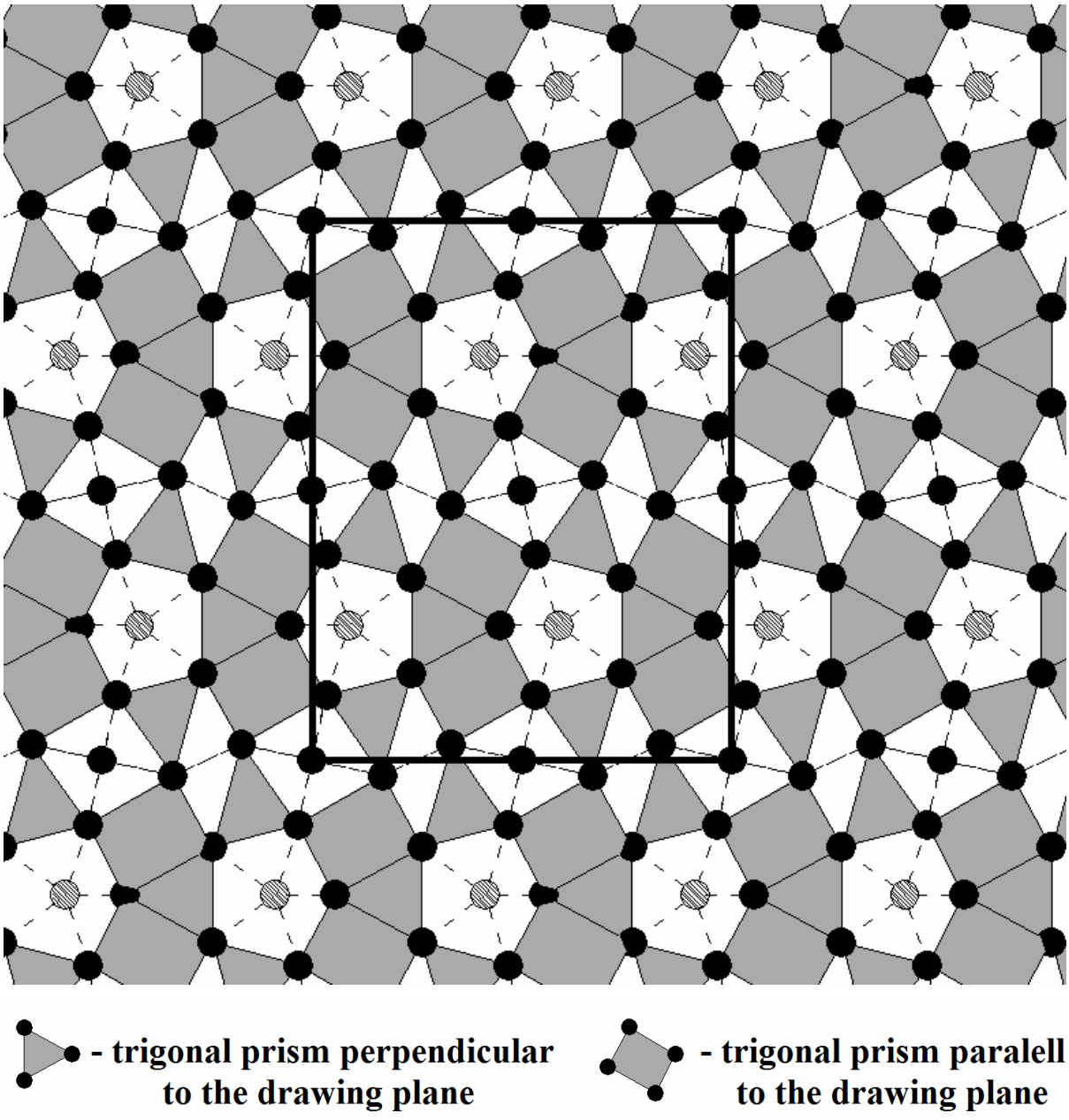


**Fig. 20. The unit cell of $Nb_4As_3$ shown as a combination of trigonal prisms – view in [$\bar{1}$00]) direction.**

- $Hf_3As_2$ (40 at.% As, Appendix A.3)

As the crystal structure of $Hf_3As_2$ phase was not refined, the structure of the isostructural $Hf_3P_2$ phase (*oP*20, [85]) will be analysed (Fig. 21 and 22). The prisms centred on P1 are aligned parallel to the short axis (*b*) direction, while the ones centred on P2 are perpendicular to them. No bcc fragments are present in the structure.

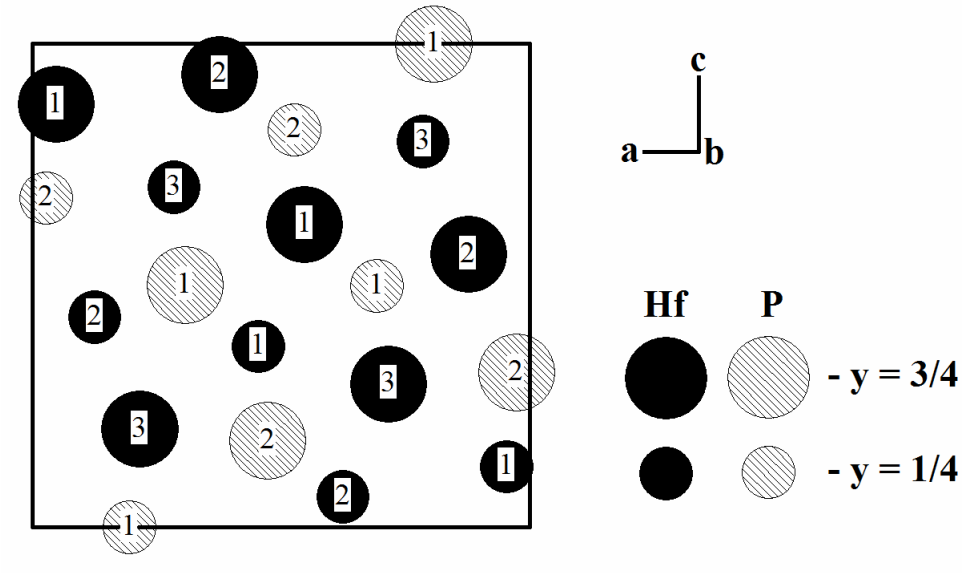


**Fig. 21. The unit cell of $Hf_3P_2$ – view in [0$\bar{1}$0]) direction. The numbers describe the atoms on the given atom position (see Appendix A.3).**

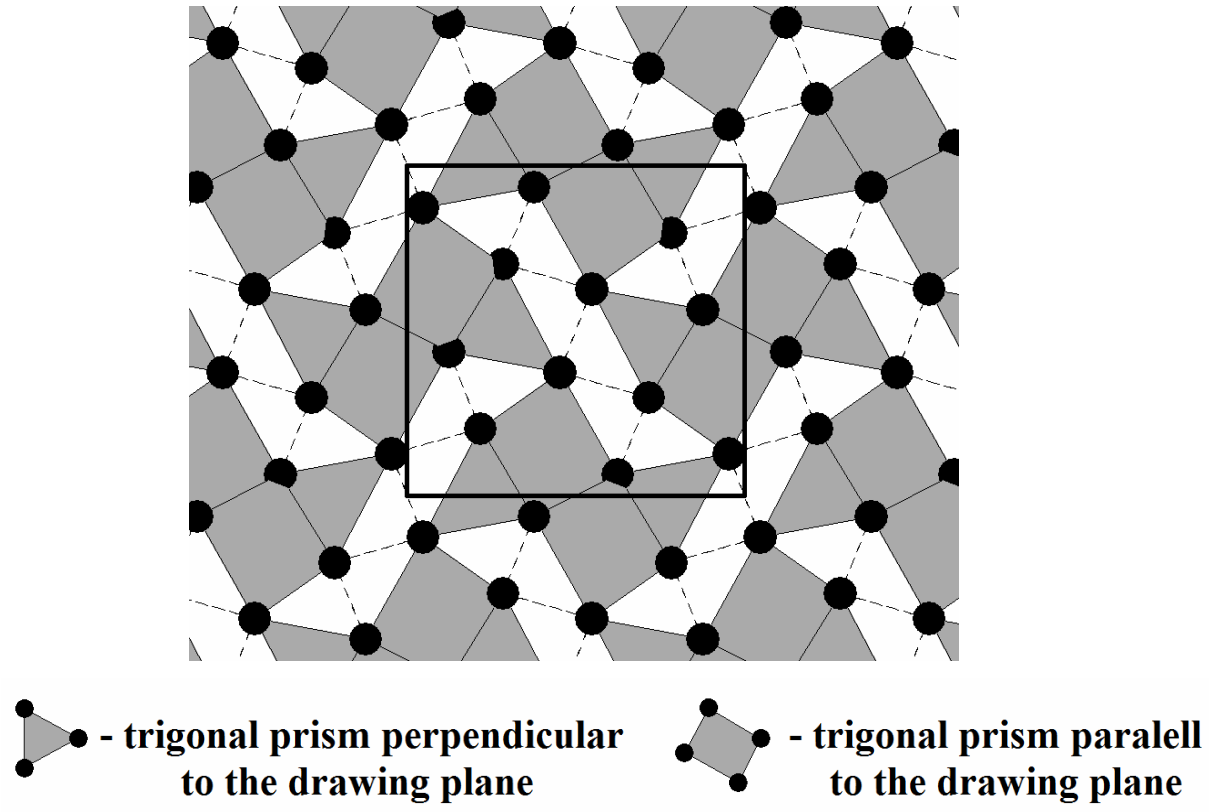


**Fig. 22. The unit cell of $Hf_3P_2$ shown as a combination of trigonal prisms – view in [0$\bar{1}$0]) direction.**

- $Hf_5As_3$ and $Nb_5As_3$ (37.5 at.% As, Appendix A.4, [45])

These two phases crystallise in the same structure type $Nb_5As_3$ (*oP*64). The structure of $Nb_5As_3$ is presented in Fig. 23 and the arrangement of trigonal prisms is shown in Fig. 24. The prisms centred on As2, As3, As5 and As6 are aligned parallel to the short axis (*b*) direction, while the ones centred on As1 and As4 are perpendicular to them. Additionally, one niobium atom (Nb6) is not included in the prisms and it is in the centre of the bcc fragment, surrounded by eight other niobium atoms in the distance range of 2.86-3.13 Å.

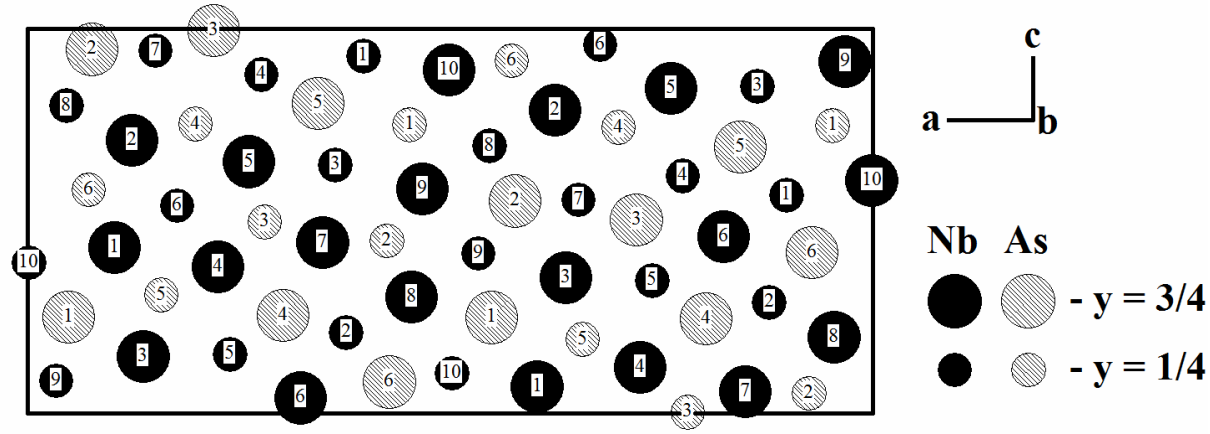


**Fig. 23. The unit cell of $Nb_5As_3$ – view in [0$\bar{1}$0]) direction. The numbers describe the atoms on the given atom position (see Appendix A.4).**

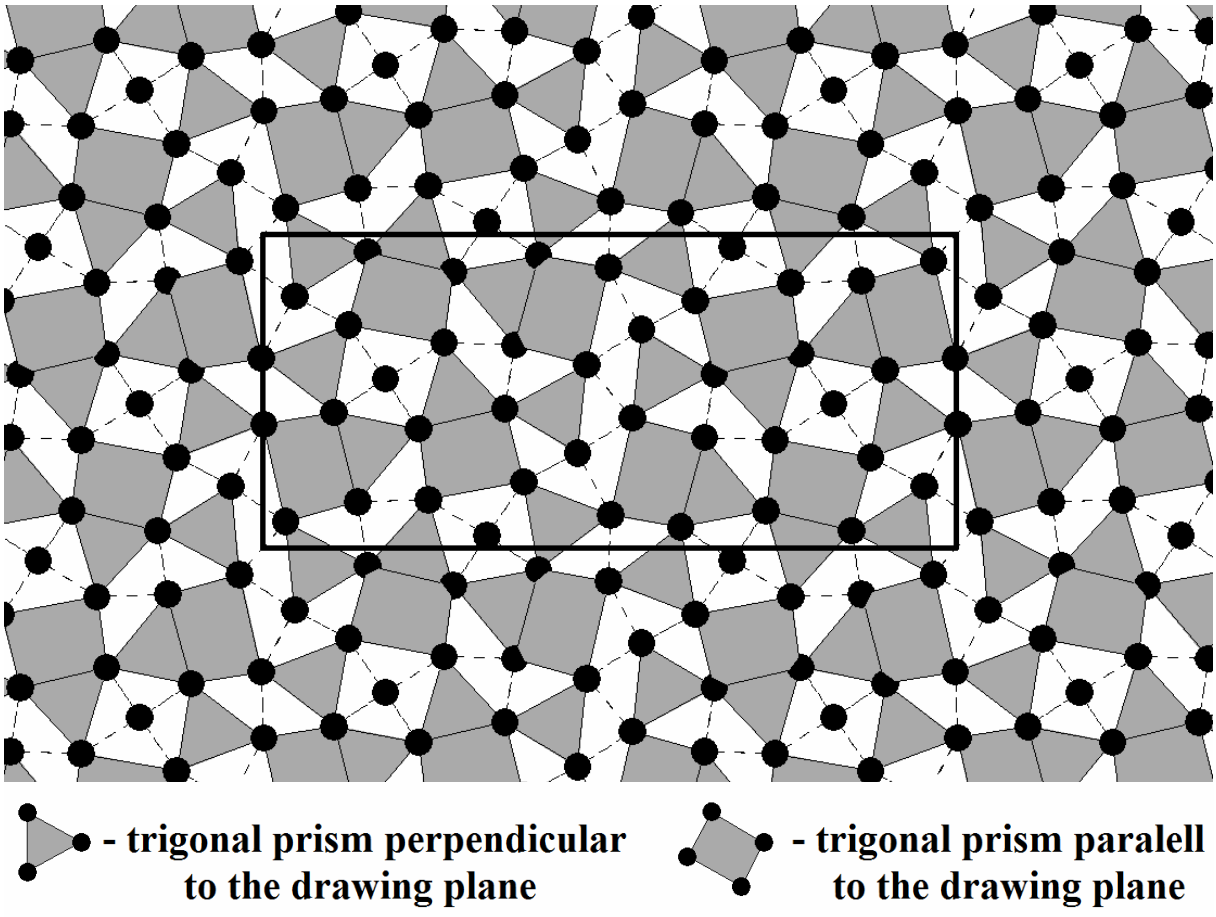


**Fig. 24. The unit cell of $Nb_5As_3$ shown as a combination of trigonal prisms – view in [0$\bar{1}$0]) direction.**

- $Hf_7As_4$ and $Nb_7As_4$ (36.4 at.% As, Appendix A.5)

The crystal structures of these phases were not refined, but they were reported to be isostructural with the $Nb_7P_4$ structure (*mC*44, [86]) so that the latter will be characterised. The unit cell is depicted in Fig. 25 and the prism arrangement is shown in Fig. 26. The prisms centred on P1, P2 and P3 are aligned parallel to the short axis (*b*) direction, while the ones centred on P4 are perpendicular to them. The niobium atoms Nb1 and Nb2 are in the centre of the body centred cubes, surrounded by eight other niobium atoms lying in the distance range of 2.99-3.20 Å to Nb1 and 2.89-3.20 Å to Nb2 atom.

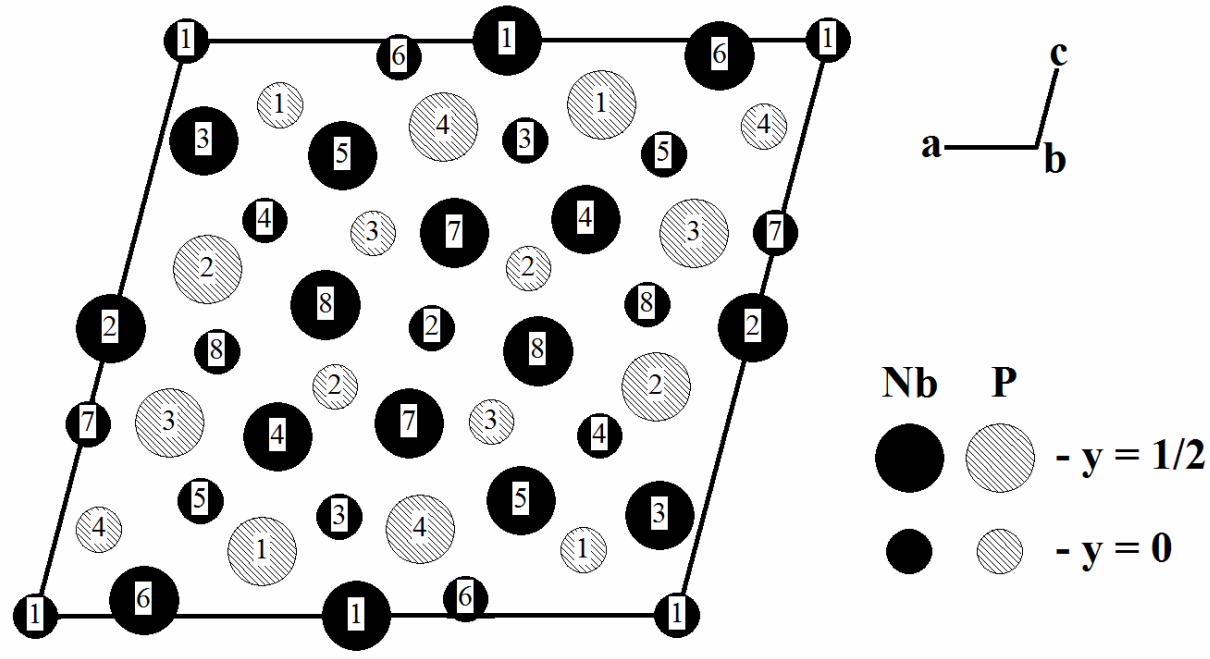


**Fig. 25. The unit cell of $Nb_7P_4$ – view in [0$\bar{1}$0]) direction. The numbers describe the atoms on the given atom position (see Appendix A.5).**

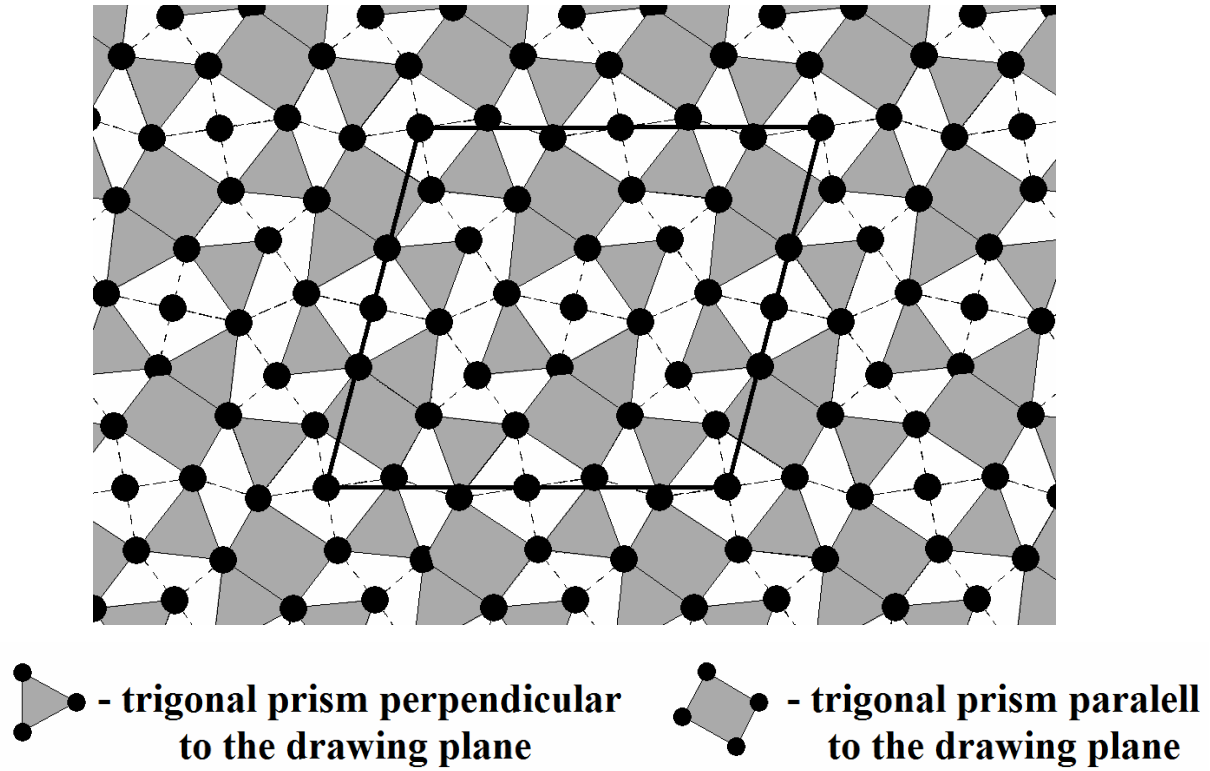


**Fig. 26. The unit cell of $Nb_7P_4$ shown as a combination of trigonal prisms – view in [0$\bar{1}$0]) direction.**

- $Hf_2As$ (33.3 at.% As, Appendix A.6)

The isostructural $Ta_2P$ structure (*oP*36, [87]) will be described as the crystal structure of the $Hf_2As$ phase has not been refined, either. The structure is depicted in Fig. 27 and the prism arrangement is shown in Fig. 28. The prisms centred on P2 and P3 are aligned parallel to the short axis (*c*) direction, while the ones centred on P1 are perpendicular to them. Ta3 atoms are surrounded by eight other tantalum atoms lying in the distance range of 3.12-3.34 Å, forming a fragment of two condensed bcc units sharing a common face.

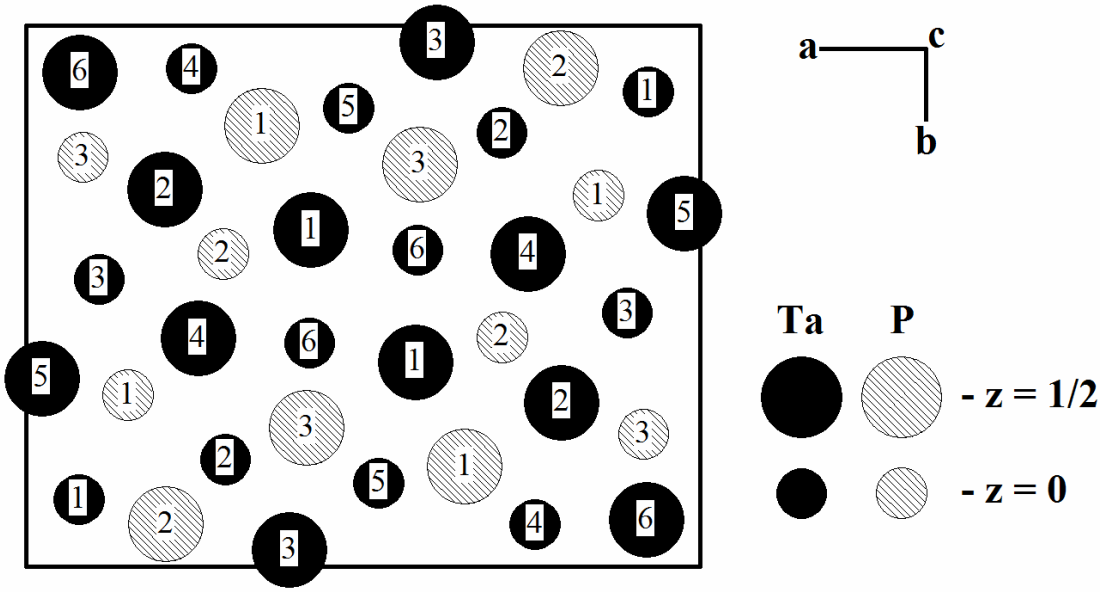


**Fig. 27. The unit cell of $Ta_2P$ – view in [00$\bar{1}$] direction. The numbers describe the atoms on the given atom position (see Appendix A.6).**

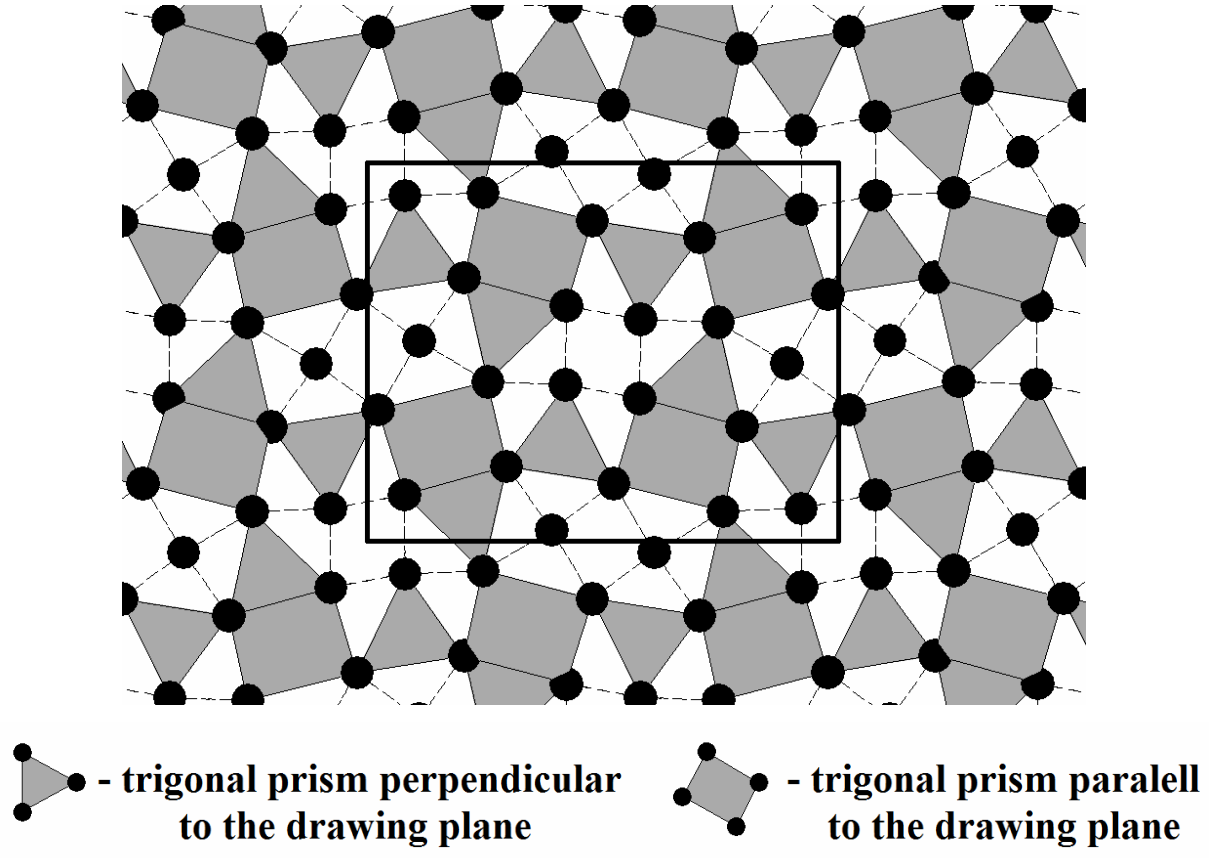


**Fig. 28. The unit cell of $Ta_2P$ shown as a combination of trigonal prisms – view in [00$\bar{1}$] direction.**

### 2.4.1.3 $Hf_3As$ and $Nb_3As$ (25 at.% As, Appendix A.7)

The structures of $Hf_3As$ (*mC*64) [30] and $Nb_3As$ (*tP*32) [44] are depicted in Fig. 29 and 30. The close relation between the two structures has already been discussed by Willerström et al. [30], the similarities can be also seen by comparing the coordination polyhedra of arsenic atoms shown on Fig. 31 and 32. The structures are different from the previous ones, as the metal atoms around arsenic atoms form distorted square antiprism linked by sharing a common edge or a common vertex. However, the angles within every prism base vary from 81° to 98° so that they are not ideal squares. It is tempting to interpret these polyhedra as deformed bicapped trigonal prisms, but in this case, there exists no pair of the parallel trigonal bases. The connected prisms create a mosaic which is difficult to describe with words. There are no fragments of the body centred cubic fragments built of metal atoms.

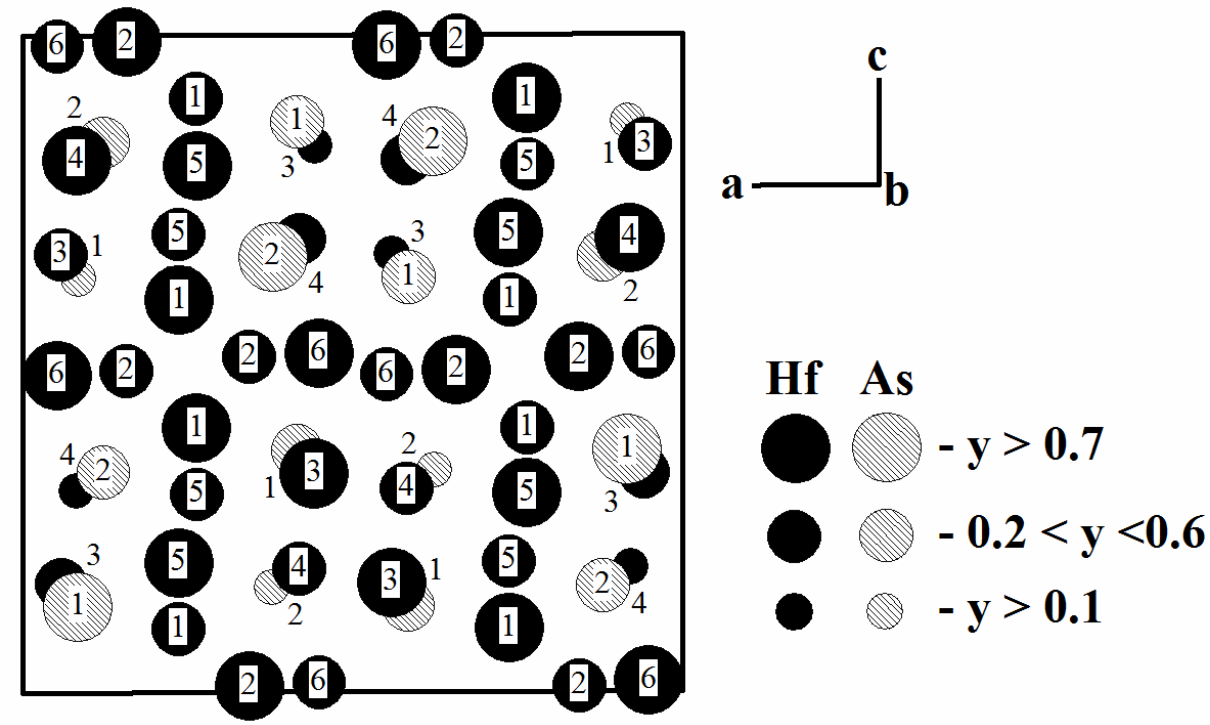


**Fig. 29. The unit cell of $Hf_3As$ – view in [0$\bar{1}$0] direction. The numbers describe the atoms on the given atom position (see Appendix A.7).**

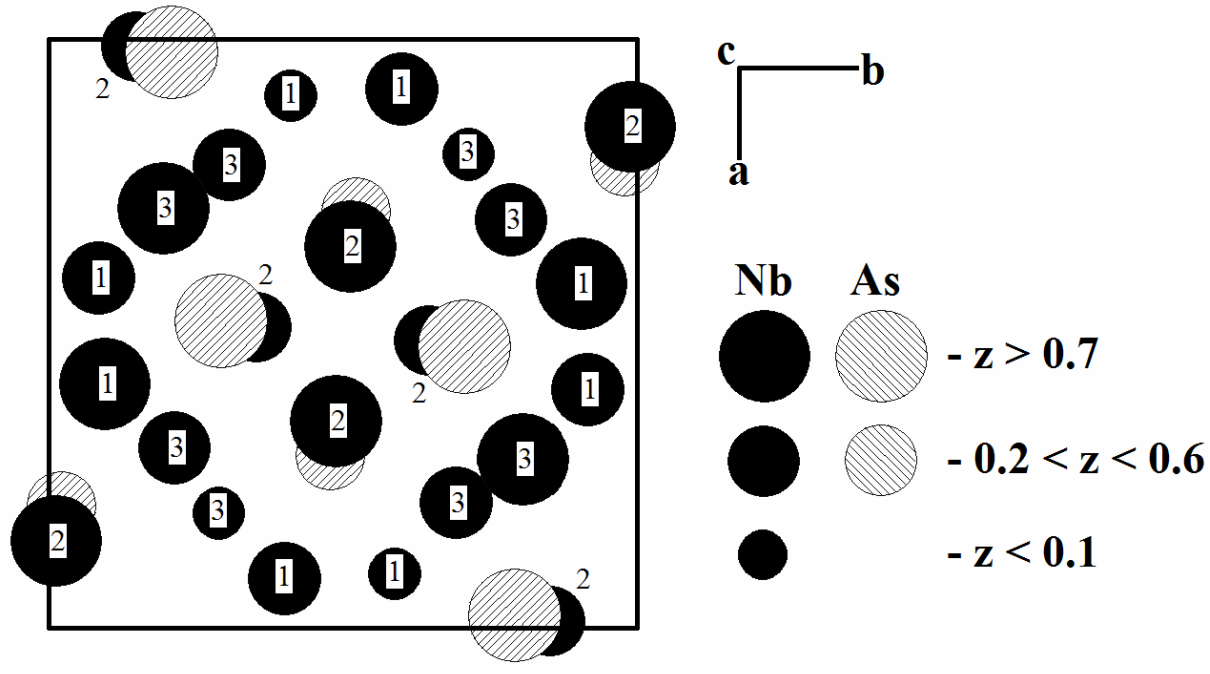


**Fig. 30. The unit cell of $Nb_3As$ – view in [00$\bar{1}$] direction. The numbers describe the atoms on the given atom position (see Appendix A.7).**

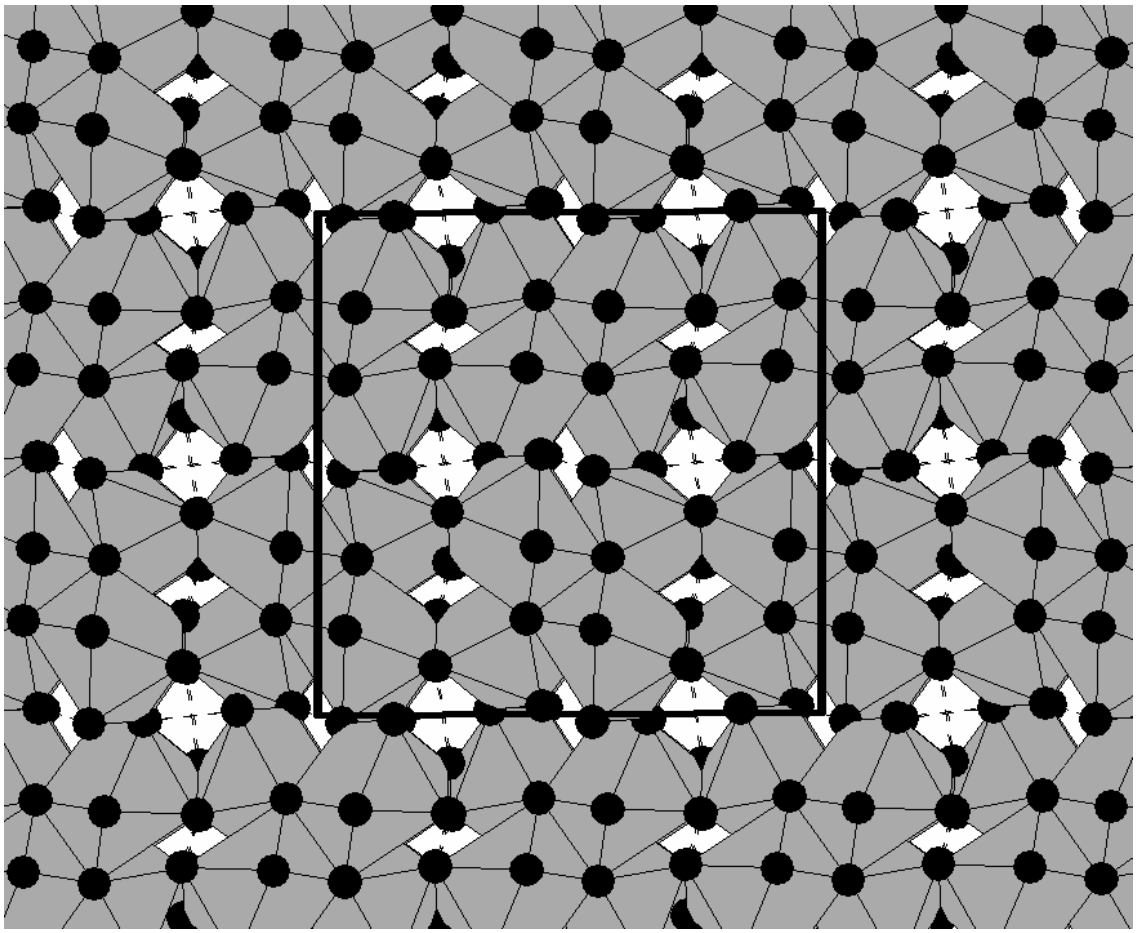

**Fig. 31. The unit cell of $Hf_3As$ shown as a combination of distorted square antiprisms – view in [$0\bar{1}0$] direction.**

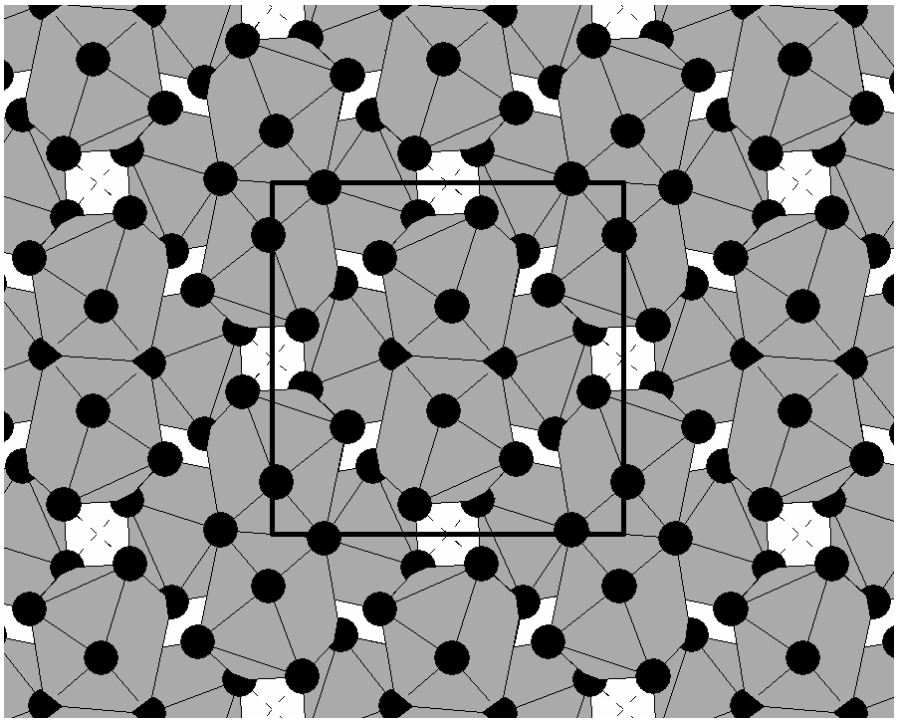

**Fig. 32.The unit cell of $Nb_3As$ shown as a combination of distorted square antiprisms– view in [$00\bar{1}$] direction**

### 2.4.2 Germanides - $Hf_5Ge_4$ (44.4 at.% Ge, Appendix B)

The crystal structure of $Hf_5Ge_4$ (*oP*36, [50]) is depicted in Fig. 33. The structure can be described with germanium atoms forming an octahedron around the Hf1 atoms, whereby every face of the octahedron is capped by the additional hafnium atoms (Hf2 and Hf3) - as it was done in ref. [82]. But it is also possible to consider the structure with regard to the coordination polyhedra of germanium atoms (Fig. 34). It is possible then to distinguish the bcc fragments with Hf1 atoms in the centre with eight nearest metal neighbours (4xHf2, 4xHf3) within 3.09 - 3.37 Å. Each bcc unit is linked to two others by sharing a common edge. Additionally, every face of a bcc unit is capped by germanium atoms (2xGe1, 2xGe2, 2xGe3). Ge1 and Ge2 atoms are surrounded by hafnium atoms in form of the trigonal prisms, so that every bcc unit is connected with four trigonal prisms with a common face. Single Ge1 and Ge2 prisms are sharing a common face, forming rhombic prisms with two germanium atoms inside. Every rhombic prism is sharing a common edge with four other perpendicularly aligned rhombic prisms. The bcc units with the Ge1 and Ge2 prisms form layers in the (010) plane. The layers are stacked alternately in *ABABAB…* manner, where layer *B* is translated by approximately 2.54 Å (~0.362*a*) in $[\bar{1}00]$ direction related to layer *A* (*A* describes the layer with Hf1 atoms on y = 0.25). Ge3 atoms are placed between the prism layers. The trigonal prisms around germanium resemble the ones around arsenic in the previously described arsenide structures.

Richter et al. substituted hafnium with niobium in this phase and observed the preferred site occupations for niobium atoms [82] (Table 18). The hafnium atoms are substituted on the consecutive sites in an almost stepwise manner, starting with the metal sites in the center of the bcc unit. This behaviour can be justified by the smaller atomic radius of niobium compared to hafnium, as the order of the substituted sites is the same as the order of increasing metal sites volumes (represented by Wigner-Seitz cells [88]). An additional reasoning was based on the atomic orbital population analysis obtained with EHTB-method (Extended Hückel tight-binding) [89], because niobium (having one more valence electron than hafnium) was found to prefer the sites with the larger orbital population numbers. Based on the experimental values, a thermodynamic model was proposed for the quantitative modelling of the site fractions.

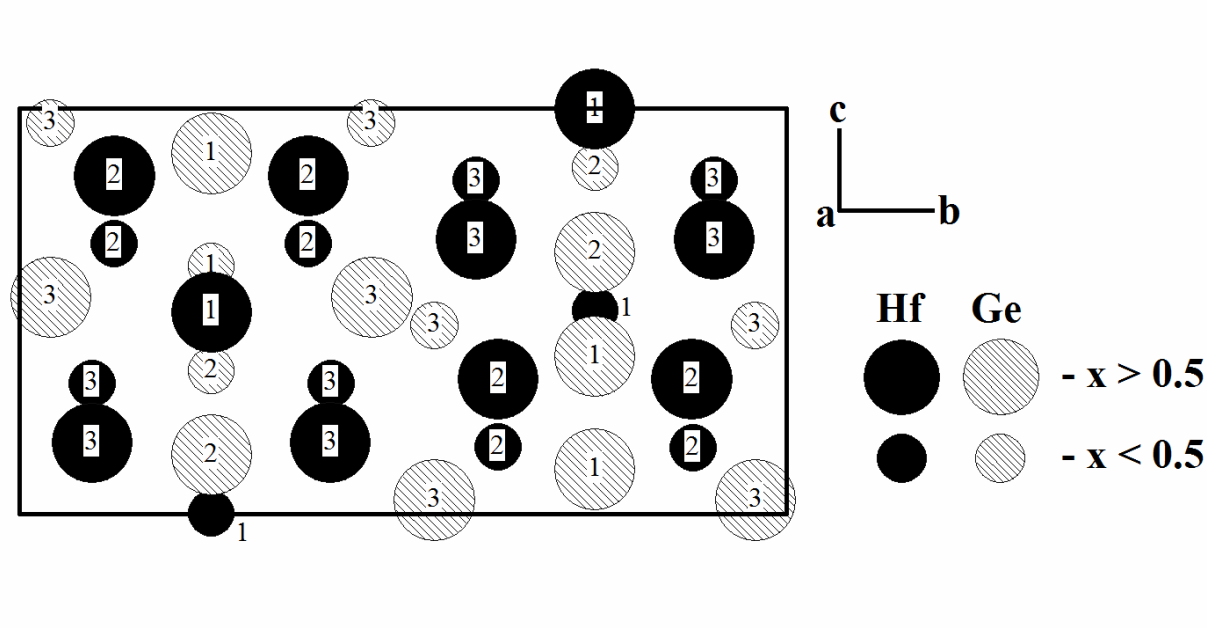


**Fig. 33. The unit cell of $Hf_5Ge_4$ – view in [$\bar{1}$00] direction. The numbers describe the atoms on the given atom position (see Appendix B).**

**Table 18. Individual site fractions for $Hf_{5-x}Nb_xGe_4$ obtained by powder diffraction [82].**

| Nominal composition | Refined niobium site fractions $y_{Nb}$ | | |
|---|---|---|---|
| | Hf1 | Hf2 | Hf3 |
| $Hf_{4.45}Nb_{0.55}Ge_4$ | 0.424(8) | 0.063(5) | 0.00 |
| $Hf_{3.36}Nb_{0.55}Ge_4$ | 0.846(8) | 0.376(5) | 0.00 |
| $Hf_{4.45}Nb_{0.55}Ge_4$ | 0.942(6) | 0.814(4) | 0.076(5) |
| $Hf_{4.45}Nb_{0.55}Ge_4$ | 1.00 | 1.00 | 0.322(9) |

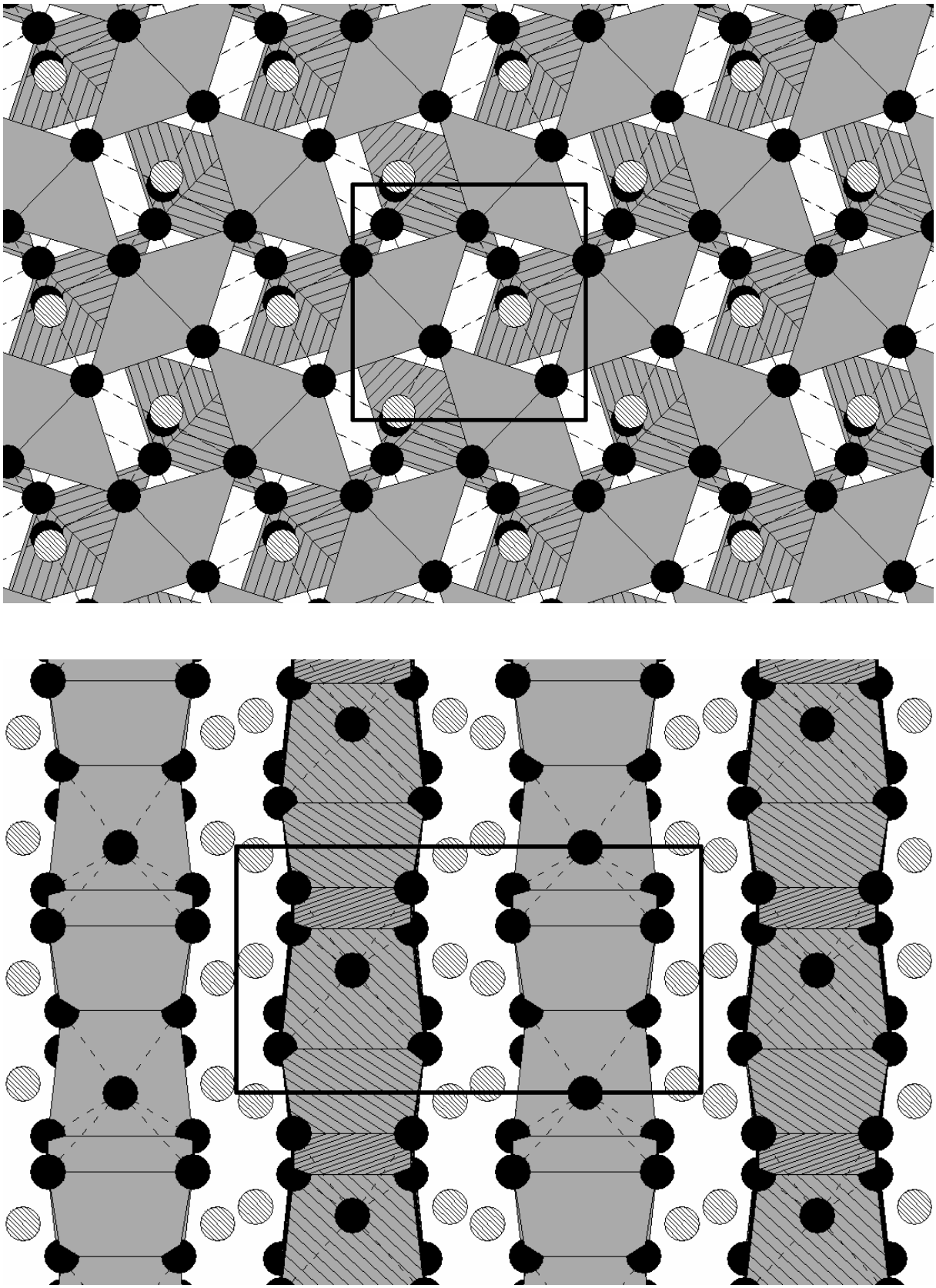

**Fig. 34. The structure of $Hf_5Ge_4$ shown as *ABABAB…* stacking of two layers of trigonal prisms (*A* – dashed shape, *B* – plain shape). The prisms are formed by Hf atoms around Ge1 and Ge2 atoms. Ge3 atoms are placed between the adjacent layers. View along [0$\bar{1}$0] (top) and [$\bar{1}$00] (bottom) directions.**

### 2.4.3 Gallides - HfGa (50 at.% Ga, Appendix C, [67])

The structure of HfGa (*oP*24) is depicted in Fig. 35. It can be described in a simple way as an arrangement of the distorted octahedra of two kinds (Fig. 36). The first one is formed by gallium atoms around Hf1 atoms, while the second one is built from hafnium atoms around Ga1. The octahedra are linked along the short axis (*c*) direction by sharing a common face and in the other directions by sharing a common edge - only octahedra of the same kind are linked. The connected polyhedra form wavy layers in the (100) plane and are alternately stacked *ABABAB*… (*A* – octahedra centred on gallium, *B* – octahedra centred on hafnium). This octahedra motif is similar to the one found in the $Hf_5Ga_3$ structure ($Mn_5Si_3$-type, [66]), where octahedra around Hf1 atoms are present (Fig. 37).

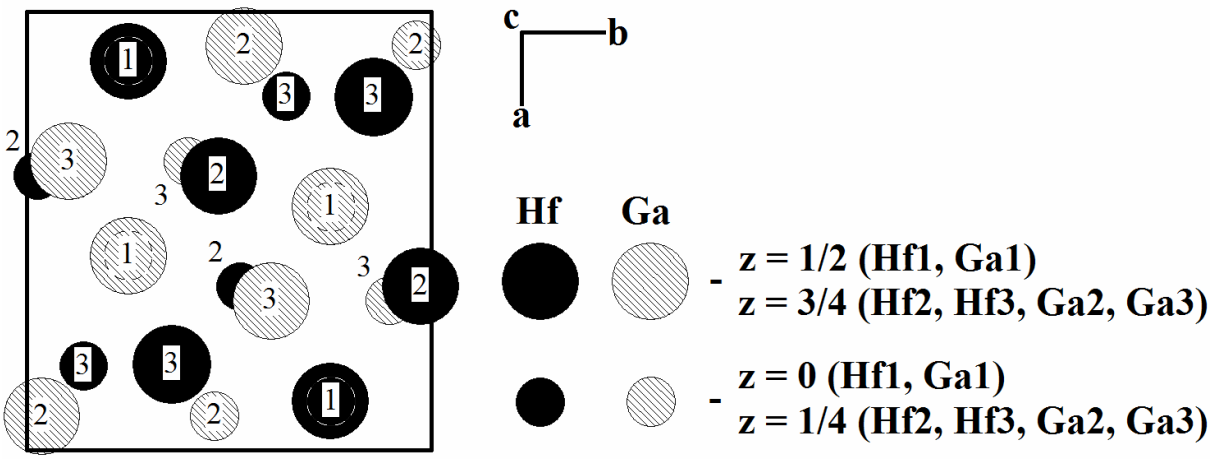


**Fig. 35. The unit cell of HfGa – view in [00$\bar{1}$] direction. The numbers describe the atoms on the given atom position (see Appendix C).**

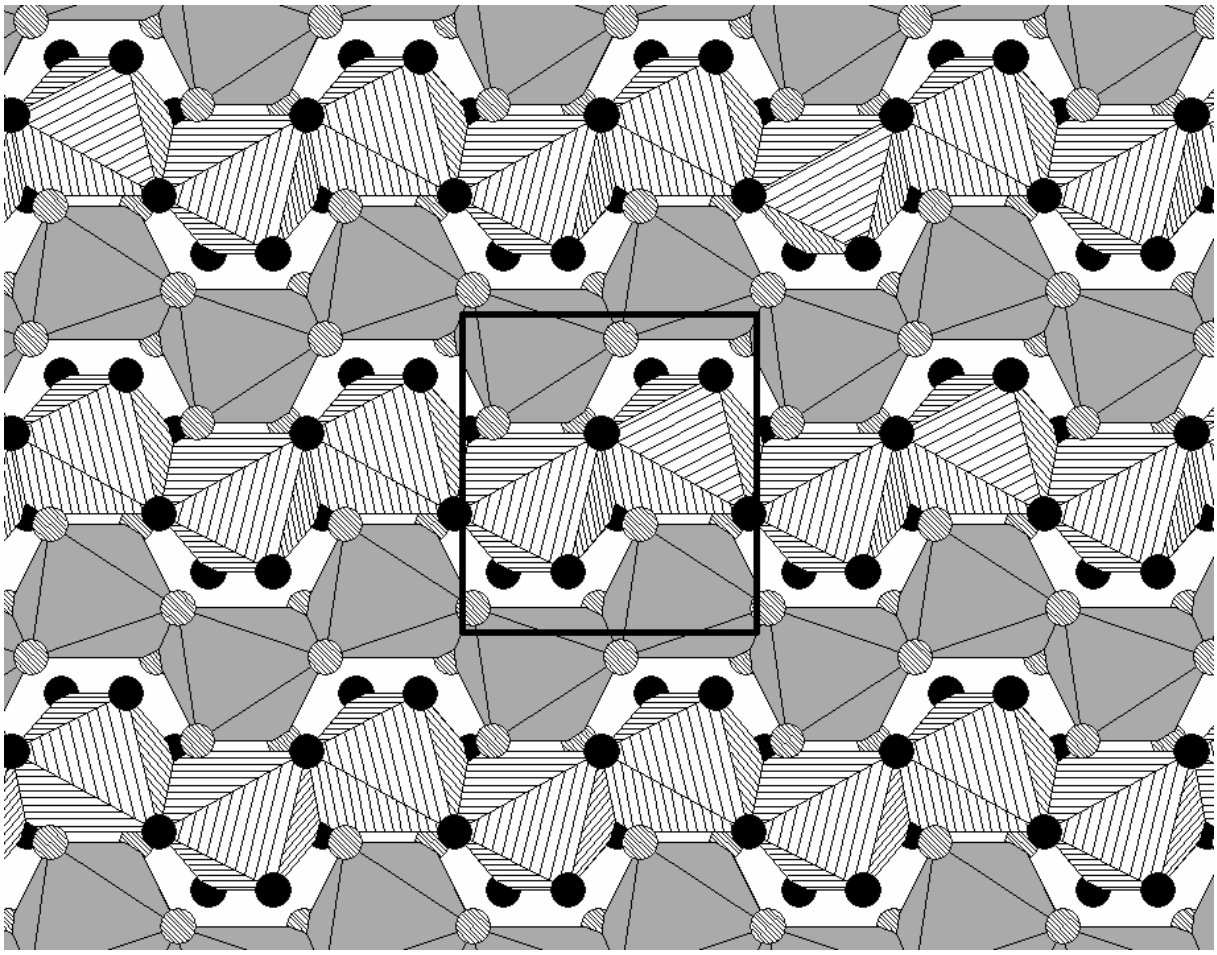

**Fig. 36. The structure of HfGa shown as an alternate stacking of octahedra layers - view along [00$\bar{1}$] direction. The octahedra are centred on Hf1 (plain shape) or Ga1 (dashed shape) atoms.**

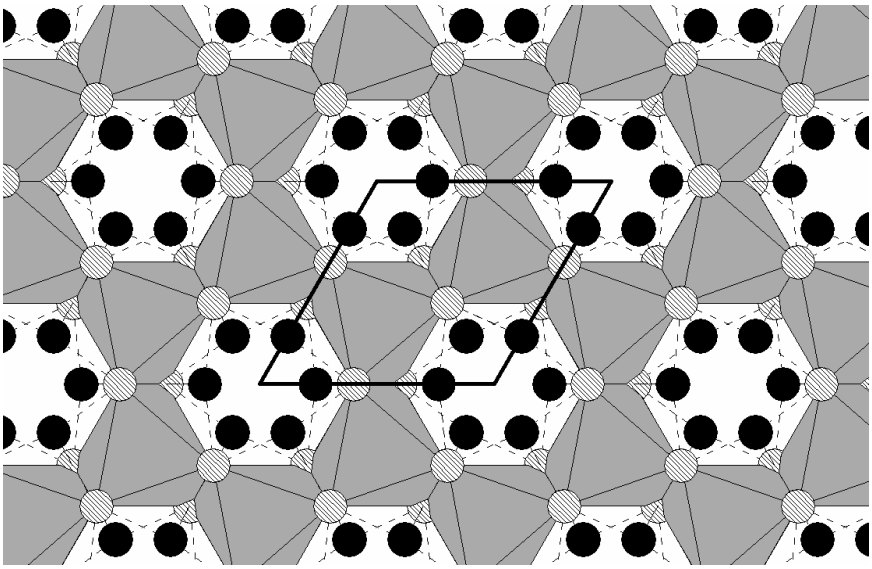

**Fig. 37. Alternate stacking of octahedra layers in $Hf_5Ga_3$ (*hP*24). The ocathedra are centred on Hf1 atoms.**

## 2.5 Summary of the literature review

The experimental work done on these three ternary systems allowed to create the phase diagrams only for the germanides and gallides. All phases present in these two systems (except $NbGa_4$) are reported to be stable also at room temperature. In case of the arsenides, the only stable phases in the low temperature range (i.e. below 1000°C) are the di- and monoarsenides, while the variety of the other metal-rich structures was obtained under high temperature conditions. This can be a result of their entropic stabilisation but, on the other hand, it is possible that due to the slow kinetics at low temperatures, the formation of the phases could not be observed at all. No work on the ternary Hf-Nb-As system is known, but the experiments done on the other systems of the ternary arsenides of the transition metals [22] may suggest the presence of a ternary phase with $Co_2Si$ structure. Although no ternary phases were found in the gallium and germanium systems of these metals, the extended solubility in the binary structures may be connected with the preferred site occupations of the substituting metal atoms, as it was shown by Richter et al. in case of the $Hf_{5-x}Nb_xGe_4$ system [82]. In the Hf-Nb-Ga system, the binary phases with an extended solubility are: $Hf_5Ga_3$, HfGa, $Nb_5Ga_3$ and $Nb_5Ga_4$. Of these four phases, only HfGa has three metal sites (the others have only two) and as such, it should be an interesting subject of an investigation of possible site preferences in the ternary field.

Previous literature reports on the synthesis clearly show that the preparation of the compounds is difficult. Due to the high melting points of hafnium and niobium, arc-melting step must be included in the synthesis of the samples. In all three systems mass losses were noticed during this step and were assumed to be connected with the evaporation of Ga, Ge or As, as these melt and vaporise before reacting with the metals. In case of the germanides and gallides, the mass loss was simply compensated by germanium or gallium addition. In case of arsenic which does not melt but sublimes at about 615°C, the use of elemental arsenic as an input material is not feasible. Instead, the di- or monoarsenides prepared by low-temperature synthesis (just over the sublimation point of arsenic) could be used as an input for the arc-melting which reduced the evaporation of this component.

As discussed above, the metal-rich arsenides of hafnium and niobium can usually be well described (in a simplified view) by the arrangement of metal trigonal prisms centred on the arsenic atom (except of the $M_3As$ compounds). The fragments consisting of metal atoms arranged in body centred cubic units can also be recognized in the majority of the arsenide

structures (exceptions are the MAs, $M_3As$ and $Hf_3As_2$ phases) and $Hf_5Ge_4$. Any new ternary phase in this system is very likely to exhibit these features as well.

As shown on the example of $Hf_{5-x}Nb_xGe_4$ [82], the order of the substituted places can be predicted by a volume analysis and by electron band structure calculation. For the quantitative description of the site fractions a thermodynamic model can be used.

# 3. Methods

## 3.1. Experimental methods

### 3.1.1 Preparation of the samples

The following substances were used for sample preparation:

- Hafnium pieces (Alfa Aesar), containing 2%Zr; the content of a metal basis (Hf+Zr) is 99.9%
- Niobium foil (Advent Research Materials Ltd.) with 0.5 mm thickness, purity of 99.9% Nb
- Hafnium powder (Alfa Aesar) Puratronic, containing 2-3.5% Zr; the content of a metal basis (Hf+Zr) is 99.6%
- Niobium powder (Alfa Aesar) Puratronic, with a content of Ta < 500 ppm; the content of a metal basis (Nb+Ta) was 99.99%
- Arsenic polycrystalline lumps (Johnson Matthey) Puratronic with 99.9999% purity
- Gallium ingot (Alfa Aesar), purity of 99.999% Ga

The metal powders and arsenic lumps were stored in the glove-box, avoiding a longer exposition to air. In order to remove any arsenic oxides from the metal surface, arsenic lumps were heated with the hydrogen flame in a silica tube under dynamic vacuum ($As_2O_3$ sublimes under 200°C).

In case of the samples in the Hf-Nb-As system, the first step was to prepare powders of HfAs and NbAs. This was achieved by sealing the relevant amounts of metal powders and arsenic lumps (aiming for 10 grams of the monoarsenide) in a silica tube, slow heating to 900°C (reached in 2 days) and annealing at this temperature for the next 3 days. The obtained powder was heated again with the hydrogen flame under dynamic vacuum to decompose any diarsenides [36]. However, the X-ray patterns of these products still showed some weak peaks of the diarsenides, but no trace of the oxide or silicide phases was observed, thus showing no reaction of metal with silica. Calculated amounts of the prepared monoarsenides and metal powders were weighed (±0.2 mg) to a sample mass of 1000 mg. All mixtures were mixed and pressed with the hydraulic press in a steel container with 15 kN, obtaining a pellet with a diameter of 5 mm. The pellets were melted in the arc-furnace under an argon atmosphere and

annealed at 1400°C for 3 days. Afterwards, the samples were analysed by X-ray powder diffraction, optical microscopy and EPMA methods.

In case of the Hf-Nb-Ga system, the procedure was slightly different. The metal pieces were weighed to a sample mass of 1000 mg (±0.2 mg) and subsequently melted three times in the arc-furnace, turning them on the other side after each melting. This was done in order to homogenise the sample. The observed mass losses (max. 50 mg) were assumed to be gallium and were replenished by the addition of $NbGa_3$ to the ground sample. The mixtures were pressed with a hydraulic press with 10 kN and the obtained pellets were annealed at 1200°C for 3 days. Next, the samples were analysed by X-ray powder diffraction. $NbGa_3$ was obtained by the synthesis from niobium and gallium sealed in an evacuated silica tube and annealed at 700°C for one week.

For melting the samples, an MAM-1 (Edmund Bühler Gmbh&Co.) arc-furnace was used. The samples were put on a water cooled copper plate. The chamber was flushed twice with argon (5N) and the final inert gas pressure was set at 0.5 atm. Before the melting of the sample, a piece of zirconium getter was melted in order to remove any impurities from the gas phase. The temperature could be regulated roughly by regulating the current intensity. Remarkably, during the melting of the arsenides, a thin black layer of arsenic evaporated from the sample condensed on the interior wall of the melting chamber which complicated the observation of the process. Therefore, the samples containing more than 30 at.% As were melted only once. The sample composition was estimated on the basis of the mass losses which were assumed to be evaporated arsenic.

Heat treatment was done in a resistance furnace “LORA-1800-32-600-1” (HTM-Reetz GmbH). The heating element was molybdenum wire wound around an alumina-ceramic tube in which the samples were placed. Both the heating element and the alumina tube were flushed with argon during the whole period of the heat treatment, as well as 12 hours before the process in order to remove the air. The temperature was measured with a thermocouple of type B (Pt-30%Rh vs. Pt-6%Rh). After the annealing phase, the furnace was tilted to a vertical position and the samples fell into the next chamber with water-cooled walls in order to quench them. Before annealing, every sample was sealed into the tantalum crucible (made by deep drawing of a tantalum sheet) in the arc-furnace under an argon atmosphere. The volume of the crucible was about 1 ccm. After annealing, the crucibles were opened with a metal saw.

### 3.1.2 Sample analysis

#### 3.1.2.1 X-ray diffraction (XRD) [90]

For the analysis of the crystallographic structure of the prepared samples, X-ray diffraction experiments were performed. In general, X-rays are electromagnetic waves with a wavelength within the range $10^{-13}$ - $10^{-8}$ m. The use of wavelengths comparable with the range of the interatomic distances (1 – 3 Å, 1Å = $10^{-10}$ m) for the irradiation on the crystalline substance results in a diffraction pattern. In other words, the crystal lattice of the irradiated substance is a diffraction grating for the X-rays. An analysis of the obtained pattern may give some information about the grating, i.e. about the crystal structure. The information about the distances between the crystallographic planes (and thus about the distances between the lattice points) can be deduced from the reflection angles of the beam. The dependence is described by the Bragg equation:

$$n * \lambda = 2 * d * \sin\theta$$

n – integer number (n=1,2,3,…)
λ – wavelength
d – distance between the crystallographic planes
θ – reflection angle

One can observe very often that some reflections are absent, although they were expected to be observed. This is the result of the symmetry operations within the unit cell. These operations can be combined in 230 ways and an analysis of the absent reflections yields information about the space group present in the investigated phase.

Every lattice point represents one or more atoms, so that a crystal lattice can be considered as a sum of single atom lattices. Thus, the wave diffracted on a crystal lattice point can be considered as a sum of the waves diffracted on the single atom lattices. The amplitude of the wave diffracted on the crystal lattice point is then the sum of the amplitudes of the diffracted component waves. Thus the wave reflected with various angles will have different intensities, as the orientation of the single atom lattices varies with the angle. This is expressed by:

$$I_{hkl} \sim K * F_{hkl}^2 * H * L * A * E$$

where:

$$F_{hkl} = \left( \sum_{j=1}^{N} S_j * N_j * f_j * \exp\left( 2\pi i \left( hx_j + ky_j + lz_j \right) - B_j * \frac{\sin^2 \theta}{\lambda^2} \right) \right)$$

$I_{hkl}$ – intensity of the wave reflected by the crystallographic plane (*hkl*)

$K$ – scale factor

$H$ – plane multiplicity factor

$L$ – Lorentz-Polarisation factor

$A$ – absorption coefficient

$E$ – extinction coefficient

$F_{hkl}$ – structure factor for a given plane (*hkl*)

$S_j$ – site fraction of atom *j*

$N_j$ – position multiplicity of the site occupied by atom *j*

$f_j$ – atomic scattering factor of atom *j*

$B_j$ – Temperature factor of atom *j*

$x_j$, $y_j$, $z_j$ – position coordinates of atom *j*

Hence, the analysis of the reflection intensities yields information about the atom arrangement in the unit cell. However, it is impossible to determine directly $F_{hkl}$ from the intensity measurements, as this is a complex number. Still, the intensity allows calculation of the modulus of the structure factor $|F_{hkl}|$.

In principle, structure investigation with X-rays can be performed on a single crystal or on powder, both obtained from the sample. In the first case, the single crystal of a given phase is put on an amorphous capillary and rotated, so that different planes can fulfil the Bragg condition for diffraction. The reflected waves form separated spots on the reading medium (e.g. photographic paper, scintillation counter), one for each crystallographic plane and the intensity of each spot is measured. The easiest method to identify the structure is to calculate a pattern of a structure model and to compare it with the experimental diffractogram. Another way is to reproduce the electron density $\rho(XYZ)$ within the unit cell. This is represented as a Fourier series of the structure factors $F_{hkl}$:

$$\rho(XYZ) = \frac{1}{V} \sum_{h=-\infty}^{+\infty} \sum_{k=-\infty}^{+\infty} \sum_{l=-\infty}^{+\infty} F_{hkl} \exp\left( 2\pi i \left( hX + kY + lZ \right) \right)$$

with:

X, Y, Z – coordinates of a given point in the unit cell

V – volume of the unit cell

Thus, the electron density within the unit cell can be deduced on the basis of an intensity measurement, and this approach is known as a *direct method*. The structure is then solved by placing the atoms on the points with the largest electron density. Any information on the atom neighbours or the interatomic distances can shorten the determination process. Still, this method is not straightforward, as the intensity measurement yields information about $|F_{hkl}|$ and not $F_{hkl}$ itself. Based on the information obtained from the direct methods, the structure model is constructed and the calculated intensities are compared with the measured ones in the subsequent refinement.

It might be difficult to find a crystal suitable for the measurement. A piece of a sample containing more than one single crystal cannot be used for a successful structure determination. The crystal should be of about 50 μm size (in the case where heavy atoms are present). If the crystal is too large, the majority of X-rays is absorbed and do not leave the crystal. On the other hand, the separation of the smaller single crystal is a difficult task. The phase equilibria determine the sample microstructure and thus influence the feasibility of a single crystal investigation of the phases. For example, it might be very difficult to find suitable crystals of a phase produced by a peritectic reaction with an adjacent narrow two-phase field.

The structure investigation with XRD can be also performed on polycrystalline samples like powders. The powder is then placed on a platform carrier and X-rays are reflected or transmitted through the sample. In both cases, X-rays meet the single crystals oriented in such a way, that the Bragg condition is met for one crystallographic plane and diffraction occurs. The diffracted waves can be read simultaneously for all angles (planes) or step-by-step in a defined $\theta$ range. Depending on the reading medium alignment, the results are depicted in the form of rings or stripes at the position appropriate for a given angle. This results in a possible overlapping of neighbouring peaks which makes the proper indexing more difficult. If more than one phase is present in the sample, the only way to identify the any structure is by comparing the experimental diffractogram with the patterns of the introduced structure models. The next step is to refine the structure parameters of the matching model. This can be done by applying the *Rietveld method* in which the modelled intensity profile is adjusted in

order to give the best fit with the measured data. The intensity $y$ for a given angle $\theta$ is represented by:

$$y_\theta = K\left(\sum_{hkl} L * \left|F_{hkl}\right|^2 * \Phi(2*\theta - 2*\theta_{hkl}) * P_{hkl} * H * A * E\right) + y_{0\theta}$$

$\Phi(2\theta\text{-}2\theta_{hkl})$ – profile function
$P_{hkl}$ – preferred orientation factor
$y_{0\theta}$ – intensity measured for the background only

In both cases (single crystal or powder sample), the modelled parameter (structure factor $F_{hkl}$ or intensity, respectively) is adjusted by varying the component parameters, which is performed by a computer program. The fit is done by applying the least squares method, in which the calculated and measured intensities are compared. For powder samples, the goodness of fit is measured by a parameter $S_y$:

$$S_y = \sum_\theta w_\theta \left(y_{m\theta} - y_{c\theta}\right)^2$$

$w_\theta$ – weight factor
$y_{m\theta}$ – measured intensity at angle $\theta$
$y_{c\theta}$ – calculated intensity at angle $\theta$

For single crystal, structure factors $F_{hkl}$ are compared. The lower the value of $S_y$ gets, the better the fit is. Except of the $S_y$ parameter, there are also other parameters describing the agreement between the model and the analysed data. For single crystal measurements the following values are defined:

$$R = \frac{\sum_i \left|\left|F_{mi}\right| - \left|F_{ci}\right|\right|}{\sum_i \left|F_{mi}\right|}$$

$$R_w = \frac{\sum_i w_i \left|\left|F_{mi}\right|^2 - \left|F_{ci}\right|^2\right|}{\sum_i w_i \left|F_{mi}\right|^2}$$

$i$ – $hkl$ values for a given plane

$w_i$ – weight factor

$F_{mi}$ – measured structure factor

$F_{ci}$ – calculated structure factor

For powder measurements the applied parameters are:

$$R_p = \sqrt{\frac{\sum_{\theta} |y_{m\theta} - y_{c\theta}|}{\sum_{\theta} |y_{m\theta} - y_{0\theta}|}}$$ - "R-pattern" with background correction

$$R_{wp} = \sqrt{\frac{\sum_{\theta} w_{\theta} (y_{m\theta} - y_{c\theta})^2}{\sum_{\theta} w_{\theta} (y_{m\theta} - y_{0\theta})^2}}$$ - "R-weighted pattern" with background correction

$$R_B = \frac{\sum_{i} |I_{mi} - I_{ci}|}{\sum_{i} I_{mi}}$$ - "R-Bragg"

$i$ – $hkl$ values for a given plane

$I_{mi}$ – measured intensity for plane $i$

$I_{ci}$ – calculated intensity for plane $i$

In both ways (single crystal or powder sample), the structure information is obtained by constructing a structure model and comparing it with the observed intensities. In case of a phase with a new structure type, this information is usually gained from a single crystal experiment. In polycrystalline samples, the selection of the model is not easy, and therefore powder experiments are usually used for the identification of known phases in the investigated sample. It is also possible to compare an unknown pattern with models based on existing structure types. More information about the atom coordinates and their site fractions can be deduced if the sample dominantly contains the phase in question and with good intensity measurement data as a function of the diffraction angle.

As can be seen, besides the structure data described by $F_{hkl}$, several other parameters must also be established in order to model the crystal structure properly. The temperature factor $B_j$

describes the dislocations oscillations of the atoms in the structure. It can be also expressed as *U*, whereby the following relation holds:

$$B = 8 * \pi^2 * U$$

with both of these parameters being tensors. Plane multiplicity factor *H* describes the number of the equivalent planes subjected to the same Bragg condition. For example in a cubic cell, the planes (123), (213) and $(\bar{1}23)$ diffract the X-rays with the same $\theta$, thus their contribution is added (for the cubic cell *H* is 48). The Lorentz-polarisation factor *L* describes the divergence of the incoming X-ray and the weakening of the wave polarised after the diffraction, being dependent on $\theta$. A part of the X-ray energy can be absorbed by the atoms in the crystal and the contribution of this effect is described by the absorption coefficient *A*. It can also happen that a part of the once diffracted wave is reflected again by the other plane so that the observed intensity gets weaker – this process is included in the model by the extinction coefficient *E*. In case of polycrystalline samples, additional factors must be considered. Although it is expected that the powder grains are randomly oriented, it may happen that the crystallites tend to align themselves with a preferred exposition of a specific plane, so that some of the measured intensities are higher than the model assumes. This is described by a preferred orientation factor $P_{hkl.}$ A single diffraction peak is not recorded as a sharp line placed on a special θ value, but is rather distributed around this value, due to the material properties (crystallite size, degree of crystallisation, microstrain) and measuring instrument geometry. The intensity profile can be described with a profile function $\Phi(2\theta - 2\theta_{hkl})$. Except of the intensity of the diffracted waves, some residual background intensity is measured and this is represented by $y_{0\theta}$.

In this work, the annealed samples were powdered in a tungsten carbide mortar. The phases contained in the powders were first examined with a Guinier imaging plate camera, model *670* (Huber). This method required placing the powder on a cellophane foil with silicon vacuum-grease used as glue. The radiation used was $CuK\alpha_1$ obtained with a crystal mirror monochromator. The exposure times were between 2 and 3 hours, depending on the observed intensity. The structure models were taken from literature data on binary gallides and arsenides of hafnium and niobium (see Table 6, 7, 12 and 13 for the reference list). In this step, the phases in the sample were either identified (i.e. found identical or isostructural with known type) or classified as unknown.

For the measurement of the site occupations in the known phases, the powders were additionally milled in a ball mill and examined with the *D8 Advance* diffractometer (Bruker AXS) with Bragg-Brentano focusing and θ/2θ geometry (immobile X-ray source) at room temperature. The samples were placed on a silicon single crystal carrier. CuKα radiation obtained with nickel filter was used and the intensities were read with a *LynxEye 1D*-detector (Bruker AXS). The data was collected every 0.01° in 2$\theta$ range of 10-120°; for every 2$\theta$ angle, the measurement took 0.6 s.

If a new phase was found in the sample, it was attempted to separate a single crystal in order to determine the structure. The single crystals were separated under an optical microscope, placed on the tip of a glass capillary with the use of the nail polish and examined on a *Nonius-Kappa-CCD* four-circle geometry diffractometer. Mo-Kα radiation obtained with graphite monochromator was used. The exposure times were about 18 hours and the crystal was held at room temperature. The observed intensities were corrected for Lorentz-polarisation and absorption effects.

Experimental data were analysed with the aid of computer programs. The data collected during the powder diffraction experiments were evaluated with the *TOPAS* program [91] which allowed the construction of structure models and compared them with the observed intensities. If the sample quality was good enough, the Rietveld refinement was performed with this tool. In this case, the profile function $\Phi(2\theta-2\theta_{hkl})$ was obtained by a convolution model [92], where the instrument (e.g. dimensions, slit parameters, divergence angle) and material parameters are taken as the fundamental parameters. The preferred orientation factor $P_{hkl}$ was represented with a symmetrised harmonics expansion [93]. The intensity profile of the background $y_{0\theta}$ was represented by Chebyshev polynomials with up to six terms.

The single crystal data were analysed first with the *DENZO* program [94] in which the observed reflexes were indexed. On the basis of the indexing, the crystallographic system and the lattice parameters were evaluated. The data were further analysed with the *SHELXL* program [95] in which the structure was solved with the use of the direct methods.

#### 3.1.2.2 Optical microscopy

The surface of the sample's cross-section was analysed with an optical microscope in order to investigate the homogeneity, the number of phases and the approximate size of the grains. About a quarter of the bulk sample was taken for embedding in a mixture of copper

powder and resin which was done in a hydraulic press (15kN) with a heated chamber (180°C). The whole block with up to 6 samples was ground and polished (with $Al_2O_3$ in water suspension) on a *Metaserv 2000* machine (Buehler). The samples were investigated with an *Axiotech 100* (Zeiss) microscope in the bright and dark field, as well as with polarised light. In the bright field, only the plain surface reflects the light, while in the dark field only the scratches, holes and cracks do so. Using polarised light, number of the phases can be identified based on their different polarising behaviour. This feature is also very helpful for a grain size determination.

#### 3.1.2.3 Electron Probe Micro-Analysis [96]

The blocks with samples used for optical microscopy were also analysed by EPMA in order to obtain information about the chemical composition of the phases present in the samples. In this method, the electron beam of an Electron Microscope is striking the sample surface. A variety of possible interactions yield information about the sample. The first interaction is the scattering of the electrons by the atoms in the sample. The intensity of the back-scattered electrons (BSE) is processed to produce an image, showing the microstructure of the sample, similar to the optical microscopy. The energy of the incoming electrons can also be transferred to one of the inner-shell electrons in the atoms of the sample, so that this is ejected and the atom remains in an excited state with a vacancy in the inner-shell. The excited state is an unstable one, and electrons from outer-shells move to the inner orbital in order to fill the vacancy. This transition can occur in subsequent steps, during which the electrons jump from one quantum state to the other, releasing the appropriate amounts of energy emitted in the form of X-rays. The energy (and thus the wavelength) of the emitted X-ray is characteristic for every element and can thus be used for a qualitative analysis of the piece of sample on which the electron beam is focused. If the sample contains more than one element (which is usual the case) the characteristic intensities can be compared and used for a quantitative analysis of this piece.

In this work, the measurements were done on a *SX100 EPMA* (Cameca) device. The electrons were obtained by the thermionic emission from a tungsten filament. The acceleration voltage used in the measurement was 20 kV and the beam current was 20 nA. The X-rays emitted from the sample were analysed with the wavelength dispersive spectrometers (WDS) using the TAP (Thallium-Acid-Phthalate) and PET (Pentaerythritol)

crystal detectors. The intensities were measured for the characteristic wavelengths of the Hf(Mα), Nb(Lα) and As(Lβ) emission lines. The calibration of the spectrometer was performed with Hf, Nb and GaAs as standard materials. The measured intensities were refined with the ZAF matrix correction which considers the atom numbers of the elements (Z), the absorption (A) and the fluorescence effects (F). The sample composition was given in weight percent which was later recalculated to mole fractions. The back scattered electrons were used for the image creation of the analysed part of the sample (BSE images).

## 3.2. Theoretical calculations

### 3.2.1 Site volume analysis

In a first approximation, the atoms in the crystal unit cell can be represented as points with the position described by the atomic coordinates. The volume of the crystal can be partitioned into a set of polyhedra, where every polyhedron is centred on the point representing an atom with every other point within a given polyhedron being closer to its centre than to the centre of any other polyhedron (Fig. 38). These polyhedra are known in mathematics as Voronoi polyhedra, also known in solid state science as Wigner-Seitz cells. Their volume is taken as the volume of the given crystal site.

For partitioning and calculating the Wigner-Seitz cells in the crystal structures, the program “DIDO95” [97] was used. For every atom position, the program found the distance and the direction to every neighbour atom, calculated the perpendicular planes which were bisecting the lines connecting the atoms, found the intersection lines of different planes which became the vertices of the polyhedra and calculated the volume for every created polyhedron.

All volumes calculated in this work are given in Appendix E.

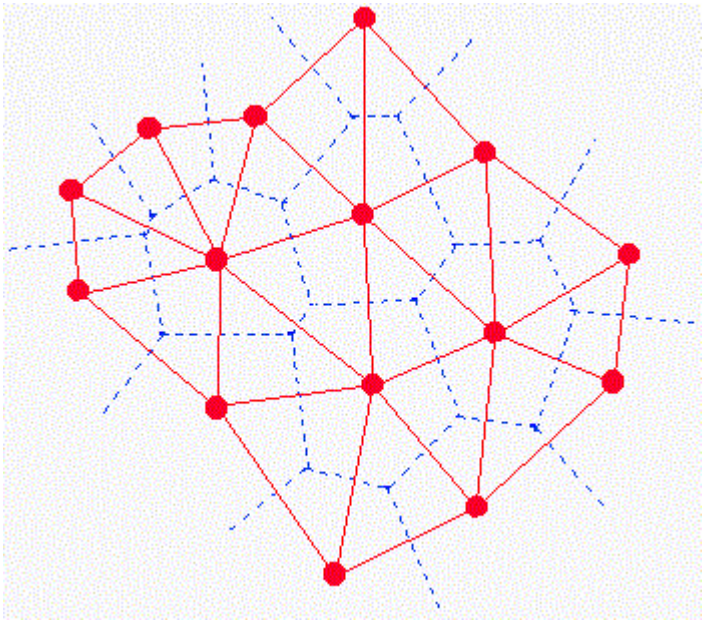

**Fig. 38. The concept of Voronoi polyhedra. Around every atom (represented by point), a polyhedron is created (marked with dashed lines). Each point within a given polyhedron is closer to the atom to which the polyhedron belongs than to any other atom.**

### 3.2.2 Bonding analysis based on Pauling Bond Order (PBO)

Observing the bond lengths in chemical compounds, Pauling suggested that there exists a correlation between the bond length and the number of electron pairs involved in a covalent bond (i.e. bond order) [98]. After analysing the coordination spheres of metals and the interatomic distances in the structures, the following quantitative relation was formulated (with the hypothetical assumption of localised bonds in this type of materials):

$$D(n) = D(1) - 0.6 * \log n$$

$n$ – bond order

$D(n)$ – Interatomic distance of the bond with order $n$

$D(1)$ – Interatomic distance of the bond with order 1 (i.e. single bond)

By making any assumptions about the contribution of the bonded atoms in terms of the number of electrons in the bonds, it is possible to calculate the number of the electrons involved in all bonds for each atom in the structure. In this work, it was assumed that for every bond, the bonded atoms contribute the same number of electrons, i.e. in a given bond

every atom contributes with the number of electrons equal to the bond order. Furthermore, it was assumed that every atom is bonded with its nearest neighbours, i.e. with the atoms constituting its first coordination sphere. With this procedure, it is possible to estimate the number of the bonding electrons for every crystal site when the structure data are given. In its original sense, the sum of Pauling Bond Orders for a given site should not exceed the number of the valence electrons of the element occupying this site but it is questionable if such a simple relation could accurately describe the complex relation of interatomic bonding with the crystal structure (especially in metallic systems). Nevertheless, previous attempts of relating this quantity with the site preferences in case of the metal sites were often successful (e.g. [18, 99]) and it was demonstrated that the sum of Pauling Bond Orders (PBO) scales with quantities (e.g. Mulliken orbital population [100]) derived from more sophisticated methods based on the wave functions description of the electron orbitals [101]. While the numbers themselves might not have a direct physical meaning, a comparison of these values might give information about the relative "electron affinity" of the different metal sites.

In this work, the sum of Pauling Bond Orders for various metal sites (further referred to as *PBO*) is calculated on the basis of the coordination polyhedra of the crystal sites obtained during the analysis of the Voronoi polyhedra (see chapter 3.2.1). All structure data were taken from the experimental results given in the next section. Additionally, the ratios of the electrons involved in the metal-metal bonding to the overall number of the bonding electrons are calculated for every metal site, in order to test the possible influence of the metallic bonds on the structure stabilisation [18]. All calculated PBOs are given in Appendix E.

### 3.2.3 Density Functional Theory calculations

In principle, by solving the Schrödinger equation:

$$\hat{H}\Psi = -\frac{\hbar^2}{2m}\nabla^2\Psi + V(r)\Psi = E\Psi$$

$\hat{H}$ - Hamilton operator

$\Psi$ – wave function

$\hbar$ - reduced Planck constant ($1.05457*10^{-34}$ J*s)

$m$ – mass

$V(r)$ – potential energy

$E$ – energy of the system

the ground state energy of the given crystal (the sum of the kinetic and potential energies of all the particles included) could be found, but this is a very complex task. In order to simplify this task, the motion of the nuclei is neglected (Born-Oppenheimer approximation) and some assumptions about the electron-electron interaction are used. Using such simplifications, and using the variational principle, the wave function for which the energy is minimal is found and the energy itself is calculated. The wave function is a combination of the wave functions of the component atoms.

The density functional theory (DFT) calculations are based on the Hohenberg-Kohn theorem [102], which states that the energy of a many-electron system is a functional of the electron density (more strictly – density probability) ρ of the system. Therefore, the knowledge of the density is as useful as the knowledge of the wavefunction. Thus finding the ground state density, allows finding the ground state energy of the system. The density can be determined using the Kohn-Sham method [103]. In this approach, the density is reproduced by the wave functions $\varphi_j$ describing fictive electrons which do not interact with each other (placed on *Kohn-Sham orbitals*). While these orbitals do not have any physical meaning, they can be used for the construction of the electron density $\rho$ in the usual way:

$$\rho(r) = \sum_j \left|\varphi_j(r)\right|^2$$

The energy dependence on the electron density is described by:

$$E_{Vext}[\rho] = T_0[\rho] + V_H[\rho] + V_{xc}[\rho] + V_{ext}[\rho]$$

$E_{Vext}$ – Energy of the system
$T_0$ – Kinetic energy of the non-interacting electrons
$V_H$ – Hartree potential energy
$V_{xc}$ – exchange – correlation energy
$V_{ext}$ – potential energy related to the nuclei

In the first approach, it is assumed that the electrons are not interacting with each other, thus the first term $T_0$ describes the kinetic energy of the non-interacting electrons.

$$T_0[\rho] = \sum_j \langle \varphi_j \mid -\frac{1}{2}\nabla_j^2 \mid \varphi_j \rangle$$

The potential energy of the electrons in the average electrostatic field of the other electrons is described by the Hartree potential energy $V_H$.

$$V_H[\rho] = \frac{1}{2}\iint \frac{\rho(r)\rho(r')}{|r-r'|} dr dr'$$

The term $V_{xc}$ describes the interaction of the electrons due to their spin number value. Additionally, it represents also the short-range Coulomb repulsion of the electrons so that it corrects the kinetic energy term $T_0$ in which no electron-electron interaction was assumed. A number of approximations were proposed in order to represent this contribution. In the calculations conducted in this work, the *generalized gradient approximation* (*GGA*) was used for this term which is the sum of the exchange part $V_x$ and the correlation part $V_c$. In this approach, the exchange term is given as:

$$V_x = \int \varepsilon_x(\rho) F(s) \rho(r) dr$$

where:

$\varepsilon_x(\rho)$ – exchange energy density
$s$ – scaled density gradient

The correlation term $V_c$ is given by:

$$V_c = \int \left[\varepsilon_c(r_s, \zeta) + H(r_s, \zeta, t)\right] \rho(r) dr$$

where:

$\varepsilon_c$ – correlation energy density
$r_s$ – effective radius of the electron (Seitz radius of the electron)
$\zeta$ – relative spin polarization
$t$ – dimensionless density gradient

More details on $\varepsilon_x$, $\varepsilon_c$, $F(s)$, $H(r_s, \zeta, t)$ are given in ref. [104]

The term $V_{ext}$ describes the potential energy of the electrons in the electrostatic field of the nuclei.

$$V_{ext} = \int \rho(r) v(r) dr$$

whereby:

$$v(r) = \sum_i -\frac{Z_i}{r_i}$$

In order to find the ground state density $\rho_0(r)$, we need to find the energy minimum, subject to the constraint: $\int \rho(r) dr = N$ i.e. the summation over the whole space should give the total number of the electrons. The energy minimum is found by:

$$\partial \left[ E(\rho(r)) - \mu \left( N - \int \rho(r) dr \right) \right] = 0$$

where:

$\mu$ – electronic chemical potential

The wave function $\varphi_j$ which reproduces $\rho_0$ is obtained by finding the one with the minimal energy $\varepsilon_j$. This is done by solving the equation:

$$\hat{h} \varphi_j = \varepsilon_j \varphi_j$$

where:

$$\hat{h} = \left[ -\frac{1}{2} \nabla^2 + v_{eff.} \right] = \left[ -\frac{1}{2} \nabla^2 + \int \frac{\rho(r')}{|r - r'|} dr' + \frac{\delta E_{xc}(\rho)}{\delta \rho(r)} + v(r) \right]$$

This set of equations (collected equations for every $\varphi_i$) is known as Kohn-Sham equations.

The single-electron wavefunction was constructed with the *PAW* (projector augumented wave) method [105, 106] in this work. In this method, the wavefunction is a combination of the plane wave set (pseudo wavefunction) and the local wavefunctions describing the electron behaviour near the atom nuclei. This combines the advantages of both the plane wave representation (performs well for the bonding region) and the pseudopotential method (simplifies the description of the region near atom nuclei). The set of the plane waves is a Fourier series limited by the *cutoff energy* parameter. The electron densities are then evaluated by the calculation of the wavefunction values in the selected points of the first Brillouin zone whereby the points are defined by the *k-points set* (strictly speaking they are defined in the irreducible part of the Brillouin zone). In this work the k-points set was generated with Monkhorst-Pack method [107] with the origin in the Γ-point of the Brillouin zone. Moreover, not every $\varphi_j$ is fully occupied with an one electron in metallic systems. The partial filling of the electronic bands is done by the *"smearing"* of the electrons on the available eigenstates for which the tetrahedron method with Blöchl corrections [108] was used in this work.

All calculations were performed with the *VASP* (**V**ienna **A**b-initio **S**imulation **P**ackage) ver. 4.6 software [107, 108]. The parameters describing the local wavefunctions for different elements are included in the code. The cutoff energy of 295 eV was used. The ground state energy is found in the iterative procedure:

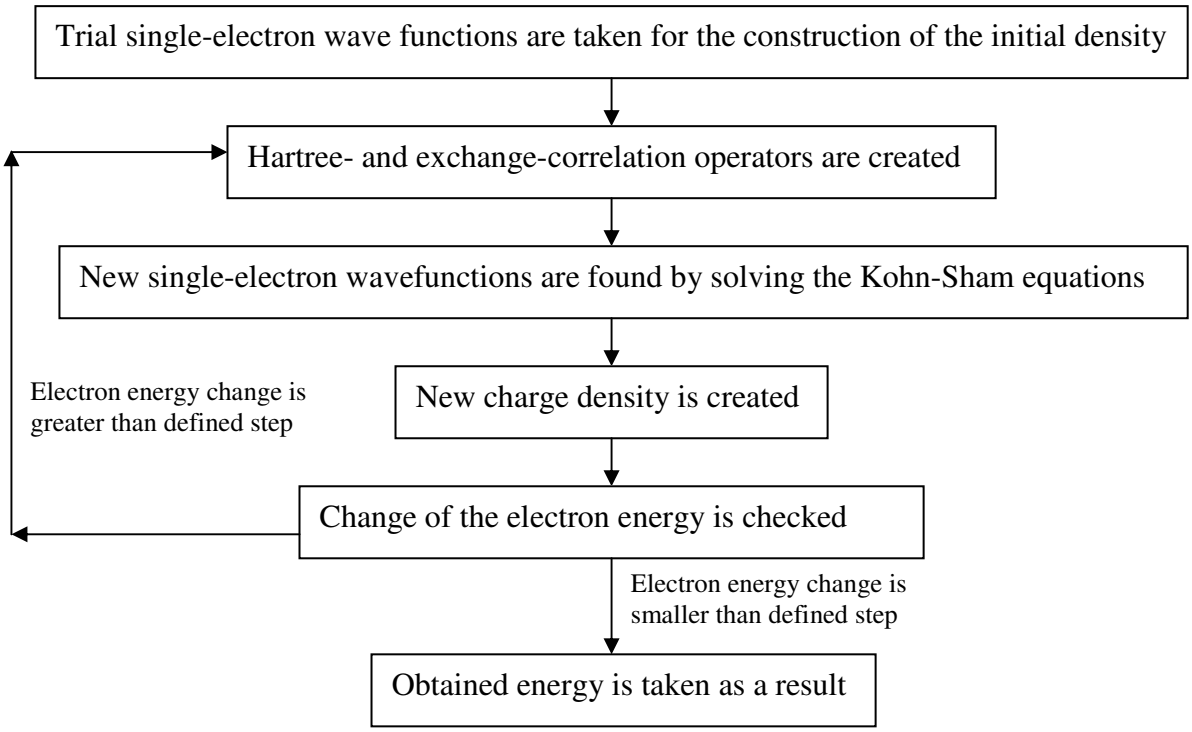

The software also allows calculating the forces acting on each atom core (referred later to as just *atoms*) the unit cell and move the atoms or change the lattice parameters of the cell. The relaxation of atoms was executed using the *conjugate-gradient algorithm* [111]. The required input data for the ground state energy were lattice parameters and atom positions of the investigated cell. In the first calculation run, the unit cell of the binary compound was allowed to change its size, and the atoms were allowed to migrate due to the calculated forces acting on them so that the general stability of the structures described in the literature was checked. The resulting relaxed structure data were taken as the input for the next calculations of the structures with some of the atoms of one element substituted by the atoms of the other element. In these calculations, the structures were allowed to further relax or kept fixed on the input parameters. The k-points sets used in the calculations are given in the corresponding sections of this work.

In addition to the structures of the compound phases, the ground state energies were calculated for the structures stable at 298 K of the elements (Hf hcp, Nb bcc, grey As, Ge diamond type, Ga). These ground state energies were subtracted from the compounds energies in order to find the corresponding formation energies.

### 3.2.4 Thermodynamic modelling

Any phase or phase mixture existing in an equilibrium state in the system has a minimal value of the thermodynamic potential chosen according to the conditions describing this system. Usually the systems are investigated at fixed temperature and fixed pressure so that the Gibbs energy is used as a thermodynamic potential for the description of the system. In a solid solution, atoms of different sorts are distributed randomly over specific crystallographic sites. If more than one site is available in a specific structure, site occupations may vary from site to site. The special combination of site fractions $y_M^A$ (i.e. the ratio of atoms of the element M on site A to all atoms on this site) found in equilibrium corresponds to the minimum of the thermodynamic potential for this solid solution. In this work, the relation between the Gibbs energy and the site fractions is described by the *Compound Energy Model* [109]. In this model a term *sublattice* is introduced which is an arbitrary chosen set of the lattice positions on one or more crystallographic sites within the crystal structure. All atoms within a unit cell are the sum of atoms in all sublattices. It must be emphasized that this meaning of sublattice is not

associated in any way with the term *lattice* used in crystallography. For a given phase MX with *i* sublattices and *j* species, the Gibbs energy $G_{MX}$ is described as:

$$G_{MX} = G_{MX}^{ref} - TS_{MX}^{id} + {}^{E}G_{MX}$$

$G_{MX}^{ref}$ – frame of reference for the Gibbs energy
$T$ – temperature [K]
$S_{MX}^{id}$ – ideal entropy of mixing
${}^{E}G_{MX}$ – excess Gibbs energy

Frame of reference for the Gibbs energy $G_{MX}^{ref}$ describes the energies of *end members* (i.e. compounds with every sublattice occupied by only one species):

$$G_{MX}^{ref} = \sum_{I} P_I(Y) G_I$$

$I$ – array describing an end member
$Y$ – matrix describing the site fractions of all species on all sublattices
$P_I(Y)$ – product of site fractions of $Y$ corresponding to the end member described by $I$
$G_I$ – Gibbs energy of the end member described by $I$

The ideal entropy of mixing $S_{MX}^{id}$ describes the contribution of the random mixing on each sublattice and is given by:

$$S_{MX}^{id} = -R \sum_{i} ai \sum_{j} y_j^i \ln y_j^i$$

where:

R – gas constant (≈ 8.314 $JK^{-1}mol^{-1}$)
ai – the stoichiometric contribution of species on sublattice $i$ ($\Sigma ai = 1$)
$y_j^i$ – the site fraction of species $j$ on sublattice $i$

The excess Gibbs energy ${}^{E}G_{MX}$ describes the contribution of various species on various sublattices and it is usually given by a product of the site fractions and the interaction energies. In this work, this part of the model was neglected.

As an example, the equation for the Gibbs energy of the phase with two sublattices with two species *A* and *B* on the first sublattice and species *C* and *D* on the second sublattice will be given. The phase formula is given as $[A,B]_{a1}[C,D]_{a2}$. The matrix Y is thus:

$$Y = \begin{bmatrix} y_A^{a1} & y_B^{a1} & y_C^{a1} & y_D^{a1} \\ y_A^{a2} & y_B^{a2} & y_C^{a2} & y_D^{a2} \end{bmatrix}$$

Whereby $y_C^{a1} = y_D^{a1} = y_A^{a2} = y_B^{a2} = 0$ as the species C and D do not occur on the sublattice a1 and elements A and B do not occur on the sublattice a2. The number of existing end members is $i^j$, so for two sublattices and four species it is $2^4 = 16$. The possible end members are: $A_{a1}A_{a2}$, $A_{a1}B_{a2}$, $A_{a1}C_{a2}$, $A_{a1}D_{a2}$, $B_{a1}A_{a2}$, $B_{a1}B_{a2}$, $B_{a1}C_{a2}$, $B_{a1}D_{a2}$, $C_{a1}A_{a2}$, $C_{a1}B_{a2}$, $C_{a1}C_{a2}$, $C_{a1}D_{a2}$, $D_{a1}A_{a2}$, $D_{a1}B_{a2}$, $D_{a1}C_{a2}$, $D_{a1}D_{a2}$ described by the corresponding arrays [A:A], [A:B], [A:C]... etc. The site fraction products corresponding to these end members are $y_A^{a1}y_A^{a2}, y_A^{a1}y_B^{a2}\ldots$ etc. As some site fractions are zero, the number of end member energies in the frame of reference part is reduced to 4, so that it looks like:

$$G^{ref} = y_A^{a1}y_C^{a2}G_{AC} + y_A^{a1}y_D^{a2}G_{AD} + y_B^{a1}y_C^{a2}G_{BC} + y_B^{a1}y_D^{a2}G_{BD}$$

The ideal entropy of mixing is then given by:

$$S^{id} = -R\left[a1\left(y_A^{a1}\ln y_A^{a1} + y_B^{a1}\ln y_B^{a1}\right) + a2\left(y_C^{a2}\ln y_C^{a2} + y_D^{a2}\ln y_D^{a2}\right)\right]$$

By setting a reference point $G_0$, such that $G_{MX} = G_0 + \Delta G_{MX}$ and $G_I = G_0 + \Delta G_I$ this formalism can be rewritten for the formation energy $\Delta G_{MX}$ using formation energies of the end members $\Delta G_I$. If the energies of the end members and the temperature are known, a set of site fractions can be found for which the Gibbs energy has a minimal value, subject to the constraint:

$$x_M = \sum_i ai * y_M^i$$

which means that the sum of the products of the site fractions and stoichiometric contributions of the sites is equal the mole fraction of the component M in the phase ($x_M$).

These calculations were performed with the *Thermo-Calc* program [110]. For the Gibbs energies of formation of the end members, the coresponding formation energies calculated by *VASP* (see the previous point) were taken. The temperature used in the model was the temperature of annealing of the compounds used for the experimental determination of site fractions with XRD methods.

# 4. Results and discussion

## 4.1 Hf-Nb-As system

### 4.1.1 Experimental results

#### 4.1.1.1 Summary of experimental results

47 samples were prepared in the metal-rich region (<50 at.% As) of the Hf-Nb-As system. The nominal compositions of these samples are listed in Table 19 and shown on a ternary Gibbs diagram (Fig. 39).

**Table 19 A list of nominal sample compositions [at.%] in Hf-Nb-As system**

| Sample | Nominal Composition [% at.] | | | Sample | Nominal Composition [% at.] | | |
|---|---|---|---|---|---|---|---|
| | As | Hf | Nb | | As | Hf | Nb |
| S1 | 50 | 50 | 0 | S25 | 40 | 24 | 36 |
| S2 | 40 | 60 | 0 | S26 | 40 | 12 | 48 |
| S3 | 37.2 | 62.8 | 0 | S27 | 35 | 62 | 3 |
| S4 | 35.5 | 64.5 | 0 | S28 | 35 | 58.5 | 6.5 |
| S5 | 30 | 70 | 0 | S29 | 35 | 52 | 13 |
| S6 | 20 | 80 | 0 | S30 | 35 | 45.5 | 19.5 |
| S7 | 50 | 0 | 50 | S31 | 35 | 32.5 | 32.5 |
| S8 | 42 | 0 | 58 | S32 | 35 | 20 | 45 |
| S9 | 40 | 0 | 60 | S33 | 35 | 6.5 | 58.5 |
| S10 | 37.2 | 0 | 62.8 | S34 | 30 | 63 | 7 |
| S11 | 33.3 | 0 | 66.7 | S35 | 30 | 56 | 14 |
| S12 | 30 | 0 | 70 | S36 | 30 | 42 | 28 |
| S13 | 20 | 0 | 80 | S37 | 30 | 35 | 35 |
| S14 | 50 | 40 | 10 | S38 | 30 | 28 | 42 |
| S15 | 50 | 30 | 20 | S39 | 30 | 14 | 56 |
| S16 | 50 | 20 | 30 | S40 | 25 | 65 | 10 |
| S17 | 50 | 10 | 40 | S41 | 25 | 40 | 35 |
| S18 | 45 | 49.5 | 5.5 | S42 | 20 | 53.3 | 26.7 |
| S19 | 45 | 38.5 | 16.5 | S43 | 20 | 40 | 40 |
| S20 | 45 | 27.5 | 27.5 | S44 | 20 | 30 | 50 |
| S21 | 45 | 16.5 | 38.5 | S45 | 20 | 26.7 | 53.3 |
| S22 | 45 | 5.5 | 49.5 | S46 | 15 | 70 | 15 |
| S23 | 40 | 48 | 12 | S47 | 15 | 60 | 25 |
| S24 | 40 | 36 | 24 | | | | |

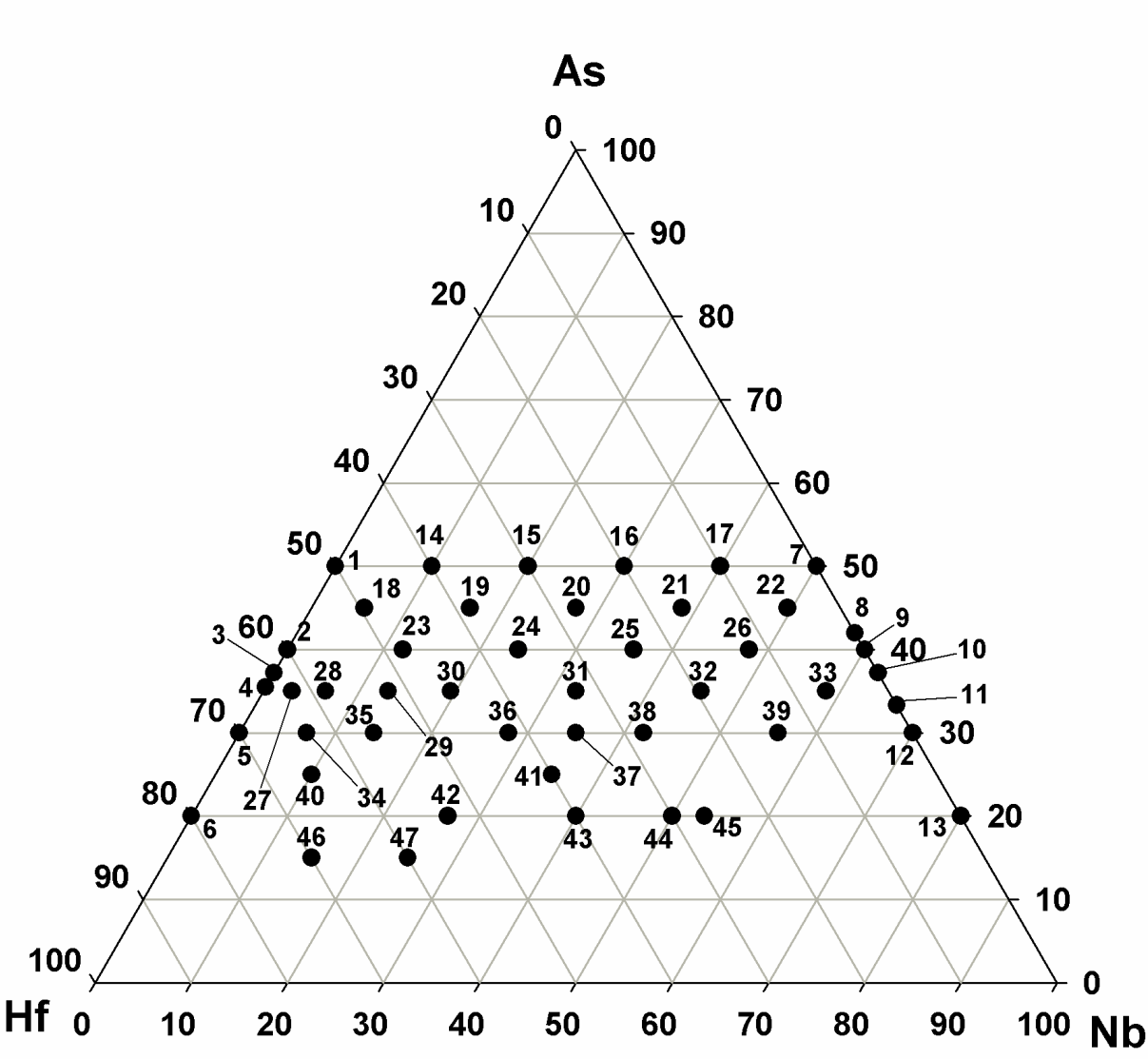


**Fig. 39. Nominal compositions of the prepared samples. The numbers refer to the sample name (e.g "1" for sample "S1").**

During the melting in the arc-melter and the annealing some mass losses were observed which were assumed to be arsenic losses, due to its low sublimation point (616°C). This agrees with the general observation that in the samples containing more metal the observed mass losses were less (e.g. S20 with 45 at. %As – 73.07 mg, S31 with 35 at. %As – 14.42 mg, S37 with 30 at. %As – 13.07 mg, S43 with 20 at. %As – 1.82 mg). Based on this assumption, the actual sample compositions were calculated (see appendix F.1). The results of the powder XRD and EPMA measurements performed on the samples in this system are given in Table 20. The EPMA results are shown also in Fig. 40.

**Table 20. The results of XRD and EPMA experiments for the investigated samples in Hf-Nb-As (annealed at 1400°C)**

| Sample | Actual Composition [% at.] | | | Phases identified by XRD method | Lattice parameters [Å] | Phase compositions found with EPMA method [% at.] | | |
|---|---|---|---|---|---|---|---|---|
| | As | Hf | Nb | | | Hf | Nb | As |
| S1 | 49.0 | 51.0 | 0.0 | HfAs | a=3.77238(4) c=12.7082(1) | 50.3 | 0.0 | 49.7 |
| | | | | $Hf_3As_2$ | a=10.4351(3) b=3.65349(9) c=10.0939(3) | 59.7 | 0.0 | 40.3 |
| S2 | 39.1 | 60.9 | 0.0 | HfAs | a=3.7746(2) c=12.7140(9) | Not found (matrix component?) | | |
| | | | | $Hf_3As_2$ | a=10.4363(2) b=3.65460(5) c=10.0949(2) | 60.3 | 0.0 | 39.7 |
| S3 | 28.4 | 71.6 | 0.0 | $Hf_2As$ | a=15.3562(3) b=12.4701(3) c=3.65563(8) | 67.1 | 0.0 | 32.9 |
| | | | | $Hf_3As$ | a=15.406(2) b=5.3754(4) c=15.327(1) β=90.359(9) | 74.8 | 0.0 | 25.2 |
| S4 | 32.8 | 67.2 | 0.0 | $Hf_5As_3$ | a=27.366(2) b=3.6145(2) c=12.2939(8) | Not found (low content?) | | |
| | | | | $Hf_7As_4$ | a=16.0870(4) b=3.59186(7) c=14.9353(4) β=104.226(2) | 63.7 | 0.0 | 36.3 |
| | | | | $Hf_2As$ | a=15.3815(7) b=12.5113(5) c=3.6425(1) | 66.7 | 0.0 | 33.3 |
| S5 | 29.6 | 70.4 | 0.0 | $Hf_2As$ | a=15.3563(2) b=12.4787(1) c=3.65247(4) | 66.4 | 0.0 | 33.6 |
| | | | | $Hf_3As$ | a=15.3916(3) b=5.38064(7) c=15.3310(3) β=90.296(1) | 75.2 | 0.0 | 24.8 |
| S6 | 19.7 | 80.3 | 0.0 | $Hf_3As$ | a=15.3965(2) b=5.37960(5) c=15.3376(2) β=90.2943(9) | 75.0 | 0.0 | 25.0 |
| | | | | Hf | a=3.21610(3) c=5.11006(8) | 95.5 | 0.0 | 4.5 |
| S7 | 45.6 | 0.0 | 54.4 | NbAs | a=3.45223(3) c=11.6723(2) | 0.0 | 50.2 | 49.8 |
| | | | | $Nb_4As_3$ | a=3.51533(3) b=14.6542(2) c=18.8376(2) | 0.0 | 57.0 | 43.0 |
| S8 | 38.2 | 0.0 | 61.8 | $Nb_4As_3$ | a=3.5142(1) b=14.6599(6) c=18.8438(8) | Not found (matrix component?) | | |
| | | | | $Nb_5As_3$ | a=26.0823(4) b=3.52033(4) c=11.7908(2) | 0.0 | 37.8 | 62.2 |
| S9 | 36.5 | 0.0 | 63.5 | $Nb_5As_3$ | a=26.0765(3) b=3.51960(3) c=11.7882(1) | 0.0 | 62.2 | 37.8 |
| S10 | 34.9 | 0.0 | 65.1 | $Nb_5As_3$ | a=26.08579(7) b=3.51984(8) c=11.7873(3) | 0.0 | 62.5 | 37.5 |
| | | | | $Nb_7As_4$ | a=15.3697(4) b=3.52308(8) c=14.1921(3) β=104.678(2) | 0.0 | 63.7 | 36.3 |
| | | | | „A“ | a=18.496(1) b=3.5056(2) c=14.1688(8) | 0.0 | 66, 5 | 33.5 |
| S11 | 32.2 | 0.0 | 67.8 | $Nb_7As_4$ | a=15.3771(5) b=3.52224(7) c=14.1909(4) β=104.689(2) | 0.0 | 63.7 | 36.3 |
| | | | | $Nb_3As$ | a=10.2949(2) c=5.1949(2) | 0.0 | 74.6 | 25.4 |
| | | | | „A“ | a=18.4987(3) b=3.50602(5) c=14.1624(2) | 0.0 | 66.7 | 33.3 |

| Sample | Actual Composition [% at.] | | | Phases identified by XRD method | Lattice parameters [Å] | Phase compositions found with EPMA method [% at.] | | |
|---|---|---|---|---|---|---|---|---|
| | As | Hf | Nb | | | Hf | Nb | As |
| S12 | 29.2 | 0.0 | 70.8 | $Nb_7As_4$ | a=15.523(1) b=3.5144(2) c=14.193(1) β=104.543(6) | 0.0 | 63.6 | 36.4 |
| | | | | $Nb_3As$ | a=10.2953(1) c=5.19657(8) | 0.0 | 74.9 | 25.1 |
| | | | | „A“ | a=18.5021(2) b=3.50527(4) c=14.1660(2) | Not found (matrix component?) | | |
| S13 | 19.7 | 0.0 | 80.3 | $Nb_3As$ | a=10.2943(2) c=5.19805(9) | 0.0 | 75.4 | 24.6 |
| | | | | Nb | a=3.31847(8) | 0.0 | 89.1 | 10.9 |
| S14 | 45.1 | 43.9 | 11.0 | HfAs | a=3.77316(4) c=12.6851(2) | 48.4 | 1.7 | 49.9 |
| | | | | $M_5As_3$ | a=26.844(2) b=3.6093(1) c=12.0229(6) | 42.0 | 21.1 | 36.9 |
| S15 | 43.8 | 33.7 | 22.5 | HfAs | a=3.77263(6) c=12.6670(3) | 45.6 | 4.4 | 50.0 |
| | | | | $M_5As_3$ | a=26.4841(9) b=3.58020(9) c=11.8950(4) | 30.4 | 32.5 | 37.1 |
| S16 | 46.1 | 21.6 | 32.3 | HfAs | a=3.77076(7) c=12.6267(4) | 42.8 | 7.3 | 49.9 |
| | | | | $Nb_4As_3$ | a=3.57502(6) b=14.7247(3) c=19.1193(4) | 15.5 | 43.3 | 41.2 |
| S17 | 43.1 | 11.4 | 45.5 | NbAs | a=3.47313(9) c=11.7868(5) | 7.7 | 42.3 | 50.0 |
| | | | | $Nb_4As_3$ | a=3.54779(5) b=14.7079(3) c=18.9730(4) | 9.4 | 47.6 | 43.0 |
| | | | | $M_5As_3$ | a=26.205(2) b=3.5414(2) c=11.842(1) | Not found (matrix component?) | | |
| S18 | 40.1 | 54.0 | 6.0 | HfAs | a=3.77146(5) c=12.7010(3) | 49.9 | 0.4 | 49.7 |
| | | | | $M_5As_3$ | a= 27.1231(6) b= 3.62492(6) c= 12.1858(2) | 54.2 | 8.7 | 37.1 |
| S19 | 41.1 | 41.3 | 17.6 | HfAs | a=3.77273(5) c=12.6918(2) | 47.8 | 2.2 | 50.0 |
| | | | | $M_5As_3$ | a=26.7362(9) b=3.60086(8) c=11.9773(4) | 39.3 | 23.3 | 37.4 |
| S20 | 38.5 | 30.7 | 30.8 | HfAs | a=3.77226(8) c=12.6768(4) | 42.6 | 7.4 | 50.0 |
| | | | | $M_5As_3$ | a=26.5822(5) b=3.58946(5) c=11.9228(2) | 31.5 | 30.9 | 37.6 |
| S21 | 38.6 | 18.3 | 43.0 | $Nb_4As_3$ | a=3.5814(2) b=14.727(1) c=19.114(1) | 17.9 | 39.4 | 42.7 |
| | | | | $M_5As_3$ | a=26.3571(4) b=3.56603(4) c=11.8651(2) | 16.9 | 45.4 | 37.7 |
| S22 | 39.3 | 6.1 | 54.7 | NbAs | a=3.46275(6) c=11.7407(3) | 5.1 | 44.9 | 50.0 |
| | | | | $Nb_4As_3$ | a=3.53011(4) b=14.6860(2) c=18.8943(2) | 4.8 | 52.2 | 43.0 |
| | | | | $M_5As_3$ | a=26.133(1) b=3.5359(1) c=11.8184(5) | Not found (matrix component?) | | |

| Sample | Actual Composition [% at.] | | | Phases identified by XRD method | Lattice parameters [Å] | Phase compositions found with EPMA method [% at.] | | |
|---|---|---|---|---|---|---|---|---|
| | As | Hf | Nb | | | Hf | Nb | As |
| S23 | 38.7 | 49.1 | 12.2 | HfAs | a=3.76786(9) c=12.7015(5) | Not found (matrix component?) | | |
| | | | | $M_5As_3$ | a=26.9866(4) b=3.62147(4) c=12.1036(2) | 47.6 | 15.1 | 37.3 |
| S24 | 39.4 | 37.2 | 23.4 | $M_5As_3$ | a=26.743(1) b=3.60103(9) c=11.9755(4) | 35.2 | 27.3 | 37.5 |
| S25 | 37.2 | 25.0 | 37.8 | $M_5As_3$ | a=26.5041(5) b=3.58299(6) c=11.8998(2) | 22.8 | 39.6 | 37.6 |
| | | | | $M_7As_4$ | a=15.506(1) b=3.5876(2) c=14.3303(9) β=104.171(6) | Not found (matrix component?) | | |
| S26 | 36.1 | 12.7 | 51.2 | $Nb_4As_3$ | a=3.5523(1) b=14.7218(5) c=18.9899(7) | Not found (matrix component?) | | |
| | | | | $M_5As_3$ | a=26.2445(4) b=3.55045(5) c=11.8414(2) | 12.3 | 50.0 | 37.7 |
| S27 | 30.0 | 66.7 | 3.3 | $M_5As_3$ | a=27.2219(5) b=3.62023(5) c=12.2396(2) | 59.3 | 3.2 | 37.5 |
| | | | | $Hf_2As$ | a=15.389(1) b=12.5392(9) c=3.6147(2) | 64.4 | 2.3 | 33.3 |
| S28 | 34.4 | 59.1 | 6.5 | $M_5As_3$ | a=27.162(1) b=3.6236(1) c=12.2020(6) | 55.8 | 6.6 | 37.6 |
| | | | | $M_7As_4$ | a=16.0243(3) b=3.60373(5) c=14.7417(3) β=104.326(2) | 57.4 | 6.2 | 36.4 |
| | | | | „B“ | a=29.6297(9) b=19.2809(6) c=3.59403(8) | 60.2 | 6.5 | 33.3 |
| S29 | 30.6 | 55.1 | 14.3 | $M_7As_4$ | a=15.9512(4) b=3.60955(7) c=14.6131(3) β=104.375(2) | 51.1 | 12.7 | 36.2 |
| | | | | “B” | a=29.462(6) b=19.188(4) c=3.5951(5) | 54.8 | 11.8 | 33.4 |
| | | | | “C” | a=7.0307(2) b=3.6058(1) c=8.6317(3) | 47.4 | 19.3 | 33.3 |
| S30 | 34.2 | 46.1 | 19.7 | $M_7As_4$ | a=15.8816(5) b=3.61251(8) c=14.5364(4) β=104.340(2) | 44.6 | 19.0 | 36.4 |
| | | | | “C” | a=7.0294(1) b=3.60248(6) c=8.6042(2) | Not found (matrix component?) | | |
| S31 | 33.4 | 33.1 | 33.5 | $M_7As_4$ | a=15.6586(5) b=3.60356(8) c=14.3925(4) β=104.104(3) | 33.2 | 30.4 | 36.4 |
| | | | | “C” | a=6.99351(8) b=3.58654(4) c=8.4883(1) | Not found (matrix component?) | | |
| S32 | 29.1 | 21.9 | 49.0 | $M_7As_4$ | a=15.5008(3) b=3.58619(5) c=14.3193(3) β=104.129(2) | Not found (matrix component?) | | |
| | | | | “D” | a=17.7397(5) b=3.55532(8) c=11.1130(3) | 23.8 | 46.2 | 30.0 |
| | | | | $Nb_3As$ | a=10.3255(3) c=5.2196(3) | 17.2 | 57.8 | 25.0 |
| S33 | 32.4 | 6.7 | 60.9 | $M_7As_4$ | a=15.3823(3) b=3.54889(7) c=14.2421(3) β=104.473(2) | 7.7 | 55.8 | 36.5 |
| | | | | $Nb_3As$ | a=10.3028(2) c=5.2038(1) | 2.6 | 72.3 | 25.1 |
| S34 | 33.8 | 26.0 | 40.2 | $M_7As_4$ | a=15.925(3) b=3.6051(5) c=14.780(3) β=104.11(2) | Not found (low content?) | | |
| | | | | „B“ | a=29.601(1) b=19.2531(8) c=3.5978(1) | 59.9 | 6.8 | 33.3 |
| | | | | „E” | a=10.7286(5) c=5.3717(5) | 64.0 | 10.9 | 25.1 |

| Sample | Actual Composition [% at.] | | | Phases identified by XRD method | Lattice parameters [Å] | Phase compositions found with EPMA method [% at.] | | |
|---|---|---|---|---|---|---|---|---|
| | As | Hf | Nb | | | Hf | Nb | As |
| S35 | 29.6 | 56.2 | 14.1 | „B“ | a=29.420(3) b=19.469(2) c=3.6122(2) | Not found (matrix component?) | | |
| | | | | „C“ | a=7.0369(5) b=3.6250(2) c=8.6507(7) | 48.2 | 18.3 | 33.5 |
| | | | | „E“ | a=10.7009(2) c=5.3795(2) | 56.9 | 18.3 | 24.8 |
| S36 | 28.7 | 42.6 | 28.6 | „C“ | a=7.0278(1) b=3.60112(7) c=8.5988(2) | 43.9 | 22.8 | 33.3 |
| | | | | „D“ | a=17.9965(5) b=3.59163(8) c=11.2910(3) | 40.8 | 29.3 | 29.9 |
| S37 | 28.6 | 35.8 | 35.5 | „C“ | a=6.9962(1) b=3.58854(7) c=8.4956(2) | 31.2 | 35.5 | 33.3 |
| | | | | „D“ | a=17.8532(7) b=3.5725(1) c=11.1653(4) | 28.3 | 41.7 | 30.0 |
| S38 | 28.8 | 28.6 | 42.6 | „C“ | a=6.9983(4) b=3.5876(2) c=8.5041(6) | Not found (low content?) | | |
| | | | | „D“ | a=17.9101(4) b=3.57793(7) c=11.1979(3) | 27.0 | 43.0 | 30.0 |
| | | | | Nb | a=3.3140(2) | 7.3 | 89.7 | 3.0 |
| S39 | 27.4 | 14.6 | 58.0 | $M_7As_4$ | a=15.460(1) b=3.5812(2) c=14.3075(9) β=104.156(6) | 18.8 | 44.6 | 36.6 |
| | | | | „D“ | a=17.7359(3) b=3.55709(5) c=11.1136(2) | Not found (matrix component?) | | |
| | | | | $Nb_3As$ | a=10.3296(1) c=5.22673(9) | 9.2 | 65.8 | 25.0 |
| S40 | 23.3 | 66.4 | 10.3 | „B” | a=29.609(3) b=19.249(2) c=3.5967(2) | 60.0 | 6.8 | 33.2 |
| | | | | „E” | a=10.7270(1) c=5.3706(1) | 64.0 | 10.9 | 25.1 |
| S41 | 21.0 | 41.9 | 37.1 | „D” | a=17.9660(5) b=3.58751(9) c=11.2532(3) | 39.5 | 30.6 | 29.9 |
| | | | | „F” | a=7.1296(2) b=3.5776(1) c=11.6039(4) | 40.6 | 34.3 | 25.1 |
| | | | | Nb | a=3.3281(1) | 13.4 | 84.7 | 1.9 |
| S42 | 19.8 | 53.4 | 26.8 | „E“ | a=10.6735(1) c=5.3713(1) | 53.7 | 21.3 | 25.0 |
| | | | | Nb | a=3.37276 | Not found (matrix component?) | | |
| S43 | 19.8 | 40.2 | 39.9 | „E“ | a=10.6430(7) c=5.3848(6) | 53.0 | 21.9 | 25.1 |
| | | | | „F“ | a=7.1443(2) b=3.58542(9) c=11.6304(3) | 40.6 | 34.5 | 24.9 |
| | | | | Nb | a=3.3462(2) | 19.7 | 79.1 | 1.2 |
| S44 | 19.8 | 30.3 | 49.9 | „D” | a=17.9297(7) b=3.5790(1) c=11.2235(4) | 31.4 | 38.7 | 29.9 |
| | | | | „F” | a= 7.1351(2) b= 3.5849(1) c= 11.5991(4) | 38.6 | 36.2 | 25.2 |
| | | | | Nb | a=3.3261(1) | 12.6 | 86.1 | 1.3 |

| Sample | Actual Composition [% at.] | | | Phases identified by XRD method | Lattice parameters [Å] | Phase compositions found with EPMA method [% at.] | | |
|---|---|---|---|---|---|---|---|---|
| | As | Hf | Nb | | | Hf | Nb | As |
| S45 | 19.6 | 26.9 | 53.6 | „D“ | a=17.9254(7) b=3.5785(1) c=11.2027(4) | 28.7 | 41.3 | 30.0 |
| | | | | Nb | a=3.3167(1) | Not found (matrix component?) | | |
| S46 | 13.9 | 60.6 | 25.5 | „E“ | a=10.7522(2) c=5.3703(2) | 66.3 | 8.7 | 25.0 |
| | | | | Hf | a=3.20566(7) c=5.0955(2) | 94.7 | 3.8 | 1.5 |
| | | | | Nb | a=3.4288647 0.0001587 | 53.4 | 45.1 | 1.5 |
| S47 | 13.0 | 71.6 | 15.4 | „E“ | a=10.7155(3) c=5.3685(3) | 58.8 | 16.2 | 25.0 |
| | | | | Nb | a=3.4136(1) | 46.4 | 51.9 | 1.7 |

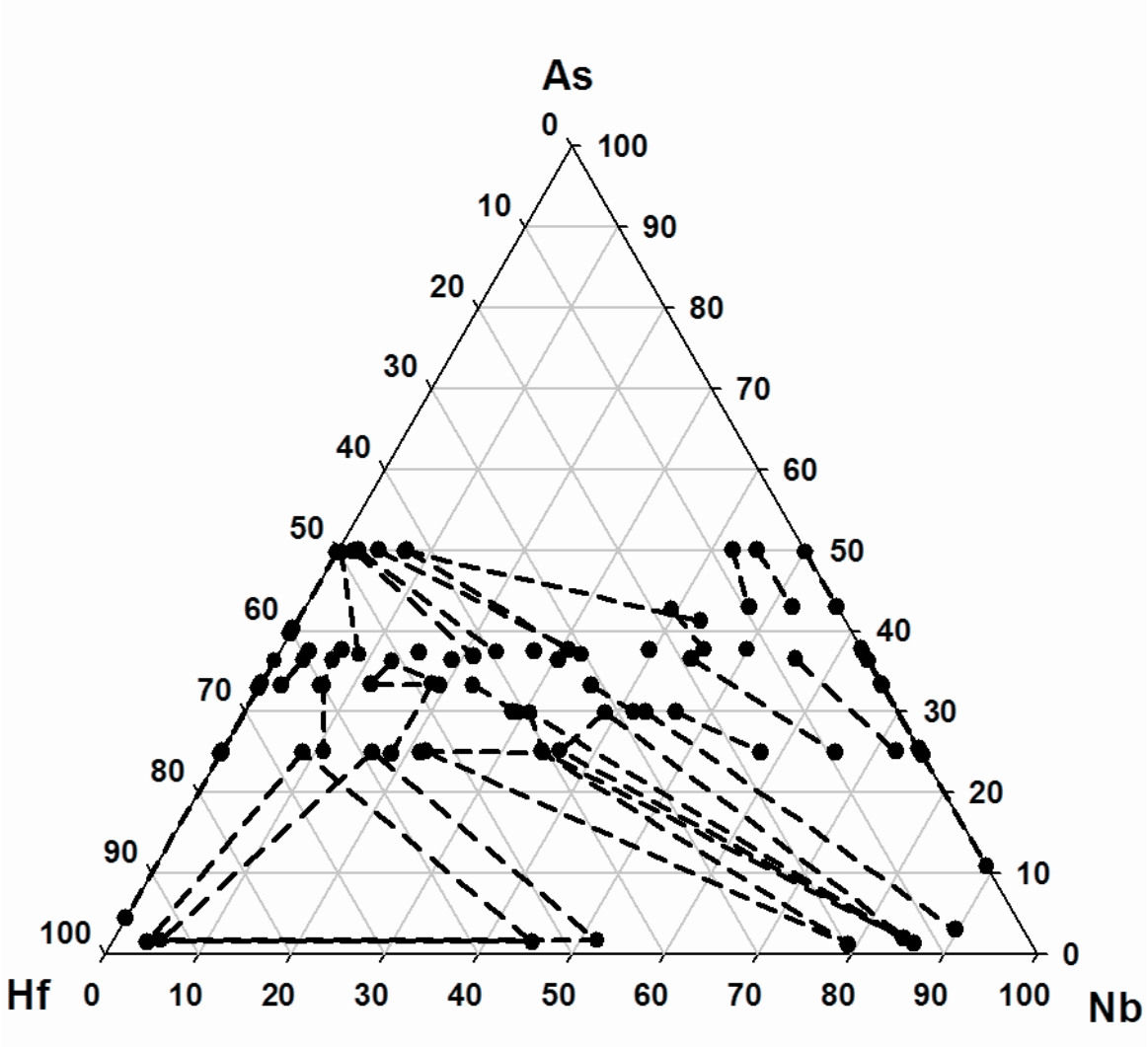


**Fig. 40. Graphical representation of EPMA results for samples annealed at 1400°C. The phase compositions are represented by points. The phase compositions found in the same sample are connected by dashed lines.**

All binary compounds reported in the literature were found in the isothermal section at 1400°C. An additional binary compound $Nb_2As$ was found (described as "A"). Also, five new ternary phases were found ("B" – $Hf_{3+x}Nb_{1-x}As_2$, "C" – $Hf_{1+x}Nb_{1-x}As$ , "D" – $Hf_{4-x}Nb_{3+x}As_3$, "E" – $Hf_{2+x}Nb_{1-x}As$ and "F" – $Hf_{3+x}Nb_{3-x}As_2$), two of which appeared to have a new structure type ($Hf_{4-x}Nb_{3+x}As_3$, $Hf_{3+x}Nb_{3-x}As_2$). The solubility ranges based on the EPMA measurements are given in Table 21. It must be noted that 4 binary samples (S4, S10, S11, S12) contain 3 phases and thus violate the Gibbs phase rule. Five of the ternary samples (S17, S22, S28, S34, S35) show overlapping phase fields (compare Fig. 40), and thus raising serious doubts if the samples describe the system in an equilibrium state. The binary phases $Hf_3As_2$, $Hf_3As$ and

**Table 21. The summary of phases found in Hf-Nb-As system at 1400°C. The solubility of the second metal for the binary phases $Hf_3As_2$, $Hf_3As$ and $Nb_2As$ is assumed to be 2 at.% or less.**

| Phase | | As content [at.%] | Second metal solubility [at.%] | Prototype |
|---|---|---|---|---|
| Binary | HfAs | 50.0 | 0-7(Nb) | AsTi |
| | $Hf_3As_2$ | 40.0 | 0-~2 (Nb) | $Hf_3P_2$ |
| | $Hf_2As$ | 33.3 | 0-2(Nb) | $PTa_2$ |
| | $Hf_3As$ | 25 | 0-~2 (Nb) | $AsTa_3$ |
| | NbAs | 50 | 0-8 (Hf) | AsNb |
| | $Nb_4As_3$ | 42.9 | 0-18 (Hf) | $As_3Nb_4$ |
| | $Nb_2As$ – **"A"** | 33.3 | 0-~2 (Hf) | $Nb_2P$ or $Zr_2P$ |
| | $Nb_3As$ | 25 | 0-17(Hf) | $PTi_3$ |
| | $M_5As_3$ | 37.5 | 0-62.5 (Hf) | $As_3Nb_5$ |
| | $M_7As_4$ | 36.4 | 0-63.7 (Hf) | $Nb_7P_4$ |
| Ternary | $Hf_{3+x}Nb_{1-x}As_2$ – **„B"** | 33.3 | 55-60 (Hf) (0.29<x<0.61) | $Nb_2P$ or $Zr_2P$ |
| | $Hf_{1+x}Nb_{1-x}As$ - **„C"** | 33.3 | 31-47 (Hf) (-0.06<x<0.42) | $Co_2Si$ |
| | $Hf_{4-x}Nb_{3+x}As_3$ – **„D"** | 30.0 | 24-41 (Hf) (-0.08<x<1.62) | new |
| | $Hf_{7.22}Nb_{3.78}As_4$* | 26.7 | 48.1 (Hf) | $Zr_{6.45}Nb_{4.55}As_4$ |
| | $Hf_{2+x}Nb_{1-x}As$ – **„E"** | 25.0 | 53-66 (Hf) (0.12<x<0.65) | $PTi_3$ |
| | $Hf_{3+x}Nb_{3-x}As_2$ – **„F"** | 25.0 | 39-41 (Hf) (0.09<x<0.25) | new |

* - Phase identified by single crystal measurement – not found in the powder diffractograms (see chapter 4.1.1.5 for details)

$Nb_2As$ were not found in any ternary samples so that they are assumed to have a minor solubility of the second metal which is set arbitrary to 2 at.%. Unfortunately, the experimental results do not allow to construct a full equilibrium phase diagram, as many binary and ternary phase fields were not determined during the current investigation. Anyway, an "orientation map" for all phases is shown in Fig. 41

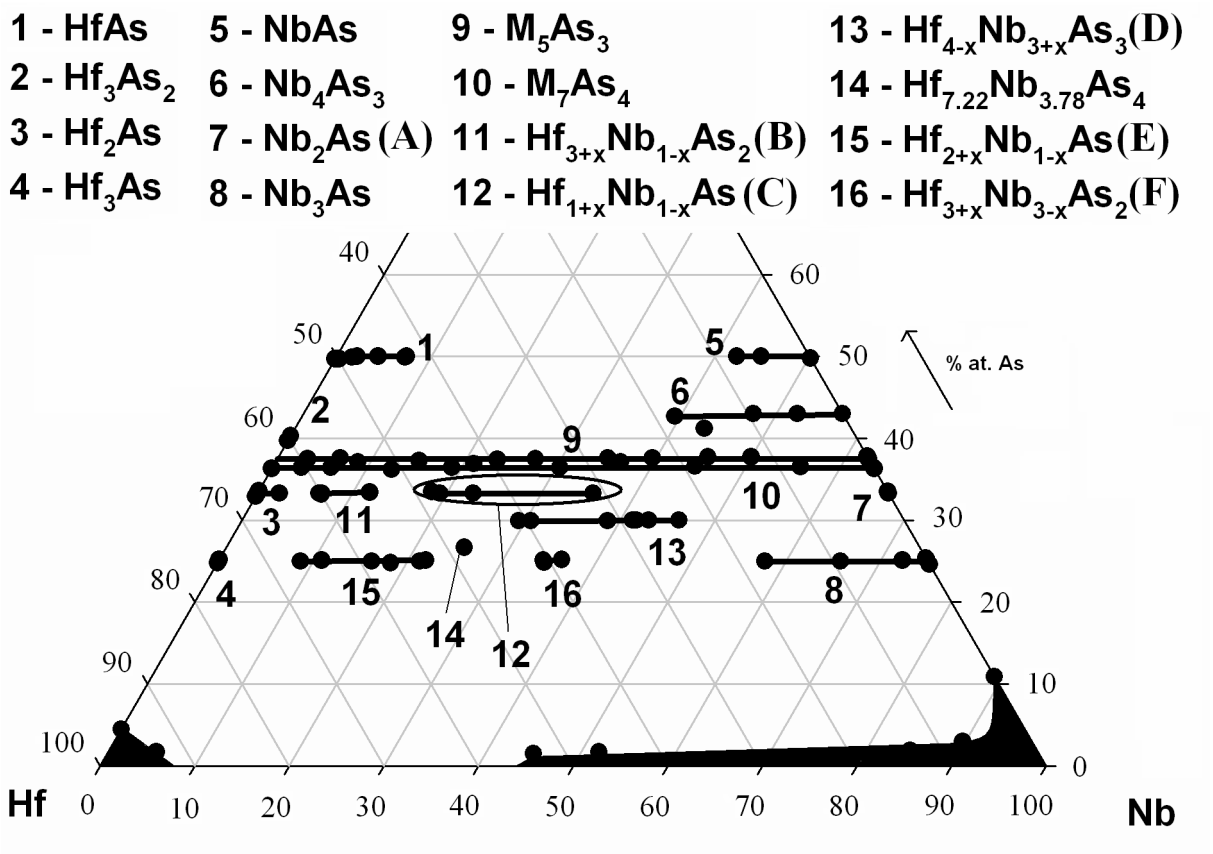


**Fig. 41. The phase ranges found in Hf-Nb-As system at 1400°C**

In many cases, the phases identified by XRD could not be found during the EPMA measurements. The author believes that the reason for that are mostly the very fine crystalline structures, found in many of the samples, of which the matrix was composed (see examples in Fig. 42) and these phases were described by "*(matrix component?)*" in Table 20. In these cases, it was not possible to measure the composition of the phase identified by XRD measurement. In three of the samples (S4, S34, S38) the phases not found in the EPMA measurements were likewise found only in a small amount by XRD (i.e. their reflexes on the diffractogram were weak) and could exist as a few single grains only – these cases are described with "*(low content?)*" in Table 20.

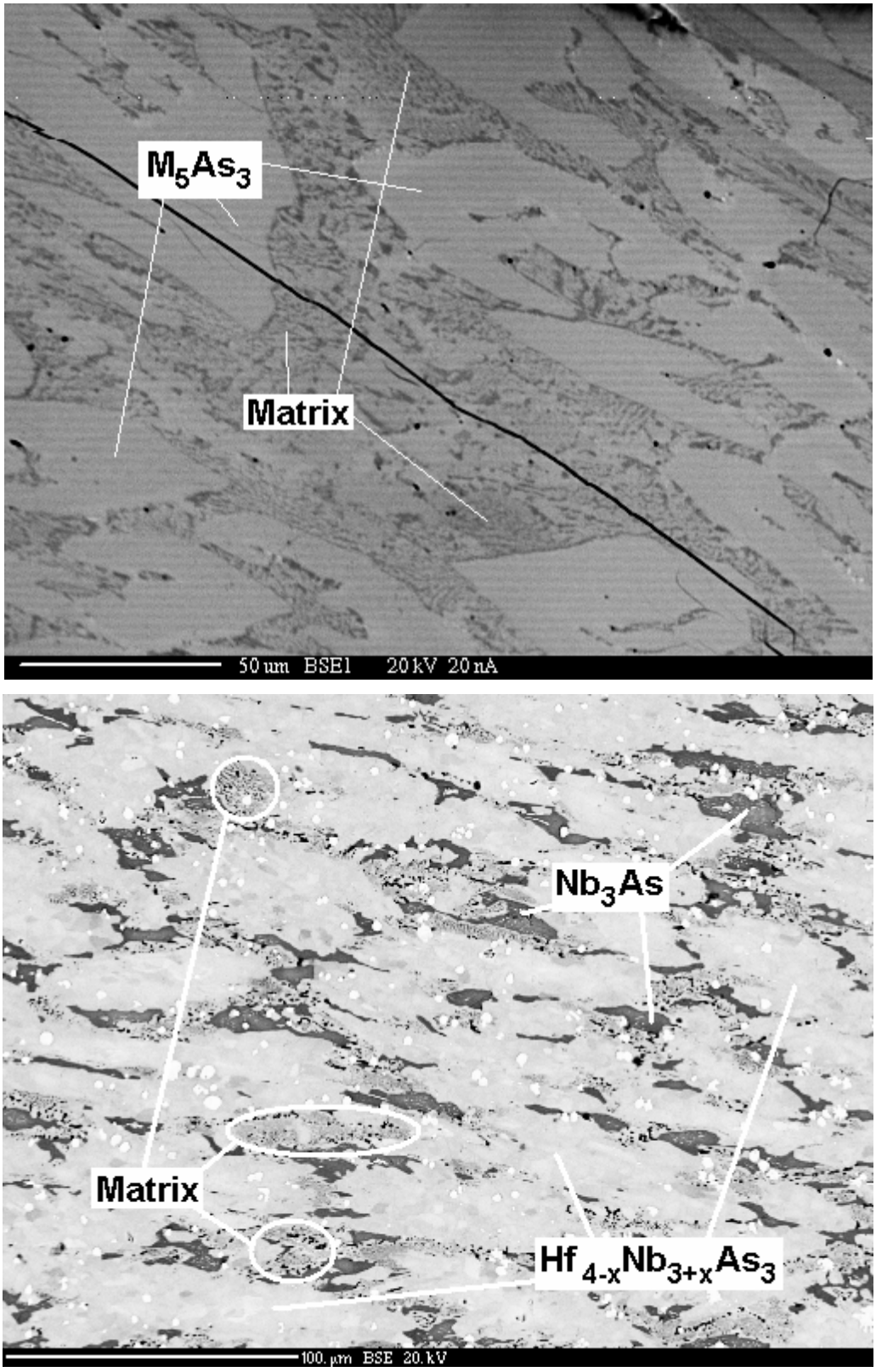


**Fig. 42. Sample pictures taken during EPMA investigation showing matrix regions. The composition of the phases present only in the matrix could not be measured (top - S23, bottom – S32). The white spots on the bottom picture are $HfO_2$ precipitates.**

The optical microscope observations together with XRD and EPMA measurements showed that all but the binary Nb-As samples contained traces of $HfO_2$ (Fig. 43-45). Since this was not found in the diffractogram obtained from the hafnium powder starting material, the oxide must have been formed during the sample preparation. Hafnium is assumed to play a role as a getter which reacts with oxygen during the synthesis steps, but surprisingly a lower content of $HfO_2$ was found in the samples containing hafnium phase in equilibrium (S6, S46) than in the other ones. It is believed that hafnium powder, used as a starting material, contained some dissolved oxygen which was released during the chemical reactions. Thus the presence of $HfO_2$ in the samples suggests that the arsenide phases themselves are not oxygen stabilised, otherwise these phases would have dissolved the oxygen and it would not have been able to react with hafnium.

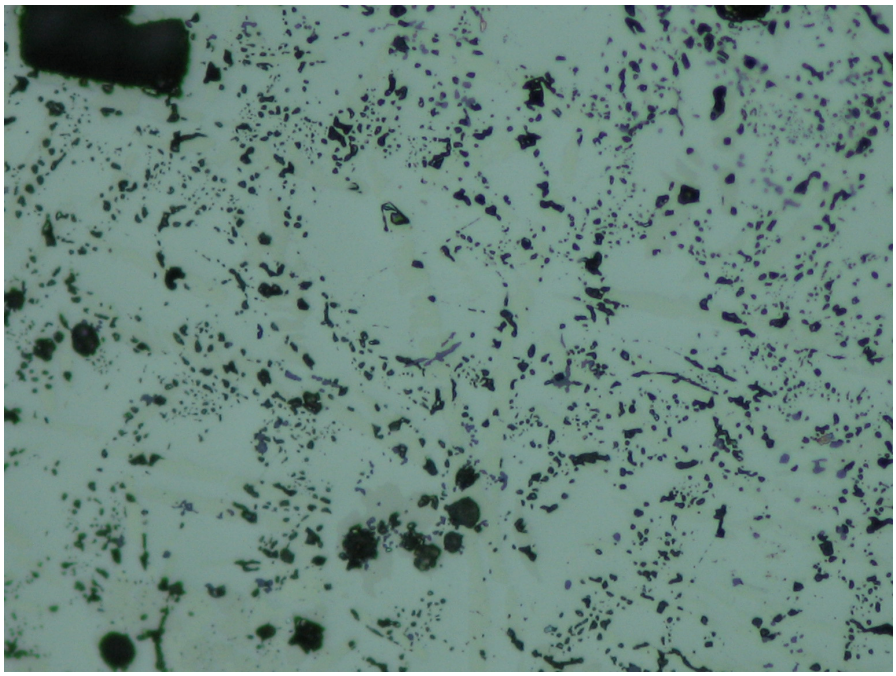

**Fig. 43. A picture of sample S16 taken under the light microscope (50x). Many black holes in the surface of the sample are believed to be a result of the arsenide decomposition into gaseous arsenic during the arc-melting step of the sample preparation**

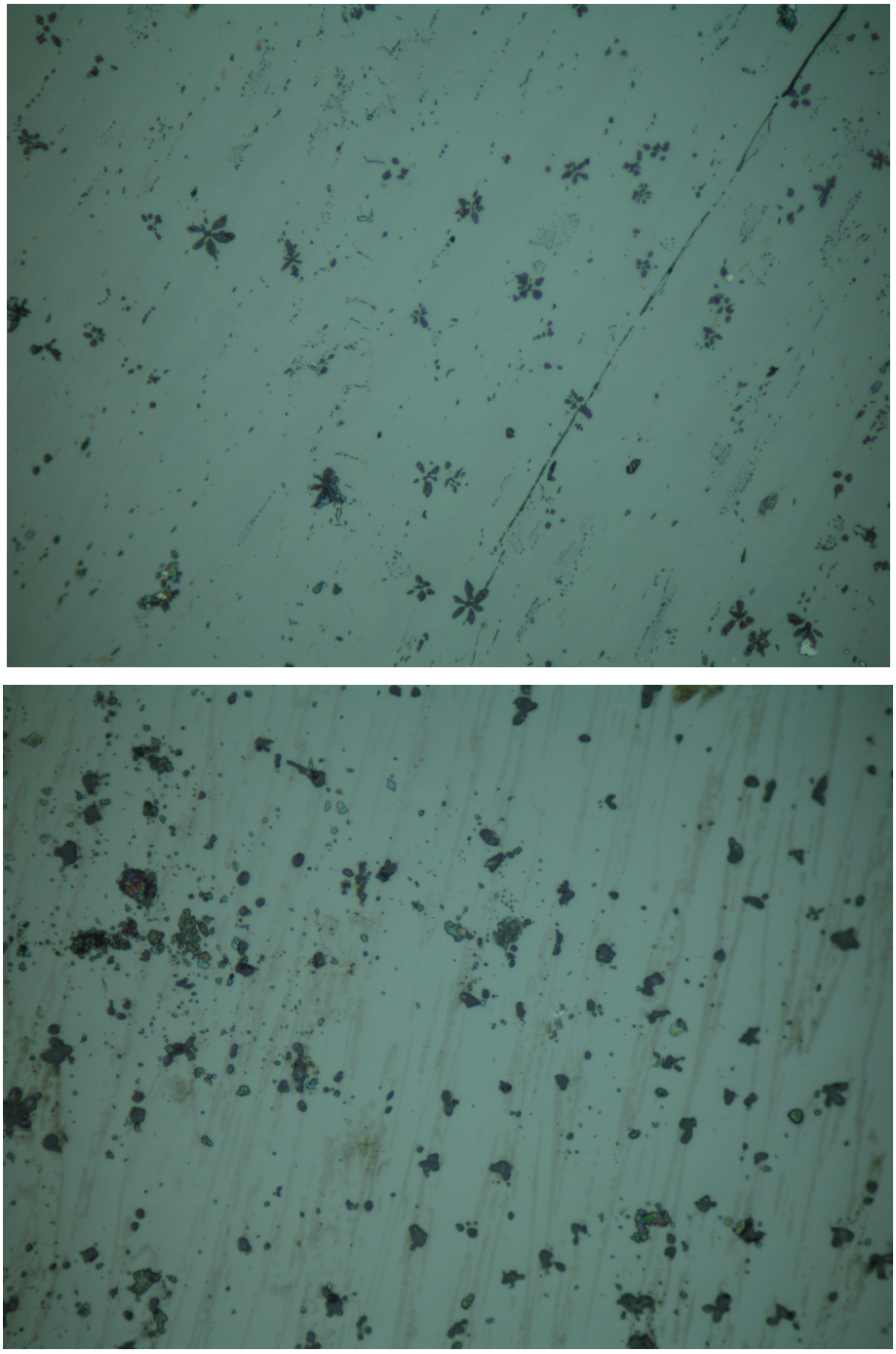

**Fig. 44. A picture of samples S37 (top) and S42 (bottom) taken under the light microscope (50x). Visible dark precipitates of $HfO_2$ are observed. In hafnium-richer S42, the precipitates are larger than in S37, where finer structures in form of "flowers" are observed.**

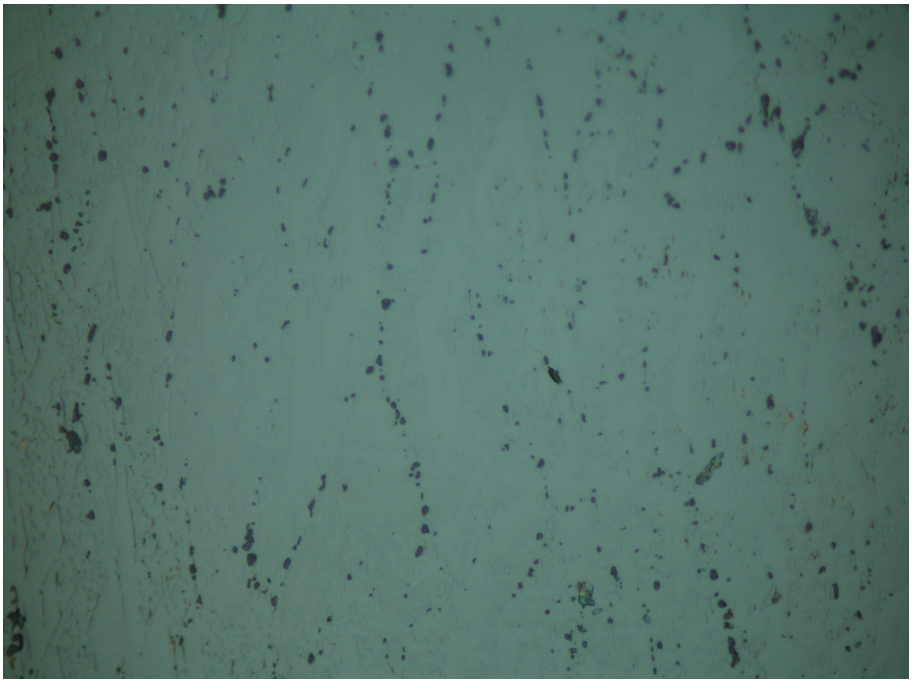

**Fig. 45. A picture of sample S6 (taken under the light microscope (50x). Dark precipitate of $HfO_2$ is observed in the smaller amount than in the previous samples (Fig. 44) which is believed to be a result of the oxygen dissolution in pure hafnium which is one of the phase present in this sample**

The further investigation of the crystal structures using single crystal measurements and Rietveld refinement of the powder samples was not possible in all cases. Unfortunately, in most samples the crystallites were found to be too small for single crystal measurements (compare with Fig. 42). Only three single crystals could be isolated from the samples – one crystal from sample S45 and two crystals from the sample S43. On the other hand, the mass losses during the preparation of the samples were generally not reproducible, so that it was impossible to prepare samples with accurate composition. Given the large number of phases with very close composition present in the ternary phase diagram, it was not possible to prepare pure phases as it would be ideal for Rietveld refinement. Consequently, Rietveld refinement was only performed in these samples which were pure enough for good refinement results. The results will be described in the subsequent discussion of some of the phases.

#### 4.1.1.2 $Hf_5As_3$ – $Nb_5As_3$ line

A continuous solid solution between the isostructural compounds $Hf_5As_3$ and $Nb_5As_3$ was found. This created a good opportunity for a Rietveld refinement of this phase, provided that pure enough samples are available. Two samples (S20, S23) were found suitable for this analysis. Both of them are situated on the arsenic rich side (i.e. >37.5 at.% As), as it was impossible to perform such a refinement on samples with the lower arsenic contents (i.e. <37.5 at.% As) due to the proximity of the $M_7As_4$ (36.4 at.% As) continuous solid solution phase. The results of the Rietveld refinement performed on these two samples are summarised in Tables 22-24 (the remaining fraction of the pattern was $HfO_2$). The site fractions found in these samples are compared in Table 25. These data, however, should be treated with some caution, as the number of the refined sites (total – 16, metal sites – 10) was large. During the refinement of sample S20, the values of temperature factor *B(eq)* for arsenic atoms dropped below 0.01, and were consequently fixed to 0.3 as a reasonable value. However, keeping this parameter fixed or relaxed did not have any substantial influence on the site fraction values.

**Table 22. Rietveld refinement results for the $M_5As_3$ phase in sample S23**

| Sample: S23 | Nominal composition: $Hf_{48}Nb_{12}As_{40}$ | | $R_p$: 2.63 | | $R_{wp}$: 3.73 | |
|---|---|---|---|---|---|---|
| Background model: Chebyshev, 4th order | | | 2$\theta$-range [°]: 10 - 120° | | | |
| Main phase: $(Hf,Nb)_5As_3$ | Structure type: $Nb_5As_3$ | | EPMA composition: $Hf_{47.6}Nb_{15.1}As_{37.3}$ | | | |
| Lattice parameters [Å] | a = 26.9908(2)<br>b = 3.6221(2)<br>c = 12.1068(8) | Cell volume [Å$^3$]: 1183.61(1) | Space group: *Pnma* (62) | | Fraction: 86.0% | $R_{Bragg}$: 1.89 |

| Site | Mpl. | x | y | z | Atom | Site fr. | B(eq.) |
|---|---|---|---|---|---|---|---|
| Hf1 | 4c | 0.1040(1) | 1/4 | 0.5644(3) | Hf | 0.84(2) | 0.18(4) |
| | | | | | Nb | 0.16(2) | |
| Hf2 | 4c | 0.1219(1) | 1/4 | 0.2849(3) | Hf | 1.00(2) | |
| | | | | | Nb | 0.00(2) | |
| Hf3 | 4c | 0.1376(1) | 1/4 | 0.8458(2) | Hf | 1.00(2) | |
| | | | | | Nb | 0.00(2) | |
| Hf4 | 4c | 0.2271(1) | 1/4 | 0.6122(2) | Hf | 0.80(2) | |
| | | | | | Nb | 0.20(2) | |
| Hf5 | 4c | 0.2591(1) | 1/4 | 0.3352(2) | Hf | 1.00(2) | |
| | | | | | Nb | 0.00(2) | |
| Hf6 | 4c | 0.3239(1) | 1/4 | 0.9593(3) | Hf | 0.37(2) | |
| | | | | | Nb | 0.63(2) | |
| Hf7 | 4c | 0.3501(1) | 1/4 | 0.5515(2) | Hf | 0.98(2) | |
| | | | | | Nb | 0.02(2) | |
| Hf8 | 4c | 0.4553(1) | 1/4 | 0.6976(3) | Hf | 0.25(2) | |
| | | | | | Nb | 0.75(2) | |
| Hf9 | 4c | 0.4686(1) | 1/4 | 0.4138(2) | Hf | 0.96(2) | |
| | | | | | Nb | 0.04(2) | |
| Hf10 | 4c | 0.4976(1) | 1/4 | 0.1108(3) | Hf | 0.84(2) | |
| | | | | | Nb | 0.16(2) | |
| As1 | 4c | 0.0503(2) | 1/4 | 0.7493(5) | As | 1 | 0.29(7) |
| As2 | 4c | 0.0771(2) | 1/4 | 0.0502(5) | As | 1 | |
| As3 | 4c | 0.2215(2) | 1/4 | 0.9917(5) | As | 1 | |
| As4 | 4c | 0.3025(2) | 1/4 | 0.7444(5) | As | 1 | |
| As5 | 4c | 0.3391(2) | 1/4 | 0.1866(5) | As | 1 | |
| As6 | 4c | 0.4269(2) | 1/4 | 0.9176(5) | As | 1 | |

| Niobium content calculated from site fractions: 13% at. | Crystallite size (Lorenzian) [nm]: 153(1) | Preferred Orientation spherical harmonics order: none |
|---|---|---|

**Table 23. Rietveld refinement results for the $M_5As_3$ phase in sample S20**

| Sample: S20 | Nominal composition: $Hf_{27.5}Nb_{27.5}As_{45.0}$ | | | $R_p$: 3.58 | | $R_{wp}$: 4.88 | |
|---|---|---|---|---|---|---|---|
| Background model: Chebyshev, 4th order | | | | 2$\theta$-range [°]: 10 - 120° | | | |
| Main phase: $(Hf,Nb)_5As_3$ | Structure type: $Nb_5As_3$ | | | EPMA composition: $Hf_{31.5}Nb_{30.9}As_{37.6}$ | | | |
| Lattice parameters [Å] | a = 26.5978(5)<br>b = 3.5901(1)<br>c = 11.9271(2) | Cell volume [Å$^3$]: 1138.92(3) | | Space group: *Pnma* (62) | Fraction: 84.9% | $R_{Bragg}$: 1.92 | |
| Site | Mpl. | x | y | z | Atom | Site fr. | B(eq.) |
| Hf1 | 4c | 0.1058(2) | 1/4 | 0.5684(5) | Hf | 0.53(2) | 0.21(3) |
| | | | | | Nb | 0.47(2) | |
| Hf2 | 4c | 0.1212(2) | 1/4 | 0.2846(4) | Hf | 0.83(2) | |
| | | | | | Nb | 0.17(2) | |
| Hf3 | 4c | 0.1364(2) | 1/4 | 0.8509(4) | Hf | 0.68(2) | |
| | | | | | Nb | 0.32(2) | |
| Hf4 | 4c | 0.2247(2) | 1/4 | 0.6144(4) | Hf | 0.26(2) | |
| | | | | | Nb | 0.74(2) | |
| Hf5 | 4c | 0.2590(2) | 1/4 | 0.3384(3) | Hf | 1.00(2) | |
| | | | | | Nb | 0.00(2) | |
| Hf6 | 4c | 0.3234(2) | 1/4 | 0.9631(5) | Hf | 0.24(2) | |
| | | | | | Nb | 0.76(2) | |
| Hf7 | 4c | 0.3505(2) | 1/4 | 0.5529(5) | Hf | 0.42(2) | |
| | | | | | Nb | 0.58(2) | |
| Hf8 | 4c | 0.4537(2) | 1/4 | 0.6970(6) | Hf | 0.08(2) | |
| | | | | | Nb | 0.92(2) | |
| Hf9 | 4c | 0.4682(2) | 1/4 | 0.4116(4) | Hf | 0.76(2) | |
| | | | | | Nb | 0.24(2) | |
| Hf10 | 4c | 0.4976(2) | 1/4 | 0.1090(4) | Hf | 0.73(2) | |
| | | | | | Nb | 0.27(2) | |
| As1 | 4c | 0.0495(3) | 1/4 | 0.7467(7) | As | 1 | 0.3 (fixed) |
| As2 | 4c | 0.0760(3) | 1/4 | 0.0484(8) | As | 1 | |
| As3 | 4c | 0.2201(3) | 1/4 | 0.9952(8) | As | 1 | |
| As4 | 4c | 0.3026(3) | 1/4 | 0.7450(8) | As | 1 | |
| As5 | 4c | 0.3407(3) | 1/4 | 0.1855(7) | As | 1 | |
| As6 | 4c | 0.4253(3) | 1/4 | 0.9187(7) | As | 1 | |
| Niobium content calculated from site fractions: 28% at. | | Crystallite size (Lorenzian) [nm]: 85(1) | | Preferred Orientation spherical harmonics order: none | | | |

**Table 24. Rietveld refinement result for the minor phase HfAs**

| Structure type: TiAs | | | Space group: $P6_3/mmc$ | | |
|---|---|---|---|---|---|
| Sample | Lattice parameters [Å] | Cell volume [Å$^3$] | Crystallite size (Lorenzian) [nm] | $R_{Bragg}$ | Fraction: |
| S23 | a = 3.7681(1)<br>c = 12.7021(4) | 156.19(1) | 100 (fixed) | 0.933 | 12.1%(1) |
| S20 | a = 3.7728(1)<br>c = 12.6818(3) | 156.33(1) | 100 (fixed) | 1.562 | 13.1%(1) |

**Table 25. The comparison of the niobium site fractions found in $M_5As_3$ phase**

| Sample | Niobium site fraction on the given site [%] | | | | | | | | | |
|---|---|---|---|---|---|---|---|---|---|---|
| | M1 | M2 | M3 | M4 | M5 | M6 | M7 | M8 | M9 | M10 |
| S23 | 16 | 0 | 0 | 20 | 0 | 63 | 2 | 75 | 4 | 16 |
| S20 | 47 | 17 | 32 | 74 | 0 | 76 | 58 | 92 | 24 | 27 |

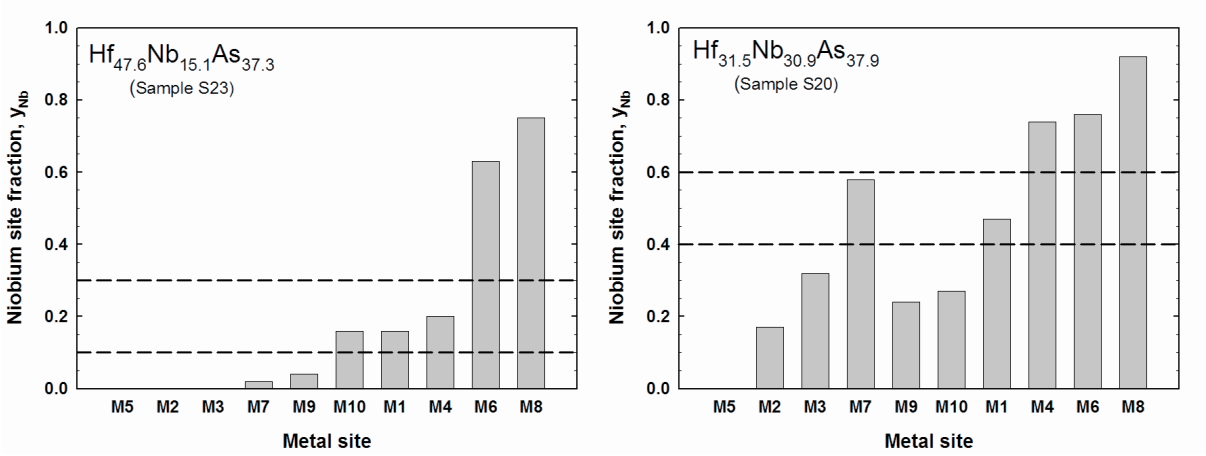


**Fig. 46. The niobium site fractions measured in $M_5As_3$ samples**

A diagram showing the niobium site fractions for metal sites is given in Fig. 46. As it can be seen, the order of the filling of this sites by niobium is somewhat different in both samples (e.g. $y_{Nb}^{M10} > y_{Nb}^{M3}$ for S23, but $y_{Nb}^{M10} < y_{Nb}^{M3}$ for S20). While the author does not consider such an exchange impossible, it seems to be more reasonable to assume that the differences reflect the limitations of refinement. Therefore, the substituted sites were classified into groups according to the niobium fraction. In sample S23 one can distinguish three site groups:

- the sites with large niobium occupation (over 30%, these are M6 and M8)
- the sites with small niobium occupation (between 10 and 30%, these are M1, M4 and M10)

- the sites with negligible niobium occupation (less than 10%, these are M2, M3, M5, M7, M9)

In sample S20 one can distinguish between four site groups:

- the sites with large niobium occupation (over 60%, these are M4, M6 and M8)
- the sites with medium niobium occupation (between 40 and 60%, these are M1 and M7)
- the sites with small niobium occupation (between 10 and 40%, these are M2, M3, M9 and M10)
- the sites with negligible niobium occupation (less than 10%, this is only M5)

Comparing these groups, one can conclude that the sites M6 and M8 (especially) are preferred by niobium in this structure, while M2, M3, M5 (especially) and M9 are the ones where the hafnium atoms are mostly found.

The volumes of the Voronoi polyhedra around the metal sites of the $M_5As_3$ structure for the structure data obtained from Rietveld refinement of samples S20 and S23 are given in Table 26 (the coordination spheres of the metal sites of the binary $Nb_5As_3$ are depicted in Appendix A.4 – these do not differ qualitatively from the ones of the ternary samples). The diagrams showing the site volumes and the niobium site fractions for both of the samples are given in Fig. 47. In case of sample S20, it can be clearly seen, that the sites with the smaller volume contain more niobium. In case of sample S23, there is no such clear distinction, as the sites M4 and M10 are found on the extrema of the diagram (i.e. they have the smallest and the largest volume, respectively) but are substituted with niobium to a similar extent. But also here, the niobium-richest sites M6 and M8 are the ones with the smallest volume (after M4). This would indicate that the size factor influences the substitution in this compound, i.e. hafnium atoms having a greater atomic radius than niobium, prefer to occupy the sites with a larger volume.

For both of the ternary structures, Pauling bond orders were calculated on the basis of the refined structure data and summarised for each metal site, yielding the cumulated PBOs. The results are given in Table 27 and the dependence of the site fraction and the cumulated PBOs are shown in Fig. 48. Although no clear correlation is observed, a certain tendency could be seen. In case of sample S20, the niobium richer sites have usually larger values of the sums (above 5.2), but the hafnium richest site M5 has the value comparable with the niobium dominated sites M4 and M6. For sample S23, the niobium richest sites also cannot be

**Table 26. The volumes of Voronoi polyhedra around metal sites of the $M_5As_3$ structure based on the refined data from samples S20 and S23 (in Å$^3$).**

| Site | S20 | S23 |
|---|---|---|
| M1 | 17.62 | 18.65 |
| M2 | 18.66 | 19.43 |
| M3 | 19.39 | 20.13 |
| M4 | 17.41 | 18.06 |
| M5 | 18.87 | 19.27 |
| M6 | 17.62 | 18.46 |
| M7 | 18.18 | 19.11 |
| M8 | 17.78 | 18.47 |
| M9 | 18.967 | 19.67 |
| M10 | 19.66 | 20.29 |

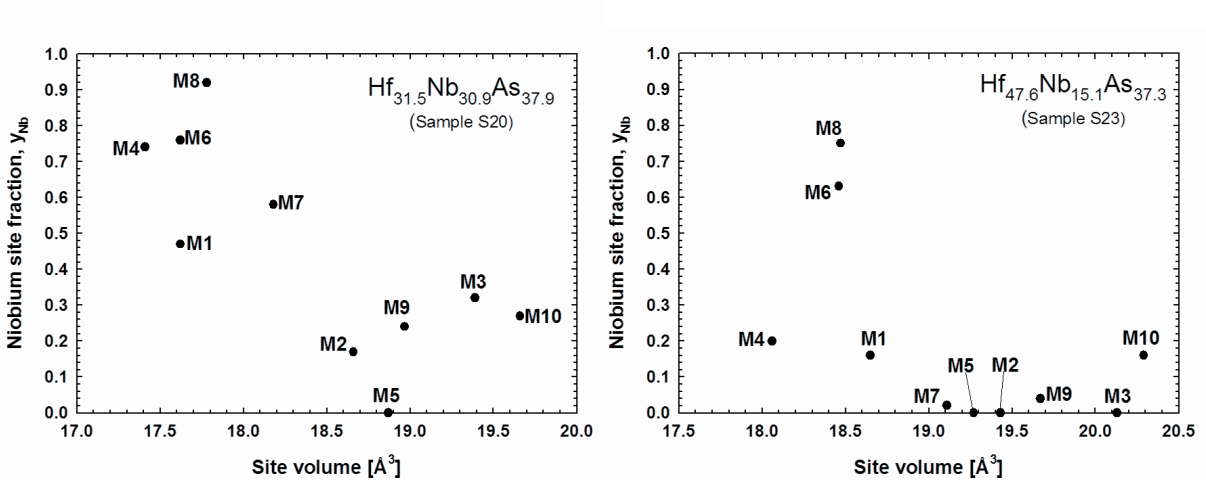


**Fig. 47. Comparison of the site volumes and the niobium site fractions calculated for $M_5As_3$ phase from the refined data – sample S20 (bottom left), sample S23 (bottom right)**

**Table 27. The values of cumulated PBOs of the metal sites for samples S20 and S23. The populations were calculated by summing the Pauling bond orders in the first coordination sphere of each metal site.**

| Site | S20 | | S23 | |
|---|---|---|---|---|
| | All bonds | Metal-metal bond (fraction of all bonds) | All bonds | Metal-metal bond (fraction of all bonds) |
| M1 | 6.05 | 1.98 (0.33) | 5.63 | 1.95 (0.35) |
| M2 | 5.37 | 2.37 (0.44) | 5.03 | 2.26 (0.45) |
| M3 | 4.72 | 1.59 (0.34) | 4.98 | 1.65 (0.33) |
| M4 | 5.74 | 2.09 (0.36) | 6.28 | 2.09 (0.33) |
| M5 | 5.77 | 1.47 (0.25) | 5.53 | 1.47 (0.27) |
| M6 | 5.79 | 3.48 (0.60) | 5.42 | 3.35 (0.62) |
| M7 | 5.30 | 1.45 (0.27) | 5.72 | 1.58 (0.28) |
| M8 | 5.35 | 2.68 (0.50) | 5.09 | 2.56 (0.50) |
| M9 | 4.97 | 1.62 (0.33) | 4.79 | 1.72 (0.36) |
| M10 | 4.27 | 1.46 (0.34) | 4.05 | 1.42 (0.35) |

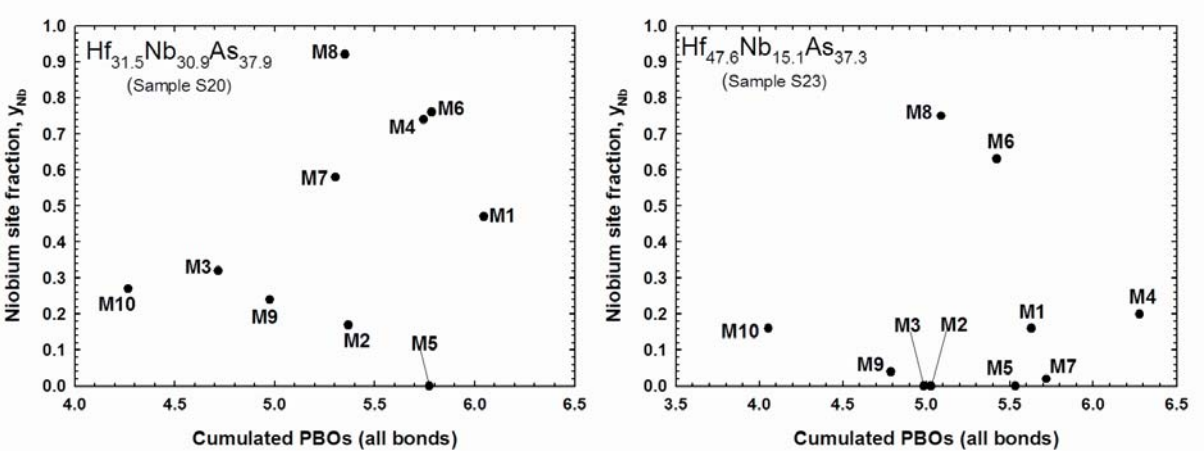


**Fig. 48. Comparison of the cumulated PBOs of all bonds and the niobium site fractions of the metal sites for samples S20 and S23.**

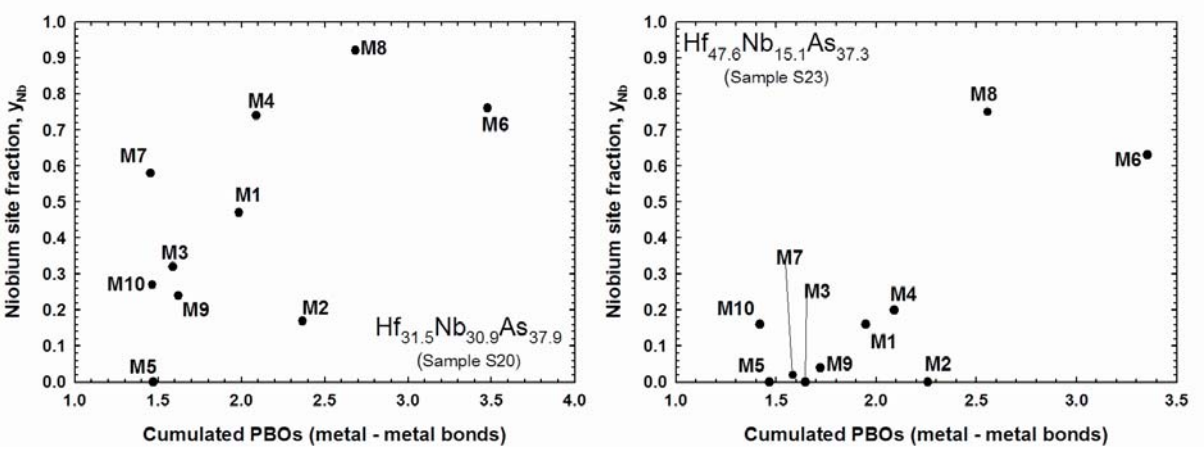


**Fig. 49. Comparison of the niobium site fractions and the the cumulated PBOs of metal-metal bonds for the metal sites in samples S20 and S23.**

distinguished by this parameter value. A somewhat better correlation is observed, if only the PBOs for metal-metal bonding are considered which is shown in Fig. 49. Here, the niobium richest M6 and M8 sites are characterised by the largest values of this parameter, suggesting the influence of the metal-metal bonding on the niobium occupation.

It seems possible to rationalise the hafnium substitution with regard of both the site volumes and the electron population involved in metal-metal bonding. As already mentioned (chapter 1.3), a smaller atomic radius is given for niobium (134.2 pm) than for hafnium (144.2 pm) [98]. Also a larger sublimation enthalpy value is reported for niobium (733.0 kJ/mol) than for hafnium (619.2 kJ/mol), suggesting a niobium preference to occupy the sites where more metal-metal bonding can be formed, as this would be energetically favourable [7]. One example would be the sites M1 and M4 having comparable or smaller volumes than M6 and M8, where the lower values of PBOs for metal-metal bonds seems to justify the lower niobium site fractions. Another example would be sites M1 and M10 having comparable values of PBOs for metal-metal bonds, but the larger volume of the latter one is probably a reason for its higher hafnium content. Thus, the site preferences are believed to be not determined by only one of the factors, but are rather a result of a compromise between both of them.

### 4.1.1.3 $Hf_2As$ – $Nb_2As$ line

As mentioned in chapter 4.1.1.1, a new binary compound with the composition of $Nb_2As$ was found. As the Gibbs phase rule was violated in all samples containing this phase (S10, S11, S12), it might be, that the phase is actually not in equilibrium at 1400°C. The phase was found to be isostructural with $Nb_2P$ (*oP*54, [114], see Appendix D.1). The powder pattern of sample S11 which had the highest content of this new binary phase, is shown in Fig. 50. The

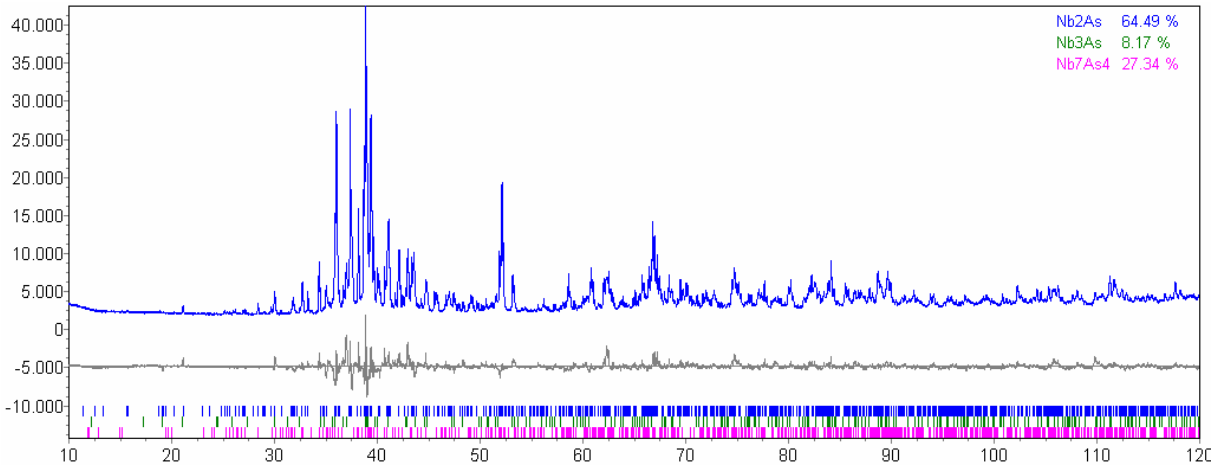


**Fig. 50. Experimental powder pattern for sample S11 including difference curve (bottom line) and Bragg positions (vertical bars).**

phase was not observed in any ternary samples so that a minor Hf solubility is assumed (~1 at.%).

The other binary compound $Hf_2As$ of $Ta_2P$-type was confirmed. It was found in two binary samples (S4, S5) and one ternary (S27). The compound was found to dissolve up to 2 at.% niobium.

Two ternary compounds containing 33.3 at.% As were also found. $Hf_{3+x}Nb_{1-x}As_2$ ($0.29<x<0.61$) with a niobium content in the range 7-12 at.% was detected in five samples (S28, S29, S34, S35, S40). Only one of them (S40) contained two phases but $Hf_{3+x}Nb_{1-x}As_2$ was the minor one, while four other samples were three-phase samples. The phase was found to be isostructural with $Zr_2P$ (*oC*108, [115], see Appendix D.2). The powder pattern of the sample S34 (three phases and $HfO_2$, $Hf_{3+x}Nb_{1-x}As_2$ majority) is shown in Fig. 51.

$Hf_{1+x}Nb_{1-x}As$ ($-0.06<x<0.42$) with a niobium content in the range of 20-36 at.% was found in seven samples (S29, S30, S31, S35, S36, S37, S38). The phase was found to be isostructural with $Co_2Si$ (*oP*12, [116], see Appendix D.3). Two of the samples were the three-phase samples (S29, S35), while the other ones contained only two phases but in all cases the

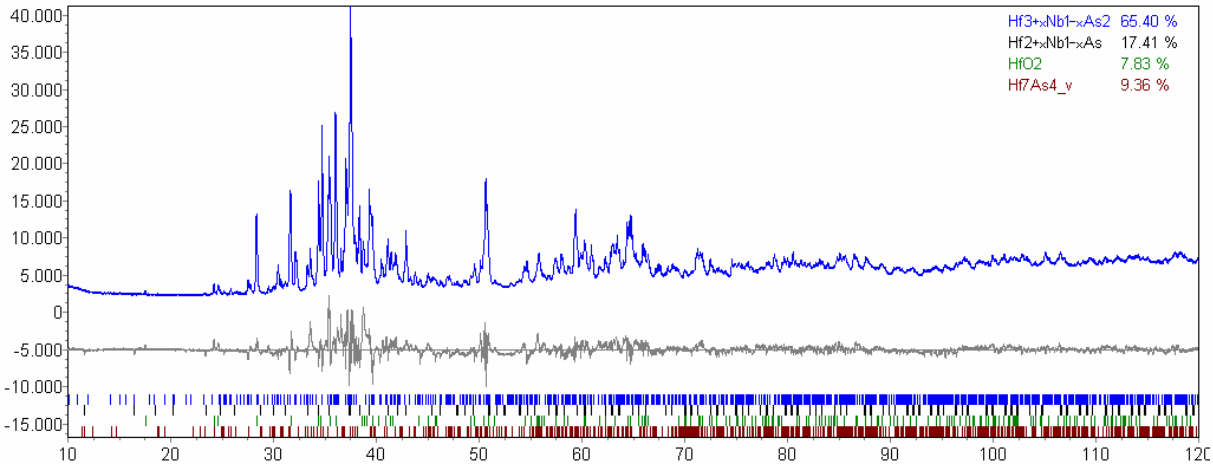


**Fig. 51. Experimental powder pattern for sample S34 including difference curve (bottom line) and Bragg positions (vertical bars).**

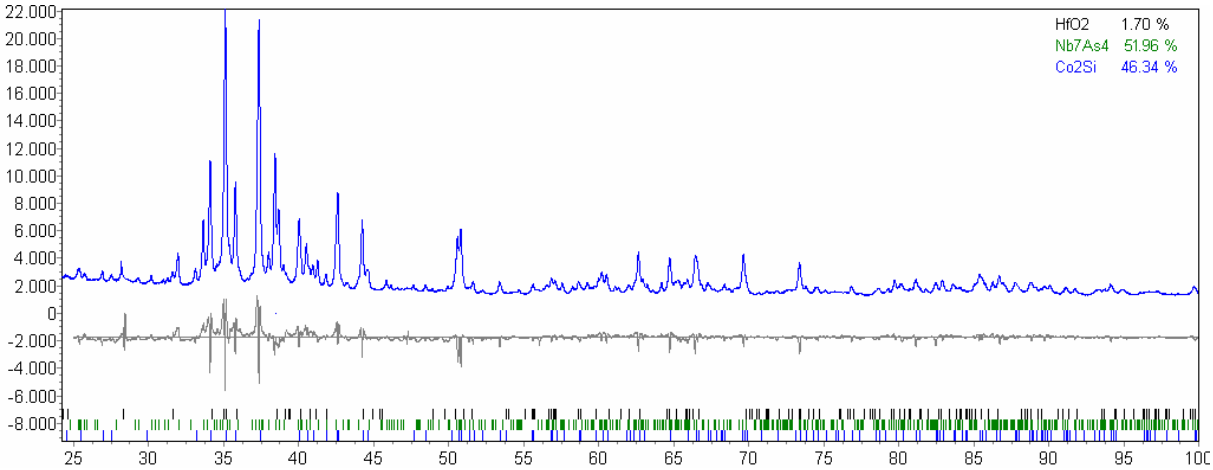


**Fig. 52. Experimental powder pattern for sample S31 including difference curve (bottom line) and Bragg positions (vertical bars).**

$Hf_{1+x}Nb_{1-x}As$ content was too small for the refinement of site occupations. The powder pattern of sample S31 which had the highest content of this new phase is shown in Fig. 52.

No single crystals of any $M_2As$ phase were found. All new structures can be described as an arrangement of the trigonal prisms formed by the metal atoms around the arsenic atoms, in the same way, as in the case of the binary structures described in chapter 2.4.1. All of these were also predicted in the published structure maps for $M_2Q$ phases [79], discussed in chapter 2.3.1.

#### 4.1.1.4 $Hf_{4-x}Nb_{3+x}As_3$ phase

One of the new ternary phases found is $Hf_{4-x}Nb_{3+x}As_3$ ($-0.08<x<1.62$) with a niobium content in range of 29-46% at. This phase was found in eight samples (S32, S36, S37, S38, S39, S41, S44, S45). A single crystal was isolated from sample S45 and the refinement results are given in Table 28.

The structure can be described with an orthorombic cell (Fig. 53), with one axis (*b*) of the very short length, similar to the other reported metal-rich arsenides, but the structure type is unique. As in the case of the other metal-rich arsenides, it is possible to describe this structure as an arrangement of arsenic-centered trigonal prisms (Fig. 54). All prisms are stacked in [010] direction. The metal atoms on one of the sites (M5) are surrounded by eight other metal atoms in the distance range of 2.86–3.19 Å forming a distorted body centered cube. Additionally, metal sites M1, M2 and M4 are surrounded by six metal and two arsenic atoms forming a bcc-like coordination. The coordination spheres of the metal sites are shown in Fig. 55.

Site occupation data obtained from the single crystal refinement show the presence of niobium on M1, M2, M4 and M5 sites, whereby the niobium site fractions on the M1 and M4 sites (0.83 and 0.81 respectively) are slightly larger than the ones on the M2 and M5 sites (0.72 and 0.74). On the remaining three metal sites, only hafnium atoms are found.

**Table 28. Single crystal data obtained from the measurement performed on $Hf_{3.89}Nb_{3.11}As_3$ crystal**

| | | | | | | | |
|---|---|---|---|---|---|---|---|
| Sample: S45 | | | Nominal sample composition: $Hf_{26.7}Nb_{53.3}As_{20}$ | | | | |
| Empirical formula: $Hf_{3.89}Nb_{3.11}As_3$ | | | Formula weight: 1208.30 | | | | |
| Calculated density: 11.051 Mg/m$^3$ | | | Structure type: new | | | | |
| Unit cell dimensions: | a | 17.964(3) Å | Crystal system: orthorhombic | | | | |
| | b | 3.5869(7) Å | Space group: *Pnma* (no. 62) | | | | |
| | c | 11.262(2) Å | Pearson symbol: *oP*40 | | | | |
| | V | 725.7(2) Å$^3$ | Z = 4 | | | | |
| Wavelength: 0.71073 Å (Mo Kα radiation) | | | Theta range for data collection: 2.90 – 27.48° | | | | |
| Absorption coefficient: 73.496 mm$^{-1}$ | | | Temperature: 293(2) K | | | | |
| Total number of the measured reflections: 5389 | | | Number of reflections with I>2σ(I): 965 | | | | |
| Number of refined parameters: 66 | | | | | | | |
| "R" – values for data with I>2σ(I) | | | "R" – values for all data | | | | |
| R : 0.0551 | | $R_w$ : 0.1364 | R : 0.0656 | | $R_w$ : 0.1407 | | |
| Values for index of measured data: h = -23 → 23, k = -4 → 3, l = -14 → 14 | | | | | | | |
| Goodness of fit for refinement reflections: 1.073 | | | Extinction coefficient: 0.00000(9) | | | | |
| Maximum/minimum values of final difference map: 6.761; -5.784 eÅ$^{-3}$ | | | | | | | |

| | Site | Wyckoff position | x | y | z | U(eq) [pm$^2$] | $y_{Nb}$ ($y_{Hf}$ = 1- $y_{Nb}$) |
|---|---|---|---|---|---|---|---|
| Atom positions | M1 | 4*c* | 0.0874(1) | 1/4 | 0.1811(2) | 0.9(1) | 0.83(1) |
| | M2 | 4*c* | 0.1310(1) | 1/4 | 0.6096(2) | 1.0(1) | 0.72(1) |
| | M3 | 4*c* | 0.2396(1) | 1/4 | 0.0026(1) | 1.0(1) | 0.00(1) |
| | M4 | 4*c* | 0.2925(1) | 1/4 | 0.7207(2) | 0.9(1) | 0.81(1) |
| | M5 | 4*c* | 0.3236(1) | 1/4 | 0.2944(2) | 0.9(1) | 0.74(1) |
| | M6 | 4*c* | 0.4408(1) | 1/4 | 0.9160(1) | 1.2(1) | 0.00(1) |
| | M7 | 4*c* | 0.5410(1) | 1/4 | 0.6162(1) | 1.1(1) | 0.00(1) |
| | As1 | 4*c* | 0.1745(2) | 1/4 | 0.3816(2) | 0.6(1) | --- |
| | As2 | 4*c* | 0.3795(2) | 1/4 | 0.5181(2) | 0.7(1) | --- |
| | As3 | 4*c* | 0.4629(2) | 1/4 | 0.1890(2) | 0.8(1) | --- |

| | Site | $U_{11}$ | $U_{22}$ | $U_{33}$ | $U_{23}$ | $U_{13}$ | $U_{12}$ |
|---|---|---|---|---|---|---|---|
| Anisotropic displacement parameters (Å$^2$ * 10$^3$) | M1 | 12(1) | 14(1) | 8(1) | 0 | -1(1) | 0 |
| | M2 | 12(1) | 12(1) | 7(1) | 0 | 1(1) | 0 |
| | M3 | 11(1) | 15(1) | 9(1) | 0 | 0(1) | 0 |
| | M4 | 11(1) | 11(1) | 6(1) | 0 | 1(1) | 0 |
| | M5 | 11(1) | 11(1) | 5(1) | 0 | 0(1) | 0 |
| | M6 | 10(1) | 11(1) | 8(1) | 0 | 0(1) | 0 |
| | M7 | 9(1) | 12(1) | 6(1) | 0 | -1(1) | 0 |
| | As1 | 5(2) | 10(1) | 4(1) | 0 | -1(1) | 0 |
| | As2 | 8(2) | 7(1) | 5(1) | 0 | -3(1) | 0 |
| | As3 | 9(2) | 7(1) | 7(1) | 0 | 0(1) | 0 |

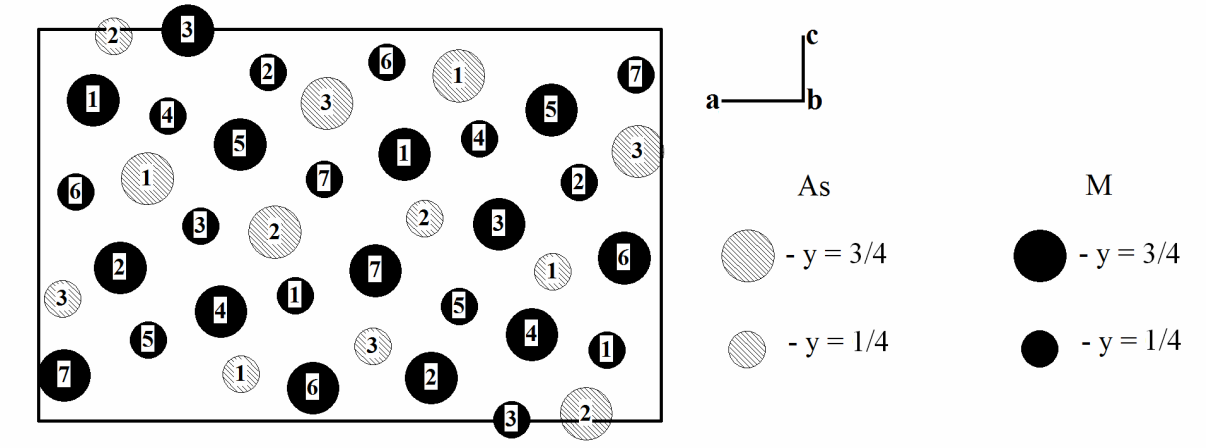


**Fig. 53. The unit cell of $Hf_{4-x}Nb_{3+x}As_3$ - view in $[0\bar{1}0]$ direction**

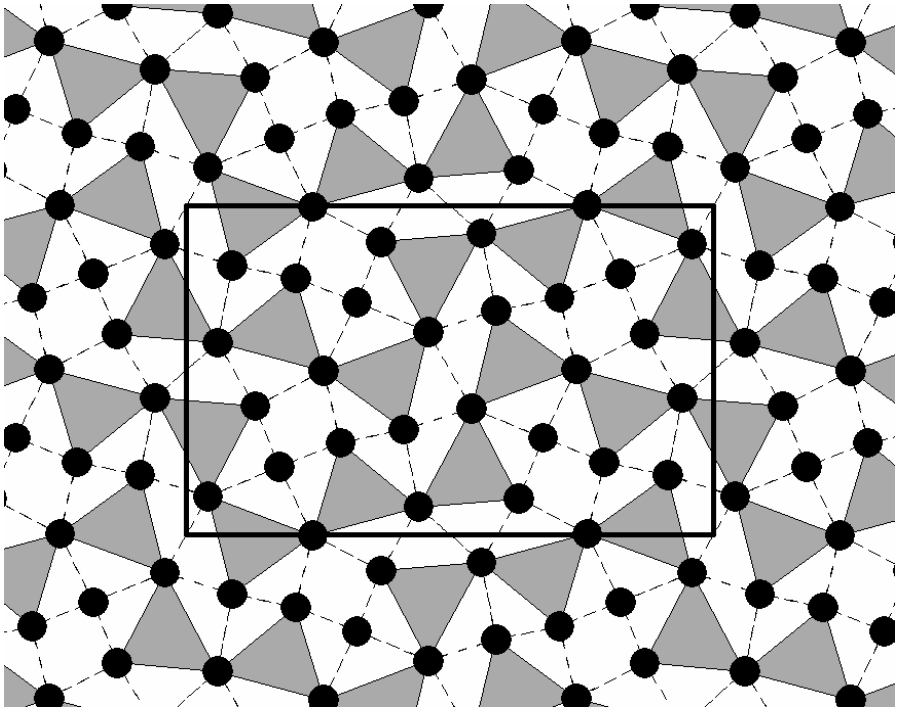

**Fig. 54. The unit cell of $Hf_{4-x}Nb_{3+x}As_3$ shown as a combination of trigonal prisms – view in $[0\bar{1}0]$ direction**

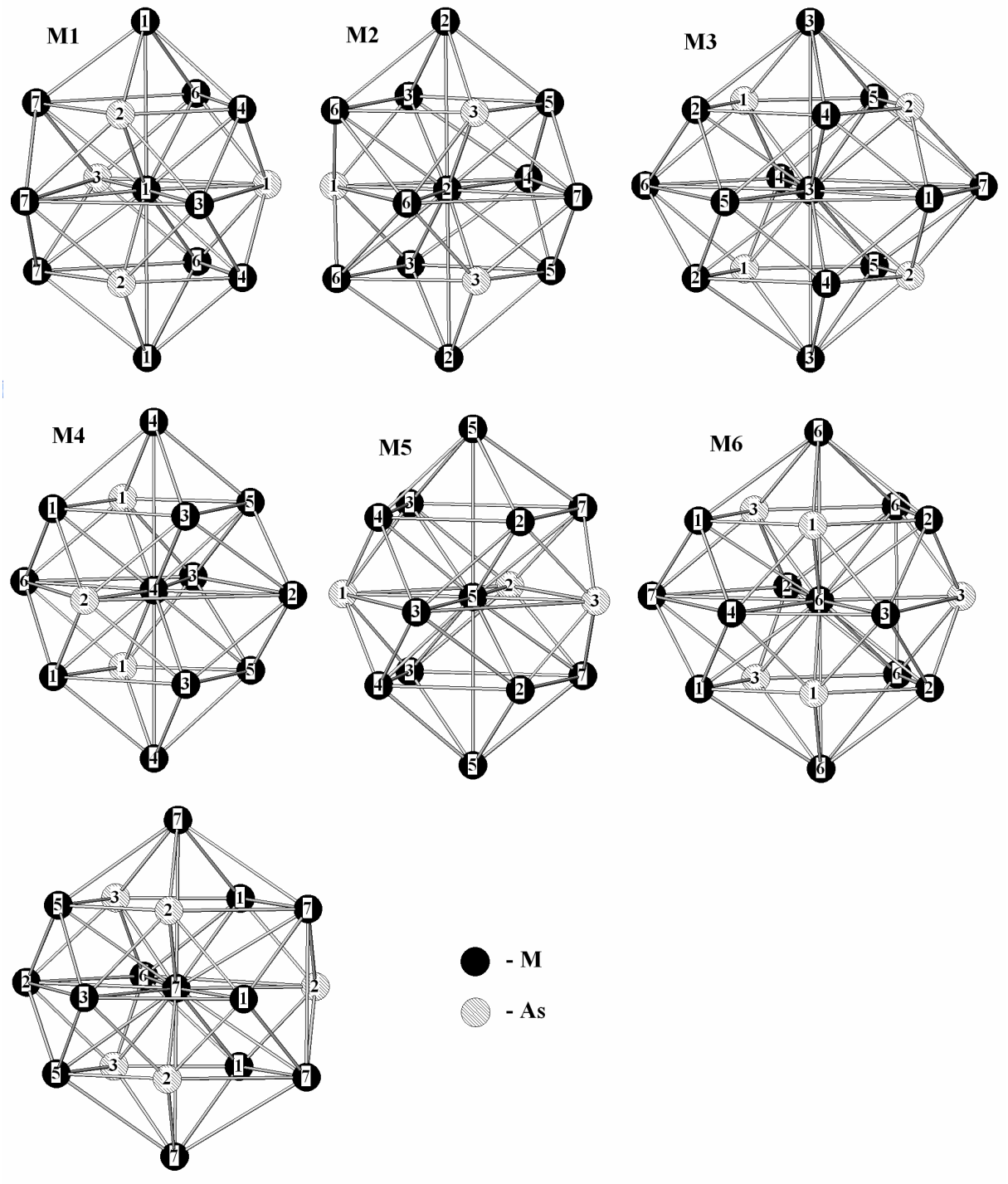


**Fig. 55. The coordination spheres of the metal sites in $Hf_{4-x}Nb_{3+x}As_3$ compound.**

The site volumes calculated for the refined structure data are given in Table 29. The diagram showing the site volumes and the niobium site fractions for various metal sites in $Hf_{4-x}Nb_{3+x}As_3$ structure is given in Fig. 56. One notices immediately, that the sites occupied by hafnium only, are the ones with the greatest volume. Additionally, the sites with the higher values of the niobium site fractions (M1 and M4) are still smaller than the ones with the slightly lower niobium content (M2 and M5). This would indicate that the smaller size of the niobium atoms plays an important role in the distribution of the hafnium and niobium atoms among the available metal sites.

**Table 29. The volumes of Voronoi polyhedra around metal sites of the $Hf_{4-x}Nb_{3+x}As_3$ structure calculated for the refined data from samples S45.**

| Site | Site volume [Å$^3$] |
|---|---|
| M1 | 17.86 |
| M2 | 18.63 |
| M3 | 19.59 |
| M4 | 17.69 |
| M5 | 18.78 |
| M6 | 19.94 |
| M7 | 20.04 |

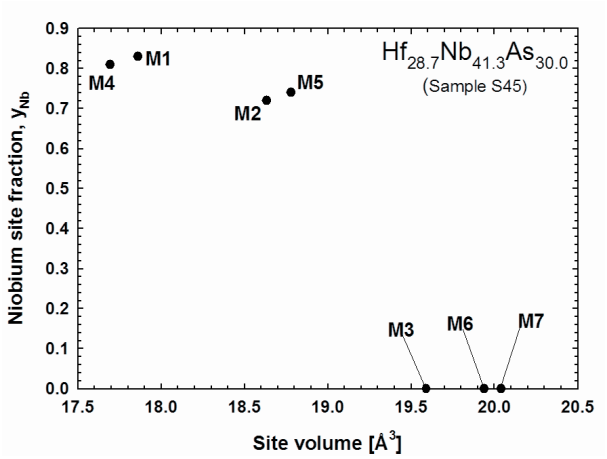


**Fig. 56. Comparison of the site volumes and the niobium site fractions calculated for the $Hf_{4-x}Nb_{3+x}As_3$ phase from the refined data of sample S45.**

The cumulated PBOs calculated for each metal site are given in Table 30, along with the number of electrons involved in metal-metal bonding. As it is shown in Fig. 57, all sites containing niobium are found to have a high value of this parameter. These are also the sites with the greatest value of cumulated PBOs for metal-metal bonding. However, the small differences between the values calculated for the sites M3 ($y_{Nb}$ = 0.00, cumulated PBO = 4.72) and M5 ($y_{Nb}$ = 0.74, cumulated PBO = 4.85) suggest, that the bonding contribution does not play such a significant role in the distribtution of these two elements, as the site volume does.

**Table 30. The values of the cumulated PBOs of the metal sites in $Hf_{4-x}Nb_{3+x}As_3$ for sample S45.**

| Site | All bonds | Metal-metal bond (fraction of all bonds) |
|---|---|---|
| M1 | 5.45 | 2.74 (0.50) |
| M2 | 5.15 | 2.77 (0.54) |
| M3 | 4.72 | 2.12 (0.45) |
| M4 | 5.63 | 3.50 (0.62) |
| M5 | 4.85 | 3.44 (0.71) |
| M6 | 4.46 | 1.69 (0.38) |
| M7 | 4.42 | 1.87 (0.42) |

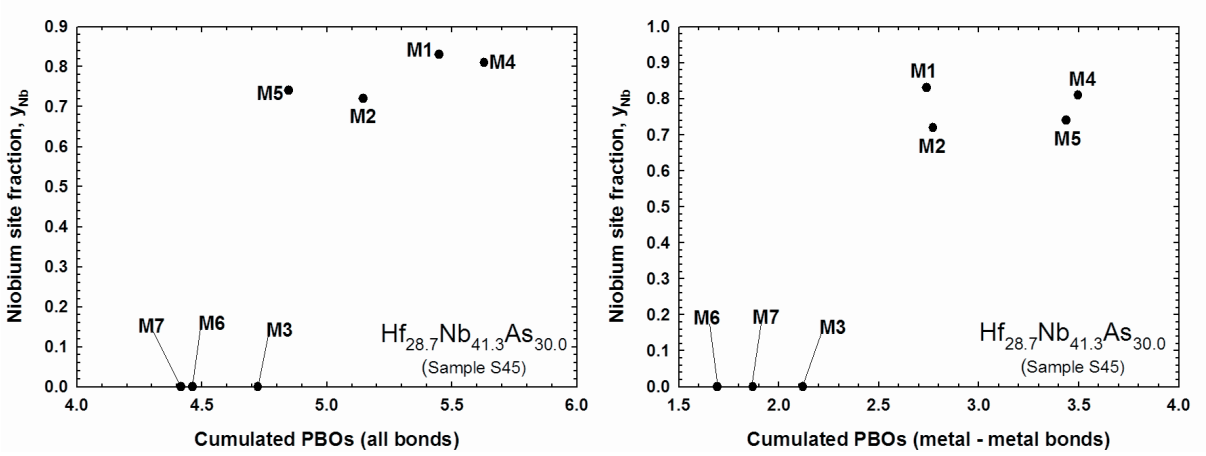


**Fig. 57. Comparison of the cumulated PBOs of all (left) and metal-metal bonds only (right), for the metal sites in the $Hf_{4-x}Nb_{3+x}As_3$ phase (single crystal data from sample S45)**

#### 4.1.1.5 $Hf_{7+x}Nb_{4-x}As_4$ phase

$Hf_{7.23}Nb_{3.77}As_4$ is another ternary phase found during the investigation of the Hf-Nb-As system. It was identified by chance, during the measurement performed on the single crystal picked from sample S43. There was not any diffractogram on which the powder pattern of this phase could be identified, even for the sample S43 from which the crystal was isolated. It is therefore concluded, that this phase is not in equilibrium at 1400°C. The phase itself is isostructural with $Zr_{6.45}Nb_{4.55}P_4$ (*oI*30) compound reported by Marking and Franzen [99] (for structure details see Appendix D.4). This phase is similar to the other metal-rich arsenides, as the trigonal prisms centred on arsenic atoms and formed by metal atoms can be easily distinguished as shown in Fig. 59. Also, a bcc-like coordination of one metal site (M5) is found in this structure. The results of the single crystal refinement are given in Table 31 and the structure is depicted in Fig. 58. The coordination spheres of the metal sites are shown in Fig. 60

Site occupation data obtained from the single crystal refinement show the presence of niobium on M1, M3 and M5 sites, whereby the niobium site fraction on M1 (0.68) is roughly double than the ones on M3 and M5 sites (0.34 and 0.31). The remaining sites are fully occupied by hafnium atoms (M4 with $y_{Nb}$=0.03 is counted to this group). This result is comparable to the data given for $Zr_{6.45}Nb_{4.55}P_4$ [99], where niobium was fully occupying the M1 site and the site fractions for the sites M3 and M5 were 0.06 and 0.42 respectively.

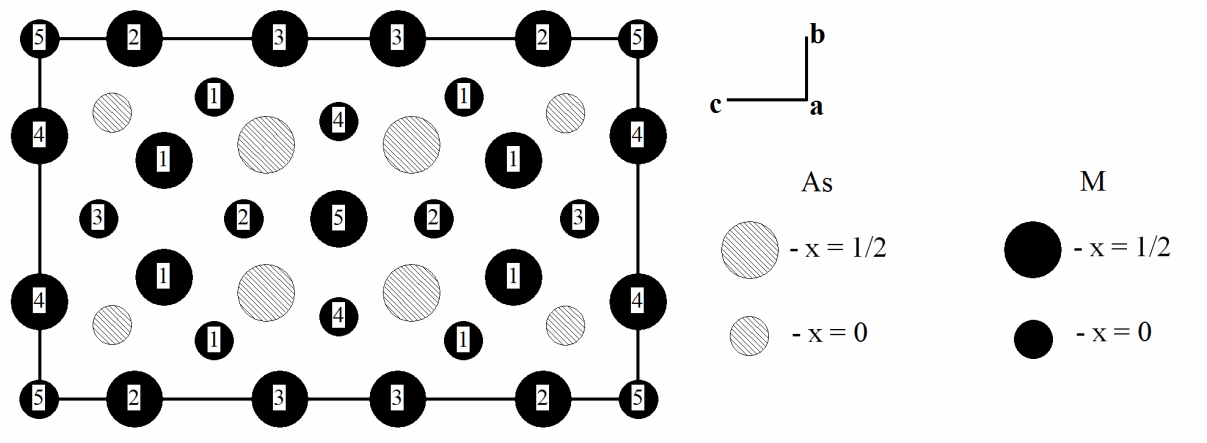


**Fig. 58. The unit cell of $Hf_{7+x}Nb_{4-x}As_4$ - view in [$\bar{1}$00] direction**

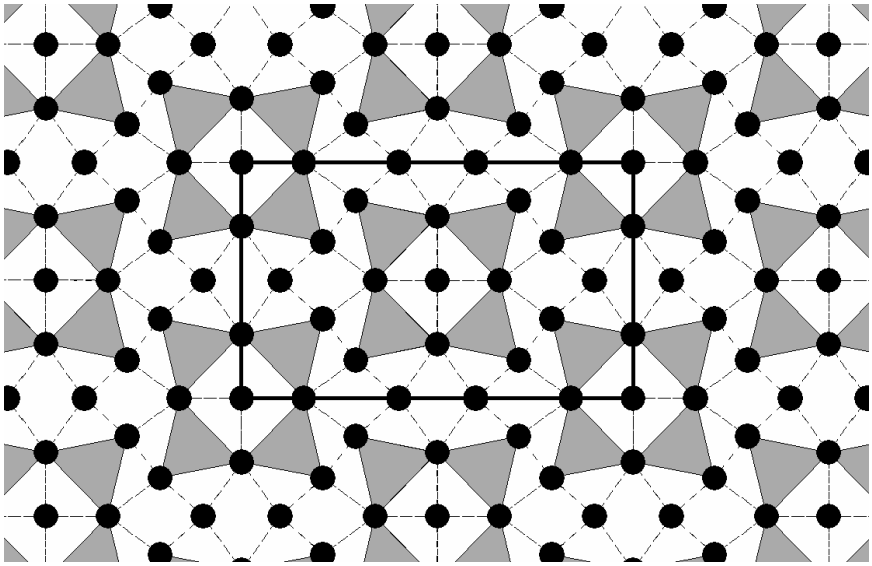

**Fig. 59. The unit cell of $Hf_{7+x}Nb_{4-x}As_4$ shown as a combination of trigonal prisms – view in [$\bar{1}$00] direction**

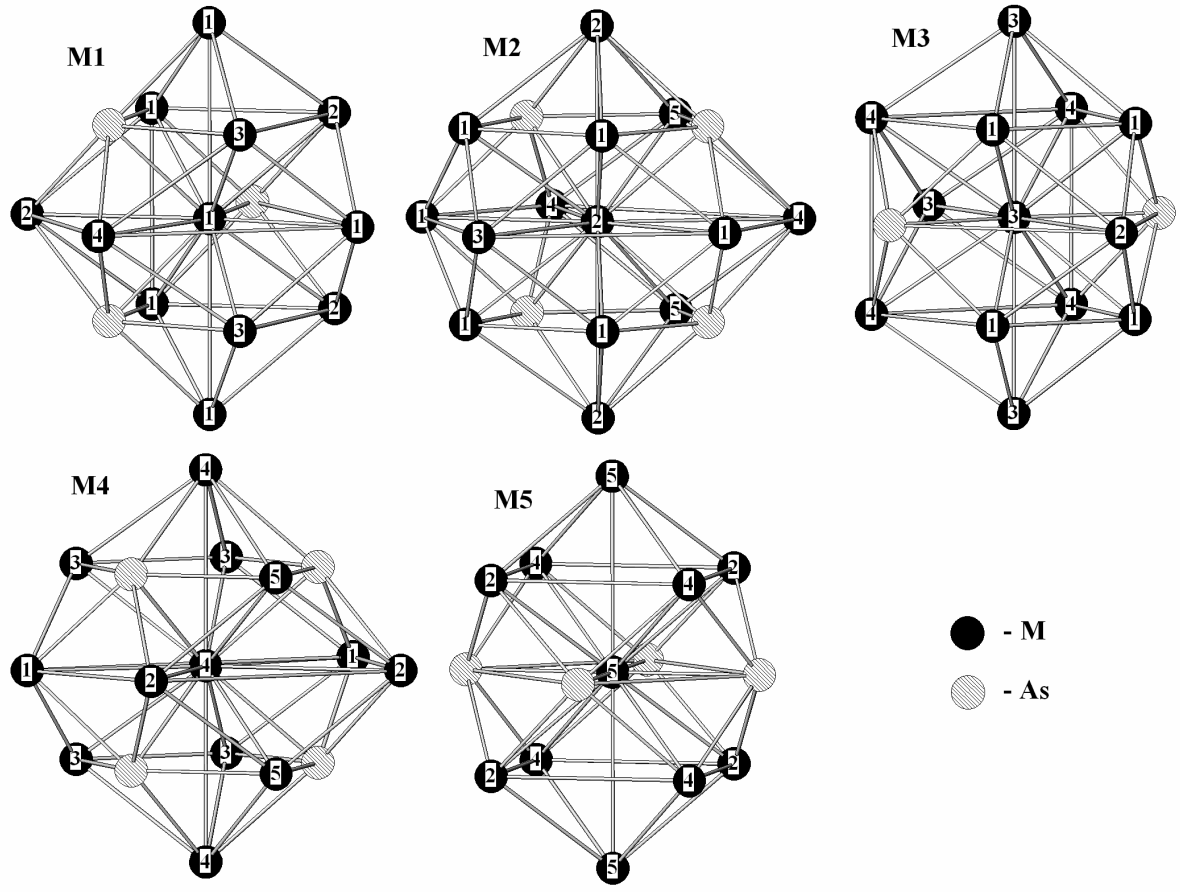


**Fig. 60. The coordination spheres of the metal sites in $Hf_{7+x}Nb_{4-x}As_4$ compound.**

**Table 31. Single crystal data obtained from the measurement performed on $Hf_{7.23}Nb_{3.77}As_4$ crystal**

| | | | | | | | |
|---|---|---|---|---|---|---|---|
| Sample: S43 | | | Nominal sample composition: $Hf_{40.0}Nb_{40.0}As_{20}$ | | | | |
| Empirical formula: $Hf_{7.23}Nb_{3.77}As_4$ | | | | Formula weight: 1939.57 | | | |
| Calculated density: 11.691 $Mg/m^3$ | | | | Structure type: $Zr_{6.45}Nb_{4.55}As_4$ | | | |
| Unit cell dimensions: | a | 3.5825(7) Å | | Crystal system: orthorhombic | | | |
| | b | 9.6162(2) Å | | Space group: *Immm* (no. 71) | | | |
| | c | 16.103(3) Å | | Pearson symbol: *oI*30 | | | |
| | V | 554.74(19) $Å^3$ | | Z = 2 | | | |
| Wavelength: 0.71073 Å (Mo Kα radiation) | | | | Theta range for data collection: 4.24 – 30.10° | | | |
| Absorption coefficient: 84.021 $mm^{-1}$ | | | | Temperature: 293(2) K | | | |
| Total number of the measured reflections: 2580 | | | | Number of reflections with I>2σ(I): 508 | | | |
| Number of refined parameters: 33 | | | | | | | |
| "R" – values for data with I>2σ(I) | | | | "R" – values for all data | | | |
| R : 0.0260 | | $R_w$ : 0.0599 | | R : 0.0339 | | $R_w$ : 0.0628 | |
| Values for index of measured data: h = -5 → 2, k = -13 → 13, l = -22 → 22 | | | | | | | |
| Goodness of fit for refinement reflections: 1.189 | | | | Extinction coefficient: 0.00043(6) | | | |
| Maximum/minimum values of final difference map: 3.734; -3.281 $eÅ^{-3}$ | | | | | | | |

| | Site | Wyckoff position | x | y | z | U(eq) [$pm^2$] | $y_{Nb}$ |
|---|---|---|---|---|---|---|---|
| Atom positions | M1 | 8*l* | 0 | 0.1559(1) | 0.2908(1) | 0.7(1) | 0.68(1) |
| | M2 | 4*j* | 1/2 | 0 | 0.1603(1) | 0.8(1) | 0.00(1) |
| | M3 | 4*j* | 1/2 | 0 | 0.4035(1) | 1.0(1) | 0.34(1) |
| | M4 | 4*h* | 0 | 0.2184(1) | 1/2 | 0.9(1) | 0.03(1) |
| | M5 | 2*a* | 0 | 0 | 0 | 0.7(1) | 0.31(1) |
| | As | 8*l* | 0 | 0.2060(1) | 0.1198(1) | 0.4(1) | --- |

| | Site | $U_{11}$ | $U_{22}$ | $U_{33}$ | $U_{23}$ | $U_{13}$ | $U_{12}$ |
|---|---|---|---|---|---|---|---|
| Anisotropic displacement parameters ($Å^2 * 10^3$) | M1 | 7(1) | 8(1) | 10(1) | 0 | 0 | 0 |
| | M2 | 10(1) | 6(1) | 8(1) | 0 | 0 | 0 |
| | M3 | 8(1) | 16(1) | 8(1) | 0 | 0 | 0 |
| | M4 | 14(1) | 8(1) | 12(1) | 0 | 0 | 0 |
| | M5 | 8(1) | 9(1) | 9(1) | 0(1) | 0 | 0 |
| | As | 4(1) | 4(1) | 6(1) | -1(1) | 0 | 0 |

Again, the influence of the size factor on the site occupations is analysed by comparing the Voronoi polyhedra of the metal sites in this structure (Table 32). The diagram showing the sites of $Hf_{7.23}Nb_{3.77}As_4$ with ascending site volumes is given in Fig. 61. It shows that the niobium- richest site M1 has a much smaller volume (less than 18.5 Å$^3$) than the others (more than 19.5 Å$^3$). On the other hand, one can see that the two other sites occupied by niobium are the largest ones. It is then clear, that the size of metal atom is not a determining factor alone (if at all) for its site preference in this structure.

**Table 32. The volumes of Voronoi polyhedra around metal sites of $Hf_{7.23}Nb_{3.77}As_4$ structure calculated for the refined data from samples S43.**

| Site | Site volume [Å$^3$] |
|---|---|
| M1 | 18.27 |
| M2 | 19.59 |
| M3 | 20.43 |
| M4 | 19.91 |
| M5 | 20.01 |

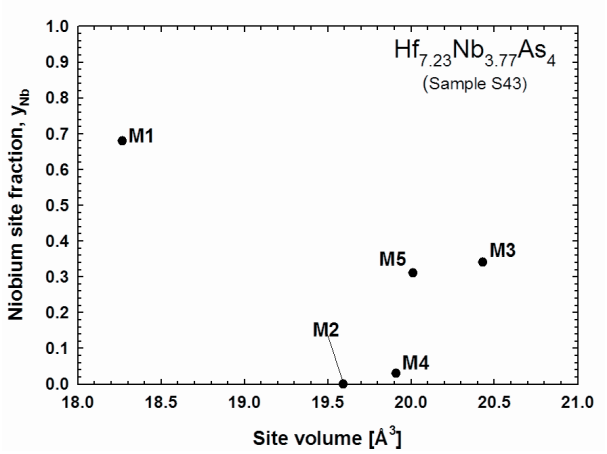


**Fig. 61. Comparison of the site volumes and the niobium site fractions calculated for $Hf_{7.23}Nb_{3.77}As_4$ phase from the refined data of sample S43.**

The cumulated PBOs for all and for the metal-metal bonds for the metal sites in this phase are given in Table 33. The comparison of these values with the niobium site fractions is shown in Fig. 62. The correlation of the cumulated PBOs with the niobium occupancies resembles a mirrored diagram showing the correlation with the site volumes (Fig. 61). An analysis of the PBOs of metal-metal bonds for every metal site shows that the niobium substituted sites M1, M3 and M5 have larger values than the hafnium dominated M2 and M4. This agrees with the trends observed in the $(Hf,Nb)_5As_3$ and $Hf_{4-x}Nb_{3+x}As_3$ phases, described earlier (chapter 4.1.1.2 and 4.1.1.4).

**Table 33. The values of the cumulated PBOs of the metal sites in $Hf_{7.23}Nb_{3.77}As_4$ (sample S43).**

| Site | All bonds | Metal-metal bond (fraction of all bonds) |
|---|---|---|
| M1 | 5.44 | 3.48 (0.64) |
| M2 | 4.95 | 2.21 (0.45) |
| M3 | 4.40 | 3.60 (0.82) |
| M4 | 4.87 | 1.97 (0.41) |
| M5 | 4.55 | 2.26 (0.50) |

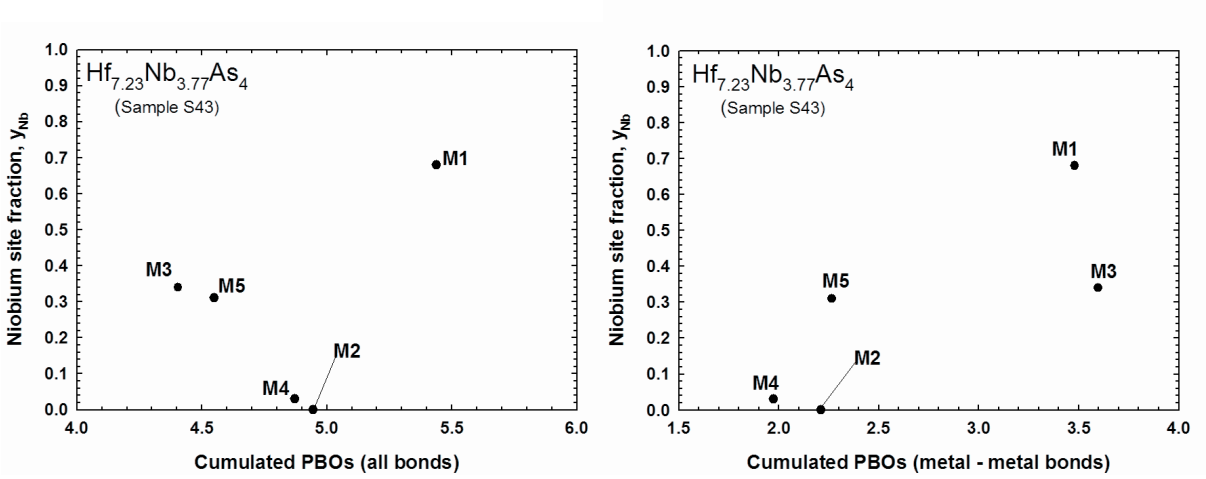


**Fig. 62. Comparison of the the cumulated PBOs of all (left) and metal-metal bonds only (right), for the metal sites in $Hf_{7.23}Nb_{3.77}As_4$ phase (single crystal data from sample S43)**

It must be noted that in this phase the site fractions can be also explained (as in the $(Hf,Nb)_5As_3$ case) in terms of the compromise between the volumes and metal-metal bonding potential of the metal sites. One example confirming this statement is the hafnium preference of the sites M2 and M4 compared to M3 and M5, though the previous ones are larger than the latter and as such, they would "easier accept" the larger hafnium atoms. Comparing the cumulated PBOs of the metal-metal bonding for these sites, the niobium preference for the M3 and M5 sites can be justified by the opportunity of creating more metal-metal bonds which would stabilise the structure, as the niobium has a larger sublimation enthalpy. On the other hand a niobium preference for the M1 site when compared to M3 can be explained by the much smaller site volume of the former (M1 and M3 are found on the extremes of Fig. 61), though the latter has a larger PBO value for metal-metal bonds.

#### 4.1.1.6 $Hf_{3+x}Nb_{3-x}As_2$ phase

On the line connecting the $Hf_3As$ and $Nb_3As$ binary phases, four phases are present. The first one is the binary $Hf_3As$ found only in three binary samples (S3, S5, S6). This phase was not found in any of the ternary samples so that a minor niobium solubility (<5% at.) is assumed. The structure type of $Ta_3As$ was confirmed for this compound.

The existence of the binary $Nb_3As$ with $Ti_3P$ structure type was also confirmed. This phase forms a solid solution extending from the binary compound $Nb_3As$ to a ternary composition limited to 17 at.% Hf. The phase was found in six samples (S11, S12, S13, S32, S33, S39) but none of them was suitable for a precise site occupation refinement.

A very small field of the ternary phase $Hf_{3+x}Nb_{3-x}As_2$ ($0.09<x<0.25$ which is equivalent to the niobium content in the range of 34-36 at.%) with a unique structure type was found. This phase was detected in 3 samples (S41, S43, S44). A single crystal of this phase was isolated from sample S43, so it was possible to determine the structure (Table 34). The unit cell of this phase is orthorhombic (Fig. 63), with one short axis (*b*) as in the other arsenides discussed here. This structure can be simply described as an arsenic-centered trigonal prism arrangement, where all prisms are stacked in [010] direction (Fig. 64). The metal atoms on M1 site are surrounded by eight other metal atoms in the distance range of 2.88 – 3.28 Å and are forming two interpenetrating (distorted) bcc units. The coordination of the metal atoms on M2 site also resembles a bcc unit built of six metal and two arsenic atoms (see Fig. 65 for the coordination spheres of the metal sites).

Site occupation data obtained from the single crystal refinement show the presence of niobium on M1 and M2 sites, leaving M3 site to be occupied predominantly by hafnium. The niobium site fraction on M2 site (0.75) is clearly greater than the one on M1 site (0.49).

**Table 34. Atom positions and niobium site fractions for $Hf_{3.38}Nb_{2.62}As_2$ crystal**

| | | | | | | | |
|---|---|---|---|---|---|---|---|
| Sample: S43 | | | Nominal sample composition: $Hf_{40.0}Nb_{40.0}As_{20}$ | | | | |
| Empirical formula: $Hf_{3.38}Nb_{2.62}As_2$ | | | | Formula weight: 498.28 | | | |
| Calculated density: 11.108 $Mg/m^3$ | | | | Structure type: new | | | |
| Unit cell dimensions: | a | 7.142(2) Å | | Crystal system: orthorhombic | | | |
| | b | 3.583(2) Å | | Space group: *Pnma* (no. 62) | | | |
| | c | 11.640(3) Å | | Pearson symbol: *oP*16 | | | |
| | V | 297.9(1) $Å^3$ | | Z = 2 | | | |
| Wavelength: 0.71073 Å (Mo Kα radiation) | | | | Theta range for data collection: 3.33 – 27.49° | | | |
| Absorption coefficient: 62.6 $mm^{-1}$ | | | | Temperature: 293(2) K | | | |
| Total number of the measured reflections: 5066 | | | | Number of reflections with I>2σ(I): 404 | | | |
| Number of refined parameters: 29 | | | | | | | |
| "R" – values for data with I>2σ(I) | | | | "R" – values for all data | | | |
| R : 0.0229 | | $R_w$ : 0.0623 | | R : 0.0231 | | $R_w$ : 0.0624 | |
| Values for index of measured data: h = -9 → 9, k = -4 → 4, l = -15 → 15 | | | | | | | |
| Goodness of fit for refinement reflections: 1.230 | | | | Extinction coefficient: 0.0032(4) | | | |
| Maximum/minimum values of final difference map: 7.27; -2.80 $eÅ^{-3}$ | | | | | | | |

| | Site | Wyckoff position | x | y | z | U(eq) [$pm^2$] | $y_{Nb}$ |
|---|---|---|---|---|---|---|---|
| Atom positions | M1 | 4*c* | 0.0559(1) | 1/4 | 0.5953(1) | 0.8(1) | 0.49(1) |
| | M2 | 4*c* | 0.1551(1) | 1/4 | 0.0181(1) | 0.6(1) | 0.75(1) |
| | M3 | 4*c* | 0.2692(1) | 1/4 | 0.3042(1) | 0.7(1) | 0.07(1) |
| | As3 | 4*c* | 0.4363(2) | 1/4 | 0.6785(1) | 0.5(1) | --- |

| | Site | $U_{11}$ | $U_{22}$ | $U_{33}$ | $U_{23}$ | $U_{13}$ | $U_{12}$ |
|---|---|---|---|---|---|---|---|
| Anisotropic displacement parameters ($Å^2 * 10^3$) | M1 | 6(1) | 6(1) | 9(1) | 0 | -3(1) | 0 |
| | M2 | 5(1) | 12(1) | 8(1) | 0 | 0(1) | 0 |
| | M3 | 5(1) | 7(1) | 5(1) | 0 | 1(1) | 0 |
| | As3 | 3(1) | 5(1) | 5(1) | 0 | 0(1) | 0 |

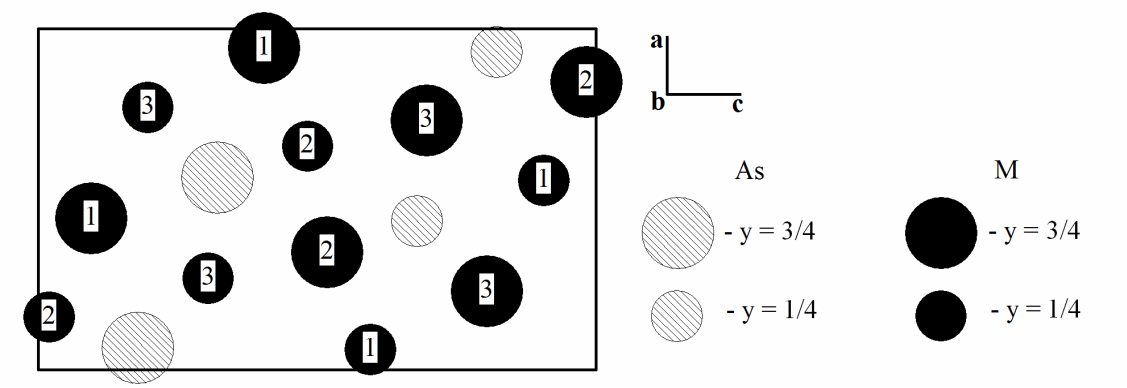


**Fig. 63. The unit cell of $Hf_{3+x}Nb_{3-x}As_2$ - view in [0$\bar{1}$0] direction**

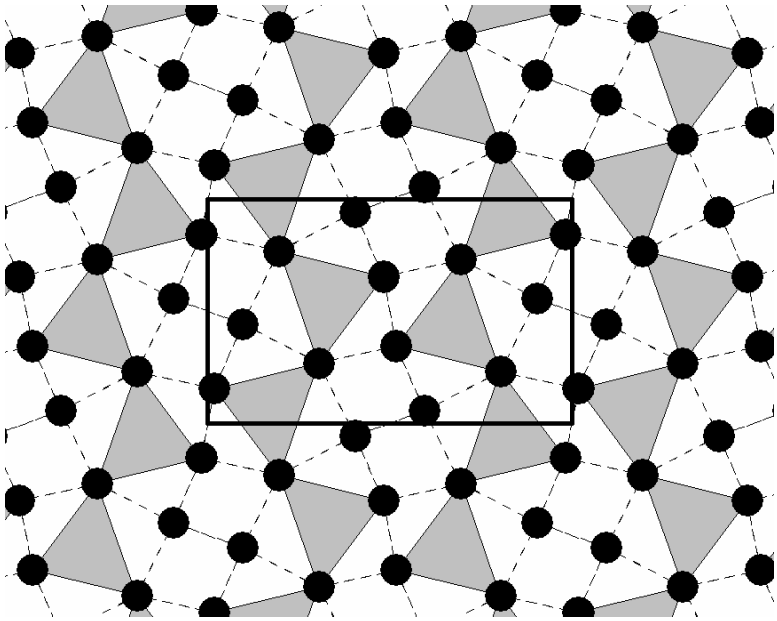

**Fig. 64. The unit cell of $Hf_{3+x}Nb_{3-x}As_2$ shown as a combination of trigonal prisms – view in [0$\bar{1}$0] direction**

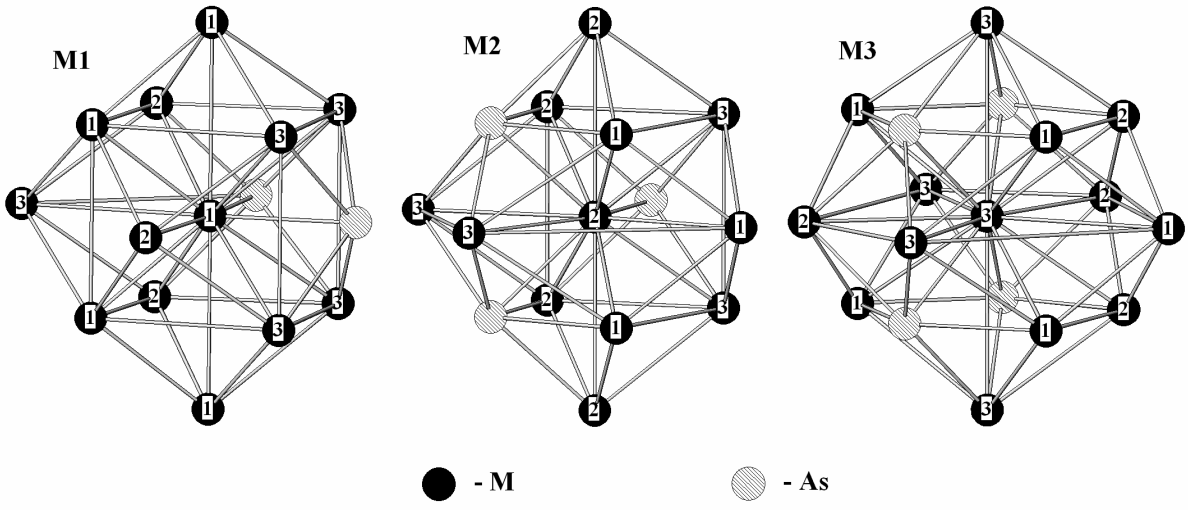


**Fig. 65. The coordination spheres of the metal sites in $Hf_{3+x}Nb_{3-x}As_2$ compound.**

An analysis of the volumes of Wigner-Seitz cells calculated from the single crystal data (Table 35) with regard to the niobium site fraction (Fig. 66) does not allow the simple correlation of these two parameters. On one hand, the site with the highest niobium occupancy (M2) is found to have the smallest volume. However, the other two have a similar volume while a significant difference in site fractions is observed ($y_{Nb}$=0.49 for M1 and $y_{Nb}$=0.07 for M3).

**Table 35. The volumes of Voronoi polyhedra around metal sites of the $Hf_{3+x}Nb_{3-x}As_2$ structure calculated for the refined data from samples S43.**

| Site | Site volume [Å$^3$] |
|---|---|
| M1 | 20.08 |
| M2 | 18.17 |
| M3 | 19.90 |

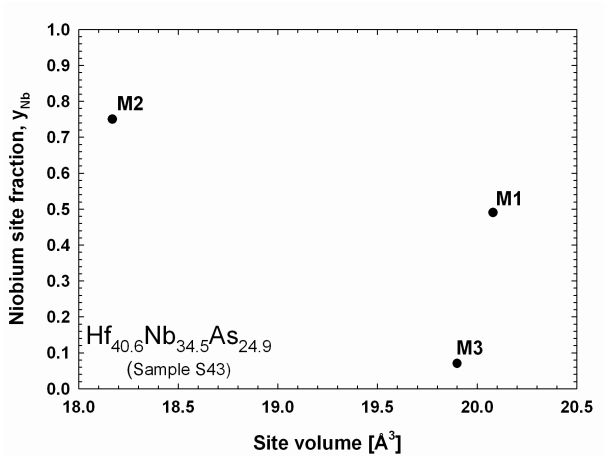


**Fig. 66. The site volumes calculated for the $Hf_{3+x}Nb_{3-x}As_2$ phase (single crystal data from sample S43)**

The influence of the cumulated PBOs for all and for metal-metal bonds are depicted in Fig. 67, based on data given in Table 36. Similar, as in the case of $Hf_{7.23}Nb_{3.77}As_4$, the diagram describing all bonds resembles a mirrored diagram of the site volumes (Fig. 66). The diagram of the PBOs of metal-metal bonds also does not show a clear correlation. The hafnium dominated site M3 has the lower value of this parameter but the niobium richest site M2 is secondary to M1 site.

As in the previous structures, the substitution of hafnium by niobium could be regarded, as a compromise between the atom size and the strength of the formed metal-metal bonding (interpreted by sublimation enthalpy). Niobium atoms tend to occupy the sites with a smaller site volume and a greater value of PBO for metal-metal bonds. Although the M1 site has a

**Table 36. The values of the cumulated PBOs of the metal sites in $Hf_{3+x}Nb_{3-x}As_2$ (sample S43).**

| Site | All bonds | Metal-metal bond (fraction of all bonds) |
|---|---|---|
| M1 | 4.39 | 3.53 (0.80) |
| M2 | 5.31 | 3.44 (0.65) |
| M3 | 4.52 | 1.90 (0.42) |

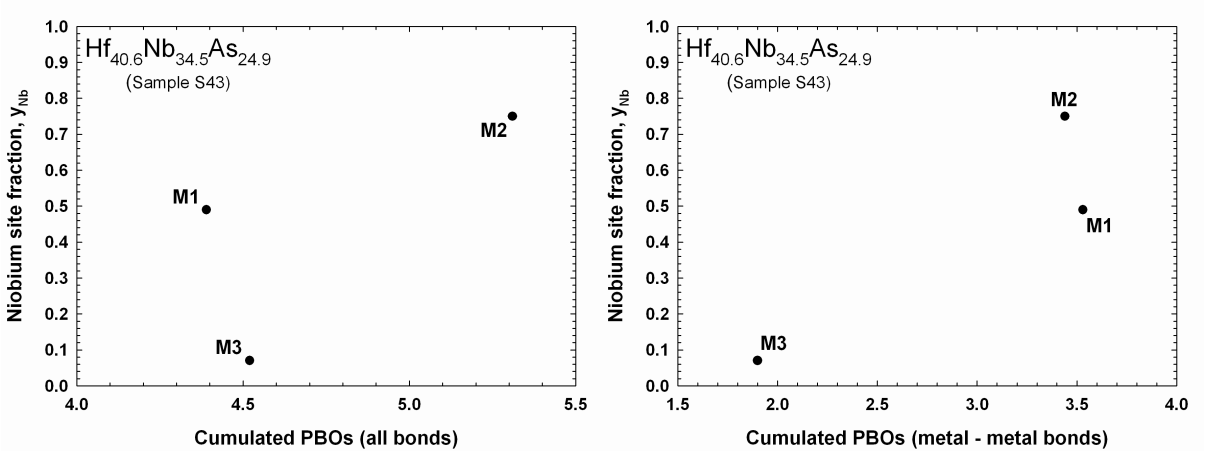


**Fig. 67. Comparison of the the cumulated PBOs of all (left) and metal-metal bonds only (right), for the metal sites in the $Hf_{3+x}Nb_{3-x}As_2$ phase (single crystal data from sample S43)**

slightly larger volume than M3 (with ~0.2 $Å^3$ difference), the greater ratio value of the previous site is probably a reason of their niobium site fractions. And while the M1 site has a larger value of PBO for metal-metal bonds than M2, its lower niobium content can be explained by a volume difference between these two sites (M2 is smaller than M1 by 1.7 $Å^3$).

#### 4.1.1.7 $Hf_{2+x}Nb_{1-x}As$ phase

The last ternary phase discussed here is $Hf_{2+x}Nb_{1-x}As$ ($0.12<x<0.65$) with a niobium content in the range of 9–22 at.%. It was found to be isostructural with binary $Nb_3As$ (*tP*32). Although the phase was found in seven samples (S34, S35, S40, S42, S43, S46, S47), only one of them was found suitable for the site fraction determination with the Rietveld refinement method (see Table 37 and 38, the remaining fraction of the pattern was $HfO_2$). The temperature factor *B(eq.)* was fixed to a constant value of 0.3 during the refinement, as setting it free caused a fall to 0 in case of the metal atoms and a rise to 1 in case of the arsenic. The

Rietveld refinement reveals the niobium presence on all the sites, in a descending order: M3, M1, M2. The coordination spheres of the metal atoms in this compound are shown in Appendix A.7.

**Table 37. Rietveld refinement results for the $Hf_{2+x}Nb_{1-x}As$ phase in sample S42**

| Sample: S42 | | Nominal composition: $Hf_{53.3}Nb_{26.7}As_{20.0}$ | | | $R_p$: 4.15 | | $R_{wp}$: 5.62 |
|---|---|---|---|---|---|---|---|
| Background model: Chebyshev, 4th order | | | | | 2$\theta$-range [°]: 10 - 120° | | |
| Main phase: $Hf_{2+x}Nb_{1-x}As$ | | | Structure type: $Ti_3P$ | | EPMA composition: $Hf_{53.7}Nb_{21.3}As_{25.0}$ | | |
| Lattice parameters [Å] | | a = 10.6739(1)<br>c = 5.36760(9) | Cell volume [Å$^3$]: 611.55(2) | | Space group: *P4$_2$/n* (86) | Fraction: 84.2% | $R_{Bragg}$: 1.88 |
| Site | Mpl. | x | y | z | Atom | Site fr. | B(eq.) |
| M1 | 8 | 0.4150(1) | 0.8943(1) | 0.9612(3) | Hf | 0.78(1) | 0.3 (fixed) |
| | | | | | Nb | 0.22(1) | |
| M2 | 8 | 0.3572(2) | 0.5281(2) | 0.7812(3) | Hf | 0.90(1) | |
| | | | | | Nb | 0.10(1) | |
| M3 | 8 | 0.3170(2) | 0.7850(2) | 0.4896(4) | Hf | 0.59(1) | |
| | | | | | Nb | 0.41(1) | |
| As | 8 | 0.2988(3) | 0.5387(3) | 0.2894(6) | As | 1 | |
| Niobium content calculated from site fractions: 18 at.% | | | Crystallite size (Lorenzian) [nm]: 53(1) | | Preferred Orientation spherical harmonics order: none | | |

**Table 38. Rietveld refinement results for the minor phase Nb**

| Structure type: W | | | Space group: $Im\bar{3}m$ | | |
|---|---|---|---|---|---|
| Sample | Lattice parameters [Å] | Cell volume [Å$^3$] | Crystallite size (Lorenzian) [nm] | $R_{Bragg}$ | Fraction: |
| S42 | a = 3.3728(1) | 38.37(1) | 20 (fixed) | 2.026 | 13.4%(1) |

The site volumes are presented in Table 39 and they are compared with the niobium site fractions in Fig. 68. The M2 site which has the smallest volume is preferably occupied by hafnium. The M3 site which has a volume lager than M2 by 0.4 Å$^3$ has the highest niobium occupancy. The site M1 still contains twice as much niobium as M2, though it is larger by 1.7 Å$^3$. This surprising result seems to prove that the size factor does not play a decisive role alone in the niobium atoms distribution in this phase.

**Table 39. The volumes of Voronoi polyhedra around metal sites of the $Hf_{2+x}Nb_{1-x}As$ structure calculated for the refined data from samples S42.**

| Site | Site volume [Å$^3$] |
|---|---|
| M1 | 21.00 |
| M2 | 19.30 |
| M3 | 19.68 |

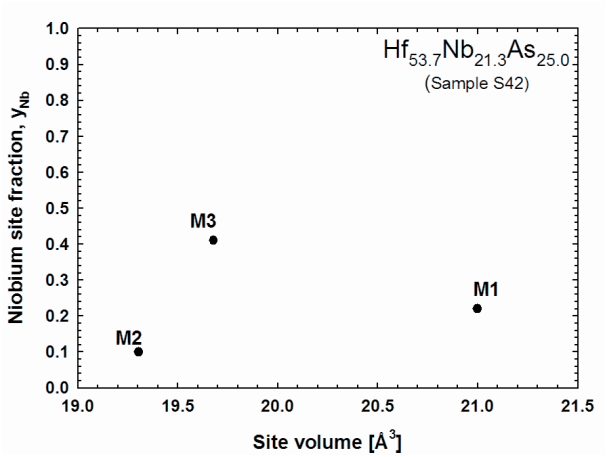


**Fig. 68. The site volumes calculated for the $Hf_{2+x}Nb_{1-x}As$ phase (Rietveld refinement data from sample S42)**

The comparison of the cumulated PBOs for all and for metal-metal bonds (Table 40) with the niobium site fractions is given in Fig. 69. It suggests that niobium prefers the sites with a low value of PBOs for all bonds but with a large value of PBOs for metal-metal bonds. Comparing these results with the phases analysed previously, the author believes that only the second argument plays a role in the substitution. The cumulated PBOs of all bonds could not be correlated with the niobium site fractions (as in the cases of $(Hf,Nb)_5As_3$ from S23, $Hf_{7+x}Nb_{4-x}As_4$, $Hf_{3+x}Nb_{3-x}As_2$) or showed the niobium preference for the sites with the large value of this parameter (as in the cases of $(Hf,Nb)_5As_3$ from S20 or $Hf_{4-x}Nb_{3+x}As_3$). The sites with the large value of cumulated PBOs for metal-metal bonds only, were in all these cases the ones with a significant niobium content.

**Table 40. The values of the cumulated PBOs of the metal sites in $Hf_{2+x}Nb_{1-x}As$ (sample S42).**

| Site | All bonds | Metal-metal bond (fraction of all bonds) |
|---|---|---|
| M1 | 4.16 | 2.99 (0.72) |
| M2 | 5.37 | 2.55 (0.47) |
| M3 | 4.66 | 3.07 (0.66) |

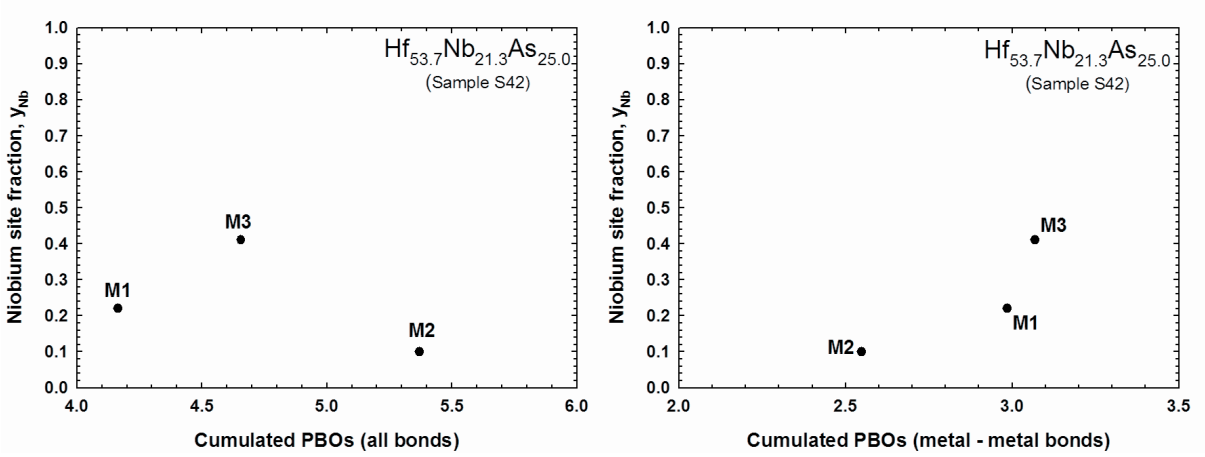


**Fig. 69. Comparison of the cumulated PBOs of all (left) and metal-metal bonds only (right), for the metal sites in $Hf_{2+x}Nb_{1-x}As$ phase (Rietveld refinement data from sample S42)**

As in all phases analysed till know, the substitution in $Hf_{2+x}Nb_{1-x}As$ seems to be an effect of two competing factors: atom size and the metal-metal bonding preference. Although the M1 site is the largest ones, it has also a high value of the cumulated PBOs of the metal-metal bonding order, thus promoting the substitution of hafnium by niobium over the site M2 which is the tightest one. On the other hand, the niobium preference for the site M3 over M1 can be additionally supported by the smaller volume of the latter one, as there is not much difference for the cumulated PBOs of the metal-metal bonds.

### 4.1.2 DFT calculations

DFT calculations were employed in the Hf-Nb-As system for the following purposes:

- to check the stability/instability of the reported binary arsenides
- to check the stability of the ternary phases found on the $Hf_3As$-$Nb_3As$ line
- to check the influence of the site preferences on the stability of the ternary phases on the $Hf_3As$-$Nb_3As$ line

The first target was set, as the metal-rich arsenides are reported at high temperatures (above 1000°C) only [29, 32]. The DFT calculations which in principle simulate the conditions at 0 K, would allow an investigation of this assumption with an independent method. The second and the third target were chosen in order to test the agreement between

the ab-initio calculations and the experimental results described in the previous section. The $Hf_3As$-$Nb_3As$ line was chosen due to the presence of the three structure types ($Ta_3As$, $Ti_3P$ and the newly reported $Hf_{3+x}Nb_{3-x}As_2$-type) and the small number of the substituted metal sites (max. 6 in the $Ta_3As$ structure type).

#### 4.1.2.1 Calculation of the ground state energies of the binary compounds

First, the ground state energies of the elements Hf, Nb and As with the crystal structures stable at 298 K were determined, with the crystal structure data taken from literature [3]. Dividing these energies by the number of atoms in the unit cell of those structures, the energies per atom were obtained (Table 41). Next, the ground state energies of the binary compounds were found in a similar procedure, but this time the atoms were allowed to migrate, as for many arsenides the crystal structure was not refined (lattice parameters were taken from literature and kept fixed during the simulation, for references see chapters 2.2.2 and 2.2.3). This relaxation was not allowed for the $M_5As_3$ compounds, as the computation of its ground state structure demanded too much time – it did not converge within 4 weeks. This is due to the huge number of atoms in the primitive cell (64) and atom sites (16) in this structure. Both $Hf_5As_3$ and $Nb_5As_3$ were calculated with atom positions taken from literature data for $Nb_5As_3$ [45]. The calculated energies per unit cell were divided by the number of formula units in the unit cell, so that the energy per formula unit was obtained, i.e. the energy of the atoms in the amount given by the chemical formula (e.g. for HfAs, the energy per unit cell was divided by 4, as the unit cell *hP*8 contains 4 HfAs formula units). Next, the formation energies per mole were calculated by subtracting the energies of a M-As mixture (with the same composition as the coresponding formula unit) from the respective compound energies per formula unit. In a final step, the formation energies were divided by the sum of the atoms in the formula unit and multiplied by 96.485 in order to obtain the value in kilojoules per mole of atoms (Table 42 and 43). The structure data after atom migration are given in Appendix G.2.

**Table 41. The calculated energies for elemental hafnium, niobium and arsenic**

| Element | Structure type | Energy per unit cell [eV] | Energy per atom [eV] |
|---|---|---|---|
| As | As(grey) | -27.9128 | -4.6521 |
| Hf | Mg(hcp) | -19.8801 | -9.9400 |
| Nb | W(bcc) | -20.4276 | -10.2138 |

**Table 42. The calculated energies for binary hafnium arsenides. $Hf_5As_3$ was calculated with atoms fixed on $Nb_5As_3$ positions. The crystal structure data was taken from literature (for references see chapter 2.2.2)**

| Compound (Formula for mole of atoms) | $x_{Hf}$ | Structure type | Energy per unit cell [eV] | Energy per formula unit [eV] | Energy of Hf-As mixture [eV] | Formation energy per formula unit [eV] | Formation energy per mole of atoms [kJ] | k-points set |
|---|---|---|---|---|---|---|---|---|
| $HfAs_2$ ($Hf_{0.333}As_{0.667}$) | 0.333 | $Co_2Si$ | -85.9681 | -21.4920 | -19.2443 | -2.2477 | -72.29 | 3 x 5 x 2 |
| HfAs $Hf_{0.5}As_{0.5}$ | 0.5 | TiAs | -66.2950 | -16.5738 | -14.5922 | -1.9816 | -95.60 | 7 x 7 x 2 |
| $Hf_3As_2$ $Hf_{0.6}As_{0.4}$ | 0.6 | $Hf_3P_2$ | -174.4300 | -43.6075 | -39.1244 | -4.4831 | -86.51 | 2 x 6 x 2 |
| $Hf_5As_3$ $Hf_{0.625}As_{0.375}$ | 0.625 | $Nb_5As_3$ | -563.4682 | -70.4335 | -63.6565 | -6.7770 | -81.73 | 2 x 15 x 5 |
| $Hf_7As_4$ $Hf_{0.636}As_{0.364}$ | 0.636 | $Nb_7P_4$ | -389.7257 | -97.4314 | -88.1887 | -9.2427 | -81.07 | 2 x 8 x 2 |
| $Hf_2As$ $Hf_{0.667}As_{0.333}$ | 0.667 | $Ta_2P$ | -322.8765 | -26.9064 | -24.5322 | -2.3742 | -76.36 | 2 x 3 x 9 |
| $Hf_3As$ $Hf_{0.75}As_{0.25}$ | 0.75 | $Ta_3As$ | -591.9972 | -36.9998 | -34.4722 | -2.5276 | -60.97 | 2 x 6 x 2 |

**Table 43. The calculated energies for binary niobium arsenides. $Nb_5As_3$ was calculated with atoms fixed on their positions. The crystal structure data was taken from literature (for references see chapter 2.2.3)**

| Compound (Formula for mole of atoms) | $x_{Nb}$ | Structure type | Energy per unit cell [eV] | Energy per formula unit [eV] | Energy of Nb-As mixture [eV] | Formation energy per formula unit [eV] | Formation energy per mole of atoms [kJ] | k-points set |
|---|---|---|---|---|---|---|---|---|
| $NbAs_2$ ($Nb_{0.333}As_{0.667}$) | 0.333 | $OsGe_2$ | -84.4216 | -21.1054 | -19.5181 | -1.5873 | -51.05 | 2 x 6 x 2 |
| NbAs ($Nb_{0.5}As_{0.5}$) | 0.5 | NbAs | -64.8989 | -16.2247 | -14.8659 | -1.3588 | -65.55 | 7 x 7 x 2 |
| $Nb_4As_3$ ($Nb_{0.571}As_{0.429}$) | 0.571 | $Nb_4As_3$ | -471.8160 | -58.9770 | -54.8116 | -4.1654 | -57.41 | 11 x 3 x 2 |
| $Nb_5As_3$ ($Nb_{0.625}As_{0.375}$) | 0.625 | $Nb_5As_3$ | -556.5592 | -69.5699 | -65.0254 | -4.5445 | -54.81 | 2 x 15 x 5 |
| $Nb_7As_4$ ($Nb_{0.636}As_{0.364}$) | 0.636 | $Nb_7P_4$ | -384.8575 | -96.2144 | -90.1051 | -6.1093 | -53.59 | 2 x 8 x 2 |
| $Nb_2As$ ($Nb_{0.667}As_{0.333}$) | 0.667 | $Nb_2P$ | -479.6765 | -26.6487 | -25.0797 | -1.5690 | -50.46 | 2 x 11 x 3 |
| $Nb_3As$ ($Nb_{0.75}As_{0.25}$) | 0.75 | $Ti_3P$ | -295.8133 | -36.9767 | -35.2935 | -1.6831 | -40.60 | 2 x 2 x 4 |

All calculated formation energies were found to be negative which would indicate that all structures are stable compared to the according stoichiometric mixture of the metal and arsenic. The next step was the investigation if the given structure is more stable than an according mixture of the neighbouring phases at 0 K. The comparison is shown in Table 44 and 45 (with an estimated error being below 0.01 kJ per mole of atoms) and depicted in Fig. 70 and 71. In the Hf-As system, all phases are found stable, except of $Hf_{0.625}As_{0.375}$ ($Hf_5As_3$). This is the reason why the phases $Hf_{0.6}As_{0.4}$ ($Hf_3As_2$) and $Hf_{0.636}As_{0.364}$ ($Hf_7As_4$) were also compared with the next stable neighbours ($Hf_{0.5}As_{0.5}$ and $Hf_{0.636}As_{0.364}$ (HfAs and $Hf_7As_4$), $Hf_{0.6}As_{0.4}$ and $Hf_{0.667}As_{0.333}$ ($Hf_3As_2$ and $Hf_2As$), respectively). One has to keep in mind that the formation energy of $Hf_{0.625}As_{0.375}$ ($Hf_5As_3$) may be not negative enough, because of fixing the atoms on the positions taken from the single crystal measurement for the $Nb_5As_3$ structure. A possible atom relaxation, could stabilise this phase, but then it might be possible that one of the other binary structures would be found unstable. In the Nb-As system all phases are found stable except for $Nb_{0.571}As_{0.429}$ ($Nb_4As_3$) and $Nb_{0.636}As_{0.364}$ ($Nb_7As_4$). Therefore, the phases $Nb_{0.5}As_{0.5}$ (NbAs), $Nb_{0.625}As_{0.375}$ ($Nb_5As_3$) and $Nb_{0.667}As_{0.333}$ ($Nb_2As$) were compared to the next stable neighbours ($Nb_{0.333}As_{0.667}$ and $Nb_{0.625}As_{0.375}$ ($NbAs_2$ and $Nb_5As_3$), $Nb_{0.5}As_{0.5}$ and $Nb_{0.667}As_{0.333}$ (NbAs and $Nb_2As$) and $Nb_{0.625}As_{0.375}$ and $Nb_{0.75}As_{0.25}$ ($Nb_5As_3$ and $Nb_3As$) respectively). The possible atom migration in the $Nb_{0.625}As_{0.375}$ ($Nb_5As_3$) structure would stabilise this phase even more which, in the extreme case, could destabilise the $Nb_{0.667}As_{0.333}$ ($Nb_2As$) structure.

Whatever the values of the calculated formation energies for the binary $M_5As_3$ structures with allowed atom relaxation would be, the calculation results allow to expect that in both of the systems at least one intermetallic phase between MAs and $M_3As$ is stable at 0 K (and probably also at higher temperatures). No such phase is reported in literature regarding the samples prepared without the use of the arc-melting furnace [29, 32], but it seems that a thermodynamic instability in the low temperature range is not the cause for this fact. Rather a slow kinetics of the phase formation in this temperature range could serve as a possible explanation.

**Table 44. The comparison of the calculated formation energies between the compounds and the mixtures of the neighbour compounds in the Hf-As system**

| Structure (Formula unit) | Formation energy [kJ/mole of atoms] | Formation energy of the neighbour structure mixture [kJ/mole of atoms] | Difference |
|---|---|---|---|
| $Hf_{0.333}As_{0.667}$ ($HfAs_2$) | -72.29 | -63.73 (As - $Hf_{0.5}As_{0.5}$) | -8.56 (stable) |
| $Hf_{0.5}As_{0.5}$ (HfAs) | -95.60 | -81.18 ($Hf_{0.333}As_{0.667}$ - $Hf_{0.6}As_{0.4}$) | -14.42 (stable) |
| $Hf_{0.6}As_{0.4}$ ($Hf_3As_2$) | -86.51 | -84.51 ($Hf_{0.5}As_{0.5}$ - $Hf_{0.625}As_{0.375}$) | -2.00 (stable) |
| $Hf_{0.6}As_{0.4}$ ($Hf_3As_2$) | -86.51 | -84.94 ($Hf_{0.5}As_{0.5}$ - $Hf_{0.636}As_{0.364}$) | -1.57 (stable) |
| $Hf_{0.625}As_{0.375}$ ($Hf_5As_3$) | -81.73 | -82.77 ($Hf_{0.6}As_{0.4}$ - $Hf_{0.636}As_{0.364}$) | 1.04 (unstable) |
| $Hf_{0.636}As_{0.364}$ ($Hf_7As_4$) | -81.07 | -80.27 ($Hf_{0.625}As_{0.375}$ - $Hf_{0.667}As_{0.333}$) | -0.80 (stable) |
| $Hf_{0.636}As_{0.364}$ ($Hf_7As_4$) | -81.07 | -80.97 ($Hf_{0.6}As_{0.4}$ - $Hf_{0.667}As_{0.333}$) | -0.10 (stable) |
| $Hf_{0.667}As_{0.333}$ ($Hf_2As$) | -76.36 | -75.71 ($Hf_{0.636}As_{0.364}$ - $Hf_{0.75}As_{0.25}$) | -0.65 (stable) |
| $Hf_{0.75}As_{0.25}$ ($Hf_3As$) | -60.97 | -57.27 ($Hf_{0.667}As_{0.333}$ - Hf) | -3.70 (stable) |

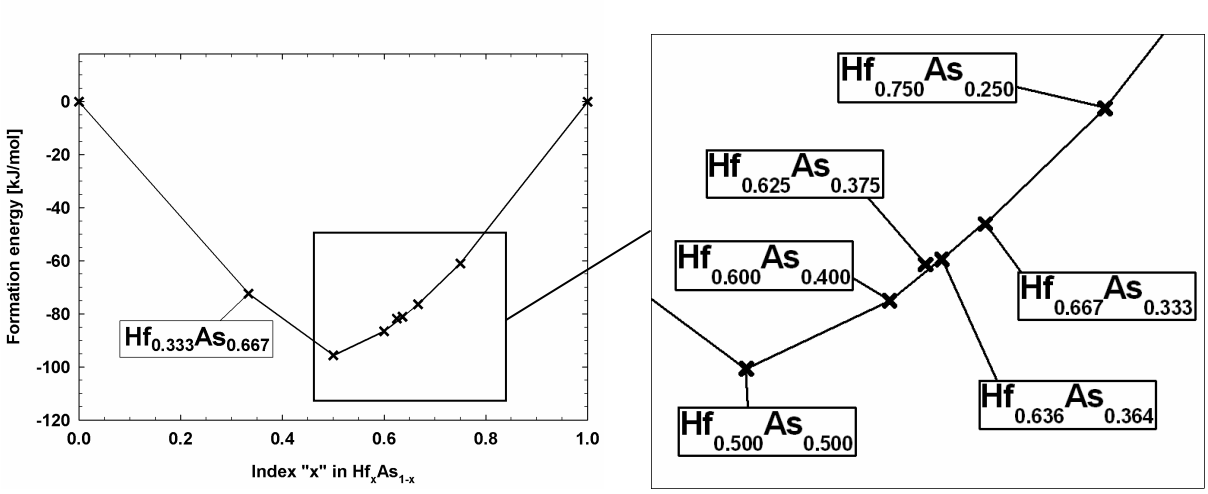


**Fig. 70. The graphic presentation of the phase stability in the Hf-As system calculated for 0 K**

**Table 45. The comparison of the calculated formation energies between the compounds and the mixtures of the neighbour compounds in the Nb-As system**

| Structure (Formula unit) | Formation energy [kJ/mole of atoms] | Formation energy of the neighbour structure mixture [kJ/mole of atoms] | Difference |
|---|---|---|---|
| $Nb_{0.333}As_{0.667}$ ($NbAs_2$) | -51.05 | -43.70 (As - $Nb_{0.5}As_{0.5}$) | -7.35 (stable) |
| $Nb_{0.5}As_{0.5}$ (NbAs) | -65.55 | -55.51 ($Nb_{0.333}As_{0.667}$ - $Nb_{0.571}As_{0.429}$) | -10.05 (stable) |
| $Nb_{0.5}As_{0.5}$ (NbAs) | -65.55 | -53.20 ($Nb_{0.333}As_{0.667}$ - $Nb_{0.625}As_{0.375}$) | -12.35 (stable) |
| $Nb_{0.571}As_{0.429}$ ($Nb_4As_3$) | -57.41 | -59.41 ($Nb_{0.5}As_{0.5}$ - $Nb_{0.625}As_{0.375}$) | 2.00 (unstable) |
| $Nb_{0.625}As_{0.375}$ ($Nb_5As_3$) | -54.81 | -54.26 ($Nb_{0.571}As_{0.429}$ - $Nb_{0.636}As_{0.364}$) | -0.55 (stable) |
| $Nb_{0.625}As_{0.375}$ ($Nb_5As_3$) | -54.81 | -54.23 ($Nb_{0.5}As_{0.5}$ - $Nb_{0.667}As_{0.333}$) | -0.58 (stable) |
| $Nb_{0.636}As_{0.364}$ ($Nb_7As_4$) | -53.59 | -53.62 ($Nb_{0.625}As_{0.375}$ - $Nb_{0.667}As_{0.333}$) | 0.04 (unstable) |
| $Nb_{0.667}As_{0.333}$ ($Nb_2As$) | -50.46 | -50.12 ($Nb_{0.636}As_{0.364}$ - $Nb_{0.75}As_{0.25}$) | -0.34 (stable) |
| $Nb_{0.667}As_{0.333}$ ($Nb_2As$) | -50.46 | -50.07 ($Nb_{0.625}As_{0.375}$ - $Nb_{0.75}As_{0.25}$) | -0.39 (stable) |
| $Nb_{0.75}As_{0.25}$ ($Nb_3As$) | -40.60 | -37.85 ($Nb_{0.667}As_{0.333}$ - Nb) | -2.75 (stable) |

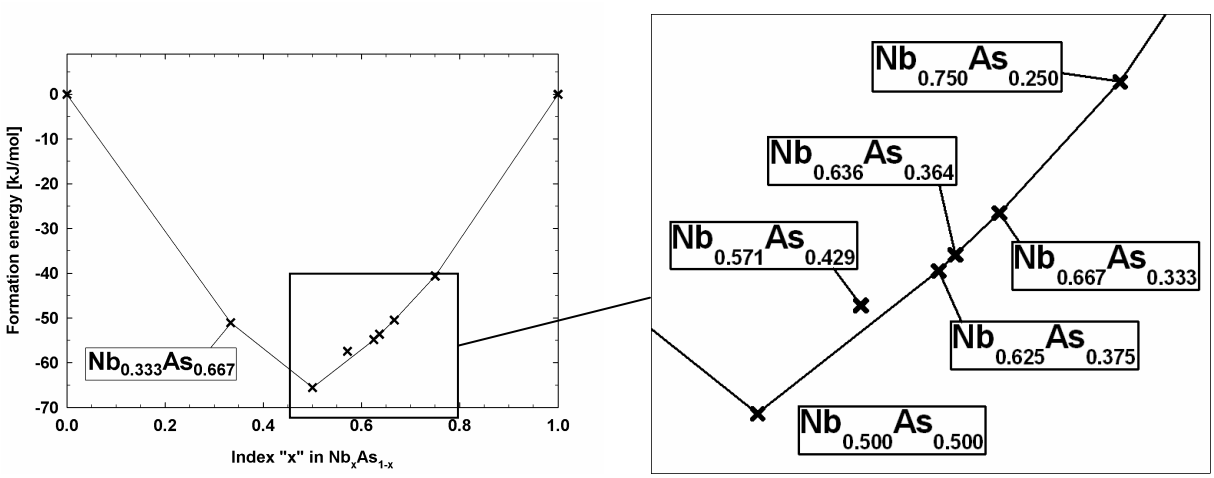


**Fig. 71. The graphic presentation of the phase stability in the Nb-As system calculated for 0 K**

#### 4.1.2.2 Calculation of the ground state energies for the $M_3As$ compounds

In this step, the ground state energies of $Hf_3As$, $Nb_3As$ and $Hf_{3+x}Nb_{3-x}As_2$ end members were calculated. In these end members, the sublattices were defined according to the metal site notation and all arsenic atoms were included in one sublattice (i.e. (M1:M2:M3:As) or (M1:M2:M3:M4:M5:M6:As)). The number of calculated end members was limited to the binary compounds (which are hypothetical, except of (Nb:Nb:Nb:As) for $Nb_3As$ and (Hf:Hf:Hf:Hf:Hf:Hf:As) for $Hf_3As$) and the binaries with atoms on only one of the sublattices substituted by another metal (i.e. the *monosubstituted* end members). This limitation was due to the fact that six metal sites in the $Ta_3As$-type phase would result in the total number of 64 ($=2^6$) possible end members for this structure. In case of the other two phases this restriction covers all possible end members, as for three metal sites only binary or monosubstituted end members are possible. The binary structures were allowed to relax their cell parameters and atom positions (see Appendix G.3 for the ground state structure data), but in order to save computation time, the atom positions taken from the relaxation of the binaries were kept in the monosubstituted ones (the cell parameters were still set free). The calculated end member energies were then recalculated, first to the energy per $M_3As$ formula unit (by dividing by the number of $M_3As$ formula units in the unit cell) and then to the formation energy per formula unit by subtracting the energy of a corresponding $Hf_{3-x}Nb_xAs$ mixture. The energy of the $Hf_{3-x}Nb_xAs$ mixture was calculated by summing the element's energies per atom according to the stoichiometry of the mixture. The formation energies were further recalculated for the values in kilojoules per mole of atoms (in $M_3As$ compound), as it was described in the previous section. The results are given in Tables 46-48.

**Table 46. The calculated end member energies for the $Hf_3As$ structure ($Ta_3As$ type) with the k-points set of 4 x 12 x 4.**

| $Hf_3As$ end members ($Ta_3As$ structure type) (M1:M2:M3:M4:M5:M6:As) | $x_{Nb}$ | Energy per unit cell [eV] | Energy per formula unit [eV] | Energy of $(Hf,Nb)_3As$ mixture [eV] | Formation energy [eV] | Formation energy per mole of atoms [kJ] |
|---|---|---|---|---|---|---|
| (Hf:Hf:Hf:Hf:Hf:Hf:As) | 0 | -592.2246 | -37.0140 | -34.4722 | -2.5418 | -61.31 |
| (Nb:Hf:Hf:Hf:Hf:Hf:As) | 0.125 | -591.0565 | -36.9410 | -34.6091 | -2.3319 | -56.25 |
| (Hf:Nb:Hf:Hf:Hf:Hf:As) | 0.125 | -591.3376 | -36.9586 | -34.6091 | -2.3495 | -56.67 |
| (Hf:Hf:Nb:Hf:Hf:Hf:As) | 0.125 | -591.1764 | -36.9485 | -34.6091 | -2.3394 | -56.43 |
| (Hf:Hf:Hf:Nb:Hf:Hf:As) | 0.125 | -590.8626 | -36.9289 | -34.6091 | -2.3198 | -55.96 |
| (Hf:Hf:Hf:Hf:Nb:Hf:As) | 0.125 | -592.3324 | -37.0208 | -34.6091 | -2.4117 | -58.17 |
| (Hf:Hf:Hf:Hf:Hf:Nb:As) | 0.125 | -592.6212 | -37.0388 | -34.6091 | -2.4297 | -58.61 |
| (Hf:Nb:Nb:Nb:Nb:Nb:As) | 0.625 | -589.6988 | -36.8562 | -35.1566 | -1.6995 | -40.99 |
| (Nb:Hf:Nb:Nb:Nb:Nb:As) | 0.625 | -590.0389 | -36.8774 | -35.1566 | -1.7208 | -41.51 |
| (Nb:Nb:Hf:Nb:Nb:Nb:As) | 0.625 | -591.1716 | -36.9482 | -35.1566 | -1.7916 | -43.22 |
| (Nb:Nb:Nb:Hf:Nb:Nb:As) | 0.625 | -591.1670 | -36.9479 | -35.1566 | -1.7913 | -43.21 |
| (Nb:Nb:Nb:Nb:Hf:Nb:As) | 0.625 | -590.7030 | -36.9189 | -35.1566 | -1.7623 | -42.51 |
| (Nb:Nb:Nb:Nb:Nb:Hf:As) | 0.625 | -589.8192 | -36.8637 | -35.1566 | -1.7071 | -41.18 |
| (Nb:Nb:Nb:Nb:Nb:Nb:As) | 0.75 | -591.0068 | -36.9379 | -35.2935 | -1.6444 | -39.66 |

**Table 47. The calculated end member energies for the $Nb_3As$ structure ($Ti_3P$ type) with the k-points set of 4 x 4 x 8.**

| $Nb_3As$ end member ($Ti_3P$ structure type) (M1:M2:M3:As) | $x_{Nb}$ | Energy per unit cell [eV] | Energy per formula unit [eV] | Energy of $(Hf,Nb)_3As$ mixture [eV] | Formation energy [eV] | Formation energy per mole of atoms [kJ] |
|---|---|---|---|---|---|---|
| (Hf:Hf:Hf:As) | 0 | -296.0165 | -37.0021 | -34.4722 | -2.5298 | -61.02 |
| (Nb:Hf:Hf:As) | 0.25 | -295.0717 | -36.8840 | -34.7460 | -2.1380 | -51.57 |
| (Hf:Nb:Hf:As) | 0.25 | -294.7992 | -36.8499 | -34.7460 | -2.1039 | -50.75 |
| (Hf:Hf:Nb:As) | 0.25 | -296.8311 | -37.1039 | -34.7460 | -2.3579 | -56.88 |
| (Hf:Nb:Nb:As) | 0.5 | -294.3260 | -36.7907 | -35.0198 | -1.7710 | -42.72 |
| (Nb:Hf:Nb:As) | 0.5 | -296.2123 | -37.0265 | -35.0198 | -2.0068 | -48.41 |
| (Nb:Nb:Hf:As) | 0.5 | -295.1511 | -36.8939 | -35.0198 | -1.8741 | -45.21 |
| (Nb:Nb:Nb:As) | 0.75 | -295.9040 | -36.9880 | -35.2935 | -1.6945 | -40.87 |

**Table 48. The calculated end member energies for the $Hf_{3+x}Nb_{3-x}As_2$ structure ($Hf_{3+x}Nb_{3-x}As_2$ type) with the k-points set of 6 x 12 x 4.**

| $Hf_{3+x}Nb_{3-x}As_2$ end member (M1:M2:M3:As) | $x_{Nb}$ | Energy per unit cell [eV] | Energy per formula unit [eV] | Energy of $(Hf,Nb)_3As$ mixture [eV] | Formation energy [eV] | Formation energy per mole of atoms [kJ] |
|---|---|---|---|---|---|---|
| (Hf:Hf:Hf:As) | 0 | -147.8613 | -36.9653 | -34.4722 | -2.4931 | -60.14 |
| (Nb:Hf:Hf:As) | 0.25 | -148.0569 | -37.0142 | -34.7460 | -2.2682 | -54.71 |
| (Hf:Nb:Hf:As) | 0.25 | -148.4435 | -37.1109 | -34.7460 | -2.3649 | -57.04 |
| (Hf:Hf:Nb:As) | 0.25 | -146.8566 | -36.7142 | -34.7460 | -1.9682 | -47.47 |
| (Hf:Nb:Nb:As) | 0.5 | -147.5161 | -36.8790 | -35.0198 | -1.8593 | -44.85 |
| (Nb:Hf:Nb:As) | 0.5 | -146.4527 | -36.6132 | -35.0198 | -1.5934 | -38.44 |
| (Nb:Nb:Hf:As) | 0.5 | -149.4776 | -37.3694 | -35.0198 | -2.3496 | -56.68 |
| (Nb:Nb:Nb:As) | 0.75 | -148.1344 | -37.0336 | -35.2935 | -1.7401 | -41.97 |

Comparing the values of the calculated energy values for monosubstituted end members some observations on the energetically favoured site preferences can be made in the different structures. In the $Ta_3As$-type structure, the lowest formation energies for the hafnium monosubstituted (i.e. with hafnium atoms on one site) end members are found for (Nb:Nb:Hf:Nb:Nb:Nb:As) and (Nb:Nb:Nb:Hf:Nb:Nb:As) which means that hafnium atoms would probably prefer M3 and M4 sites. As the lowest niobium monosubstituted end member formation energies are found for (Hf:Hf:Hf:Hf:Hf:Nb:As) and (Hf:Hf:Hf:Hf:Nb:Hf:As), the niobium is predicted to substitute preferably at the sites M5 and M6. Assuming a stepwise substitution on the metal sites, the substituted sites can be ordered according to their formation energies for both types of the monosubstituted end members. Thus, two orders of substituted sites are obtained, depending on the chosen binary end member. Starting from the binary (Hf:Hf:Hf:Hf:Hf:Hf:As), niobium atoms are predicted to substitute the sites in the following order with increasing formation energy: M6→M5→M2→M3→M1→M4. Starting from the binary (Nb:Nb:Nb:Nb:Nb:Nb:As), hafnium atoms are expected to substitute the sites in the following order with increasing formation energy: M3→M4→M5→M2→M6→M1. It can be seen that both orders are not symmetric so that a further assumption is made, that the niobium monosubstituted end member formation energies are considered only for the hafnium-rich end members and vice versa. Hence, it is assumed that the most stable endmembers are (Hf:Hf:Hf:Hf:Hf:Nb:As) and (Hf:Hf:Hf:Hf:Nb:Nb:As) for the hafnium-rich side and (Nb:Nb:Hf:Nb:Nb:Nb:As) and (Nb:Nb:Hf:Hf:Nb:Nb:As) for the niobium-rich side. The formation energies for these end members were calculated by the addition of the substitution energies of the monosubstituted end members (defined as the difference between the formation energies of the monosubstituted and the binary end members, see Table 49 and 50). The formation energy for the most stable end member with the $Hf_{1.5}Nb_{1.5}As$ stoichiometry, was found by comparing the formation energies referred to the two binary end members. As the estimated energy for (Hf:Nb:Hf:Hf:Nb:Nb:As) (-50.83 kJ/mol, referred to $Hf_3As$ end member) is lower than the one for (Nb:Nb:Hf:Hf:Hf:Nb:As) (-49.60 kJ/mol, referred to $Nb_3As$ end member), the former is taken as the most stable one so that a substitution order for niobium substituting hafnium is taken as: M6→M5→M2→M1→M4→M3. For hafnium substituting niobium the reverse one is assumed. The calculated formation energies for the most stable end members are given in Table 51.

**Table 49. The substitution enengies for the niobium monosubstituted end members of the $Ta_3As$-type calculated as a difference between the formation energies of the monosubstituted and binary end member**

| End member $Ta_3As$-type | Formation energy per mole of atoms [kJ] | Substitution energy per mole of atoms [kJ] |
|---|---|---|
| (Hf:Hf:Hf:Hf:Hf:Hf:As) | -61.31 | 0 |
| (Nb:Hf:Hf:Hf:Hf:Hf:As) | -56.25 | 5.06 |
| (Hf:Nb:Hf:Hf:Hf:Hf:As) | -56.67 | 4.64 |
| (Hf:Hf:Nb:Hf:Hf:Hf:As) | -56.43 | 4.88 |
| (Hf:Hf:Hf:Nb:Hf:Hf:As) | -55.96 | 5.36 |
| (Hf:Hf:Hf:Hf:Nb:Hf:As) | -58.17 | 3.14 |
| (Hf:Hf:Hf:Hf:Hf:Nb:As) | -58.61 | 2.70 |

**Table 50. The substitution enengies for the hafnium monosubstituted end members of the $Ta_3As$-type calculated as a difference between the formation energies of the monosubstituted and binary end member**

| End member $Ta_3As$-type | Formation energy per mole of atoms [kJ] | Substitution energy per mole of atoms [kJ] |
|---|---|---|
| (Nb:Nb:Nb:Nb:Nb:Nb:As) | -39.66 | 0 |
| (Hf:Nb:Nb:Nb:Nb:Nb:As) | -40.99 | -1.33 |
| (Nb:Hf:Nb:Nb:Nb:Nb:As) | -41.51 | -1.85 |
| (Nb:Nb:Hf:Nb:Nb:Nb:As) | -43.22 | -3.56 |
| (Nb:Nb:Nb:Hf:Nb:Nb:As) | -43.21 | -3.55 |
| (Nb:Nb:Nb:Nb:Hf:Nb:As) | -42.51 | -2.85 |
| (Nb:Nb:Nb:Nb:Nb:Hf:As) | -41.18 | -1.52 |

**Table 51. The most stable end member energies of the $Ta_3As$-type obtained by the summation of the substitution energies of the according monosubstituted end members (see text).**

| End member $Ta_3As$-type | Composition | Formation energy [kJ/mol] |
|---|---|---|
| (Hf:Hf:Hf:Hf:Hf:As) | $Hf_{0.750}As_{0.250}$ | -61.31 |
| (Hf:Hf:Hf:Hf:Hf:Nb:As) | $Hf_{0.625}Nb_{0.125}As_{0.250}$ | -58.61 |
| (Hf:Hf:Hf:Hf:Nb:Nb:As) | $Hf_{0.500}Nb_{0.250}As_{0.250}$ | -55.47 |
| (Hf:Nb:Hf:Hf:Nb:Nb:As) | $Hf_{0.375}Nb_{0.375}As_{0.250}$ | -50.83 |
| (Nb:Nb:Hf:Hf:Nb:Nb:As) | $Hf_{0.250}Nb_{0.500}As_{0.250}$ | -46.76 |
| (Nb:Nb:Hf:Nb:Nb:Nb:As) | $Hf_{0.125}Nb_{0.625}As_{0.250}$ | -43.22 |
| (Nb:Nb:Nb:Nb:Nb:Nb:As) | $Nb_{0.750}As_{0.250}$ | -39.66 |

In the $Ti_3P$-type structure, the lowest formation energy value for hafnium monosubstituted endmembers is the one for (Nb:Hf:Nb:As) which means that hafnium atoms prefer the M2 site. (Hf:Hf:Nb:As) is the niobium monosubstituted endmember with the lowest energy value, suggesting the niobium preference for the M3 sites. As the $Ti_3P$ and $Ta_3As$ structure types are related to each other (see Appendix A.7) and it is also possible to relate the metal sites in these structures, a good agreement between the site preferences for both metals in the two structures is observed in the DFT calculations. Moreover, the predicted site preferences agree qualitatively with the site fractions obtained from the Rietveld refinement in the $Hf_{2+x}Nb_{1-x}As$ phase (chapter 4.1.1.7), which were decreasing in order $y_{Nb}^{M3} > y_{Nb}^{M1} > y_{Nb}^{M2}$. The calculated formation energies for the most stable elements are collected in Table 52.

**Table 52. The most stable end member energies of the $Ti_3P$-type**

| End member $Ti_3P$-type | Composition | Formation energy [kJ/mol] |
|---|---|---|
| (Hf:Hf:Hf:As) | $Hf_{0.750}As_{0.250}$ | -61.02 |
| (Hf:Hf:Nb:As) | $Hf_{0.500}Nb_{0.250}As_{0.250}$ | -56.88 |
| (Nb:Hf:Nb:As) | $Hf_{0.250}Nb_{0.500}As_{0.250}$ | -48.41 |
| (Nb:Nb:Nb:As) | $Nb_{0.750}As_{0.250}$ | -40.87 |

An analogue analysis for $Hf_{3+x}Nb_{3-x}As_2$ shows that hafnium atoms prefer the M3 site and niobium atoms prefer the M2 site. This is also in a good agreement with the site fractions obtained from the single crystal data refinement which were decreasing in the order $y_{Nb}^{M2} > y_{Nb}^{M1} > y_{Nb}^{M3}$. Remarkably, the formation energy of (Nb:Hf:Nb:As) (-38.44kJ/mol) is higher than the one of binary (Nb:Nb:Nb:As) (-41.97 kJ/mol), while in all other cases an energy gain is observed when hafnium substitutes niobium (compare Table 48). This would suggest a kind of “repulsion” of hafnium atoms from M2 site. The calculated formation energies for the most stable end members are shown in Table 53. One can see that there is a huge energetic gap (14.7 kJ/mol) between the (Nb:Nb:Nb:As) and (Nb:Nb:Hf:As) endmembers compared to the other one-site substitution steps which underlines the strong “attraction” of hafnium atoms to the M3 site.

**Table 53. The most stable end member energies of the $Hf_{3+x}Nb_{3-x}As_2$-type**

| End member $Hf_{3+x}Nb_{3-x}As_2$ | Composition | Formation energy [kJ/mol] |
|---|---|---|
| (Hf:Hf:Hf:As) | $Hf_{0.750}As_{0.250}$ | -60.14 |
| (Hf:Nb:Hf:As) | $Hf_{0.500}Nb_{0.250}As_{0.250}$ | -57.04 |
| (Nb:Nb:Hf:As) | $Hf_{0.250}Nb_{0.500}As_{0.250}$ | -56.68 |
| (Nb:Nb:Nb:As) | $Nb_{0.750}As_{0.250}$ | -41.97 |

The calculated formation energies of the most stable end members for all three structures are compared in Fig. 72. Comparing these, one can confirm that the $Ta_3As$-type structure is found to be the most stable one for the binary $Hf_3As$ composition with the formation energy differences being 0.29 kJ for the $Ti_3P$-type and 1.17 kJ for $Hf_{3+x}Nb_{3-x}As_2$ structures. The predicted most stable structure for the binary $Nb_3As$ composition is the $Hf_{3+x}Nb_{3-x}As_2$ structure with the more distinct energy differences of 1.10 kJ for the $Ti_3P$-type and 2.31 kJ for the $Ta_3As$-type structure. Also, for the two ternary compositions $Hf_{0.50}Nb_{0.25}As_{0.25}$ and $Hf_{0.25}Nb_{0.50}As_{0.25}$, the $Hf_{3+x}Nb_{3-x}As_2$ end members were found to be the most stable ones. It can be seen that an ordered system with the lowest possible energy is expected to include the (Hf:Hf:Hf:Hf:Hf:Hf:As) end member of the $Ta_3As$-type, and the (Nb:Nb:Hf:As) and (Nb:Nb:Nb:As) end members of the $Hf_{3+x}Nb_{3-x}As_2$-type.

The modelling conclusions agree with the experimental results only in the case of the stability of the $Ta_3As$-type structure for the binary $Hf_{0.75}As_{0.25}$ ($Hf_3As$). The experiment shows the presence of the $Ti_3P$-type phase rather than the predicted $Hf_{3+x}Nb_{3-x}As_2$ structure for binary $Nb_{0.75}As_{0.25}$ ($Nb_3As$). This may suggest that the former is a high-temperature phase. This conclusion can be extended on the ternary field $Hf_3As$ – $Nb_3As$, as the $Ti_3P$-type structure is found to dissolve hafnium up to 17 at.%. An appearance of a $Ti_3P$-type structure on the hafnium-rich side in form of the $Hf_{2+x}Nb_{1-x}As$ phase is somewhat surprising and is not predicted by DFT calculations. The same is true for the appearance of the $Hf_{3+x}Nb_{3-x}As_2$ structure for the hafnium content of 39-41 at.%, i.e around the composition of $Hf_{0.40}Nb_{0.35}As_{0.25}$ ($Hf_{1.6}Nb_{1.4}As$), where a mixture of $Hf_3As$ and $HfNb_2As$ (Nb:Nb:Hf:As) is predicted. However, it must be pointed out that the calculated data reflects only hypothetical completely ordered end members. Therefore, a direct comparison with the experimental data regarding the equilibrium phase fields might be not plausible.

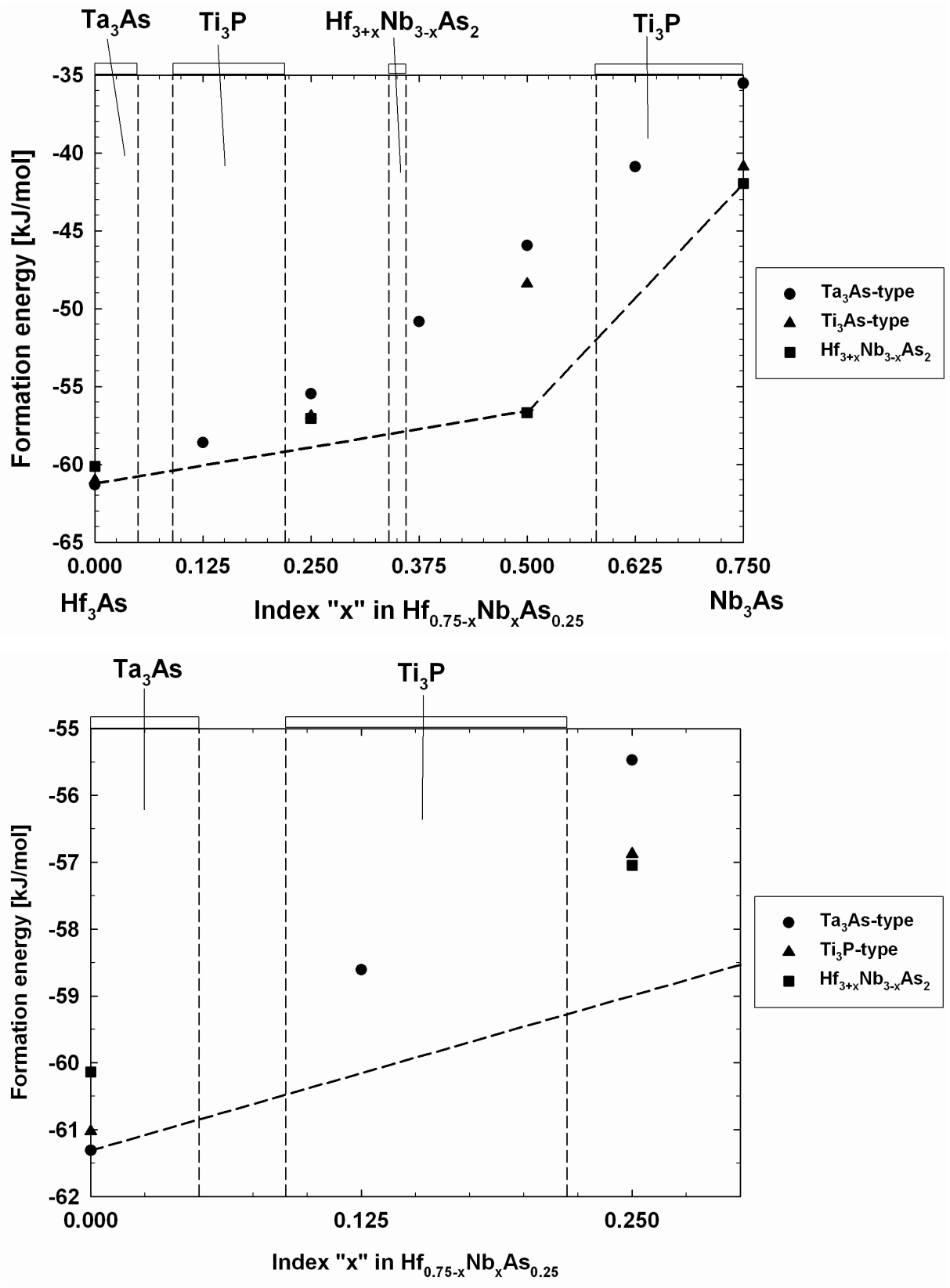


**Fig. 72. The graphic presentation of the end member energies for $Ta_3As$-, $Ti_3P$- and $Hf_{3+x}Nb_{3-x}As_2$-type. The diagram on the top covers the whole composition range, while the diagram on the bottom is a magnification of the hafnium richer range. Dashed lines represent the experimentally found existemce range for each structure type at 1400°C.**

### 4.1.3 Thermodynamic modeling of the site fractions in $M_3As$ phases

Thermodynamic modelling of the site fraction was possible for all phases where the end member energies were known from DFT calculations. Therefore, this modelling was restricted only to the $M_3As$ phases, for which these calculations were performed. The site fractions were experimentally refined for the phases $Hf_{2+x}Nb_{1-x}As$ and $Hf_{3+x}Nb_{3-x}As_2$ and it would be interesting to check the agreement of the experimental values with the ones based on ab-initio calculations.

In case of the $Hf_{2+x}Nb_{1-x}As$ phase ($Ti_3P$ structure type), the formation energies of the end members given in the last column of Table 47 were used in the Compound Energy Model in order to find the site fractions which minimise the Gibbs energy of this phase. The calculated niobium site fractions are depicted in Fig. 73, together with the experimentally determined values from the Rietveld refinement of sample S42 (see chapter 4.1.1.7). Selected site fraction values are given in Table 54. It can be seen that the experimental site fractions are in good agreement with the modelled curves, yielding a satisfactory fit. The site fractions for M1 site are underestimated and the ones for the M3 site are overestimated. On the niobium-rich side (>65 at.% Nb), a clear distinction of the niobium occupation between M2 and the other sites is predicted, whereby the site fractions on M1 and M3 sites should be very close to each other (<0.05). Unfortunately, this could not be confirmed, as no sample containing the solid solution extending from binary $Nb_3As$ was found suitable for a Rietveld refinement.

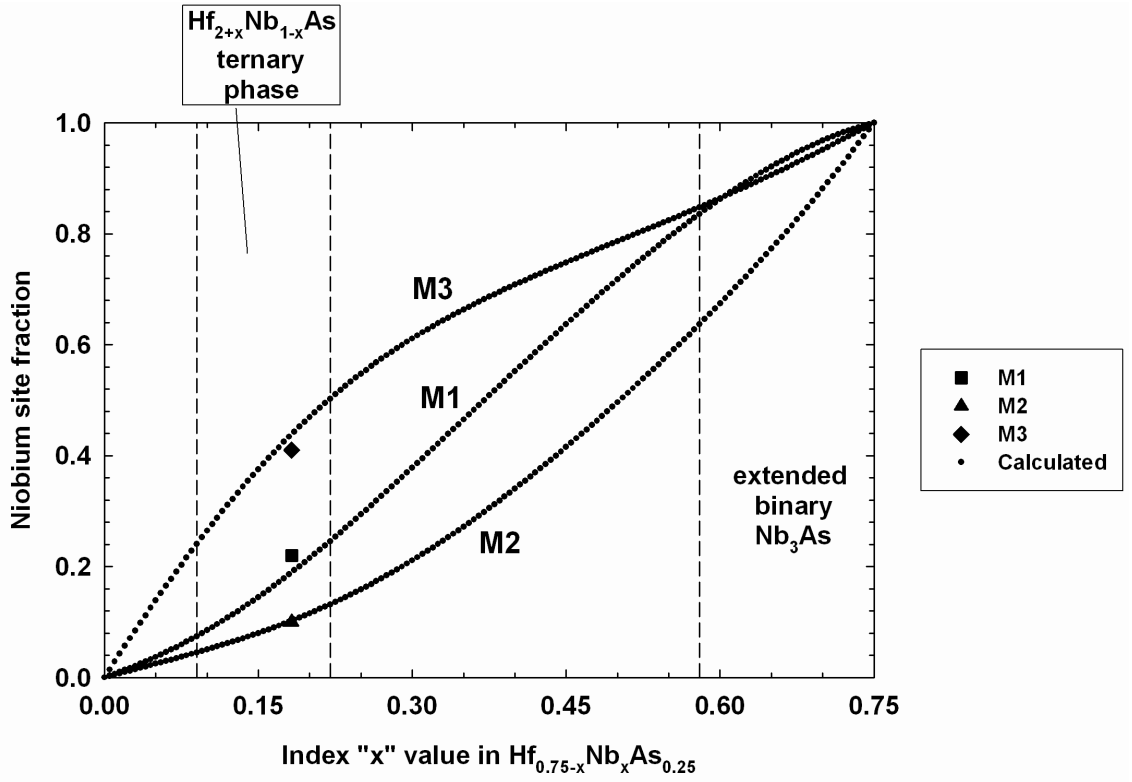


**Fig. 73. The comparison of the niobium site fractions found experimentally for the $Hf_{2+x}Nb_{1-x}As$ phase (Rietveld refinement of sample S42, marked by symbols) and calculated for the $Ti_3P$ structure type. Dashed lines show the experimentally found (EPMA measurement) existence range of the $Ti_3P$-type structure at 1400°C.**

**Table 54. The calculated site fractions for the $M_3As$ phase with the $Ti_3P$-type structure**

| $Hf_{0.75-x}Nb_xAs_{0.25}$ $Ti_3P$-type | Nb site fraction, $y_{Nb}$ ($y_{Nb} + y_{Hf} = 1$) | | |
|---|---|---|---|
| $x_{Nb}$ | M1 | M2 | M3 |
| 0.00 | 0 | 0 | 0 |
| 0.05 | 0.0368 | 0.0246 | 0.1387 |
| 0.10 | 0.0850 | 0.0504 | 0.2646 |
| 0.15 | 0.1448 | 0.0798 | 0.3754 |
| 0.20 | 0.2152 | 0.1153 | 0.4695 |
| 0.25 | 0.2939 | 0.1588 | 0.5474 |
| 0.30 | 0.3781 | 0.2110 | 0.6109 |
| 0.35 | 0.4650 | 0.2718 | 0.6633 |
| 0.40 | 0.5518 | 0.3402 | 0.7080 |
| 0.45 | 0.6366 | 0.4153 | 0.7481 |
| 0.50 | 0.7177 | 0.4961 | 0.7862 |
| 0.55 | 0.7935 | 0.5823 | 0.8242 |
| 0.60 | 0.8620 | 0.6743 | 0.8638 |
| 0.65 | 0.9210 | 0.7731 | 0.9059 |
| 0.70 | 0.9678 | 0.8809 | 0.9514 |
| 0.75 | 1 | 1 | 1 |

In Fig. 74, the comparison of the modelled and experimentally found niobium site fractions for the $Hf_{3+x}Nb_{3-x}As_2$ phase ($Hf_{3+x}Nb_{3-x}As_2$ structure type) is shown. The calculation was based on the formation energies of the end members given in Table 48 (the last column) and some calculated site fraction values are given in Table 55. The experimental site fractions are taken from the single crystal refinement of $Hf_{3+x}Nb_{3-x}As_2$ taken from sample S43 (see chapter 4.1.1.6). The refined single crystal composition lies outside the phase field range determined by EPMA and the author believes that this is due to the fact that the crystal was picked near the crystal surface, where the composition may differ from the one measured in the bulk of the sample. In this case, the experimental site fractions deviate noticeably from the modelled curves with a maximal difference of nearly 0.1 for the M1 and M2 sites. Still, the fit with the experimental data is quite reasonable. The site fractions for M1 site are overestimated while the ones for M2 and M3 sites are underestimated. A large difference between the niobium site fraction on M3 compared to M1 and M2 is confirmed, but the modelled difference between M1 and M2 site fractions is smaller than the measured one.

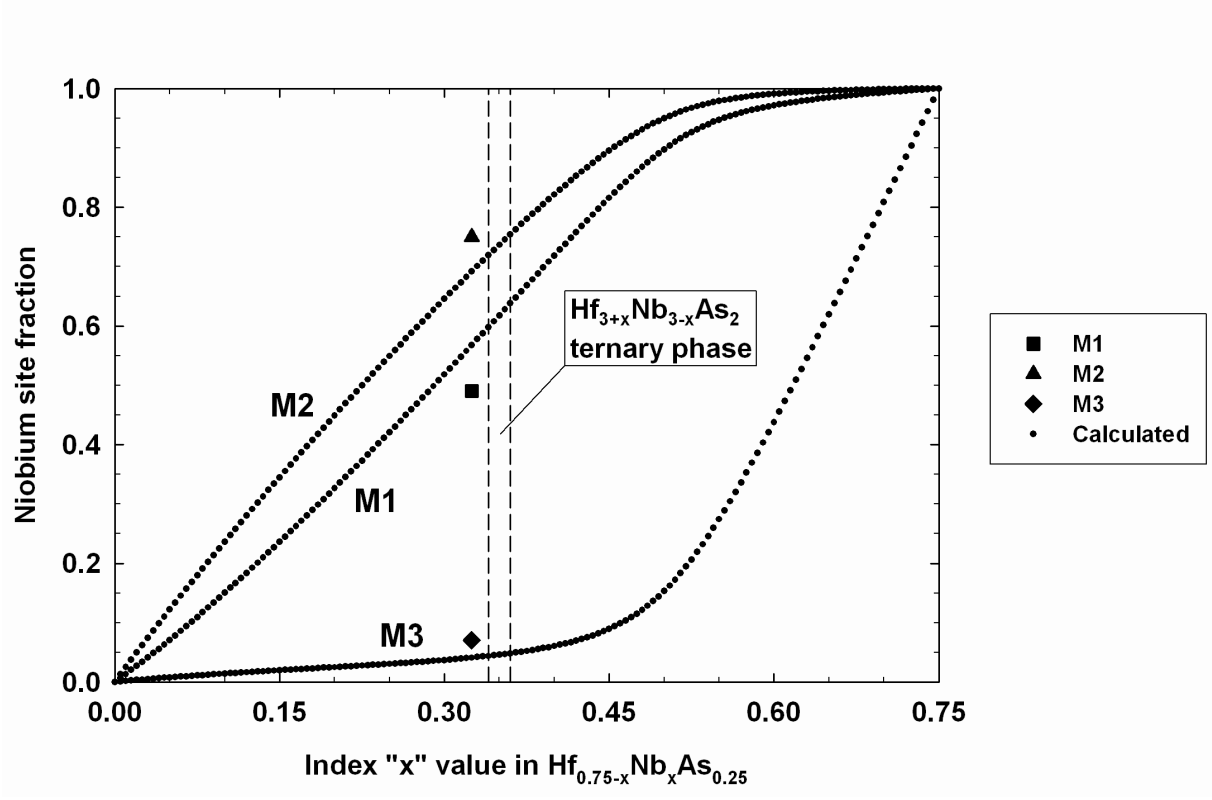


**Fig. 74. The comparison of the niobium site fractions found experimentally for the $Hf_{3+x}Nb_{3-x}As_2$ phase (single crystal data of sample S43, marked by symbols) with those calculated for the $Hf_{3+x}Nb_{3-x}As_2$ structure type. Dashed lines show the experimentally found (EPMA measurement) existence range of the $Hf_{3+x}Nb_{3-x}As_2$-type structure at 1400°C.**

**Table 55. The calculated site fractions for $M_3As$ phase with $Hf_{3+x}Nb_{3-x}As_2$-type structure**

| $Hf_{0.75-x}Nb_xAs_{0.25}$ $Hf_{3+x}Nb_{3-x}As_2$-type | Nb site fraction, $y_{Nb}$ ($y_{Nb} + y_{Hf} = 1$) | | |
|---|---|---|---|
| $x_{Nb}$ | M1 | M2 | M3 |
| 0.00 | 0 | 0 | 0 |
| 0.05 | 0.0706 | 0.1219 | 0.0075 |
| 0.10 | 0.1500 | 0.2361 | 0.0139 |
| 0.15 | 0.2358 | 0.3447 | 0.0195 |
| 0.20 | 0.3263 | 0.4489 | 0.0248 |
| 0.25 | 0.4206 | 0.5491 | 0.0303 |
| 0.30 | 0.5180 | 0.6453 | 0.0368 |
| 0.35 | 0.6176 | 0.7366 | 0.0459 |
| 0.40 | 0.7182 | 0.8212 | 0.0606 |
| 0.45 | 0.8157 | 0.8951 | 0.0893 |
| 0.50 | 0.8975 | 0.9498 | 0.1528 |
| 0.55 | 0.9472 | 0.9788 | 0.2741 |
| 0.60 | 0.9714 | 0.9908 | 0.4379 |
| 0.65 | 0.9844 | 0.9960 | 0.6196 |
| 0.70 | 0.9931 | 0.9986 | 0.8083 |
| 0.75 | 1 | 1 | 1 |

The Gibbs energies per mole of atom for both of these structure types are compared in Fig. 75. Starting from $Nb_3As$, both of them are falling with the increasing hafnium content. After reaching a minimum at the hafnium-rich composition, the energies rise slightly again. The minimum value for the $Ti_3P$-type is reached at the $Hf_{0.72}Nb_{0.03}As_{0.25}$ ($Hf_{2.88}Nb_{0.12}As$) composition and for the $Hf_{3+x}Nb_{3-x}As_2$-type at the $Hf_{0.69}Nb_{0.06}As_{0.25}$ ($Hf_{2.76}Nb_{0.24}As$) composition. The highest value of the Gibbs energy of mixing (in terms of absolute value) for the $Ti_3P$-type is observed for $Hf_{0.40}Nb_{0.35}As_{0.25}$ ($Hf_{1.2}Nb_{1.8}As$) composition and for $Hf_{3+x}Nb_{3-x}As_2$-type for $Hf_{0.30}Nb_{0.45}As_{0.25}$ ($Hf_{1.4}Nb_{1.6}As$). Some selected Gibbs energies for both of the phases are given in Table 56.

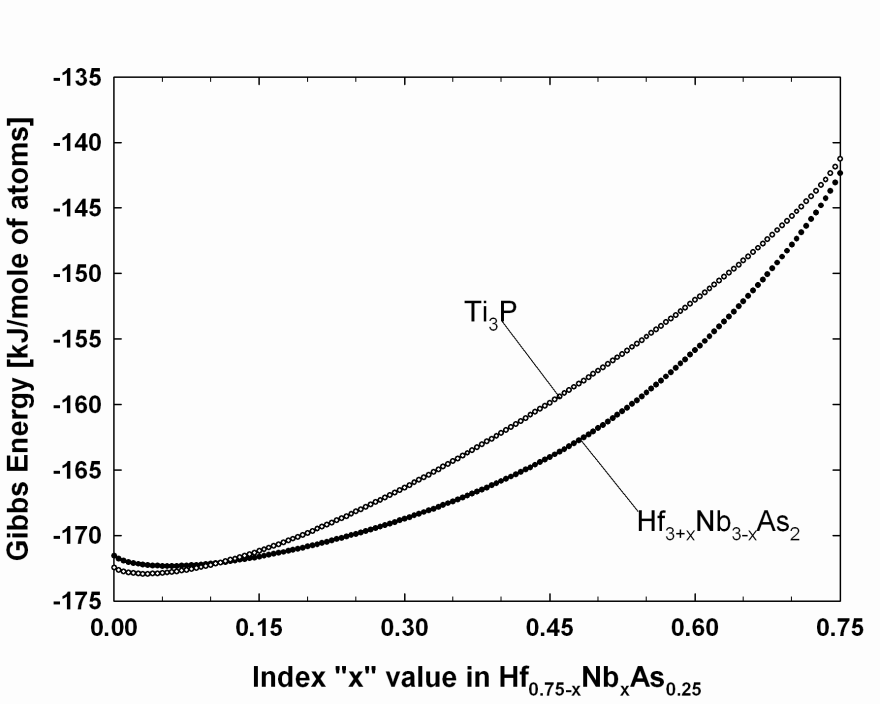


**Fig. 75. The comparison of the modelled Gibbs energies for the $Ti_3P$ and $Hf_{3+x}Nb_{3-x}As$ structures at 1400°C.**

**Table 56. The calculated Gibbs energies for the $M_3As$ phase with $Hf_{3+x}Nb_{3-x}As_2$- and $Ti_3P$ structure.**

| $Hf_{0.75-x}Nb_xAs_{0.25}$ $x_{Nb}$ | Gibbs energy [kJ/mole of atoms] | | Gibbs energy of mixing [kJ/mole of atoms] | |
|---|---|---|---|---|
| | $Hf_{3+x}Nb_{3-x}As$ | $Ti_3P$ | $Hf_{3+x}Nb_{3-x}As$ | $Ti_3P$ |
| 0.00 | -171.55 | -172.45 | 0.00 | 0.00 |
| 0.05 | -172.34 | -172.89 | -2.74 | -2.52 |
| 0.10 | -172.17 | -172.27 | -4.51 | -3.98 |
| 0.15 | -171.64 | -171.20 | -5.93 | -4.99 |
| 0.20 | -170.86 | -169.82 | -7.09 | -5.68 |
| 0.25 | -169.89 | -168.19 | -8.07 | -6.13 |
| 0.30 | -168.75 | -166.35 | -8.87 | -6.37 |
| 0.35 | -167.41 | -164.35 | -9.48 | -6.45 |
| 0.40 | -165.86 | -162.18 | -9.87 | -6.36 |
| 0.45 | -164.04 | -159.88 | -10.00 | -6.14 |
| 0.50 | -161.83 | -157.43 | -9.73 | -5.77 |
| 0.55 | -159.11 | -154.83 | -8.96 | -5.25 |
| 0.60 | -155.88 | -152.05 | -7.67 | -4.54 |
| 0.65 | -152.13 | -149.03 | -5.87 | -3.60 |
| 0.70 | -147.82 | -145.64 | -3.50 | -2.29 |
| 0.75 | -142.37 | -141.27 | 0.00 | 0.00 |

## 4.2 Hf-Nb-Ge system

### 4.2.1 DFT calculations

As mentioned in the literature review (chapters 2.3.2 and 2.4.2), site preferences are observed in the $Hf_{5-x}Nb_xGe_4$ solid solution (oP36, $Sm_5Ge_4$-type) [82]. Thus, this phase was chosen for the DFT calculations in order to examine the formation energies of the end members in the ground state. First, the ground state energy of Ge with the crystal structure stable at 298 K (cubic diamond) was determined, with the crystal structure data taken from literature [3]. After dividing this energy by the number of atoms in the unit cell of this structure, the energy per germanium atom was obtained. The calculated energies of the elements which were used in this modelling are given in Table 57 (the energies for hafnium and niobium were already determined in chapter 4.1.2.1).

**Table 57. The calculated energies for elemental hafnium, niobium and germanium**

| Element | Structure type | Energy per unit cell [eV] | Energy per atom [eV] |
|---|---|---|---|
| Ge | C(diamond) | -9.2419 | -4.6209 |
| Hf | Mg(hcp) | -19.8801 | -9.9400 |
| Nb | W(bcc) | -20.4276 | -10.2138 |

Next, the ground state energies of the $Hf_5Ge_4$ end members were calculated, with all structures allowed to relax their cell parameters and change the atom positions (see Appendix G.4 for the ground state structure data). The sublattices were defined in form of (M1:M2:M3:Ge), i.e. consitent with the metal site notation, and germanium atoms were restricted to one separate sublattice. The ground state energies were divided by four to obtain the energies per formula unit (the *oP*36 unit cell contains four $M_5Ge_4$ units). Formation energies were found by subtracting the energies of $Hf_{5-x}Nb_xGe_4$ mixtures from the energies per formula unit, whereby the former were calculated by summing the element's energies per atom according to the mixture's stoichiometry. The last step was the recalculation of these mixture's values to kilojoules per mole of atoms by division by nine (as nine atoms are included in the $M_5Ge_4$ formula) and multiplication by 96.485. The results are given in Table 58. Analysing these data, it was found that the energies for (Hf:Nb:Hf:Ge) and (Hf:Hf:Nb:Ge) end members were identical and this would mean that the substitution of the hafnium atoms

**Table 58. The calculated end member energies for the $Hf_5Ge_4$ structure ($Sm_5Ge_4$ type) with the k-points set of 5 x 10 x 5. The atoms were allowed to migrate during the calculation.**

| $Hf_5Ge_4$ end member | $x_{Nb}$ | Energy per unit cell [eV] | Energy per formula unit [eV] | Energy of $(Hf,Nb)_5Ge_4$ mixture [eV] | Formation energy [eV] | Formation energy per mole of atoms [kJ] |
|---|---|---|---|---|---|---|
| (Hf:Hf:Hf:Ge) | 0 | -297.9808 | -74.4952 | -68.1840 | -6.3112 | -67.66 |
| (Nb:Hf:Hf:Ge) | 0.111 | -299.0222 | -74.7556 | -68.4577 | -6.2978 | -67.52 |
| (Hf:Nb:Hf:Ge) | 0.222 | -298.2232 | -74.5558 | -68.7315 | -5.8243 | -62.44 |
| (Hf:Hf:Nb:Ge) | 0.222 | -298.2230 | -74.5557 | -68.7315 | -5.8242 | -62.44 |
| (Nb:Nb:Hf:Ge) | 0.333 | -298.2795 | -74.5699 | -69.0053 | -5.5646 | -59.66 |
| (Nb:Hf:Nb:Ge) | 0.333 | -293.9612 | -73.4903 | -69.0053 | -4.4850 | -48.08 |
| (Hf:Nb:Nb:Ge) | 0.444 | -292.2558 | -73.0639 | -69.2790 | -3.7849 | -40.58 |
| (Nb:Nb:Nb:Ge) | 0.555 | -292.0609 | -73.0152 | -69.5528 | -3.4624 | -37.12 |

**Table 59. The calculated end member energies for the $Hf_5Ge_4$ structure ($Sm_5Ge_4$ type) with with the k-points set of 5 x 10 x 5. The atoms were held on atom positions calculated for binary $Hf_5Ge_4$ (i.e. (Hf:Hf:Hf:Ge)) end member).**

| $Hf_5Ge_4$ end member | $x_{Nb}$ | Energy per unit cell [eV] | Energy per formula unit [eV] | Energy of $(Hf,Nb)_5Ge_4$ mixture [eV] | Formation energy [eV] | Formation energy per mole of atoms [kJ] |
|---|---|---|---|---|---|---|
| (Nb:Hf:Hf:Ge) | 0.111 | -298.9222 | -74.7306 | -68.4577 | -6.2728 | -67.25 |
| (Hf:Nb:Hf:Ge) | 0.222 | -297.6697 | -74.4174 | -68.7315 | -5.6859 | -60.96 |
| (Hf:Hf:Nb:Ge) | 0.222 | -293.3867 | -73.3467 | -68.7315 | -4.6152 | -49.48 |

by niobium on the sites Hf2 and Hf3 requires the same amount of energy. If that was the case, identical or very similar values would be expected for the energies of (Nb:Nb:Hf:Ge) and (Nb:Hf:Nb:Ge) members, while the calculated difference for those was about 10 kJ/mol.

Comparing the calculated ground state structures (see Appendix G.4), one notes immediately the significant difference of the atom positions of the (Hf:Hf:Nb:Ge) end member compared to the other ones. But a careful analysis of this structure shows that in fact it is the same structure as the one of the (Hf:Nb:Hf:Ge) member. By moving the cell origin of (Hf:Hf:Nb:Ge) by a vector [0.5; 0.5; 0] and keeping in mind the symmetry operations in the cell, one can see that the M3 site atoms in (Hf:Hf:Nb:Ge) are the same as the ones on M2 site in (Hf:Nb:Hb:Ge). Also, the M2 atoms of (Hf:Hf:Nb:Ge) are the same as the ones on M3 site in (Hf:Nb:Hf:Ge). A similar exchange of germanium atoms in these two end members is observed for Ge1 and Ge2 sites. Also, the lattice parameters of both of the unit cells differ by less than 0.01 Å. This means that due to the atom migration during the iteration, the initial structures of these two end members transferred to the same final structure.

As a result of this fact, the end members with no atom relaxation allowed must be calculated to estimate the energy contribution of niobium substituting hafnium. By doing this (with the allowed change of the cell parameters), an energy difference of about 10 kJ/mol is found between the two end members with (Hf:Nb:Hf:Ge) being more stable (see Table 59). The values of the formation energies for the various end members are compared in Fig. 76. By connecting the end members with the lowest formation energy with a line, the substitution order for niobium substituting hafnium can be created: M1→M2→M3. This agrees with the reported site preferences. The formation energies for the end members with the atoms immobilised on the atom positions of the (Hf:Hf:Hf:Ge) ground structure were calculated by the corresponding addition of the substitution energies of the monosubstituted end members and are given in Table 60.

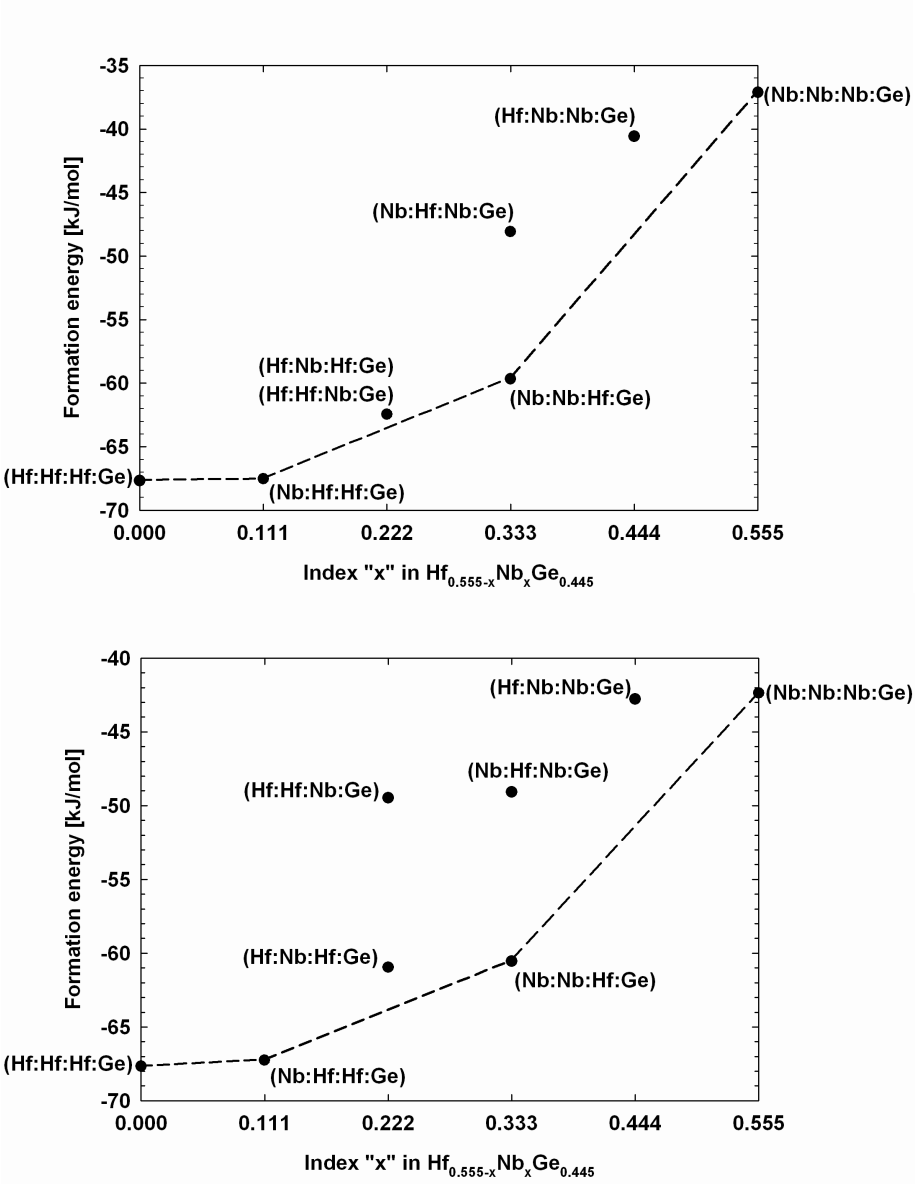


**Fig. 76. The graphic presentation of the end member energies for the calculation with the atoms relaxed (top) and kept on positions calculated for binary $Hf_5Ge_4$ (bottom)**

The comparison of the calculated lattice parameters for binary $Hf_5Ge_4$ with those reported in literature [50] shows that the calculated lattice parameters are ~1% larger than the experimental ones. The fractional coordinates of the atom positions agree within an accuracy of 0.001. The values of the lattice parameters for the ternary compounds found experimentally [82] can be compared with the values of the most stable end members (i.e. (Hf:Hf:Hf:Ge), (Nb:Hf:Hf:Ge), (Nb:Nb:Hf:Ge) and (Nb:Nb:Nb:Ge)), though it is clear that the latter are the ordered compounds which are not found in the investigated samples. This comparison is shown in Fig. 77. Again, the calculated lattice parameters are larger than the experimental ones. But the comparison of the lattice parameter ratio for the experimental samples and the computed end members (Fig. 78) yields an interesting observation. It can be clearly seen that

the trends observed experimentally are reproduced very well by the calculated cell parameters. This shows that the influence of the almost stepwise substitution of hafnium by niobium on the lattice parameters can be reproduced by lattice parameters calculated for the corresponding ordered compounds.

**Table 60. The formation and substitution enengies for the end members calculated with atoms fixed on (Hf:Hf:Hf:Ge) ground structure. The substitution energies are referred to the formation energy of (Hf:Hf:Hf:Ge) end member. The substitution energies of the monosubstituted end members are added accordingly for the construction of the other substitution energies (e.g. the formation energy of (Nb:Hf:Nb:Ge) member is taken as a sum of the formation energy of (Hf:Hf:Hf:Ge) with the substitution energies of (Nb:Hf:Hf:Ge) and (Hf:Hf:Nb:Ge) members)**

| $Hf_5Ge_4$ end member | Formation energy per mole of atoms [kJ] | Substitution energy per mole of atoms [kJ] |
|---|---|---|
| (Hf:Hf:Hf:Ge) | -67.66 | 0 |
| (Nb:Hf:Hf:Ge) | -67.25 | 0.41 |
| (Hf:Nb:Hf:Ge) | -60.96 | 6.70 |
| (Hf:Hf:Nb:Ge) | -49.48 | 18.18 |
| (Nb:Nb:Hf:Ge) | -60.55 | 7.11 |
| (Nb:Hf:Nb:Ge) | -49.07 | 18.59 |
| (Hf:Nb:Nb:Ge) | -42.78 | 24.88 |
| (Nb:Nb:Nb:Ge) | -42.37 | 25.29 |

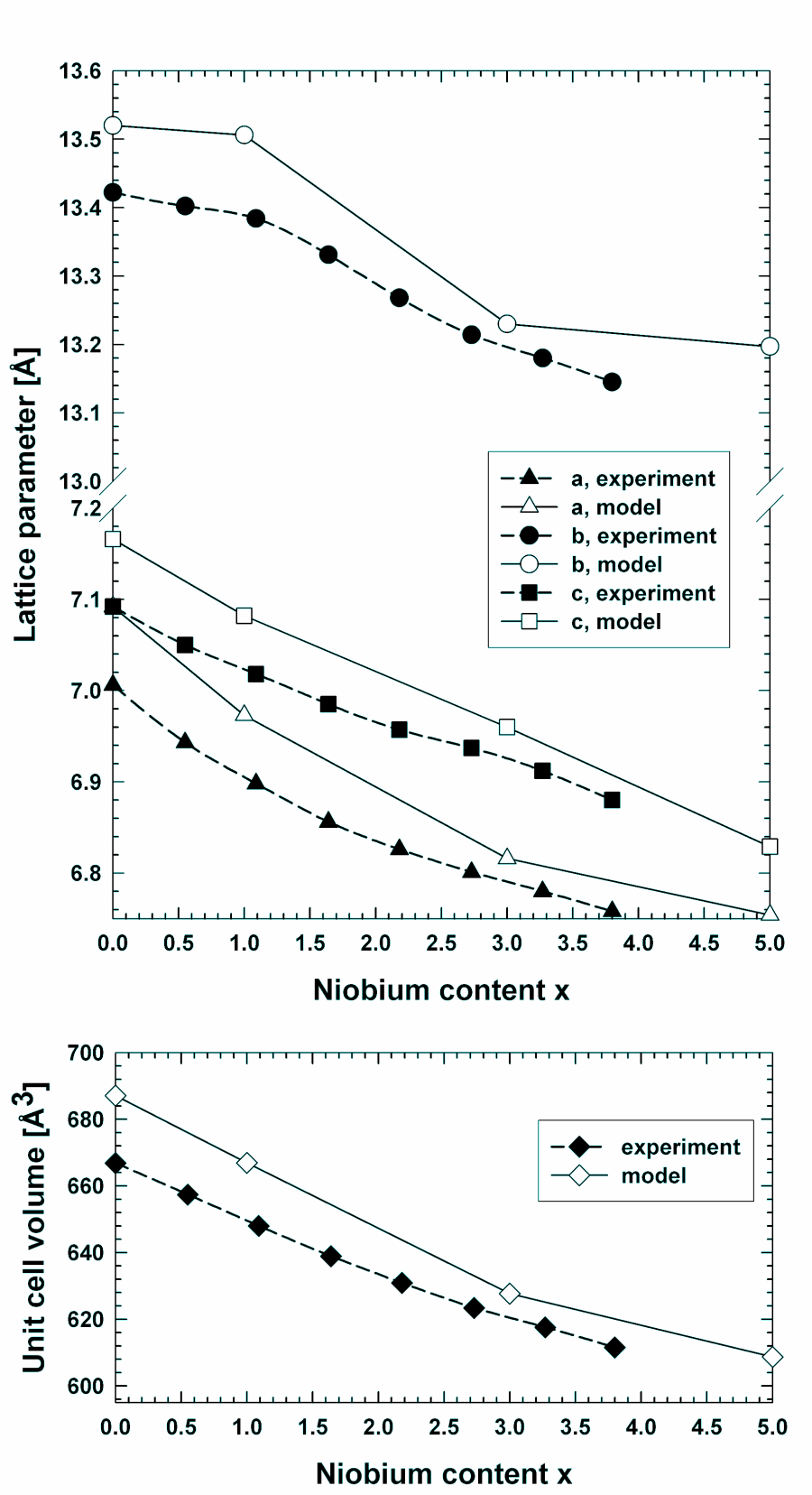


**Fig. 77. The comparison of the reported lattice parameters (top) and cell volumes [82] (bottom) with the values obtained for the most stable end members of the $Hf_{5-x}Nb_xGe_4$ phase.**

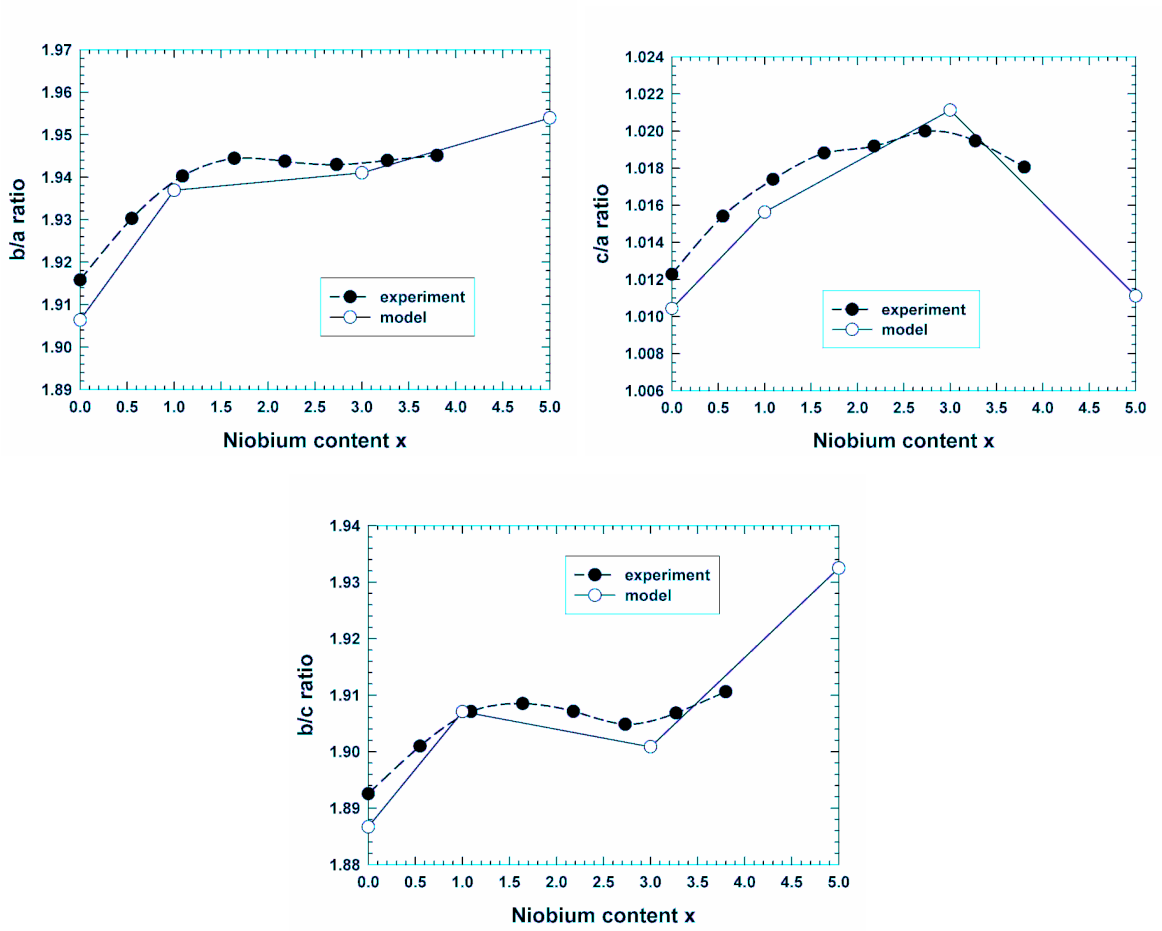


**Fig. 78. The comparison of the reported lattice parameter ratios [82] and the ones taken for the most stable end members of the $Hf_{5-x}Nb_xGe_4$ phase.**

### 4.2.2 Thermodynamic modeling of the site fractions in $Hf_{5-x}Nb_xGe_4$ phase

The ground state energies for the end members of the $Hf_{5-x}Nb_xGe_4$ phase were used as input into the Compound Energy Model. First, the calculation with the energies for the ground state structures (relaxed atoms) was taken (the last column of Table 58). As the structure of the (Hf:Hf:Nb:Ge) end member transformed to the (Hf:Nb:Hf:Ge) structure, when the atoms were allowed to relax, the energy for this compound was taken from the calculation where the atoms were kept fixed on the positions of the calculated binary $Hf_5Ge_4$ structure (the value is given in the last column in Table 59 for this end member). All other energies were taken from the calculations where the atoms were allowed to move (given in the last column of Table 58). Selected values for the calculated site fractions are given in Table 61. Although, the calculation underestimates the niobium occupancy on the M1 site and overestimates it slightly

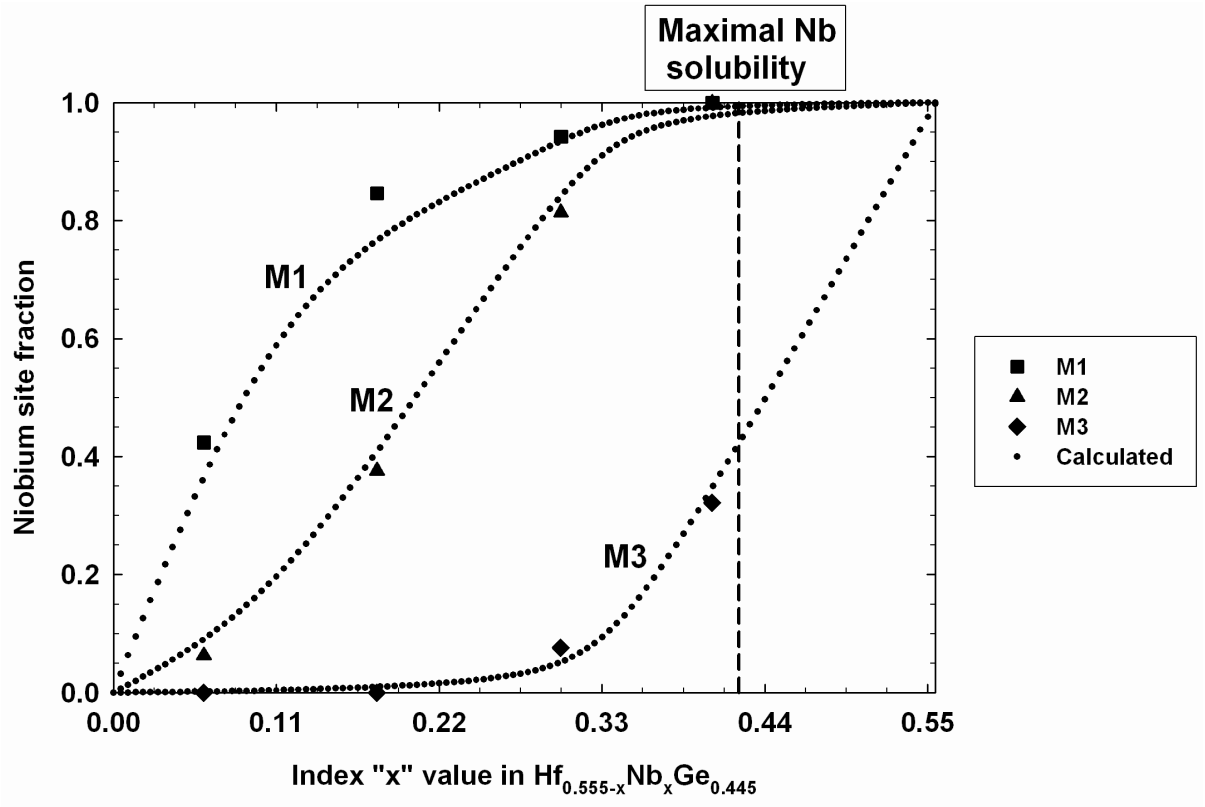


**Fig. 79. The comparison of the niobium site fractions reported for the $Hf_{5-x}Nb_xGe_4$ phase ([82], marked by symbols) with the ones calculated on basis of the formation energies taken from the calculations with relaxed atom positions (except (Hf:Hf:Nb:Ge)). Dashed lines show the reported niobium solubility range in this phase at 1400°C.**

**Table 61. The calculated site fractions for the $Hf_{5-x}Nb_xGe_4$ phase. Except of (Hf:Hf:Nb:Ge), all formation energies are taken from the calculations with relaxed atom positions.**

| $Hf_{0.555-x}Nb_xGe_{0.445}$ $Sm_5Ge_4$-type | Nb site fraction, $y_{Nb}$ ($y_{Nb} + y_{Hf} = 1$) | | |
|---|---|---|---|
| $x_{Nb}$ | M1 | M2 | M3 |
| 0.000 | 0 | 0 | 0 |
| 0.050 | 0.3042 | 0.0717 | 0.0012 |
| 0.100 | 0.5498 | 0.1718 | 0.0033 |
| 0.150 | 0.7080 | 0.3142 | 0.0068 |
| 0.200 | 0.8024 | 0.4865 | 0.0124 |
| 0.250 | 0.8707 | 0.6672 | 0.0225 |
| 0.300 | 0.9316 | 0.8347 | 0.0495 |
| 0.350 | 0.9756 | 0.9420 | 0.1453 |
| 0.400 | 0.9905 | 0.9756 | 0.3292 |
| 0.450 | 0.9956 | 0.9873 | 0.5399 |
| 0.500 | 0.9982 | 0.9941 | 0.7569 |
| 0.555 | 1 | 1 | 1 |

on the M2 site, a good agreement between the calculated and reported [82] (see Table 18 in chapter 2.4.2) site fractions can be observed in Fig. 79.

The next attempt was based on a simplified approach, with reduced computational cost. In this case, only the formation energies for the niobium monosubstituted end members (i.e. (Nb:Hf:Hf:Ge), (Hf:Nb:Hf:Ge) and (Hf:Hf:Nb:Ge)), together with the formation energy of the binary (Hf:Hf:Hf:Ge) end member were taken from the DFT calculations. The other energies were obtained from the corresponding addition of the substitution energies of the monosusbtituted energies and the formation energy of the (Hf:Hf:Hf:Ge) end member (e.g., the formation energy of the (Nb:Hf:Nb:Ge) member is taken as a sum of the formation energy of (Hf:Hf:Hf:Ge) with the substitution energies of the (Nb:Hf:Hf:Ge) and (Hf:Hf:Nb:Ge) members). The next simplification step was obtained by considering the energies for the structures with the atoms fixed on positions found in the ground state structure of $Hf_5Ge_4$, as the calculations with allowed atom relaxation require more time. The set of the applied formation energies was already given in Table 60 and the results are shown in Fig. 80. It is quite surprising that the simplified model yields values which are closer to the ones reported in the literature compared to the model where all energies were taken for the relaxed structures. The reason for that must obviously be the formation energy differences in the two sets. The relaxation of the atoms results in an energy gain of 0.3 kJ in case of (Nb:Hf:Hf:Ge) and 1.4 kJ in case of (Hf:Nb:Hf:Ge), as it can be seen when the formation energies for these end members are compared (for (Hf:Hf:Hf:Ge) the same formation energy was used). Thus the relaxation of the atoms will increase the number of niobium atoms present on M2 sites in the thermodynamic calculation. Starting from the almost ideal fit found in the “fixed” model, the atom relaxation leads to the situation found in the previous model, where the niobium site fraction on the M2 site was overrated and the fraction on the M1 site was underrated. As the multiplicity of the M2 site is twice the multiplicity of the M1 site, the small variation of site fractions on the M2 site has a proportionally greater effect on the site fractions on the M1 site, being subject to the same composition constraint. Selected values for the site fractions predicted by the simplified approach are given in Table 62.

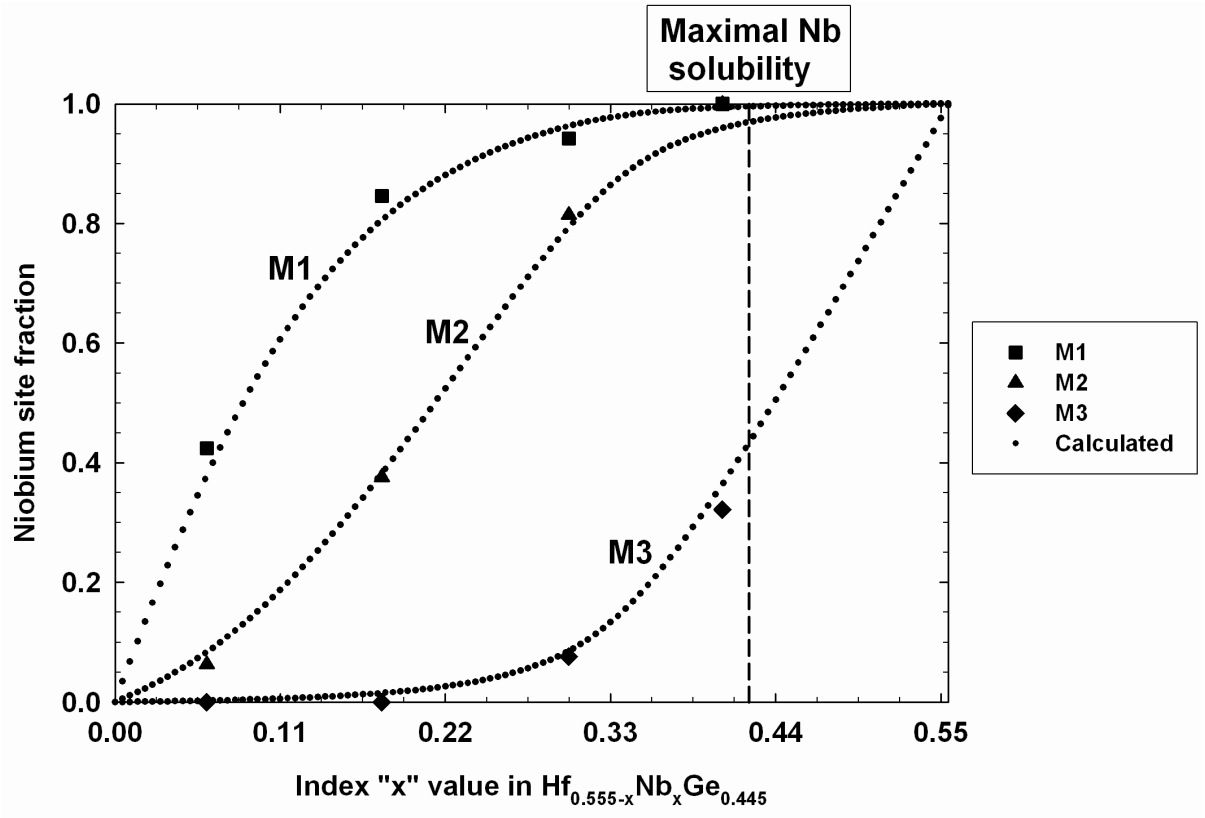


**Fig. 80. The comparison of the niobium site fractions reported for the $Hf_{5-x}Nb_xGe_4$ phase ([82], marked by symbols) with the ones calculated on basis of the formation energies of the niobium monosubstituted end members taken from the calculations with atoms fixed on positions of the ground state structure of binary $Hf_5Ge_4$ end member. Dashed lines show the reported niobium solubility range in this phase at 1400°C.**

**Table 62. The calculated site fractions for the $Hf_{5-x}Nb_xGe_4$ phase. The energies of the monosubstituted end members were used as a base for the calculation of the other energies.**

| $Hf_{0.555-x}Nb_xGe_{0.445}$ $Sm_5Ge_4$-type | Nb site fraction, $y_{Nb}$ ($y_{Nb} + y_{Hf} = 1$) | | |
|---|---|---|---|
| $x_{Nb}$ | M1 | M2 | M3 |
| 0.000 | 0 | 0 | 0 |
| 0.050 | 0.3170 | 0.0649 | 0.0017 |
| 0.100 | 0.5652 | 0.1627 | 0.0047 |
| 0.150 | 0.7378 | 0.2960 | 0.0101 |
| 0.200 | 0.8487 | 0.4558 | 0.0199 |
| 0.250 | 0.9184 | 0.6267 | 0.0392 |
| 0.300 | 0.9613 | 0.7871 | 0.0823 |
| 0.350 | 0.9840 | 0.9015 | 0.1816 |
| 0.400 | 0.9932 | 0.9564 | 0.3471 |
| 0.450 | 0.9970 | 0.9802 | 0.5463 |
| 0.500 | 0.9988 | 0.9923 | 0.7583 |
| 0.555 | 1 | 1 | 1 |

The third modelling calculation was based on the basis of the energies given in ref. [82], where the same simplification was used, as in the previous model, i.e. the energies of the niobium monosubstituted end members were used for the calculation of the other end member energies. The set of energies is given in Table 63 and the calculation results are depicted in Fig. 81. It can be seen that with this set the niobium occupancy on the M1 site is clearly overestimated in comparison with the previous two modelling results - this must be due to the negative substitution energy for the (Nb:Hf:Hf:Ge) end member used in this set of energies. Selected values of the predicted site fractions are given in Table 64.

**Table 63. The list of formation energies used in the ref. [82] for the simplified model**

| $Hf_{5-x}Nb_xGe_4$ $Sm_5Ge_4$-type (M1:M2:M3:Ge) | Formation energy per mole of atoms [kJ] | Substitution energy per mole of atoms [kJ] |
|---|---|---|
| (Hf:Hf:Hf:Ge) | -55.0 | 0 |
| (Nb:Hf:Hf:Ge) | -57.8 | -2.8 |
| (Hf:Nb:Hf:Ge) | -47.6 | 7.4 |
| (Hf:Hf:Nb:Ge) | -27.6 | 27.4 |
| (Nb:Nb:Hf:Ge) | -50.4 | 4.6 |
| (Nb:Hf:Nb:Ge) | -30.4 | 24.6 |
| (Hf:Nb:Nb:Ge) | -20.2 | 34.8 |
| (Nb:Nb:Nb:Ge) | -23.0 | 32.0 |

**Table 64. The calculated site fractions for the $Hf_{5-x}Nb_xGe_4$ phase. The energies of the monosubstituted end members were used as a base for the calculation of the other energies.**

| $Hf_{0.555-x}Nb_xGe_{0.445}$ $Sm_5Ge_4$-type | Nb site fraction, $y_{Nb}$ ($y_{Nb} + y_{Hf} = 1$) | | |
|---|---|---|---|
| $x_{Nb}$ | M1 | M2 | M3 |
| 0.00 | 0 | 0 | 0 |
| 0.05 | 0.4280 | 0.0110 | 0.0000 |
| 0.100 | 0.7923 | 0.0538 | 0.0001 |
| 0.150 | 0.9445 | 0.2024 | 0.0004 |
| 0.200 | 0.9789 | 0.4095 | 0.0011 |
| 0.250 | 0.9912 | 0.6268 | 0.0026 |
| 0.300 | 0.9972 | 0.8432 | 0.0083 |
| 0.350 | 0.9998 | 0.9847 | 0.0905 |
| 0.400 | 0.9999 | 0.9965 | 0.3036 |
| 0.450 | 1.0000 | 0.9986 | 0.5264 |
| 0.500 | 1.0000 | 0.9995 | 0.7506 |
| 0.555 | 1 | 1 | 1 |

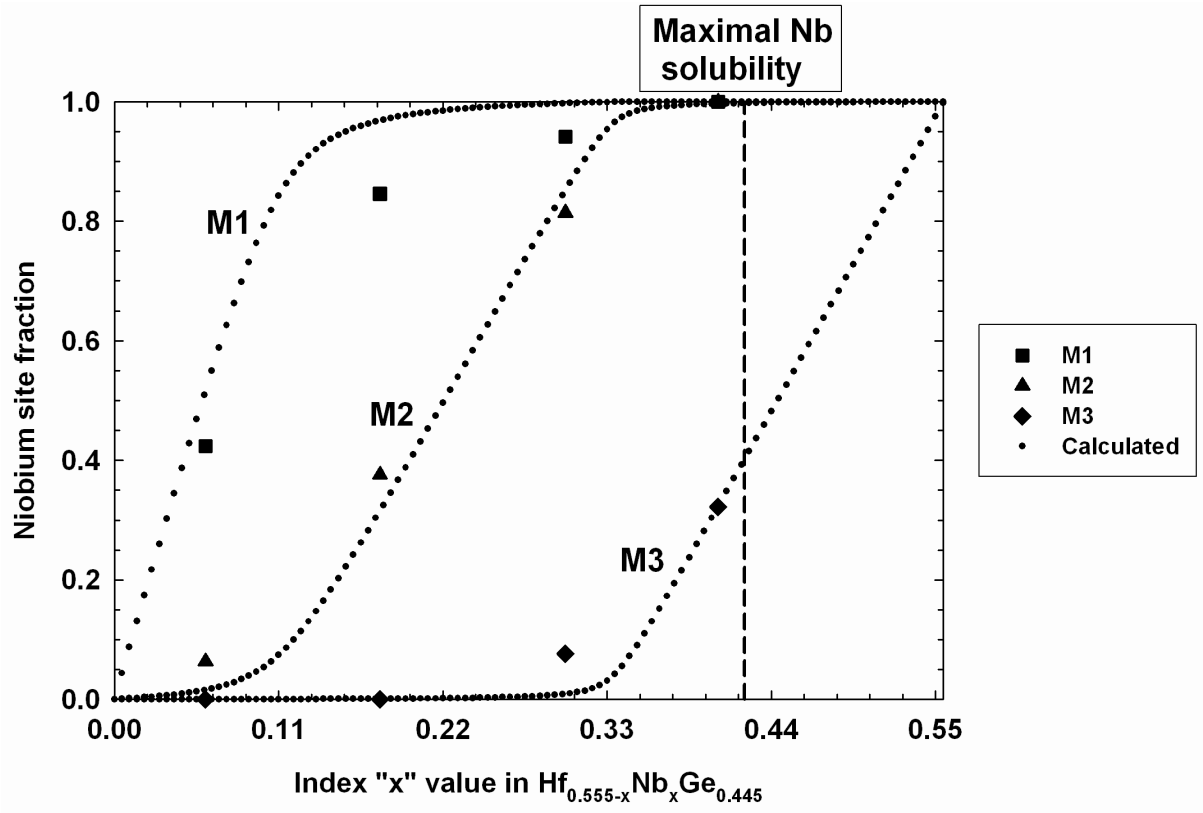


**Fig. 81. The comparison of the niobium site fractions reported for the $Hf_{5-x}Nb_xGe_4$ phase ([82], marked by symbols) with the ones calculated on basis of the formation energies given in ref. [82]. Dashed lines show the reported niobium solubility range in this phase at 1400°C.**

All used sets of energies are summarised in Table 65**,** and labelled as *A*, *B* and *C*. The modelled Gibbs energies of the $Hf_{5-x}Nb_xGe_4$ phase calculated with each set are shown in Fig. 82 and a few values are given in Table 66. The values for set *C* are less negative than the ones for set *A* and *B*, as the formation energies of the binary germanides in this set are less negative than in the other two (-55.0 kJ in *C* compared to -67.7 kJ in *A* and *B* for $Hf_5Ge_4$, -23.0 kJ in *C* compared to ~-40 kJ in *A* and *B* for $Nb_5Ge_4$) – this is due to the fact that these parameters were estimated based on the reported thermodynamic data [82]. With increasing niobium content in the phase, the energies obtained with set *A* give higher values than the ones obtained with set *B*, because of the difference in the energy values for the (Nb:Nb:Nb:Ge) end member (-37.12 kJ in *A* and -42.37 kJ for *B*). The minimal values are found for $Hf_{0.520}Nb_{0.035}Ge_{0.445}$ (Set *A* and *B*) and $Hf_{0.475}Nb_{0.080}Ge_{0.445}$ (Set *C*) compositons. The maximal Gibbs energies of mixing are found for the compositions: $Hf_{0.265}Nb_{0.290}Ge_{0.445}$ (Set *A* and *B*) and $Hf_{0.255}Nb_{0.300}Ge_{0.445}$ (Set *C*).

**Table 65. The summary of the energies taken for the various sets used for the thermodynamic modelling of the $Hf_{5-x}Nb_xGe_4$ phase.**

| $Hf_{5-x}Nb_xGe_4$ $Sm_5Ge_4$-type (M1:M2:M3:Ge) | Formation energy per mole of atoms [kJ] | | |
|---|---|---|---|
| | Set A | Set B | Set C [82] |
| (Hf:Hf:Hf:Ge) | -67.66 | -67.66 | -55.0 |
| (Nb:Hf:Hf:Ge) | -67.52 | -67.25 | -57.8 |
| (Hf:Nb:Hf:Ge) | -62.44 | -60.96 | -47.6 |
| (Hf:Hf:Nb:Ge) | -49.48 | -49.48 | -27.6 |
| (Nb:Nb:Hf:Ge) | -59.66 | -60.55 | -50.4 |
| (Nb:Hf:Nb:Ge) | -48.08 | -49.07 | -30.4 |
| (Hf:Nb:Nb:Ge) | -40.58 | -42.78 | -20.2 |
| (Nb:Nb:Nb:Ge) | -37.12 | -42.37 | -23.0 |

**Table 66. The calculated Gibbs energies for the $Hf_{5-x}Nb_xGe_4$ phase.**

| $Hf_{0.555-x}Nb_xGe_{0.445}$ $Sm_5Ge_4$-type $x_{Nb}$ | Gibbs energy [kJ/mole of atoms] | | | Gibbs energy of mixing [kJ/mole of atoms] | | |
|---|---|---|---|---|---|---|
| | Set *A* | Set *B* | Set *C* | Set *A* | Set *B* | Set *C* |
| 0.000 | -171.84 | -171.84 | -159.18 | 0.00 | 0.00 | 0.00 |
| 0.050 | -172.38 | -172.25 | -160.81 | -4.02 | -3.41 | -5.24 |
| 0.100 | -171.63 | -171.48 | -160.97 | -6.74 | -5.65 | -9.00 |
| 0.150 | -170.15 | -170.11 | -160.01 | -8.74 | -7.28 | -11.65 |
| 0.200 | -168.07 | -168.23 | -158.20 | -10.14 | -8.41 | -13.45 |
| 0.250 | -165.43 | -165.87 | -155.75 | -10.97 | -9.05 | -14.61 |
| 0.300 | -162.18 | -163.00 | -152.62 | -11.20 | -9.19 | -15.08 |
| 0.350 | -158.11 | -159.54 | -148.26 | -10.61 | -8.73 | -14.33 |
| 0.400 | -153.18 | -155.45 | -142.38 | -9.15 | -7.65 | -12.06 |
| 0.450 | -147.58 | -150.78 | -135.72 | -7.03 | -5.98 | -9.00 |
| 0.500 | -141.34 | -145.51 | -128.42 | -4.27 | -3.72 | -5.31 |
| 0.555 | -133.25 | -138.49 | -119.14 | 0.00 | 0.00 | 0.00 |

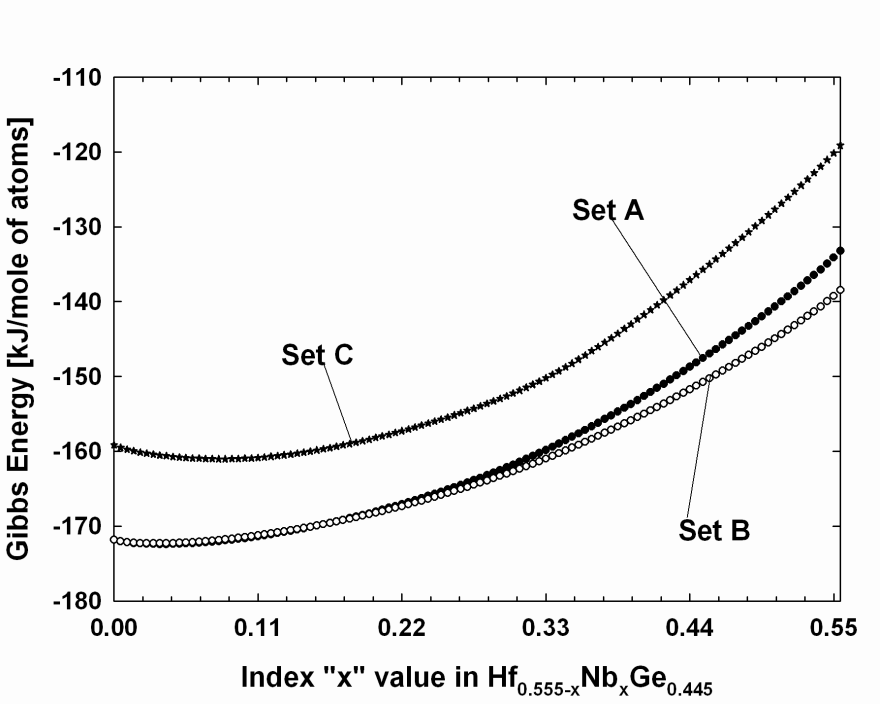


**Fig. 82. Gibbs energy of the $Hf_{5-x}Nb_xGe_4$ phase obtained with different sets of formation energies at 1400°C.**

## 4.3 Hf-Nb-Ga system

### 4.3.1 Experimental results

A series of 6 samples was prepared along the $Hf_{1-x}Nb_xGa$ phase field. The nominal compositions of the samples are listed in Table 67 and shown on a ternary Gibbs diagram in Fig. 83. Small mass losses were observed after arc-melting and annealing which are believed to be caused by gallium evaporation, as the boiling point of this metal (2403°C) lies close to the melting points of hafnium and niobium (2230°C and 2468°C respectively). Based on this assumption, the sample compositions were calculated (see Appendix F.2) and used for further consideration. The losses did not affect the sample compositions as dramatic as in the case of the arsenide samples – the gallium content did not drop below 49 at.%.

Powder XRD measurements showed that all samples contained the phases crystallising with HfGa and $Hf_5Ga_3$ structures. Small amounts of hafnium dioxide were also detected in all samples, which is believed to be a product of the reaction with the oxygen contained in the metal powders used for the synthesis. The niobium-richest samples (G6 and G7) contained also a phase crystallising with $Nb_5Ga_4$ structure. The results of the Rietveld refinement of the samples containing three intermetallic phases and a small but detectable amount of $HfO_2$ might be of doubtful quality, however, this method was applied also to sample G6 which contained ~87% of the HfGa-type phase. The content of the $Nb_5Ga_4$ phase in sample G7 was larger than 20%, so no refinement was done on this sample. The results of Rietveld refinement are given in Tables 68-75 (the remaining fraction of the pattern was $HfO_2$).

**Table 67. The composition of the investigated samples in the Hf-Nb-Ga system**

| Sample | Nominal Composition [at.%] | | | Calculated composition [at.%] | | |
|---|---|---|---|---|---|---|
| | Ga | Hf | Nb | Ga | Hf | Nb |
| G1 | 50 | 45 | 5 | 49.5 | 44.7 | 5.8 |
| G2 | 50 | 40 | 10 | 49.3 | 40.3 | 10.4 |
| G3 | 50 | 35 | 15 | 49.8 | 34.9 | 15.3 |
| G4 | 50 | 30 | 20 | 49.7 | 29.7 | 20.5 |
| G5 | 50 | 25 | 25 | 49.1 | 25.3 | 25.6 |
| G6 | 50 | 20 | 30 | 49.4 | 19.8 | 30.8 |
| G7 | 50 | 15 | 35 | 49.7 | 14.8 | 35.5 |

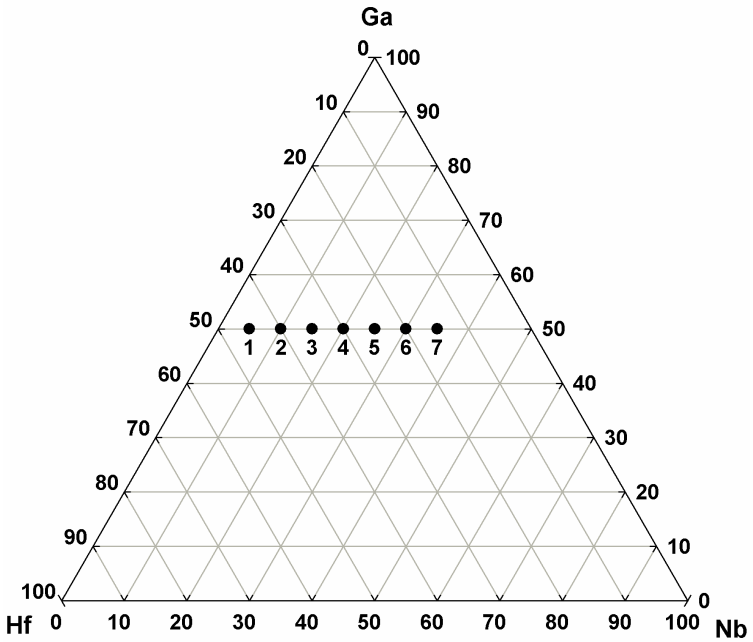


**Fig. 83. The nominal compositions of the samples prepared in the Hf-Nb-Ga system. The numbers refer to the sample name (e.g "1" for sample "G1").**

**Table 68. Rietveld refinement results for the HfGa phase in sample G1**

| Sample: G1 | | Nominal composition: $Hf_{45}Nb_5Ga_{50}$ | | | $R_p$: 4.16 | | $R_{wp}$: 5.64 |
|---|---|---|---|---|---|---|---|
| Background model: Chebyshev, 4th order | | | | | 2$\theta$-range [°]: 10 - 120° | | |
| Main phase: (Hf,Nb)Ga | | Structure type: ThTl | | | Space group: *Pbcm* (57) | | |
| Lattice parameters [Å] | | a = 9.17102(6)<br>b = 8.47586(6)<br>c = 5.59860(3) | Cell volume [Å$^3$]: 435.192(5) | | Fraction: 93.2(1)% | | $R_{Bragg}$: 1.83 |
| Site | Mpl. | x | y | z | Atom | Site fr. | B(eq.) |
| M1 | 4c | 0.1124(1) | 1/4 | 0 | Hf | 0.64(1) | 0.14(8) |
| | | | | | Nb | 0.36(1) | |
| M2 | 4d | 0.6198(1) | 0.5265(1) | 1/4 | Hf | 0.89(1) | |
| | | | | | Nb | 0.11(1) | |
| M3 | 4d | 0.1884(1) | 0.6349(1) | 1/4 | Hf | 0.91(1) | |
| | | | | | Nb | 0.09(1) | |
| Ga1 | 4c | 0.5685(3) | 1/4 | 0 | Ga | 1 | 0.43(9) |
| Ga2 | 4d | 0.0831(3) | 0.9524(4) | 1/4 | Ga | | |
| Ga3 | 4d | 0.6511(3) | 0.8659(4) | 1/4 | Ga | | |
| Niobium content calculated from site fractions: 9.3 at.% | | | Crystallite size (Lorenzian) [nm]: 140(1) | | | Preferred Orientation spherical harmonics order: 6 | |

**Table 69. Rietveld refinement results for the HfGa phase in sample G2**

| Sample: G2 | | Nominal composition: $Hf_{40}Nb_{10}Ga_{50}$ | | | $R_p$: 3.55 | | $R_{wp}$: 4.75 |
|---|---|---|---|---|---|---|---|
| Background model: Chebyshev, 4th order | | | | | 2$\theta$-range [°]: 10 – 120° | | |
| Main phase: (Hf,Nb)Ga | | Structure type: ThTl | | | Space group: *Pbcm* (57) | | |
| Lattice parameters [Å] | a = 9.16210(4)<br>b = 8.44986(4)<br>c = 5.55821(2) | Cell volume [Å$^3$]: 430.308(3) | | | Fraction: 93.7(1)% | | $R_{Bragg}$: 1.89 |
| Site | Mpl. | x | y | z | Atom | Site fr. | B(eq.) |
| M1 | 4c | 0.1118(1) | 1/4 | 0 | Hf | 0.463(8) | 0.19(9) |
| | | | | | Nb | 0.537(8) | |
| M2 | 4d | 0.62112(9) | 0.5284(1) | 1/4 | Hf | 0.952(9) | |
| | | | | | Nb | 0.048(9) | |
| M3 | 4d | 0.18634(9) | 0.6346(1) | 1/4 | Hf | 0.956(9) | |
| | | | | | Nb | 0.044(9) | |
| Ga1 | 4c | 0.5689(2) | 1/4 | 0 | Ga | 1 | 0.2(1) |
| Ga2 | 4d | 0.0815(2) | 0.9551(3) | 1/4 | Ga | | |
| Ga3 | 4d | 0.6507(2) | 0.8672(3) | 1/4 | Ga | | |
| Niobium content calculated from site fractions: 9.8 at.% | | Crystallite size (Lorenzian) [nm]: 169(1) | | | Preferred Orientation spherical harmonics order: 6 | | |

**Table 70. Rietveld refinement results for the HfGa phase in sample G3**

| Sample: G3 | | Nominal composition: $Hf_{35}Nb_{15}Ga_{50}$ | | | $R_p$: 4.81 | | $R_{wp}$: 6.33 |
|---|---|---|---|---|---|---|---|
| Background model: Chebyshev, 4th order | | | | | 2$\theta$-range [°]: 10 – 120° | | |
| Main phase: (Hf,Nb)Ga | | Structure type: ThTl | | | Space group: *Pbcm* (57) | | |
| Lattice parameters [Å] | a = 9.14366(6)<br>b = 8.42336(6)<br>c = 5.51973(4) | Cell volume [Å$^3$]: 425.132(5) | | | Fraction: 89.1(1)% | | $R_{Bragg}$: 1.81 |
| Site | Mpl. | x | y | z | Atom | Site fr. | B(eq.) |
| M1 | 4c | 0.1110(2) | 1/4 | 0 | Hf | 0.274(8) | 0.87(2) |
| | | | | | Nb | 0.726(9) | |
| M2 | 4d | 0.6223(1) | 0.5296(1) | 1/4 | Hf | 0.88(1) | |
| | | | | | Nb | 0.12(1) | |
| M3 | 4d | 0.1844(1) | 0.6344(1) | 1/4 | Hf | 0.92(1) | |
| | | | | | Nb | 0.08(1) | |
| Ga1 | 4c | 0.5693(3) | 1/4 | 0 | Ga | 1 | 0.89(4) |
| Ga2 | 4d | 0.0810(3) | 0.9548(4) | 1/4 | Ga | | |
| Ga3 | 4d | 0.6511(3) | 0.8676(4) | 1/4 | Ga | | |
| Niobium content calculated from site fractions: 15.4 at.% | | Crystallite size (Lorenzian) [nm]: 140(1) | | | Preferred Orientation spherical harmonics order: 4 | | |

**Table 71. Rietveld refinement results for the HfGa phase in sample G4**

| Sample: G4 | Nominal composition: $Hf_{30}Nb_{20}Ga_{50}$ | | | $R_p$: 3.84 | | $R_{wp}$: 5.04 |
|---|---|---|---|---|---|---|
| Background model: Chebyshev, 4th order | | | | 2$\theta$-range [°]: 10 – 120° | | |
| Main phase: (Hf,Nb)Ga | Structure type: ThTl | | | Space group: *Pbcm* (57) | | |
| Lattice parameters [Å] | a = 9.12771(5)<br>b = 8.38282(5)<br>c = 5.49169(3) | Cell volume [Å$^3$]: 420.202(4) | | Fraction: 96.5(1)% | | $R_{Bragg}$: 1.73 |
| Site | Mpl. | x | y | z | Atom | Site fr. | B(eq.) |
| M1 | 4c | 0.1121(1) | 1/4 | 0 | Hf | 0.190(7) | 0.4(1) |
| | | | | | Nb | 0.810(7) | |
| M2 | 4d | 0.6236(1) | 0.5307(1) | 1/4 | Hf | 0.726(8) | |
| | | | | | Nb | 0.274(8) | |
| M3 | 4d | 0.18284(9) | 0.6343(1) | 1/4 | Hf | 0.827(8) | |
| | | | | | Nb | 0.173(8) | |
| Ga1 | 4c | 0.5710(2) | 1/4 | 0 | Ga | 1 | 0.6(2) |
| Ga2 | 4d | 0.0806(2) | 0.9553(3) | 1/4 | Ga | | |
| Ga3 | 4d | 0.6505(2) | 0.8687(3) | 1/4 | Ga | | |
| Niobium content calculated from site fractions: 20.9 at.% | | Crystallite size (Lorenzian) [nm]: 124(1) | | Preferred Orientation spherical harmonics order: 4 | | | |

**Table 72. Rietveld refinement results for the HfGa phase in sample G5**

| Sample: G5 | Nominal composition: $Hf_{25}Nb_{25}Ga_{50}$ | | | $R_p$: 3.85 | | $R_{wp}$: 5.06 |
|---|---|---|---|---|---|---|
| Background model: Chebyshev, 4th order | | | | 2$\theta$-range [°]: 10 – 120° | | |
| Main phase: (Hf,Nb)Ga | Structure type: ThTl | | | Space group: *Pbcm* (57) | | |
| Lattice parameters [Å] | a = 9.10753(5)<br>b = 8.35035(6)<br>c = 5.46943(3) | Cell volume [Å$^3$]: 415.956(4) | | Fraction: 96.4(1)% | | $R_{Bragg}$: 1.83 |
| Site | Mpl. | x | y | z | Atom | Site fr. | B(eq.) |
| M1 | 4c | 0.1125(1) | 1/4 | 0 | Hf | 0.112(7) | 0.3(1) |
| | | | | | Nb | 0.888(7) | |
| M2 | 4d | 0.6246(1) | 0.5308(1) | 1/4 | Hf | 0.605(7) | |
| | | | | | Nb | 0.395(7) | |
| M3 | 4d | 0.1821(1) | 0.6337(1) | 1/4 | Hf | 0.713(8) | |
| | | | | | Nb | 0.287(8) | |
| Ga1 | 4c | 0.5723(2) | 1/4 | 0 | Ga | 1 | 0.3(1) |
| Ga2 | 4d | 0.0805(2) | 0.9536(3) | 1/4 | Ga | | |
| Ga3 | 4d | 0.6498(2) | 0.8698(3) | 1/4 | Ga | | |
| Niobium content calculated from site fractions: 26.2 at.% | | Crystallite size (Lorenzian) [nm]: 118(1) | | Preferred Orientation spherical harmonics order: 2 | | | |

**Table 73. Rietveld refinement results for the HfGa phase in sample G6**

| Sample: G6 | Nominal composition: $Hf_{20}Nb_{30}Ga_{50}$ | | $R_p$: 3.99 | $R_{wp}$: 5.24 |
|---|---|---|---|---|
| Background model: Chebyshev, 4th order | | | 2$\theta$-range [°]: 10 – 120° | |
| Main phase: (Hf,Nb)Ga | Structure type: ThTl | | Space group: *Pbcm* (57) | |
| Lattice parameters [Å] | a= 9.09318(6)<br>b= 8.30442(6)<br>c = 5.44968(4) | Cell volume [Å$^3$]: 411.525(5) | Fraction: 87.5(1)% | $R_{Bragg}$: 1.74 |

| Site | Mpl. | x | y | z | Atom | Site fr. | B(eq.) |
|---|---|---|---|---|---|---|---|
| M1 | 4c | 0.1137(2) | 1/4 | 0 | Hf | 0.120(7) | 0.30(5) |
| | | | | | Nb | 0.880(7) | |
| M2 | 4d | 0.6264(1) | 0.5306(1) | 1/4 | Hf | 0.451(7) | |
| | | | | | Nb | 0.550(7) | |
| M3 | 4d | 0.1820(1) | 0.6334(1) | 1/4 | Hf | 0.611(8) | |
| | | | | | Nb | 0.389(8) | |
| Ga1 | 4c | 0.5728(3) | 1/4 | 0 | Ga | 1 | 0.41(6) |
| Ga2 | 4d | 0.0793(2) | 0.9534(3) | 1/4 | Ga | | |
| Ga3 | 4d | 0.6510(2) | 0.8681(3) | 1/4 | Ga | | |

| Niobium content calculated from site fractions: 30.3 at.% | Crystallite size (Lorenzian) [nm]: 125(1) | Preferred Orientation spherical harmonics order: 4 |
|---|---|---|

**Table 74. Rietveld refinement results for the minor phase $Hf_5Ga_3$**

| Structure type: $Mn_5Si_3$ | | | Space group: $P6_3/mcm$ | | |
|---|---|---|---|---|---|
| Sample | Lattice parameters [Å] | Cell volume [Å$^3$] | Crystallite size (Lorenzian) [nm] | $R_{Bragg}$ | Fraction: |
| G1 | a = 7.9251(3)<br>c = 5.5593(4) | 302.38(3) | 90 (fixed) | 2.24 | 6.5(1)% |
| G2 | a = 7.9104(3)<br>c = 5.5009(4) | 298.10(3) | 90 (fixed) | 2.27 | 5.8(1)% |
| G3 | a = 7.8825(2)<br>c = 5.4524(2) | 293.39(2) | 110 (fixed) | 3.94 | 9.6(1)% |
| G4 | a = 7.8640(5)<br>c = 5.4144(9) | 289.98(6) | 100 (fixed) | 2.71 | 2.5(1)% |
| G5 | a = 7.8443(5)<br>c = 5.372(1) | 286.28(7) | 80 (fixed) | 4.33 | 2.6(1)% |
| G6 | a = 7.8255(9)<br>c = 5.343(1) | 283.36(9) | 60 (fixed) | 2.51 | 2.6(1)% |

**Table 75. Rietveld refinement results for the minor phase $Nb_5Ga_4$**

| Structure type: $Ti_5Ga_4$ | | | Space group: $P6_3/mcm$ | | |
|---|---|---|---|---|---|
| Sample | Lattice parameters [Å] | Cell volume [Å$^3$] | Crystallite size (Lorenzian) [nm] | $R_{Bragg}$ | Fraction: |
| G6 | a = 7.9650(4)<br>c = 5.4566(5) | 299.80(4) | 80 (fixed) | 1.78 | 5.2(1)% |

A solid solution ranging from binary HfGa to $Hf_{0.4}Nb_{0.6}Ga$ was found to exist at 1200°C during the investigation. This range is estimated only on the basis of the composition calculation from the refined site fractions. It was impossible to obtain samples suitable for EPMA measurement because the samples were in form of the pressed powders which could not be polished. Comparing the sample composition calculated on basis of the refined site fractions with the composition calculated on basis of the nominal compositions considering the mass losses assumed to be due to gallium evaporation (Appendix F.2), it can be seen that for all samples except of G1, the difference is within 1 at.%. For the sample G1 the niobium content calculated from the site fraction is 9 at.%, while according to the sample preparation data it would contain about 6 at.% Nb. The reported maximal niobium solubility of 36 at.% ($Hf_{0.28}Nb_{0.72}Ga$) based on the EPMA measurement of the arc-melted samples [84] could not be directly confirmed. The arc-melted samples were found inhomogeneous and thus not suitable for the Rietveld refinement.

The observed site fractions are represented in Fig. 84, where niobium content is calculated on the basis of the site fractions obtained from the Rietveld refinement. The first observation is the distinct niobium site preference for M1 (the sites within the distorted gallium octahedra, see appendix C) and a less distinct preference for M2 compared to the M3 site. The order of the metal sites with increasing niobium content is the same in all samples so there is little doubt about the existence of the site preferences. Site fraction data for sample G1 do not fit well to the trend, as the site fraction values for sites M2 and M3 are larger than the corresponding values in the next sample G2. The overestimation of the site fractions results in the already mentioned high (3%) difference between the compositions calculated from the refined site fractions and the nominal compositions. Therefore, the results for this sample will be excluded from the further analysis.

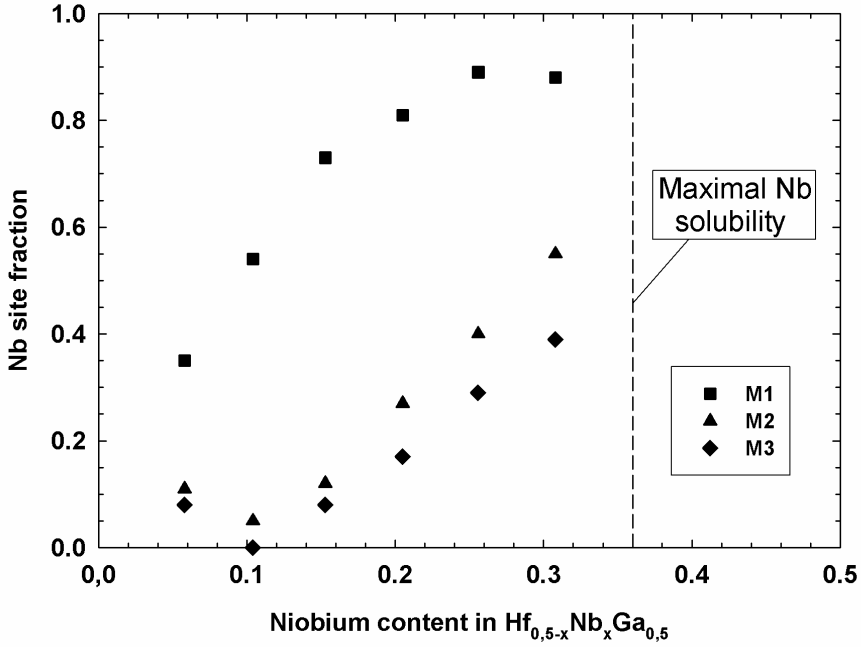


**Fig. 84. The niobium site fractions measured in the investigated samples in the Hf-Nb-Ga system. The niobium content is calculated from the refined site fractions. The maximal niobium solubility range for 1200°C is taken from ref. [84]**

For the site volume calculation, the structure data of $Hf_{0.5}Nb_{0.5}Ga$ (obtained from a refinement of sample G5) was taken (Table 76). The coordination spheres of the transition metal sites of the binary HfGa are depicted in Appendix C – these do not differ qualitatively from the ones of the sample G5. A comparison of the site volumes and the niobium site fractions is shown in Fig. 85. The M1 site (preferred by niobium) has the smallest volume, while the hafnium richest site has the largest one. This suggests an important role of the atom size factor for the substitution, due to the atom radii differences between these two metal atoms. However, this should not be overrated, as the volume difference between M2 and M3 sites (~0.9 $Å^3$) is larger than the difference between the sites M1 and M2 (~0.6 $Å^3$) while the refined site fraction difference is smaller in the previous case (~0.11) than in the latter (~0.49).

**Table 76. The volumes of Voronoi polyhedra around metal sites of $Hf_{0.5}Nb_{0.5}Ga$ structure calculated for the refined data from sample G5.**

| Site | Site volume [$Å^3$] |
|---|---|
| M1 | 17.16 |
| M2 | 17.80 |
| M3 | 18.66 |

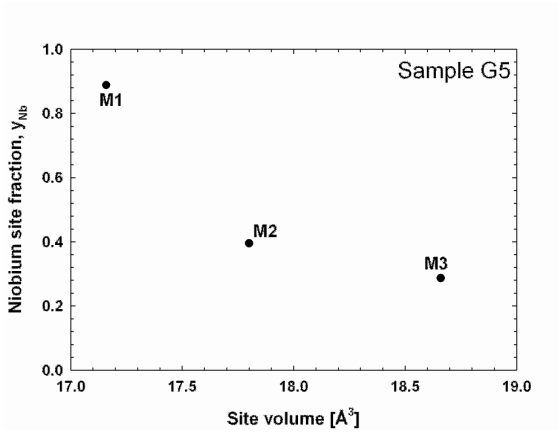


**Fig. 85. The comparison of the site volumes and the niobium site fractions calculated for the $Hf_{0.5}Nb_{0.5}Ga$ phase (Rietveld refinement of sample G5).**

The cumulated PBOs for the metal sites of all and of transition metal-transition metal bonds is given in Table 77. The correlation of these data with the niobium site fractions is depicted in Fig. 86. The sites ordered with increasing niobium occupation are also ordered with increasing values of cumulated PBOs which does not surprise, as the niobium atom has one more valence electron than hafnium. Also, the niobium-richest metal site (M1) has the largest value of PBOs for transition metal-transition metal bonds. On the other hand, the M2 site which has the smallest value of his parameter (0.53) contains more niobium than the M3 site for which the value is about twice as great (1.02).

**Table 77. The values of the cumulated PBOs of the transition metal sites in $Hf_{0.5}Nb_{0.5}Ga$ (Rietveld refinement of sample G5).**

| Site | All bonds | Bonds between tranition metal sites (fraction of all bonds) |
|---|---|---|
| M1 | 5.37 | 3.55 (0.66) |
| M2 | 5.03 | 0.53 (0.11) |
| M3 | 4.68 | 1.02 (0.22) |

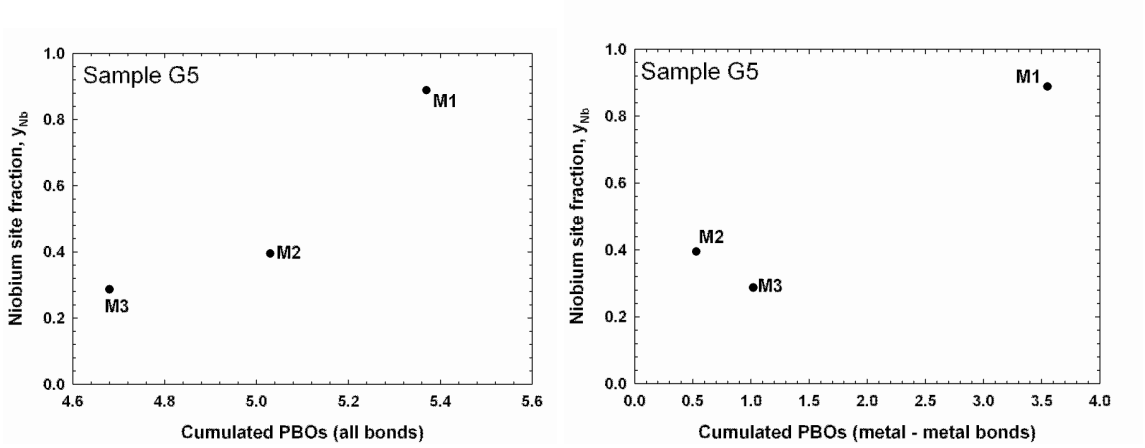


**Fig. 86. Comparison of the cumulated PBO for all (left) and for transition metal - transition metal bonds (right) for the metal sites in the $Hf_{1-x}Nb_xGa$ phase (Rietveld refinement of sample G5)**

Similar, as in the case of the arsenide compounds, the site preferences can still be rationalised in terms of a compromise between the tendency of the hafnium occupation of the sites with the larger volume (due to it's larger atom volume) and the preference of the niobium occupation of the sites where more electrons can participate in the bonding between the transition metal sites (due to it's higher sublimation enthalpy). The comparison of the site volumes only, showed the correct order of the niobium substituted sites. Although the smaller volume of the M2 site might favour the niobium occupation compared to the M3 site, the smallest value of cumulated PBOs for transition metal-transition metal bond might inhibit the niobium substitution on this site, thus resulting in the relative small site fraction difference between these two sites ($y_{Nb}^{M2} = 0.40$, $y_{Nb}^{M3} = 0.29$) when compared to the M1 site ($y_{Nb}^{M1} = 0.88$).

### 4.3.2 DFT calculations

Similar to the procedure for $Hf_{5-x}Nb_xGe_4$, the formation energies of all end members for the $Hf_{1-x}Nb_xGa$ compound with the ThTl structure type were calculated in order to examine their stability and to check if the experimentally found site preferences can be explained in terms of the ground state energies of the end members. First, the ground state energy of Ga with the crystal structure stable at 298 K was determined (Ga-type), with the unit cell data taken from literature [3]. By dividing this energy by eight (the number of gallium atoms in its unit cell, chapter 2.1), the energy per gallium atom was obtained. The set of energies for the

elements used in the following modelling is given in Table 78 (the energies for hafnium and niobium were already determined in chapter 4.1.2.1).

**Table 78. The calculated energies for elemental hafnium, niobium and gallium**

| Element | Structure type | Energy per unit cell [eV] | Energy per atom [eV] |
|---|---|---|---|
| Ga | Ga (unique) | -24.2373 | -3.0297 |
| Hf | Mg(hcp) | -19.8801 | -9.9400 |
| Nb | W(bcc) | -20.4276 | -10.2138 |

Next, the ground state energies of the end members of the HfGa structure were calculated, similar as it was done in the case of the $Hf_5Ge_4$ structure (chapter 4.2.1), i.e. the calculation was performed with the relaxation of the lattice parameters and the atoms allowed to migrate in case of all structures. Additionally the niobium monosubstituted end members were calculated also with the atoms held on the positions found for the ground state structure of the binary HfGa end member and the lattice parameters were relaxed. The sublattices were again defined in the form (M1:M2:M3:Ga). The energies per formula unit were obtained from the ground state energies by dividing the latter by twelve, as the oP24 unit cell contains twelve MGa units. The $Hf_{1-x}Nb_xGa$ mixture energies were calculated by the summation of the energies per element atom, according to the mixture's stoichiometry. The mixture energies were subtracted from the energies per formula unit giving the formation energies of a given end member. These were again divided by two (MGa consists of two atoms) and multiplied by 96.485, giving the value in kilojoule per mole of atoms. The calculated energies are given in Table 79. The ground state structure data for the end members are collected in Appendix G.5 - no structure identity after iteration was found, as it was the case for the (Hf:Nb:Hf:Ge) and (Hf:Hf:Nb:Ge) end members (chapter 4.2.1).

The formation energies for the end members for which also relaxation was allowed are shown in Fig. 87 (top). The order of the substituted sites can be found by connecting the end members with the lowest energy and the most stable end members are (Hf:Hf:Hf:Ga), (Nb:Hf:Hf:Ga), (Nb:Nb:Hf:Ga) and (Nb:Nb:Nb:Ga) so that the predicted order of the sites substituted by niobium is M1→M2→M3. Remarkably, there is a small difference between the energies for (Hf:Nb:Hf:Ge) and (Hf:Hf:Nb:Ga) (0.2 kJ/mol), as well as for (Nb:Nb:Hf:Ga) and (Nb:Hf:Nb:Ga) members (1.3 kJ/mol) which suggests only a minor niobium preference for M2 over the M3 site. This is in a very good agreement with the experimental data. A

calculation of the monosubstituted end members with atoms kept on the position of binary HfGa showed that the maximal energy gained by the migration of atoms was about 1.5 kJ/mol for (Nb:Hf:Hf:Ga) end member (see results in Table 80). The formation energies of the end members with atoms kept on the positions found for the ground state structure of the (Hf:Hf:Hf:Ga) end member are shown also in Fig. 87 (bottom). The values for the end members other than the monosubstituted members, were calculated by the according addition of the substitution energies found for the monosubstituted ones and are shown in Table 81.

**Table 79. The calculated end member energies for the HfGa structure (ThTl type) with the k-points set of 5 x 5 x 8. The atoms were allowed to migrate during the calculation.**

| End member HfGa | $x_{Nb}$ | Energy per unit cell [eV] | Energy per formula unit [eV] | Energy of (Hf,Nb)Ga mixture [eV] | Formation energy [eV] | Formation energy per mole of atoms [kJ] |
|---|---|---|---|---|---|---|
| (Hf:Hf:Hf:Ga) | 0 | -167.7833 | -13.9819 | -12.9697 | -1.0123 | -48.8339 |
| (Nb:Hf:Hf:Ga) | 0.167 | -168.5858 | -14.0488 | -13.0609 | -0.9879 | -47.6575 |
| (Hf:Nb:Hf:Ga) | 0.167 | -166.6210 | -13.8851 | -13.0609 | -0.8241 | -39.7585 |
| (Hf:Hf:Nb:Ga) | 0.167 | -166.5751 | -13.8813 | -13.0609 | -0.8203 | -39.5741 |
| (Nb:Nb:Hf:Ga) | 0.333 | -167.7501 | -13.9792 | -13.1522 | -0.8270 | -39.8955 |
| (Nb:Hf:Nb:Ga) | 0.333 | -167.4265 | -13.9522 | -13.1522 | -0.8000 | -38.5942 |
| (Hf:Nb:Nb:Ga) | 0.333 | -165.2984 | -13.7749 | -13.1522 | -0.6227 | -30.0389 |
| (Nb:Nb:Nb:Ga) | 0.5 | -166.4753 | -13.8729 | -13.2435 | -0.6295 | -30.3680 |

**Table 80. The calculated end member energies for the HfGa structure (ThTl type) with the k-points set of 5 x 5 x 8. The atoms were held on atom positions calculated for binary HfGa (i.e. (Hf:Hf:Hf:Ga) end member).**

| End member HfGa | $x_{Nb}$ | Energy per unit cell [eV] | Energy per formula unit [eV] | Energy of (Hf,Nb)Ga mixture [eV] | Formation energy [eV] | Formation energy per mole of atoms [kJ] |
|---|---|---|---|---|---|---|
| (Nb:Hf:Hf:Ga) | 0.167 | -168.2302 | -14.0192 | -13.0609 | -0.9582 | -46.2277 |
| (Hf:Nb:Hf:Ga) | 0.167 | -166.4950 | -13.8746 | -13.0609 | -0.8136 | -39.2521 |
| (Hf:Hf:Nb:Ga) | 0.167 | -166.3114 | -13.8593 | -13.0609 | -0.7983 | -38.5140 |

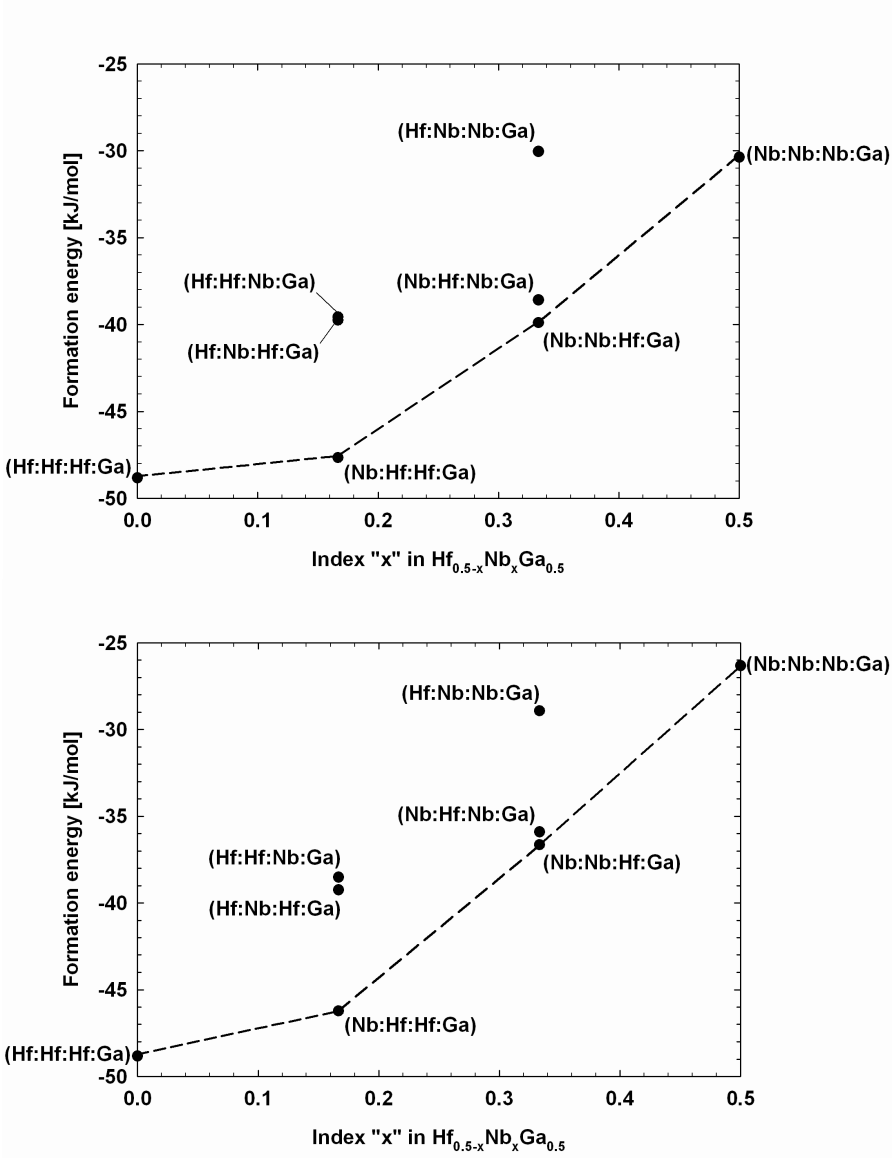


**Fig. 87. The graphic presentation of the end member energies for the calculation with the atoms relaxed (top) and kept on positions calculated for binary HfGa (bottom)**

**Table 81. The formation and substitution energies for the end members calculated with atoms fixed on the (Hf:Hf:Hf:Ga) ground structure. The substitution energies are referred to the formation energy of (Hf:Hf:Hf:Ga) end member. The substitution energies of the monosubstituted end members are added accordingly for the construction of the other substitution energies (e.g. the formation energy of the (Nb:Hf:Nb:Ga) member is taken as the sum of the formation energy of (Hf:Hf:Hf:Ga) with the substitution energies of (Nb:Hf:Hf:Ga) and (Hf:Hf:Nb:Ga) members)**

| End member ThTl-type | Formation energy per mole of atoms [kJ] | Substitution energy per mole of atoms [kJ] |
|---|---|---|
| (Hf:Hf:Hf:Ga) | -48.83 | 0 |
| (Nb:Hf:Hf:Ga) | -46.23 | 2.60 |
| (Hf:Nb:Hf:Ga) | -39.25 | 9.58 |
| (Hf:Hf:Nb:Ga) | -38.51 | 10.32 |
| (Nb:Nb:Hf:Ga) | -36.65 | 12.18 |
| (Nb:Hf:Nb:Ga) | -35.91 | 12.92 |
| (Hf:Nb:Nb:Ga) | -28.93 | 19.90 |
| (Nb:Nb:Nb:Ga) | -26.33 | 22.50 |

The comparison of the calculated structure data with those reported in the literature [67] for the binary HfGa phase shows that also in this case the computed cell is larger than the one found experimentally. The calculated lattice parameters exceed the experimental ones by approx. 0.5%. The fractional coordinates of the atom positions differ maximally by ±0.03 (*y* coordinate of Ga3) so the fit to the experimental data is significantly worse than in the case of $Hf_5Ge_4$. The values of the lattice parameters for the ternary compounds found experimentally can be compared with the values of the most stable end members (i.e. (Hf:Hf:Hf:Ga), (Nb:Hf:Hf:Ga), (Nb:Nb:Hf:Ga) and (Nb:Nb:Nb:Ga) ), as well as the lattice parameter ratios. This comparison is shown in Fig. 88 and 89. The calculated lattice parameters *a* and *b* are slightly larger than the experimental ones, while the lattice parameter *c* is almost equal with the measured value. The trends in lattice parameter ratios observed experimentally are reproduced very well by the calculated cell parameters.

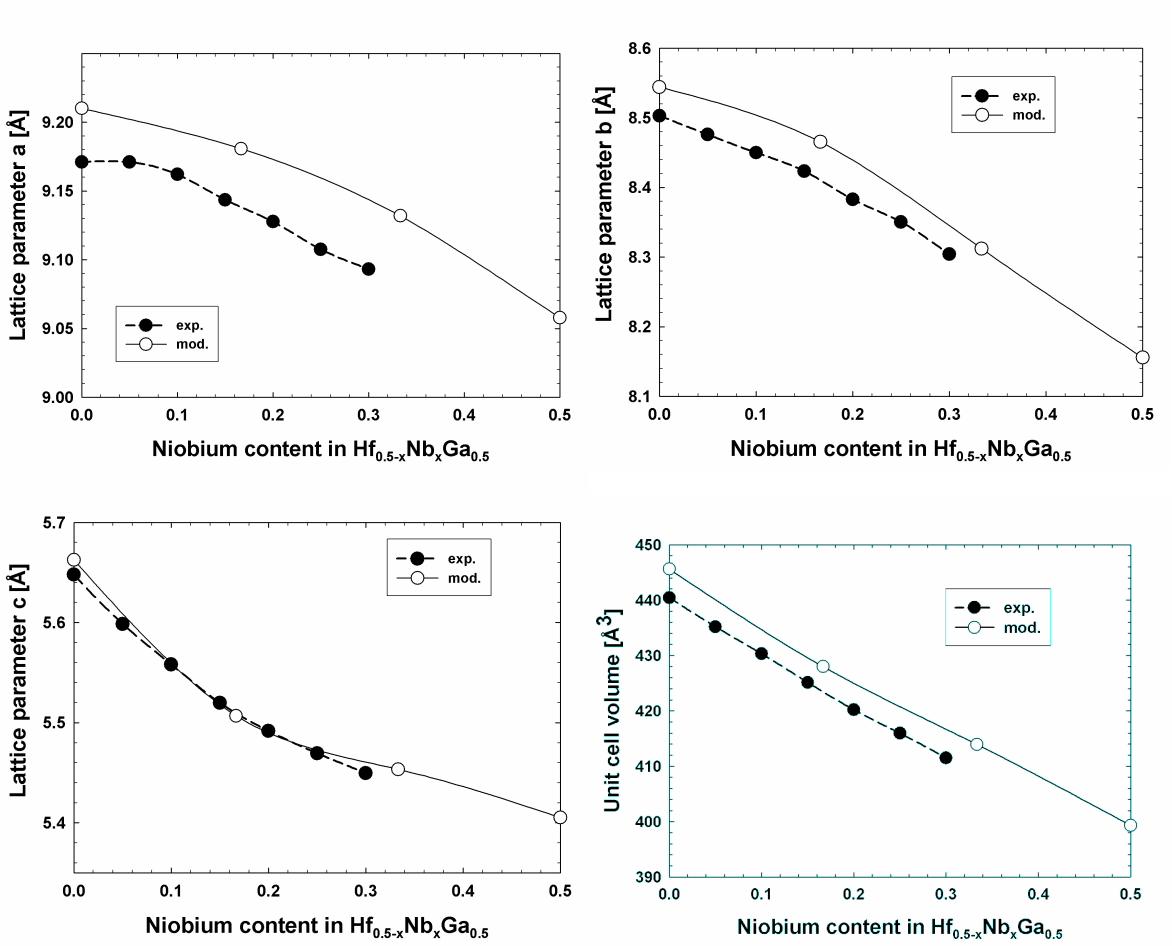


**Fig. 88. The comparison of the experimentally found lattice parameters and cell volumes with the values obtained for the most stable end members of the $Hf_{1-x}Nb_xGa$ phase.**

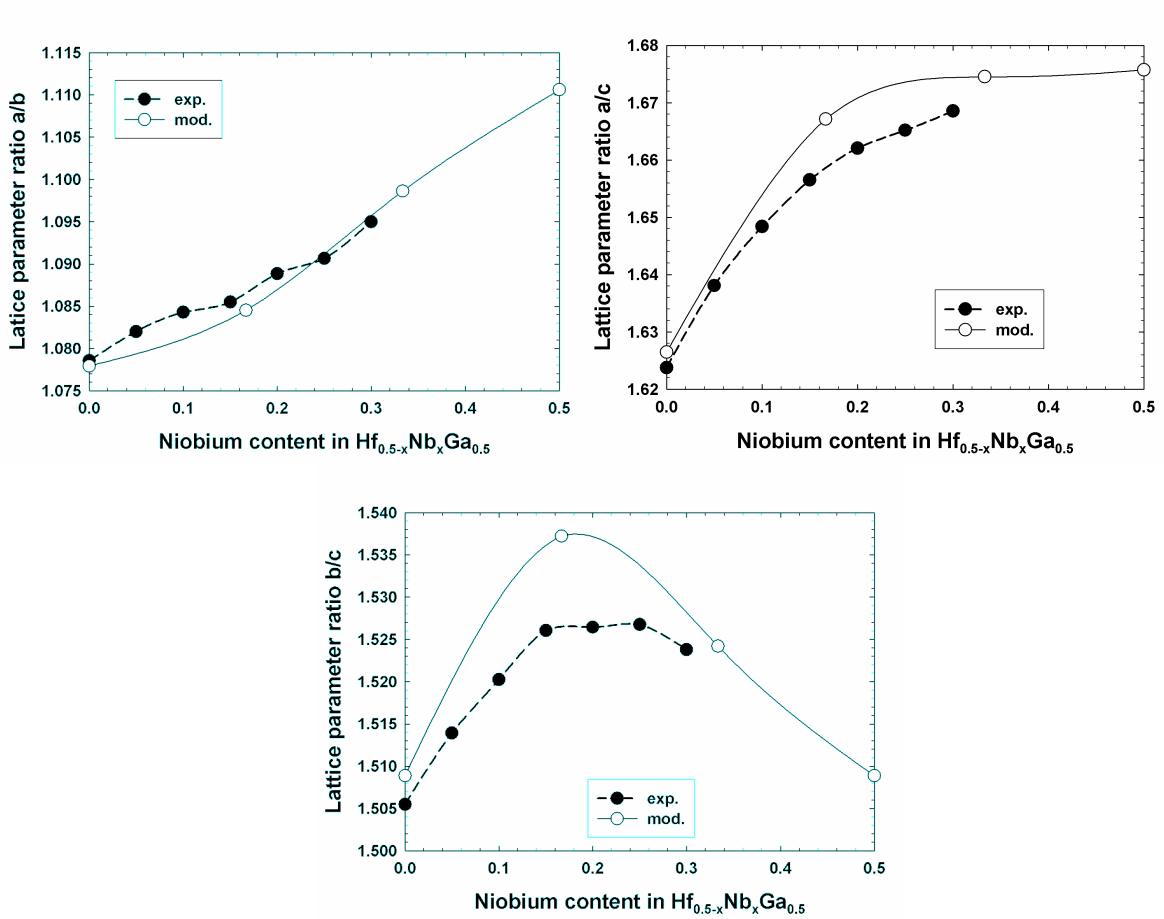


**Fig. 89. The comparison of the experimentally found lattice parameter ratios and the ones taken for the most stable end members of the $Hf_{1-x}Nb_xGa$ phase.**

### 4.3.3 Thermodynamic modelling of the site fractions in $Hf_{1-x}Nb_xGa$ phase

Two sets of formation energies were used in the thermodynamic modelling of the site occupations in the $Hf_{1-x}Nb_xGa$ phase. The first one (Set "*A*") contained the energies given in the last column of Table 79, i.e. the ones referred to the ground state structures (relaxed lattice parameter, atom migration allowed). Selected values of the calculated site fractions are given in Table 82 and the comparison of the modelling results with the experimentally found site fractions is given in Fig. 90. The niobium site fractions are overestimated for site M1 and underestimated for the sites M2 and M3. Yet, the agreement between the modelled and the experimental values is still quite satisfactory.

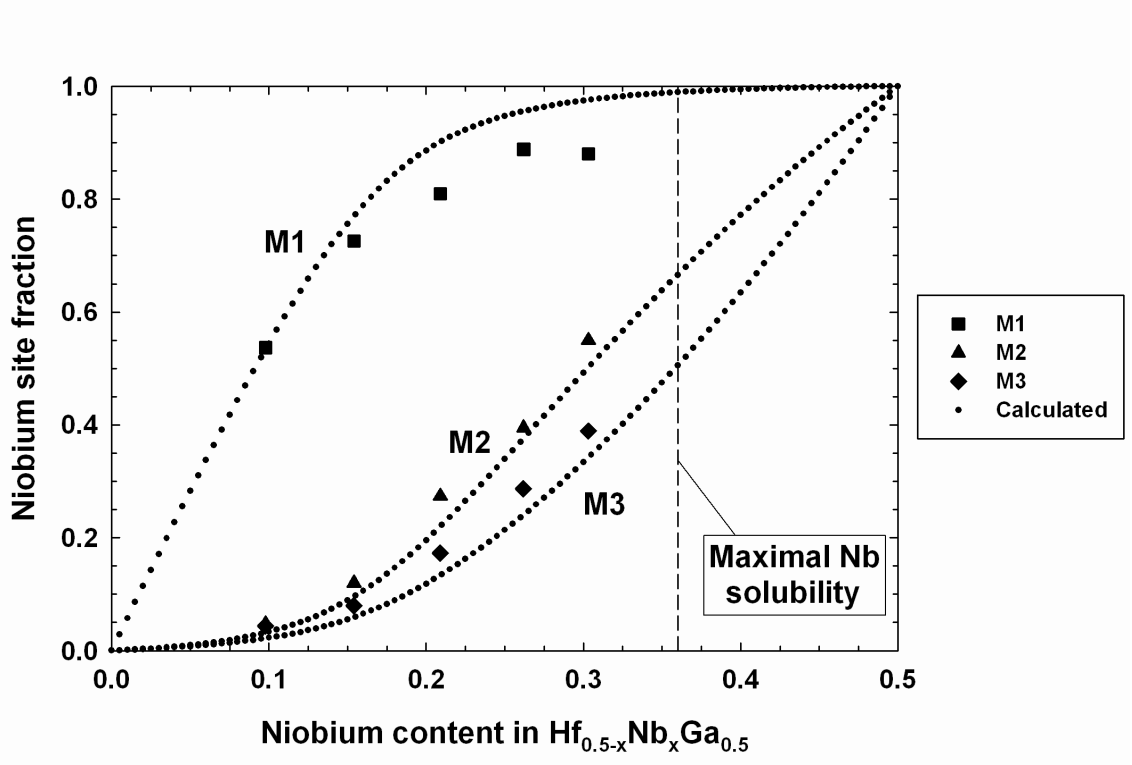


**Fig. 90. The comparison of the niobium site fractions refined for the $Hf_{1-x}Nb_xGa$ phase (marked by symbols) with the ones calculated on basis of the formation energies taken from the calculations with allowed atom relaxation. Dashed lines show the reported niobium solubility range in this phase at 1200°C.**

**Table 82. The calculated site fractions for the $Hf_{1-x}Nb_xGa$ phase. All formation energies are taken from the calculations with allowed atom relaxation.**

| $Hf_{1-x}Nb_xGa$ ThTl-type | Nb site fraction $y_{Nb}$ ($y_{Nb} + y_{Hf} = 1$) | | |
|---|---|---|---|
| $x_{Nb}$ | M1 | M2 | M3 |
| 0.00 | 0 | 0 | 0 |
| 0.10 | 0.2827 | 0.0097 | 0.0076 |
| 0.20 | 0.5441 | 0.0332 | 0.0227 |
| 0.30 | 0.7559 | 0.0888 | 0.0552 |
| 0.40 | 0.8859 | 0.1956 | 0.1185 |
| 0.50 | 0.9469 | 0.3394 | 0.2137 |
| 0.60 | 0.9743 | 0.4920 | 0.3337 |
| 0.70 | 0.9874 | 0.6379 | 0.4747 |
| 0.80 | 0.9942 | 0.7714 | 0.6343 |
| 0.90 | 0.9979 | 0.8917 | 0.8104 |
| 1.00 | 1 | 1 | 1 |

Similar to the approach used in the modelling of the $Hf_{5-x}Nb_xGe_4$ phase, the second set (Set "*B*") of the formation energies was used, based on the calculation of the niobium monosubstituted end member energies (last column of Table 80). From these three energies the formation energies of the other end members were calculated as a sum of the corresponding substitution energies and the formation energy of the binary HfGa end member (as given in Table 81). The selected site fraction values for this energy set are given in Table 83. The comparison of the refined and computed site fraction values (Fig. 91) shows that the fit of the modelled curve is almost identical with the one obtained with the previous set (i.e. energies for the relaxed structures). Minor differences are noticed for the curves describing the fractions of M2 (lower than before) and M3 (higher than before) sites. Similar to the case of the $Hf_{5-x}Nb_xGe_4$ phase, the simplification of the model does not worsen the quality of the modelled data.

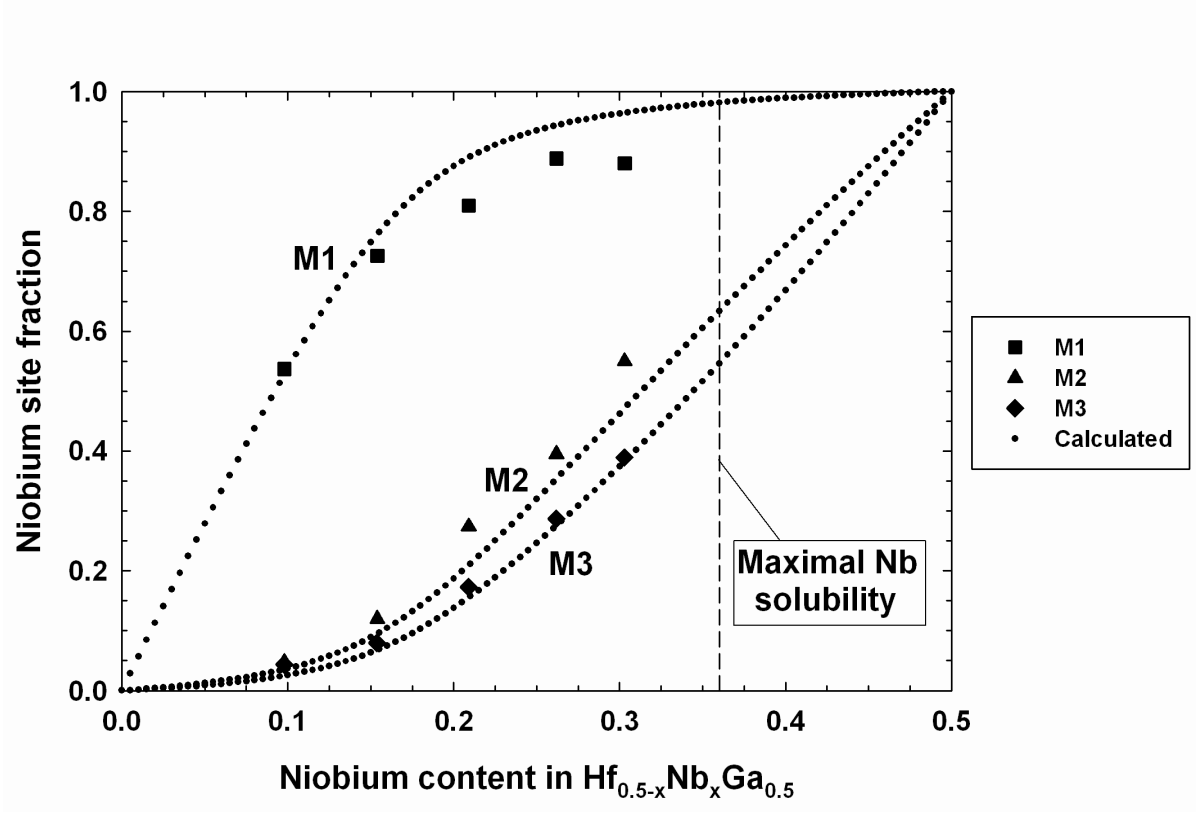


**Fig. 91. The comparison of the niobium site fractions refined for the $Hf_{1-x}Nb_xGa$ phase (marked by symbols) with the ones calculated on basis of the formation energies of the niobium monosubstituted end members taken from the calculations with atoms kept on positions of the ground state structure of binary HfGa end member. Dashed lines show the reported niobium solubility range in this phase at 1200°C.**

**Table 83. The calculated site fractions for the $Hf_{1-x}Nb_xGa$ phase. The energies of the monosubstituted end members were used as a base for the calculation of the other energies.**

| $Hf_{1-x}Nb_xGa$ ThTl-type | Nb site fraction $y_{Nb}$ ($y_{Nb} + y_{Hf} = 1$) | | |
|---|---|---|---|
| $x_{Nb}$ | M1 | M2 | M3 |
| 0.00 | 0 | 0 | 0 |
| 0.10 | 0.2787 | 0.0125 | 0.0088 |
| 0.20 | 0.5374 | 0.0367 | 0.0259 |
| 0.30 | 0.7479 | 0.0887 | 0.0635 |
| 0.40 | 0.8751 | 0.1869 | 0.138 |
| 0.50 | 0.9346 | 0.3192 | 0.2462 |
| 0.60 | 0.9632 | 0.4622 | 0.3745 |
| 0.70 | 0.9791 | 0.6049 | 0.5161 |
| 0.80 | 0.9888 | 0.743 | 0.6682 |
| 0.90 | 0.9953 | 0.8749 | 0.8297 |
| 1.00 | 1 | 1 | 1 |

The end member energies used in both of the sets are summarised in Table 84. The modelled Gibbs energies calculated for both sets are depicted in Fig. 92 and a few selected values are given in Table 85. As the end members used in set "A" were stabilised by the atom migration, this set obviously returns the lower values of the Gibbs energies than set "B" where atoms were not allowed to move. The Gibbs energy difference for the hypothetical binary NbGa compound (i.e. (Nb:Nb:Nb:Ga) endmember) is about 4.0 kJ/mole of atoms (i.e. 8 kJ/mol)

**Table 84. The summary of the energies taken for the various sets used for the thermodynamic modelling of $Hf_{1-x}Nb_xGa$ phase.**

| $Hf_{1-x}Nb_xGa$ ThTl-type (M1:M2:M3:Ga) | Formation energy per mole of atoms [kJ] | |
|---|---|---|
| | Set A | Set B |
| (Hf:Hf:Hf:Ga) | -48.83 | -48.83 |
| (Nb:Hf:Hf:Ga) | -47.66 | -46.23 |
| (Hf:Nb:Hf:Ga) | -39.76 | -39.25 |
| (Hf:Hf:Nb:Ga) | -39.57 | -38.51 |
| (Nb:Nb:Hf:Ga) | -39.90 | -36.65 |
| (Nb:Hf:Nb:Ga) | -38.59 | -35.91 |
| (Hf:Nb:Nb:Ga) | -30.04 | -28.93 |
| (Nb:Nb:Nb:Ga) | -30.37 | -26.33 |

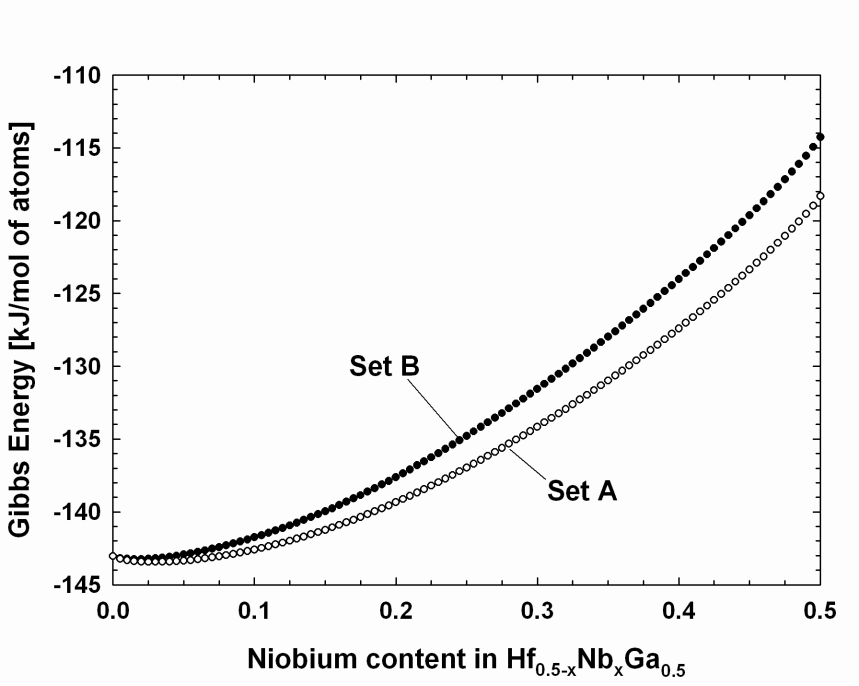


**Fig. 92. Gibbs energy of $Hf_{0.5-x}Nb_xGa_{0.5}$ phase obtained with various sets of formation energies at 1200°C.**

**Table 85. The calculated Gibbs energies for the $Hf_{0.5-x}Nb_xGa_{0.5}$ phase.**

| $Hf_{0.5-x}Nb_xGa_{0.5}$ ThTl-type | Gibbs energy [kJ/mole of atoms] | | Gibbs energy of mixing [kJ/mole of atoms] | |
|---|---|---|---|---|
| $x_{Nb}$ | Set *A* | Set *B* | Set *A* | Set *B* |
| 0.00 | -143.05 | -143.05 | 0.00 | 0.00 |
| 0.05 | -142.94 | -143.36 | -2.77 | -2.78 |
| 0.10 | -141.76 | -142.60 | -4.46 | -4.50 |
| 0.15 | -139.97 | -141.24 | -5.55 | -5.61 |
| 0.20 | -137.62 | -139.35 | -6.08 | -6.19 |
| 0.25 | -134.80 | -136.97 | -6.13 | -6.29 |
| 0.30 | -131.57 | -134.17 | -5.78 | -5.96 |
| 0.35 | -127.98 | -130.99 | -5.07 | -5.25 |
| 0.40 | -124.03 | -127.41 | -4.00 | -4.14 |
| 0.45 | -119.63 | -123.36 | -2.47 | -2.57 |
| 0.50 | -114.28 | -118.32 | 0.00 | 0.00 |

## 4.4. Site occupations – trend in arsenides, germanides and gallides.

The investigation in the Hf-Nb-As, Hf-Nb-Ge and Hf-Nb-Ga systems shows that in all of these systems solid solutions are found in which site preferences occur. This suggests that the change of the third element in the Hf-Nb-X combination from the element from the $15^{th}$ to $13^{th}$ group does not eliminate this phenomenon at all. Unfortunately, there does not exist any structure type which would appear in all three systems, making the direct comparison of the site preference effect on the stabilisation of the ternary compound possible. The differences between the ternary diagrams of these three systems also do not allow to draw a straightforward conclusion. The experimental investigation of the Hf-Nb-As system described in this work shows an abundance of ternary phases (five new phases detected plus one probably metastable), while the available literature data show that no ternary phase is present in the metal-rich region of the Hf-Nb-Ge and Hf-Nb-Ga systems which consist mostly of the extended binaries (see chapters 2.3.2 and 2.3.3). Although the literature data on the gallides and germanides refer to lower temperatures (800°C and 897°C respectively) than the one used in the experiments with the arsenides (1400°C), the samples in all those systems were prepared by arc-melting and the occurrence of any trace of the high-temperature ternary phase would be likely. It appears that preferred site occupation is formed in all these systems, so it is obvious that this kind of partial ordering is "stabilising" in the sense that the Gibbs energy is lowered for the partially ordered compounds in comparison with either the fully ordered or the completely disordered structure. In case of the arsenides, this partial ordering is realised in solid solutions extending from the binary compounds, as well as in new ternary phases, while the germanides and gallides show only the solid solutions of the binary structures. This difference apparently is to be attributed to the different levels of structural complexity of these compounds. While the arsenides show many and complex crystal structures also in the binaries, the germanides and the gallides are structurally rather simple. Therefore, the author believes that the DFSO concept of the phase stabilisation is not restricted to the "classic" DFSO phases only which are restricted to posses the structure type not found in the binary compounds of the given system. The stabilising role of both the mixed occupations and the site preferences is also observed in the solid solutions extended from the binary structures as in the case of $(Hf,Nb)_5As_3$, $Hf_{5-x}Nb_xGe_4$, $Hf_{1-x}Nb_xGa$ phases.

## 5. Summary and conclusions

Site preferences were found in the ternary compounds present in the Hf-Nb-As (the solid solutions of $(Hf,Nb)_5As_3$, $Hf_{4-x}Nb_{3+x}As_3$, $Hf_{3+x}Nb_{3-x}As_2$ and $Hf_{2+x}Nb_{1-x}As$; the $Hf_{7.22}Nb_{3.78}As_4$ phase) and Hf-Nb-Ga (the solid solution of $Hf_{1-x}Nb_xGa$) systems. The preferences are believed to be the result of the compromise between the tendency of hafnium atoms to occupy the sites with a larger volume and the preference of niobium atoms to occupy the sites, where more metal-metal bonds can be formed. The influence of the site volumes can be explained by a comparison of the atom radii of these two metals, as hafnium has a radius greater by 10 pm than niobium, according to the values given by Pauling. The tendency of niobium occupying the sites where more electrons can be included in the metal-metal bonds can be supported by the comparison of the sublimation enthalpies reported for both of these metals. As niobium has a larger value (in absolute terms) than hafnium, it is believed that the possibility of creating more metal-metal bonds by niobium atoms stabilises the compounds energetically. Even if the sublimation enthalpy values were not accurate, the higher melting point of niobium compared to hafnium suggests stronger intermetallic bonding for niobium. The Pauling bond orders in the systems with metallic bonding obviously cannot be directly interpreted as a number of electrons taking part in the bonds, as the summation of these yields sometimes the total number of electrons greater than the possible sum of the valence electrons. But it is believed that even if the numbers cannot be interpreted in the physical sense, they still carry valuable information about the quantitative share of the various interatomic bonds.

Six new phases were found in the Hf-Nb-As system, where two of them ($Hf_{4-x}Nb_{3+x}As_3$, $Hf_{3+x}Nb_{3-x}As_2$) crystallise in new structure types. Two other phases ($Nb_2As$ and $Hf_{7.22}Nb_{3.78}As_4$) are believed to be metastable at 1400°C. All of the new phases can be described in terms of the arsenic-centred trigonal prisms arrangement made of metal atoms. The crystal structures found for $(Hf,Nb)_2As$ phases agree with the predictions made with the structure maps.

The DFT calculations yield the results which allow a successful prediction of the site preferences as it was demonstrated on the $Hf_{3+x}Nb_{3-x}As_2$, $Hf_{2+x}Nb_{1-x}As$, $Hf_{5-x}Nb_xGe_4$ and $Hf_{1-x}Nb_xGa$ phases. Although the method examines the stability of the ordered structures at 0 K temperature, its validity is useful for the analysis of the experimental data obtained at the elevated temperatures. It is found that the site preferences stabilise the compounds energetically

and thus, comparing the ground state energies of the substituted compounds, the site preferences can be explained. The lattice parameters of the calculated ground state structures are slightly larger than the experimentally found ones (~1%), they can be still useful for the analysis of the trends related to the variation of these parameters with the composition of the solid solutions. The calculations predict also the stability of the majority of the binary hafnium and niobium arsenides. As only a few are observed below 1000°C, it is believed that their formation is impeded by kinetic reasons. The stability of binary $Nb_3As$ with the $Hf_{3+x}Nb_{3-x}As_2$ structure type could not be experimentally proven but it may well be that this structure appears in the lower temperature range (below 1000°C). Unfortunately, the computation cost for the complicated structures is still considerable and the method is not feasible if too many end members are to be calculated (the cases of $(Hf,Nb)_5As_3$ and $Hf_3As$ phases).

The results of the ab-initio calculations yield the valuable data for the thermodynamic modelling of the phase Gibbs energy of the phase by the CEM formalism. Predicted site fractions are in a very good agreement with the values obtained from the refinement of the experimental values for the $Hf_{3+x}Nb_{3-x}As_2$, $Hf_{2+x}Nb_{1-x}As$, $Hf_{5-x}Nb_xGe_4$ and $Hf_{1-x}Nb_xGa$ phases. This proves the usefulness of DFT calculation for qualitative predictions regarding the observed site preferences. The agreement of the modelling based on the input data relevant to 0 K with results observed at 1400°C might suggest a weak influence of the vibrational entropy effects. The implementation of the simplified model based on the energies calculated for the monosubstituted end members only did not affect the quality of the data significantly. However, it must be noted that entering the data for the end members into the software turns into the serious effort in the case of many sublattices. Even if no calculation of end member energies by DFT methods is necessary, they must be defined in the case of thermodynamic modelling. This may be a demanding task if the number of possible end members becomes very large (several hundreds in extreme cases).

## 6. Acknowledgments

The author was supported by many persons during his work and can hardly express his gratefulness for their contribution. In fact, some of them should be considered as coauthors.

I would like to thank Prof. Herbert Ipser for his supervision on this work and my scientific activity. Despite his numerous duties as the Head of the Institute of Inorganic Chemistry/Materialchemistry, he was always open to my doubts and questions, guiding me with his advise through many problems of not only scientific importance. It was an honour to have him as my "Doktorvater".

It is impossible to overrate the contribution of Prof. Klaus Richter, with whom I had the master-apprentice relation. This manuscript has it's root in his idea which was expressed in the form of the scientific project. Klaus taught me literally everything about the experimental methods and directed me through all my modelling attempts with his unlimited patience and optimism. I would like to thank him also for showing me what the life of the scientist is, especially the fact that thinking must not be inferior to the knowledge.

Next, I would like to thank the co-workers on the project FWF P16946. Among them, I would like mention Dr. Igor Chumak (Ігор Чумак) who helped me with the single crystal experiments and the structure determination. My results on $Hf_{1-x}Nb_xGa$ phase were merely a coronation of the efforts of Dipl.-Ing. Michael Oberseider, who investigated this ternary system. Of course, the contribution of FWF (Austrian Science Fund) for supporting the project is gratefully acknowledged.

The measurements of the single crystals were performed at the Institute of Mineralogy and Crystallography with the comprehensive and cordial support of Prof. Herta Silvia Effenberger.

The DFT calculations are an important part of this work. I had the luck of learning this method from Dr. Florian Mittendorfer and discuss the results with Prof. Georg Kresse, both being the members of Computational Materials Physics group at the University of Vienna. I would like to thank them also for the smooth processing of the license agreement of the VASP software.

The secrets of the thermodynamic modelling were revealed to me by Dr. Aleš Kroupa of Institute of Physics of Materials in Brno (Czech Republic). The approach and the results were also discussed with Prof. Jan Vřešťál (Masaryk University, Brno) and Dr. Suzana G. Fries.

I would like to thank the whole staff of the Institute of Inorganic Chemistry/ Materialchemistry for the atmosphere in which I was studying and working in for almost five years. Regardless of age or position (scientific or non-scientific), everybody here supported me making this place my second home. Especially, I would like to thank all the fellow-students of the doctorate studies for all happy moments we had together.

It is trivial to say, that the authors mentioned in the literature citations built the fundaments for my work. Still, I would reach nothing if they had not done their work and published the results.

Last, but not least, I thank my whole family for their love and support. I guess it would not be possible to finish this work at all, if my wife was not next to me during all these days with her smile and patience. For sure, it would be not possible to start this work at all, if my parents have not devoted nearly everything for my upbringing. As in the case of the institute staff, all family members have their important contribution and their role can be hardly overrated. A lot of thanks goes also to all my teachers and my friends. KOCHANI, DZIĘKUJĘ WAM WSZYSTKIM !!!

## 7. Literature

[1] – "Encyclopaedia Britannica – the Online Encyclopedia", http://www.britannica.com

[2] – A.R. West, „Solid state chemistry and its applications", John Willey & Sons, 1989

[3] – P. Villars, L.D. Calvert, "Pearson's Handbook of Crystallographic Data for Intermetallic Phases, 2nd Edition" ASM International, 1991

[4] – J.L.C. Daams, P. Villars, J.H.N. van Vucht, "Atlas of crystal structure types for intermetallic phases", ASM International, 1991

[5] – T.B. Massalski (Ed.), "Binary alloy phase diagrams, 2nd Edition", ASM International, 1996

[6] – P. Villars, A. Prince, H. Okamoto (Eds.), "Handbook of ternary alloy phase diagrams", ASM International, 1995

[7] – O. Knacke, O. Kubaschewski, K. Hesselmann (Eds.), „Thermochemical Properties of Inorganic Substances", Springer Verlag, 1991

[8] – A. Dinsdale, Calphad 15 (1991) 317.

[9] – R. Ferro, A. Saccone, „Materials science and technology – a comprehensive treatment, vol. 1", Wiley-VCH, 2005

[10] – Inorganic Crystal Strucutre Data, FIZ Karlsruhe, 2006

[11] – H. F. Franzen, Prog. Solid St. Chem., 12 (1978), p.1

[12] – S. Debus, B. Harbrecht, J. Alloys Compd., 338 (2002) p.253

[13] – X. Yao, H.F. Franzen, Z. Anorg. Allg. Chem., 598/599 (1991), p.353

[14] – X. Yao, H.F. Franzen, J. Solid State Chem., 86 (1990), p.88

[15] – X. Yao, H.F. Franzen, J. Am. Chem. Soc., 113 (1991), p.1426

[16] – X. Yao, G.J. Miller, H.F. Franzen, J. Alloys Compd., 183 (1992), p.7

[17] – X Yao, G.A. Marking, H.F. Franzen, Ber. Bunsenges. Phys. Chem., 96 (1992), p.1552

[18] – H.F. Franzen, M. Köckerling, Prog. Solid State Chem., 23 (1995) p.265

[19] – H. Kleinke, Trends in Inorg. Chem., 7 (2001), p.135

[20] – C.-S. Lee, E. Dashjav, H. Kleinke, Chem. Mater., 13 (2001) p.4053

[21] – H. Kleinke, H.F. Franzen, J. Solid State Chem., 136 (1998), p.221

[22] – $0 < x < 0.5$, $-0.25 < y < 0.25$; S. Derakhshan, E. Dashjav, H. Kleinke, Eur. J. Inorg. Chem., (2004) p.1183

[23] – $0.1 < x < 0.4$, $0.1 < y < 1.1$; K.W. Richter, H.F. Franzen, J. Solid State Chem., 150 (2000), p.347

[24] – Dictionary of Inorganic Compounds, Chapman&Hall, London, 1992

[25] – J. Emsley, "The elements", Clarendon Press, Oxford, 1989

[26] – A.F. Holleman, N. Wiberg, "Lehrbuch der Anorganischen Chemie", 101 Aufl., de Gruyter, Berlin, 1995

[27] – R.W. Carpenter, C.T.Liu, P.G. Mardon, Metall. Trans., 2 (1971), p.125

[28] – W. Jeitschko, H. Nowotny, Monatsh. Chem., 93 (1962), p.1284

[29] – S. Rundqvist, B. Carlsson, Acta Chem. Scand., 22 (1968), p.2395

[30] – J.-O. Willerström, B. Carlsson, S. Rundqvist, J. Solid State Chem., 31 (1980) p.227

[31] – J.-O. Willerström, Acta Chem. Scand., A38 (1984), p.91

[32] – S. Rundqvist, B. Carlsson, C.-O. Pontchour, Acta Chem. Scand., 23 (1969), p.2188

[33] – E. Heinerth, W. Biltz, Z. Anorg. Chem., 198 (1931), p.175

[34] – H. Boller, E. Parthé, Acta Cryst., 16 (1963), p.1095

[35] – S. Furuseth, A. Kjekshus, Acta Cryst., 17 (1964), p.1077

[36] – S. Furuseth, A. Kjekshus, Acta Chem. Scand., 18 (1964), p.1180

[37] – S. Furuseth, A. Kjekshus, Nature, 203 (1964), p.512

[38] – S. Furuseth, A. Kjekshus, Acta Cryst., 18 (1965), p.320

[39] – G.S. Saini, L.D. Calvert, J.B. Taylor, Canad. J. Chem. 42 (1964), p.630

[40] – H. Schäfer, W. Fuhr, J. Less-Common Met., 8 (1965), p.375

[41] – E. Ganglberger, Dissertation, Univ. Wien (1966)

[42] – E. Ganglberger, H. Nowotny, F. Benesovsky, Monatsh. Chem., 97 (1966), p.1696

[43] – B. Carlsson, S. Rundqvist, Acta Chem. Scand., 25 (1971), p.1742

[44] – R.M. Waterstrat, K. Yvon, H.D. Flack, E. Parthé, Acta Cryst., B31 (1975), p.2765

[45] – S. Laohavanich, S. Thanomkul, S. Pramatus, Acta Cryst., B37 (1981), p.227

[46] – W. Bensch, W. Heid, Acta Cryst., C51 (1995), p.2205

[47] – H. Nowotny, H. Braun, F. Benesovsky, Radex Rundsch., 6 ,(1960), p.367

[48] – K. Schubert, H.G. Meissner, W. Rossteutscher, Naturwissenschaften, 51 (1964), p.506

[49] – W. Rossteutscher, K. Schubert, Z. Metallkd., 56 (1965), p.813

[50] – J.T. Zhao, E. Parthé, J. Less-Common Met., 162 (1990), L27

[51] – E.E Havinga, H. Damsma, P. Hokkelig, J. Less-Common Met., 27 (1972), p.169

[52] – E. Parthé, Acta Cryst., 12 (1959), p.559

[53] – H. Nowotny, F. Benesovsky, O. Schob, Monatsh. Chem., 91 (1960), p.270

[54] – J.F. Smith, D.M. Bailey, Acta Cryst., 10 (1957), p.341

[55] – V.M. Pan, V.I. Latysheva, E.A. Shishkin, "Metallurgy, Physical Chemistry and Metal Physics of Superconductors", Nauka, Moscow (1967), p.157-160

[56] – K.W. Richter, H. Flandorfer, H.F. Franzen, J. Alloys and Comp., 320 (2001), 87

[57] – J.L. Jorda, R. Flükiger, J. Müller, J. Less-Common Met., 62 (1978), p.25

[58] – R. Horyń, R. Kubiak, Bull. Acad. Pol. Sci., Sér. Sci. Chim., 19 (1971), p.185

[59] – C.P. Umbach, L.E. Toth, A.M. Goldman, J. Less-Common Met., 69 (1980), p.319

[60] – A.I. Evstyukhin, G.N. Elmanov, V.I. Statsenko, R.R. Shakirov, Inorg. Mat., 19 (1983), p.213

[61] – M. Arita, H.-U. Nissen, W. Schauer, J. Solid State Chem., 84 (1990) p.386

[62] – R. Kubiak, R. Horyn, H. Broda, K. Łukaszewicz, Bull. Acad. Pol. Sci., Sér. Sci. Chim., 20 (1972), p.429

[63] – M. Pötzschke, K. Schubert, Z. Metallkd., 53 (1962), p.474

[64] – V.Ya. Markiv, N.N. Belyavina, A.S. Kazachkova, Russ. Metall., 1989 (3), p.191

[65] – Y. Le Page, J.R. Rodgers, P.S. White, J. Appl. Crystallogr., 35 (2002), p.364

[66] – H. Boller, E. Parthé, Monatsh. Chem., 94 (1963), p. 225

[67] – V.Ya. Markiv, N.N. Belyavina, Dokl. Akad. Nauk USSR, Ser. B, 1986 (4), p.44

[68] – J.L. Jorda, R. Flükiger, J. Müller, J. Less-Common Met., 55 (1977), p.249

[69] – V.M. Pan, V.I. Latysheva, "Superconducting alloys and compounds", Nauka, Moscow (1972), p.70-77

[70] – W. Jeitschko, H. Nowotny, F. Benesovsky, Monatsh. Chem., 94 (1963), p.1242

[71] – M. Dryś, R. Kubiak, J. Less-Common Met., 71 (1980), p.323

[72] – M. Dryś, J. Less-Common Met., 58 (1978), p.111

[73] – H. Holleck, W. Rieger, H. Nowotny, F. Benesovsky, Monatsh. Chem., 95 (1964), p.552

[74] – E.A. Wood, V.B. Compton, B.T. Matthias, E. Corenzwit, Acta Cryst., 11 (1958), p.604

[75] – V.V. Baron, L.F. Myzenkova, E.M. Savitskii, E.I. Gladyshevskii, Russ. J. Inorg. Chem., 9 (1964), p.1172

[76] – M. Dryś, R. Kubiak, K. Łukaszewicz, Bull. Acad. Pol. Sci., Sér. Sci. Chim., 21 (1973), p.901

[77] – H.G. Meissner, K. Schubert, Z. Metallkd., 56 (1965), p.475

[78] – H. Kleinke, B. Harbrecht, Z. Anorg. Allg. Chem., 626 (2000), p.1851

[79] – S. Derakhshan, E. Dashjav, H. Kleinke, Mat. Res. Soc. Symp. Proc., 755 (2003), p.341

[80] – Yu.D. Seropegin, M.V. Rudometkina, J. Less-Common Met., 135 (1987), p.127

[81] – Yu.D. Seropegin, V.V. Tabachenko, M.G. Myskiv, Kristallogr., 29 (1984), p.161

[82] – K.W. Richter, R. Picha, H. Ipser, H.F. Franzen, Solid State Sci., 5 (2003), 653

[83] – N.N. Belyavina, V.Ya. Markiv, Dop. Akad. Nauk USSR, Ser. A, 1979(7), p.577

[84] – M. Oberseider, private comumnication

[85] – H. Kleinke, H.F. Franzen, Acta Cryst., C52 (1996), p.2127

[86] – S. Rundqvist, Acta Chem. Scand., 20 (1966), p.2427

[87] – A. Nylund, Acta Chem. Scand., 20 (1966), p.2393

[88] – E. Wigner, F. Seitz, Phys. Rev., 43 (1933), p.804

[89] – R.A. Hoffmann, J. Chem. Phys., 39 (1963), p.1397

[90] – H. Krischner, B. Koppelhuber-Bitschnau, „Röntgenstrukturanalyse und Rietveldmethode“, Verlag Friedrich Vieweg&Sohn, Braunschweig (1994)

[91] – TOPAS, version 3, Bruker AXS Inc., Karlsruhe, Germany (2005)

[92] – R.W. Cheary, A. Coelho, J. Appl. Cryst. 25 (1992), 109

[93] – M. Järvinen, J. Appl. Cryst. (1993). 26, 525-531

[94] – Nonius Kappa CCD Program Package COLLECT, DENZO, SCALEPACK, SORTAV, Nonius Delft, The Netherlands, 1998

[95] – G.M. Sheldrick. SHELXL-97, Program for Crystal Structure Refinement. University of Göttingen, Germany

[96] - J.I. Goldstein, D.E. Newbury, P. Echlin, D.C. Joy, C. Fiori, E. Lifshin, "Scanning Electron Microscopy and X-ray Microanalysis", Plenum, New York, 1981

[97] – E. Koch, W. Fischer, Z. Kristallogr. 211 (1996), p.251

[98] – L. Pauling, „The nature of the chemical bond“ (3rd Ed.), Cornell University Press, Ithaca (1960)

[99] – G.A. Marking, H.F. Franzen, Chem. Mater. 5 (1993) p.678

[100] – R.S. Mulliken, J. Chem. Phys., 23 (1955) 1833

[101] – M. Köckerling, H.F. Franzen, Croatica Chemica Acta, 68 (1995) 709

[102] - P. Hohenberg, W. Kohn, Phys. Rev. 136 (1964), p. B864

[103] - W. Kohn, L. J. Sham, Phys. Rev. 140 (1965), p. A1133

[104] – J.P. Perdew, J.A. Chevary, S.H. Vosko, K.A. Jackson, M.R. Pederson, D.J. Singh, C. Fiolhais, Phys. Rev. B 46 (1992), p.6671.

[105] – P.E. Blöchl, Phys. Rev. B 50 (1994) 17953.

[106] – G. Kresse, D. Joubert, Phys. Rev. B 59 (1999) 1758.

[107] – H.J. Monkhorst, J.D. Pack, Phys. Rev. B 13 (1976) 5188.

[108] – P.E. Blöchl, O. Jepsen, O.K. Anderson, Phys. Rev. B 49 (1994) 16223.

[109] – G. Kresse, J. Hafner, Phys. Rev. B 47 (1993) 558.

[110] – G. Kresse, J. Furthmüller, Comput. Mater. Sci. 6 (1996) 15.

[111] – W.H. Press, B.P. Flannery, S.A. Teukolsky, W.T. Vetterling, "Numerical Recipes', Cambridge University Press, New York (1986).

[112] – B. Sundman, J. Ågren, J. Phys. Chem. Solids 42 (1981) 297.

[113] – Thermo-Calc, version P, Software for Thermodynamic Calculations in Multi-component Systems, Thermo-Calc AB, Stockholm, Sweden.

[114] – Y.B. Kuzma, S.V. Orishchin, Y.F. Lomnitskaya, T. Głowiak, Dop. AN Uk.RSR, Ser.B, 1988(2), p.47

[115] – P.J. Ahlzén, S. Rundqvist, Z. Kristallogr. 189 (1989) p.117

[116] – S. Geller, Acta Cryst., 8 (1955) p.83

[117] – Th. Hahn (Ed.), "International Tables for Crystallography, Vol. A, 5$^{th}$ Edition", Springer (The Netherlands), 2005, p.325; (available also online: http://it.iucr.org/Ab/contents/ )

[118] – P.A.Romans, O.G. Paasche, H. Kato, J. Less-Common Met., 8 (1965), p.213

[119] – A. Pialoux, M.L. Joyeux, G. Cizeron, J. Less-Common Met., 87 (1982), p.1

[120] – D. Schiferl, C.S. Barrett, J. Appl. Crystallogr., 2 (1969), p.30

[121] – M.E. Straumanis, E.Z. Aka, J. Appl. Phys., 23 (1952), p.330

[122] – B.D. Sharma, J. Donohue, Z. Kristallogr. Kristallgeom. Kristallphys. Kristallchem., 117 (1962), p.293

## Appendix A – Reported hafnium- and niobium-rich arsenides

### A.1. Crystal structures of HfAs and NbAs

The crystallographic data for the HfAs and NbAs are summarised in Table A.1 and A.2, respectively, and depicted in Fig. A.1 and A.2

**Table A.1. The crystal structure data for the HfAs compound [28]**

| Formula | | HfAs | | |
|---|---|---|---|---|
| Structure type | | AsTi | | |
| Pearson symbol | | *hP*8 | | |
| Space group | | $P6_3/mmc$ (no. 194) | | |
| Lattice parameters [Å] | a | 3.7681(3) | | |
| | c | 12.7034(17) | | |
| Atomic position | Wyckoff number | Coordinates | | |
| | | x | y | z |
| Hf | 4*f* | 1/3 | 2/3 | 0.116 |
| As1 | 2*a* | 0 | 0 | 0 |
| As2 | 2*d* | 1/3 | 2/3 | 3/4 |

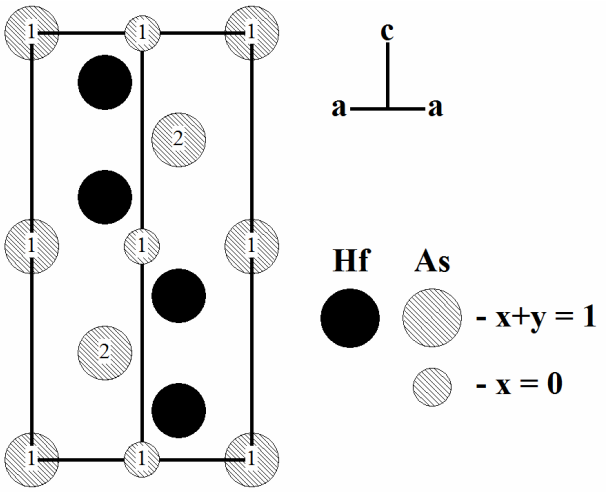


**Fig.A.1. The unit cell of HfAs – view in [$\bar{1}\,\bar{1}$0]) direction. The numbers describe the atoms on the given atom position (see Table A.1).**

**Table A.2. The crystal structure data for the NbAs compound [37]**

| Formula | | NbAs | | |
|---|---|---|---|---|
| Structure type | | AsNb | | |
| Pearson symbol | | *tI*8 | | |
| Space group | | $I4_1md$ (no. 109) | | |
| Lattice parameters [Å] | a | 3.4517 | | |
| | c | 11.680 | | |
| Atomic position | Wyckoff number | Coordinates | | |
| | | x | y | z |
| Nb | 4*a* | 0 | 0 | 0.000 |
| As | 4*a* | 0 | 0 | 0.416(1) |

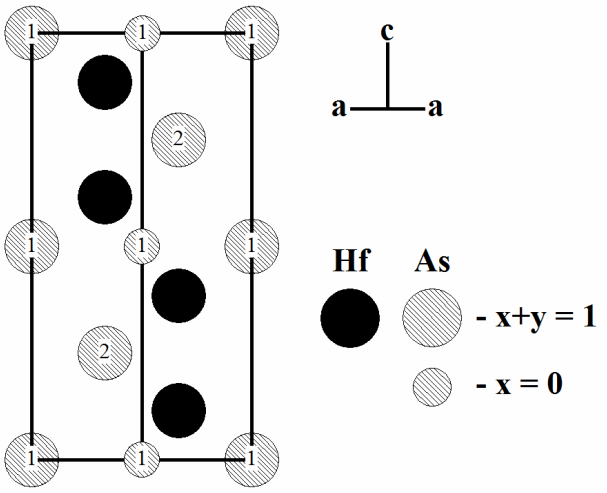


**Fig.A.2. The unit cell of HfAs – view in [$\bar{1}\,\bar{1}$0]) direction. The numbers describe the atoms on the given atom position (see Table A.2).**

## A.2. Crystal structure of $Nb_4As_3$

The crystallographic data for the $Nb_4As_3$ phase are summarised in Table A.3. and the structure is depicted in Fig. A.3.

**Table A.3. The crystal structure data for the $Nb_4As_3$ compound [43]**

| Formula | | $Nb_4As_3$ | | |
|---|---|---|---|---|
| Structure type | | $As_3Nb_4$ | | |
| Pearson symbol | | *oC*56 | | |
| Space group | | *Cmcm* (no. 63) | | |
| Lattice parameters [Å] | a | 3.5161(3) | | |
| | b | 14.6605(10) | | |
| | c | 18.8303(11) | | |
| Atomic position | Wyckoff number | Coordinates | | |
| | | X | y | z |
| Nb1 | 4*a* | 0 | 0 | 0 |
| Nb2 | 4*c* | 0 | 0.94676(15) | 1/4 |
| Nb3 | 8*f* | 0 | 0.26241(11) | 0.8382(8) |
| Nb4 | 8*f* | 0 | 0.46616(10) | 0.88002(8) |
| Nb5 | 8*f* | 0 | 0.33177(11) | 0.02848(8) |
| As1 | 4*c* | 0 | 0.30758(19) | 1/4 |
| As2 | 4*c* | 0 | 0.58790(17) | 1/4 |
| As3 | 8*f* | 0 | 0.09818(12) | 0.88215(9) |
| As4 | 8*f* | 0 | 0.15774(12) | 0.07725(9) |

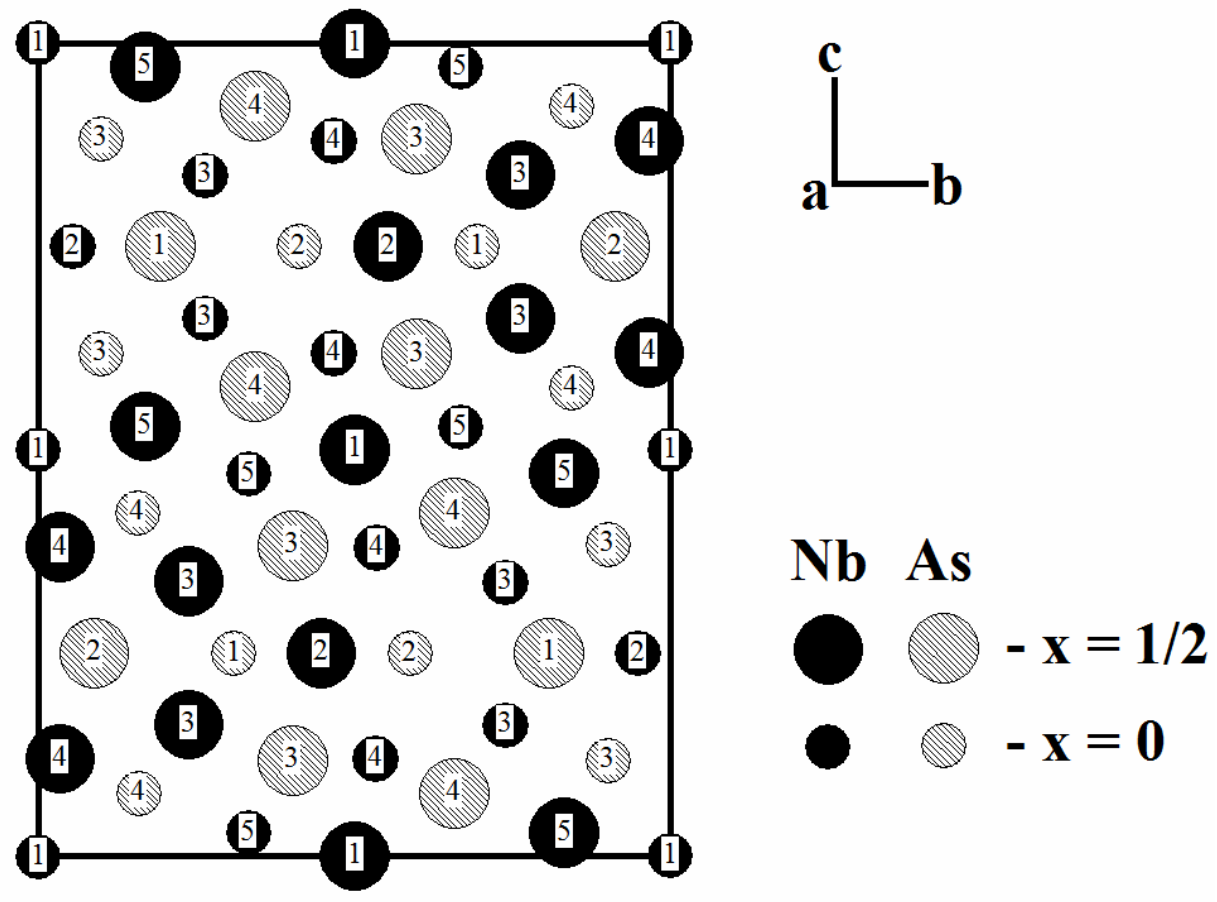


**Fig.A.3. The unit cell of the $Nb_4As_3$ compound view - in [$\bar{1}$00]) direction. The numbers describe the atoms on the given atom position (see Table A.3).**

.

### A.3. Crystal structure of $Hf_3As_2$

No crystallographic data for the $Hf_3As_2$ structure is reported. The phase was found isostructural with $Hf_3P_2$ by Rundqvist and Carlsson [29] who also gave the lattice parameters (orthorhombic cell, a = 10,4362 Å , b = 3,6521 Å, c = 10,1465 Å). The structure data for $Hf_3P_2$ [85] is given in Table A.4 and the structure is depicted in Fig.A.4. It is a representative of the anti-$Sb_3S_2$ structure type, i.e. the metal and non-metal atoms occupy the contrary sites compared to the ones occupied in original $Sb_3S_2$ compound (Hf occupies S sites and P occupies Sb sites).

**Table A.4. The crystal structure data for the $Hf_3P_2$ compound [85]**

| Formula | | $Hf_3P_2$ | | |
|---|---|---|---|---|
| Structure type | | $Hf_3P_2$ | | |
| Pearson symbol | | *oP*20 | | |
| Space group | | *Pnma* (no. 62) | | |
| Lattice parameters [Å] | a | 10.128(2) | | |
| | b | 3.5707(6) | | |
| | c | 9.868(2) | | |
| Atomic position | Wyckoff number | Coordinates | | |
| | | x | y | z |
| Hf1 | 4*c* | 0.04686(6) | 1/4 | 0.12605(6) |
| Hf2 | 4*c* | 0.37636(7) | 1/4 | 0.06432(5) |
| Hf3 | 4*c* | 0.21585(7) | 1/4 | 0.79665(6) |
| P1 | 4*c* | 0.3066(4) | 1/4 | 0.4991(4) |
| P2 | 4*c* | 0.4729(4) | 1/4 | 0.8203(4) |

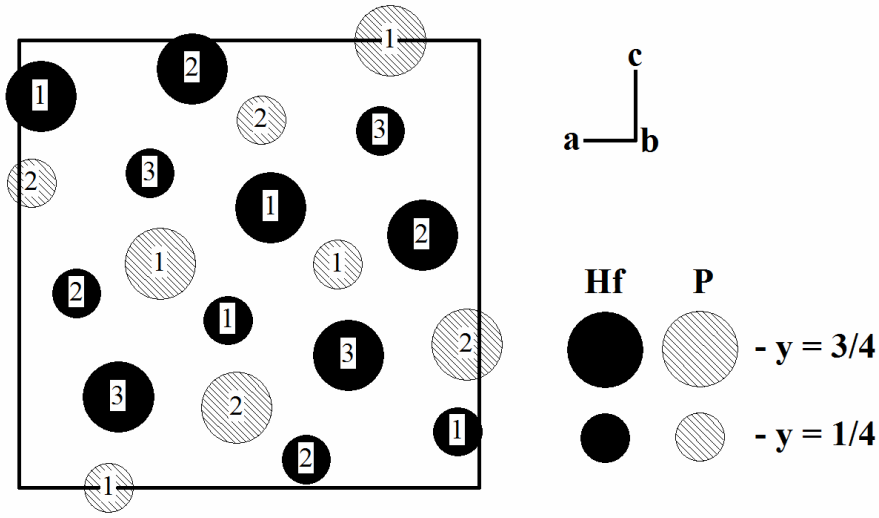


**Fig.A.4. The unit cell of the $Hf_3P_2$ compound - view in [$0\bar{1}0$]) direction. The numbers describe the atoms on the given atom position (see Table A.4).**

### A.4. Crystal structures of $Hf_5As_3$ and $Nb_5As_3$

Both of the phases crystallises in the $Nb_5As_3$ structure type. While the structural details for $Nb_5As_3$ were given by Laohavanich et al. [45], only the lattice parameters (orthorhombic cell, a = 27,3884(13) Å , b = 3,6114(2) Å, c = 12,3049(5) Å) and its structure type are known for $Hf_5As_3$ [32]. The structure data of $Nb_5As_3$ is given in Table A.5. and it is presented in Fig.A.5. The coordination spheres of the metal sites which are analysed in chapter 4.1.1.2 are shown in Fig.A.6.

**Table A.5. The crystal structure data for the $Nb_5As_3$ compound [45].**

| Formula | | $Nb_5As_3$ | | |
|---|---|---|---|---|
| Structure type | | $As_3Nb_5$ | | |
| Pearson symbol | | *oP*64 | | |
| Space group | | *Pnma* (no. 62) | | |
| Lattice parameters [Å] | a | 26.0701(10) | | |
| | b | 3.5198(2) | | |
| | c | 11.7869(5) | | |
| Atomic position | Wyckoff number | Coordinates | | |
| | | x | y | z |
| Nb1 | 4*c* | 0.1027(2) | 1/4 | 0.5682(4) |
| Nb2 | 4*c* | 0.1236(2) | 1/4 | 0.2888(4) |
| Nb3 | 4*c* | 0.1368(2) | 1/4 | 0.8523(4) |
| Nb4 | 4*c* | 0.2248(2) | 1/4 | 0.6192(4) |
| Nb5 | 4*c* | 0.2613(2) | 1/4 | 0.3452(4) |
| Nb6 | 4*c* | 0.3232(2) | 1/4 | 0.9604(4) |
| Nb7 | 4*c* | 0.3490(2) | 1/4 | 0.5557(4) |
| Nb8 | 4*c* | 0.4539(2) | 1/4 | 0.6972(4) |
| Nb9 | 4*c* | 0.4668(2) | 1/4 | 0.4159(4) |
| Nb10 | 4*c* | 0.4984(2) | 1/4 | 0.1056(4) |
| As1 | 4*c* | 0.0485(2) | 1/4 | 0.7491(5) |
| As2 | 4*c* | 0.0763(2) | 1/4 | 0.0525(5) |
| As3 | 4*c* | 0.2201(2) | 1/4 | 0.0033(4) |
| As4 | 4*c* | 0.3022(2) | 1/4 | 0.7462(5) |
| As5 | 4*c* | 0.3433(2) | 1/4 | 0.1926(4) |
| As6 | 4*c* | 0.4279(2) | 1/4 | 0.9189(5) |

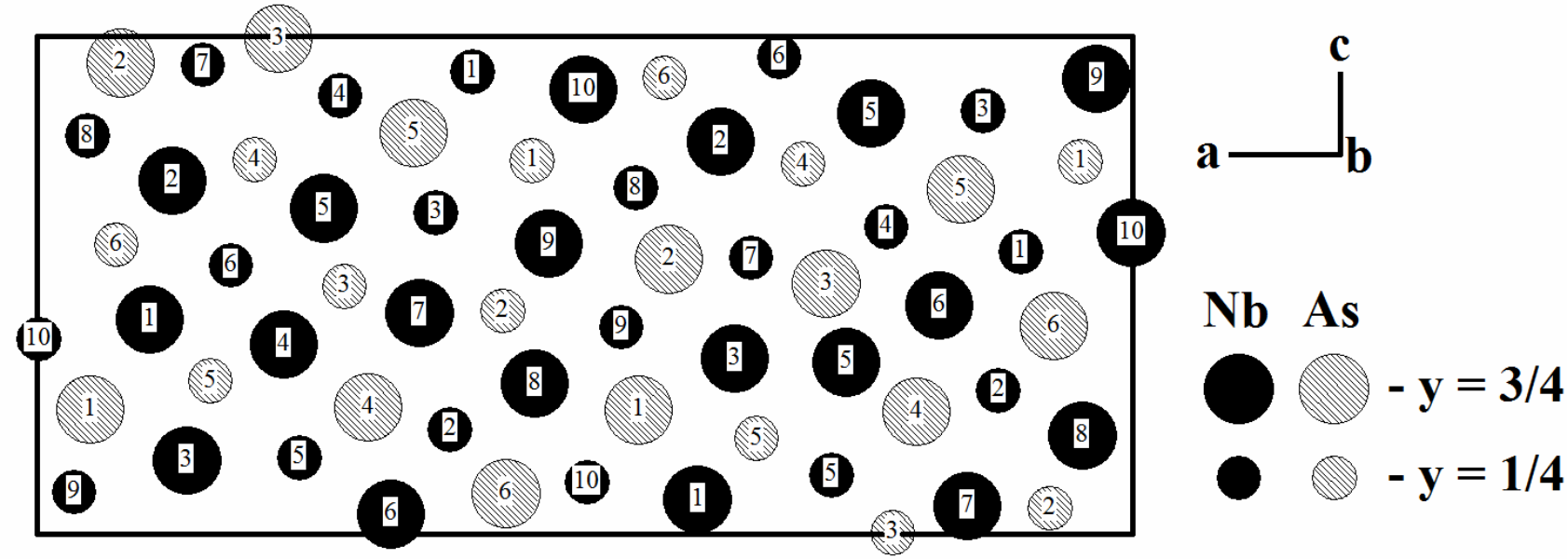


**Fig.A.5. The unit cell of $Nb_5As_3$ compound - view in [$0\bar{1}0$]) direction. The numbers describe the atoms on the given atom position (see Table A.5).**

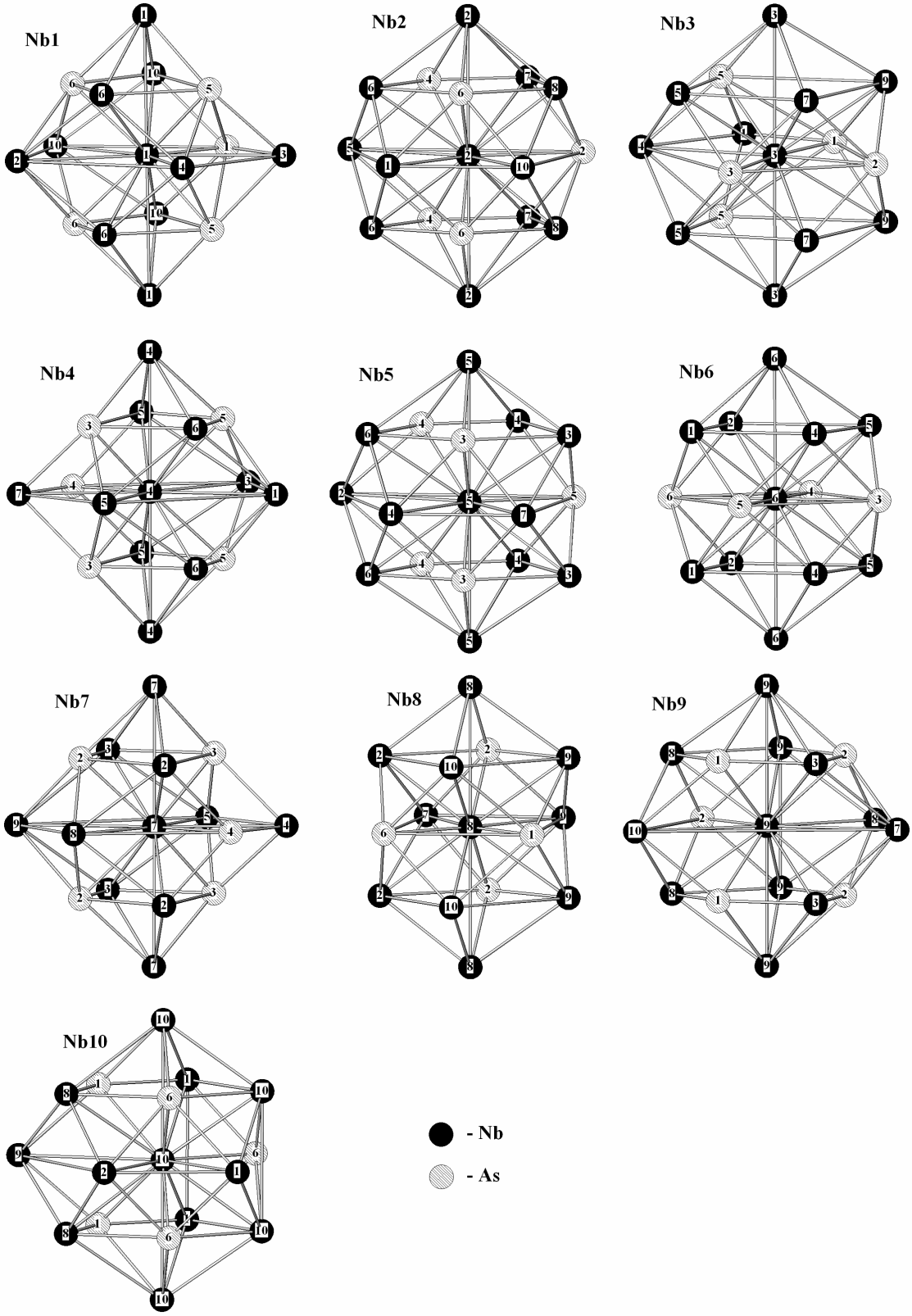


**Fig.A.6. The coordination spheres of the metal sites in $Nb_5As_3$ compound.**

### A.5. Crystal structures of $Hf_7As_4$ and $Nb_7As_4$

These both phases are isostructural with the $Nb_7P_4$ structure type, but unfortunately, the only available data are the lattice parameters (monoclinic cell; $Hf_7As_4$: a = 16,1150(21) Å , b = 3,5912(3) Å, c = 14,9283(15) Å, β = 104,24(1), [31]; $Nb_7As_4$: a = 15,3716(7) Å , b = 3,5242(2) Å, c = 14,1920(7) Å, β = 104,74(6)°, [32]). Therefore, the structure data of the $Nb_7P_4$ [86] phase are given in Table A.6 and the unit cell is depicted in Fig.A.7.

**Table A.6. The crystal structure data for the $Nb_7P_4$ compound [86].**

| Formula | | $Nb_7P_4$ | | |
|---|---|---|---|---|
| Structure type | | $Nb_7P_4$ | | |
| Pearson symbol | | *mC*44 | | |
| Space group | | *C*2/*m* (no. 12) | | |
| Lattice parameters [Å] | a | 14.9503(9) | | |
| | b | 3.4398(3) | | |
| | c | 13.8478(9) | | |
| | β [°] | 104.743(6) | | |
| Atomic position | Wyckoff number | Coordinates | | |
| | | x | y | z |
| Nb1 | 2*a* | 0 | 0 | 0 |
| Nb2 | 2*d* | 0 | 1/2 | 1/2 |
| Nb3 | 4*i* | 0.43126(8) | 0 | 0.82675(9) |
| Nb4 | 4*i* | 0.19530(8) | 0 | 0.31188(8) |
| Nb5 | 4*i* | 0.20981(8) | 0 | 0.80030(8) |
| Nb6 | 4*i* | 0.33760(8) | 0 | 0.02775(9) |
| Nb7 | 4*i* | 0.00322(8) | 0 | 0.66537(8) |
| Nb8 | 4*i* | 0.17502(9) | 0 | 0.54042(9) |
| P1 | 4*i* | 0.17403(26) | 0 | 0.11243(28) |
| P2 | 4*i* | 0.37360(27) | 0 | 0.60229(28) |
| P3 | 4*i* | 0.36956(25) | 0 | 0.33571(27) |
| P4 | 4*i* | 0.06355(25) | 0 | 0.84915(26) |

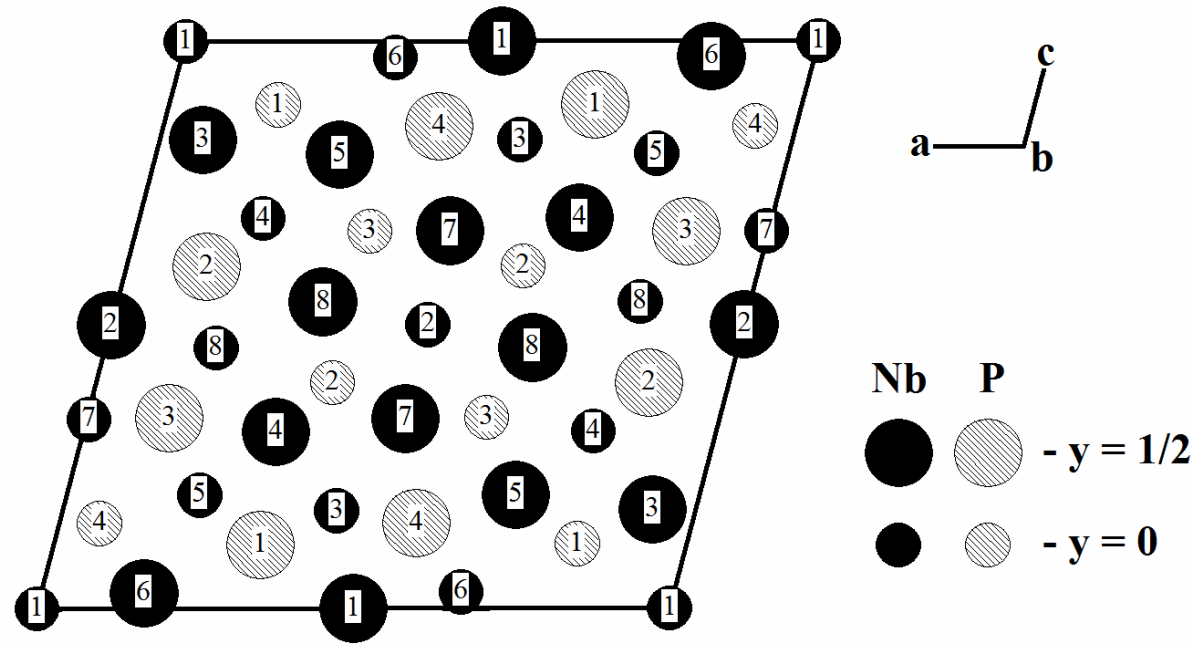


**Fig.A.7. The unit cell of the $Nb_7P_4$ compound - view in [0$\bar{1}$0]) direction. The numbers describe the atoms on the given atom position (see Table A.6).**

### A.6. Crystal structure of $Hf_2As$

No crystallographic data for the $Hf_2As$ structure is reported. The phase is isostructural with $Ta_2P$ by Rundqvist and Carlsson [29] who also gave the lattice parameters (orthorhombic cell, a = 15,3606(6) Å , b = 12,4892(6) Å, c = 3,6498(2) Å). Therefore, the structure data of the $Ta_2P$ phase [87] is given in Table A.7. and the structure is depicted in Fig.A.8.

**Table A.7. The crystal structure data for the $Ta_2P$ compound [87]**

| Formula | | $Ta_2P$ | | |
|---|---|---|---|---|
| Structure type | | $PTa_2$ | | |
| Pearson symbol | | *oP*36 | | |
| Space group | | *Pnnm* (no. 58) | | |
| Lattice parameters [Å] | a | 14.419 | | |
| | b | 11.552 | | |
| | c | 3.399 | | |
| Atomic position | Wyckoff number | Coordinates | | |
| | | x | y | z |
| Ta1 | 4*g* | 0.07775(8) | 0.12237(10) | 0 |
| Ta2 | 4*g* | 0.29501(8) | 0.19686(9) | 0 |
| Ta3 | 4*g* | 0.10897(8) | 0.52997(10) | 0 |
| Ta4 | 4*g* | 0.24502(8) | 0.92143(10) | 0 |
| Ta5 | 4*g* | 0.47722(9) | 0.84758(11) | 0 |
| Ta6 | 4*g* | 0.42028(8) | 0.41362(10) | 0 |
| P1 | 4*g* | 0.1511 (6) | 0.3153(7) | 0 |
| P2 | 4*g* | 0.2930(6) | 0.5778(8) | 0 |
| P3 | 4*g* | 0.0840(6) | 0.7562(8) | 0 |

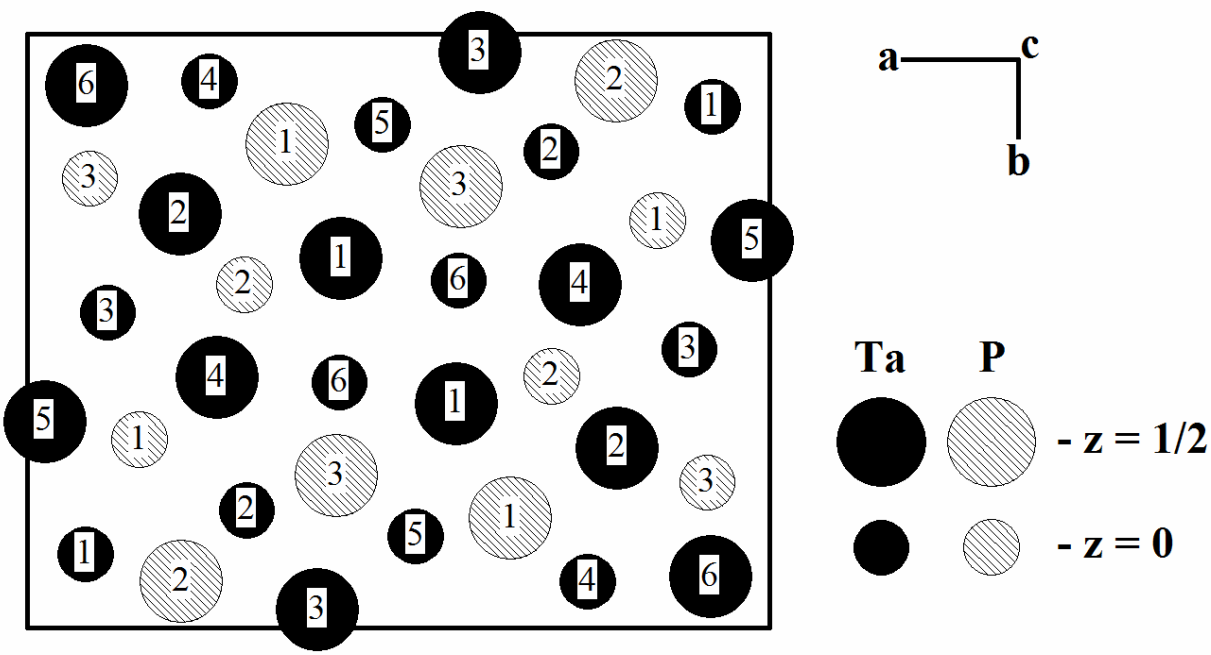


**Fig.A.8. The unit cell of the $Ta_2P$ compound - view in [00$\bar{1}$]) direction. The numbers describe the atoms on the given atom position (see Table A.7).**

## A.7. Crystal structures of $Hf_3As$ and $Nb_3As$

The crystallographic data for the $Hf_3As$ ($Ta_3As$ structure type) [30] and $Nb_3As$ ($Ti_3P$ structure type) [44] are gathered in Table A.8 and A.9, respectively. Both structures are depicted in Fig.A.9 and A.10. Although both compounds are described with the unit cells having different symmetry, they are both related to each other, as it was demonstrated by Willerström et al. [30]. Additionally, the coordination spheres of the metal sites which are analysed for the $Hf_{2+x}Nb_{1-x}As$ phase isostructural with $Nb_3As$ in chapter 4.1.1.7 are depicted in Fig.A.11.

**Table A.8. The crystal structure data for the $Hf_3As$ compound [30].**

| Formula | | $Hf_3As$ | | |
|---|---|---|---|---|
| Structure type | | $AsTa_3$ | | |
| Pearson symbol | | *mC*64 | | |
| Space group | | $C2/c$ (no. 15) | | |
| Lattice parameters [Å] | a | 15.3898(14) | | |
| | b | 5.3795(5) | | |
| | c | 15.3330(14) | | |
| | β [°] | 90.291(6) | | |
| Atomic position | Wyckoff number | Coordinates | | |
| | | x | y | z |
| Hf1 | 8*f* | 0.7367(5) | 0.7895(12) | 0.4026(6) |
| Hf2 | 8*f* | 0.1570(5) | 0.7231(15) | 0.5100(5) |
| Hf3 | 8*f* | 0.9415(5) | 0.4802(15) | 0.1669(5) |
| Hf4 | 8*f* | 0.0808(5) | 0.9664(14) | 0.6899(5) |
| Hf5 | 8*f* | 0.7362(5) | 0.2672(13) | 0.3021(5) |
| Hf6 | 8*f* | 0.9487(5) | 0.7556(14) | 0.4835(5) |
| As1 | 8*f* | 0.9161(9) | 0.9916(35) | 0.1317(10) |
| As2 | 8*f* | 0.1214(9) | 0.4602(31) | 0.6627(12) |

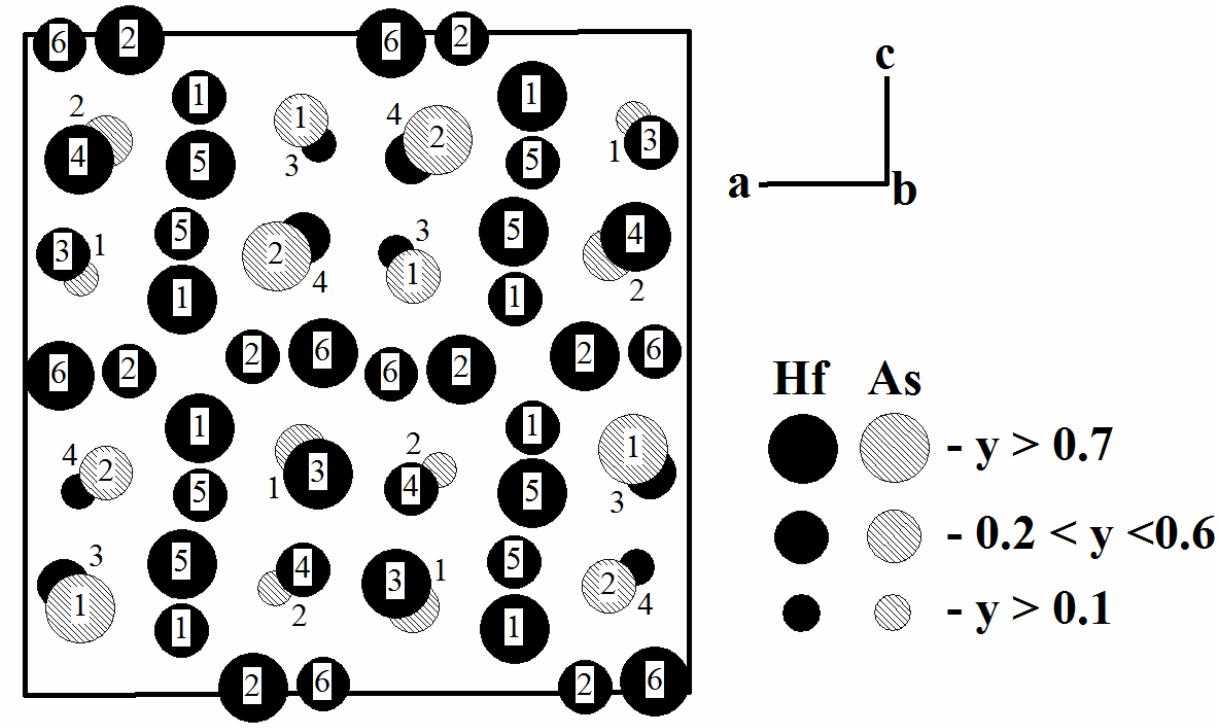


**Fig.A.9. The unit cell of the $Hf_3As$ compound - view in [0$\bar{1}$0]) direction. The numbers describe the atoms on the given atom position (see Table A.8).**

**Table A.9. The crystal structure data for the $Nb_3As$ compound [44].**

| Formula | | $Nb_3As$ | | |
|---|---|---|---|---|
| Structure type | | $PTi_3$ | | |
| Pearson symbol | | *tP*32 | | |
| Space group | | $P4_2/n$ (no. 86) | | |
| Lattice parameters [Å] | a | 10.294(4) | | |
| | c | 5.199(2) | | |
| Atomic position | Wyckoff number | Coordinates | | |
| | | x | y | z |
| Nb1 | 8*f* | 0.4152(1) | 0.9054(1) | 0.9772(2) |
| Nb2 | 8*f* | 0.3521(1) | 0.5117(1) | 0.7681(2) |
| Nb3 | 8*f* | 0.3062(1) | 0.7864(1) | 0.4911(1) |
| As1 | 8*f* | 0.2930(1) | 0.5214(1) | 0.2703(3) |

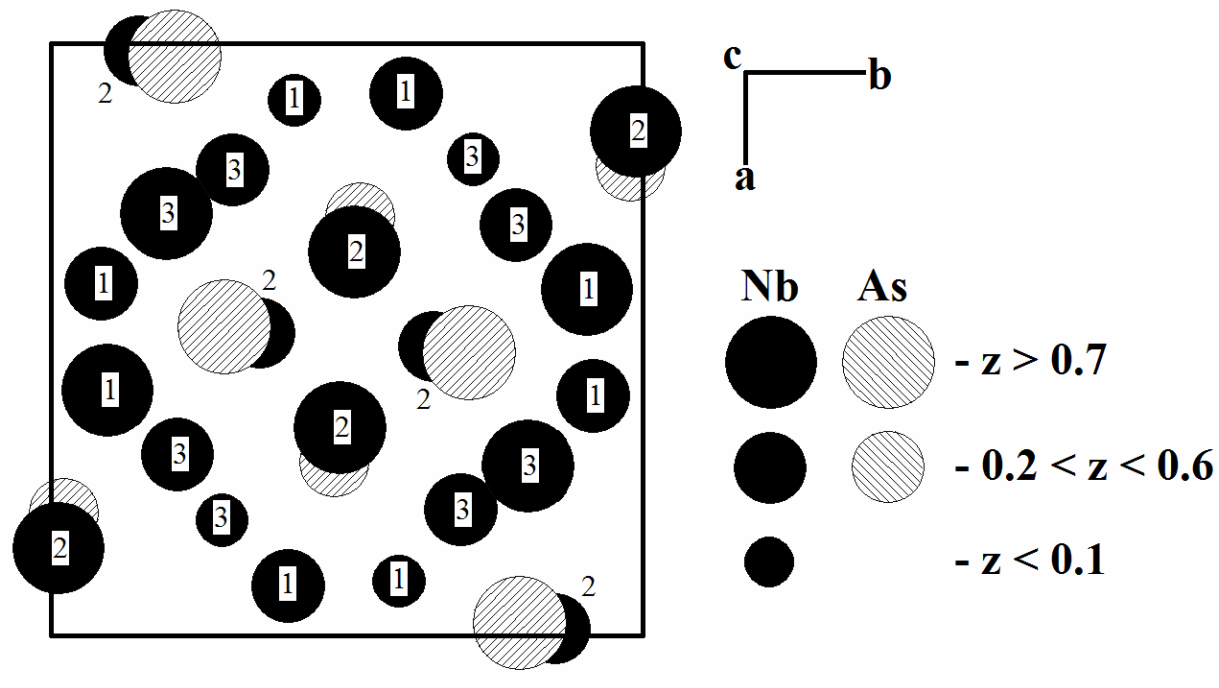


**Fig.A.10. The unit cell of the $Nb_3As$ compound - view in [00$\bar{1}$]) direction. The numbers describe the atoms on the given atom position (see Table A.9).**

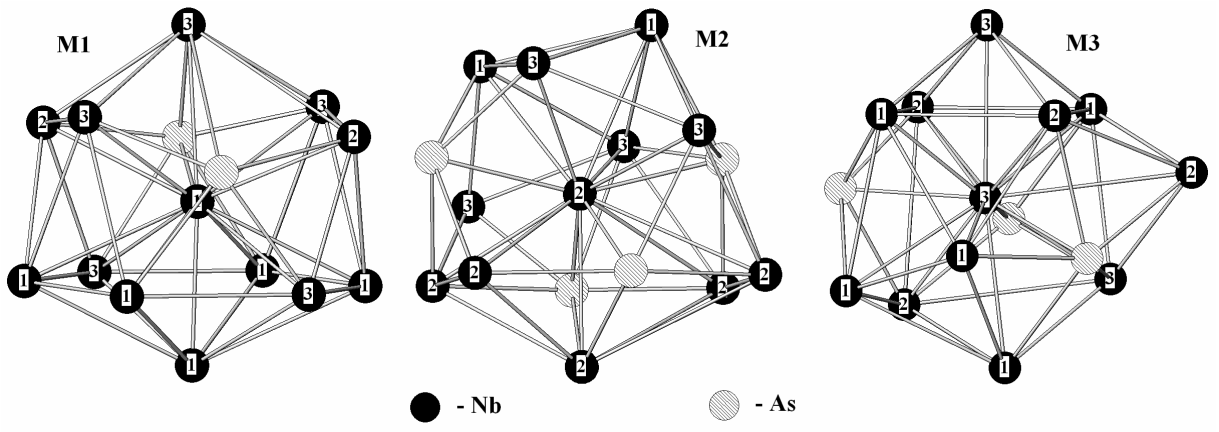


**Fig.A.11. The coordination spheres of the metal sites in the $Hf_{2+x}Nb_{1-x}As$ phase (isostructural with $Nb_3As$).**

## Appendix B – Crystal structure of $Hf_5Ge_4$

The crystallographic data for the $Hf_5Ge_4$ given by Zhao and Parthe [50] are summarised in Table B.1 and the structure is depicted in Fig. B.1.

**Table B.1. The crystal structure data for the $Hf_5Ge_4$ compound [50].**

| Formula | | $Hf_5Ge_4$ | | |
|---|---|---|---|---|
| Structure type | | $Ge_4Sm_5$ | | |
| Pearson symbol | | *oP*36 | | |
| Space group | | *Pnma* (no. 62) | | |
| Lattice parameters [Å] | a | 7.017(1) | | |
| | b | 13.434(4) | | |
| | c | 7.105(1) | | |
| Atomic position | Wyckoff number | Coordinates | | |
| | | x | y | z |
| Hf1 | 4*c* | 0.1811(2) | 1/4 | 0.0021(3) |
| Hf2 | 8*d* | 0.1457(2) | 0.6239(1) | 0.1671(2) |
| Hf3 | 8*d* | 0.0141(2) | 0.0946(1) | 0.3229(2) |
| Ge1 | 4*c* | 0.0534(6) | 1/4 | 0.6110(6) |
| Ge2 | 4*c* | 0.3212(6) | 1/4 | 0.3540(6) |
| Ge3 | 8*d* | 0.3039(4) | 0.5407(3) | 0.4648(4) |

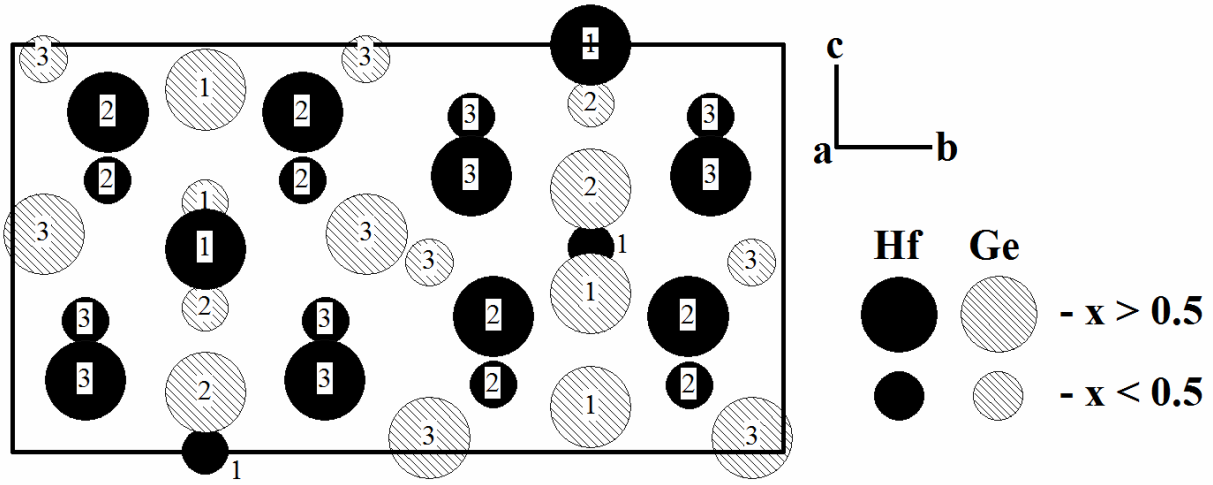


**Fig.B.1. The unit cell of the $Hf_5Ge_4$ compound - view in [$\bar{1}$00]) direction. The numbers describe the atoms on the given atom position (see Table B.1).**

## Appendix C – Crystal structure of HfGa

The crystallographic data for the HfGa given by Markiv and Belyavina [67] are given in Table C.1. The coordination spheres of the crystal sites occupied by transition metals which are analysed in chapter 4.3.1 are depicted in Fig.C.1. and the unit cell itsef is shown in Fig.C.2.

**Table C.1. The crystal structure data for the HfGa compound [67].**

| Formula | | HfGa | | |
|---|---|---|---|---|
| Structure type | | ThTl | | |
| Pearson symbol | | *oP*24 | | |
| Space group | | *Pbcm* (no. 57) | | |
| Lattice parameters [Å] | a | 9.171 | | |
| | b | 8.503 | | |
| | c | 5.648 | | |
| Atomic position | Wyckoff number | Coordinates | | |
| | | x | y | z |
| Hf1 | 4c | 0.112 | 1/4 | 0 |
| Hf2 | 4d | 0.626 | 0.527 | 1/4 |
| Hf3 | 4d | 0.1918 | 0.6407 | 1/4 |
| Ga1 | 4c | 0.556 | 1/4 | 0 |
| Ga2 | 4d | 0.077 | 0.963 | 1/4 |
| Ga3 | 4d | 0.659 | 0.897 | 1/4 |

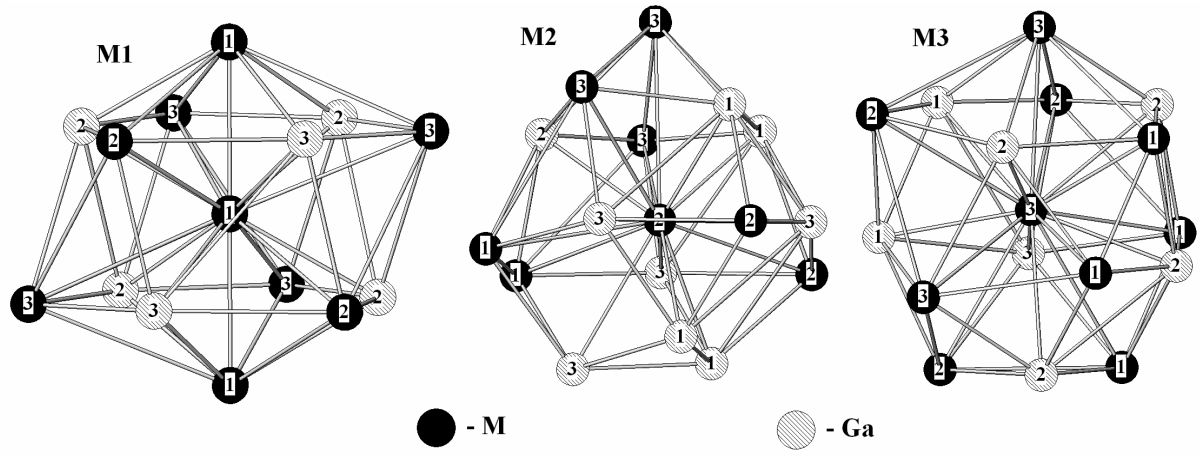


**Fig.C.1. The coordination spheres of the metal sites in the HfGa phase.**

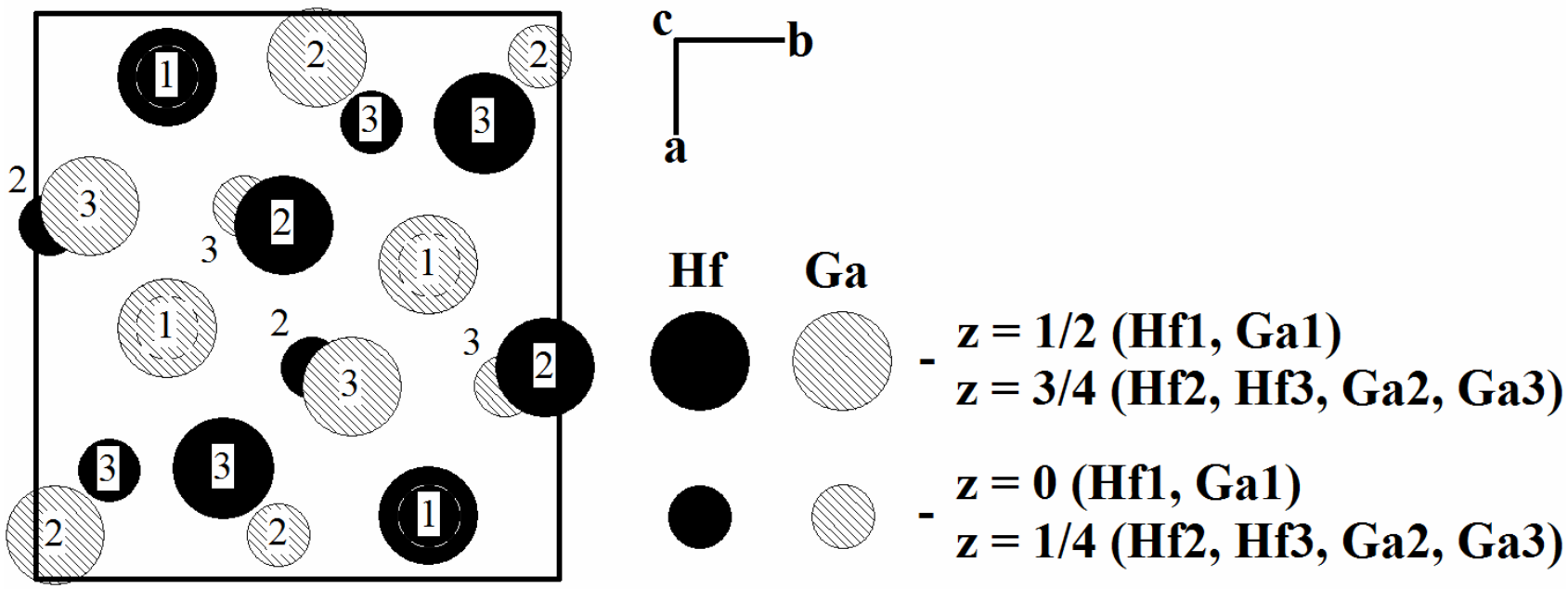


**Fig.C.2. The unit cell of the HfGa compound - view in [00$\bar{1}$]) direction. The numbers describe the atoms on the given atom position (see Table C.1).**

## Appendix D – Reported prototypes of the structures found in this work

### D.1. Crystal structure of $Nb_2P$

As it was mentioned in chapter 4.1.1.3, $Nb_2As$ was found isostructural with the $Nb_2P$ phase reported by Kuzma et al. [114]. The reported data for $Nb_2P$ data are given in Table D.1 and the structure is depicted in Fig. D.1. The arrangement of the trigonal prisms around arsenic atoms is shown in Fig. D.2.

**Table D.1. The crystal structure data for the $Nb_2P$ compound [114]**

| Formula | | $Nb_2P$ | | |
|---|---|---|---|---|
| Structure type | | $Nb_2P$ | | |
| Pearson symbol | | *oP*54 | | |
| Space group | | *Pmma* (no. 51) | | |
| Lattice parameters [Å] | a | 18.079(5) | | |
| | b | 3.425(1) | | |
| | c | 13.858(4) | | |
| Atomic position | Wyckoff number | Coordinates | | |
| | | x | y | z |
| Nb1 | 2*a* | 0 | 0 | 0 |
| Nb2 | 2*d* | 0 | 1/2 | 1/2 |
| Nb3 | 2*e* | 1/4 | 0 | 0.1098 |
| Nb4 | 2*e* | 1/4 | 0 | 0.3878 |
| Nb5 | 2*e* | 1/4 | 0 | 0.8898 |
| Nb6 | 2*f* | 1/4 | 1/2 | 0.5612 |
| Nb7 | 4*i* | 0.0616 | 0 | 0.3437 |
| Nb8 | 4*i* | 0.1216 | 0 | 0.5704 |
| Nb9 | 4*j* | 0.0016 | 1/2 | 0.1628 |
| Nb10 | 4*j* | 0.1375 | 1/2 | 0.0044 |
| Nb11 | 4*j* | 0.1661 | 1/2 | 0.2413 |
| Nb12 | 4*j* | 0.6621 | 1/2 | 0.2392 |
| P1 | 2*e* | 1/4 | 0 | 0.6891 |
| P2 | 4*i* | 0.1049 | 0 | 0.1378 |
| P3 | 4*i* | 0.6037 | 0 | 0.1282 |
| P4 | 4*j* | 0.1442 | 1/2 | 0.4304 |
| P5 | 4*j* | 0.5463 | 1/2 | 0.3275 |

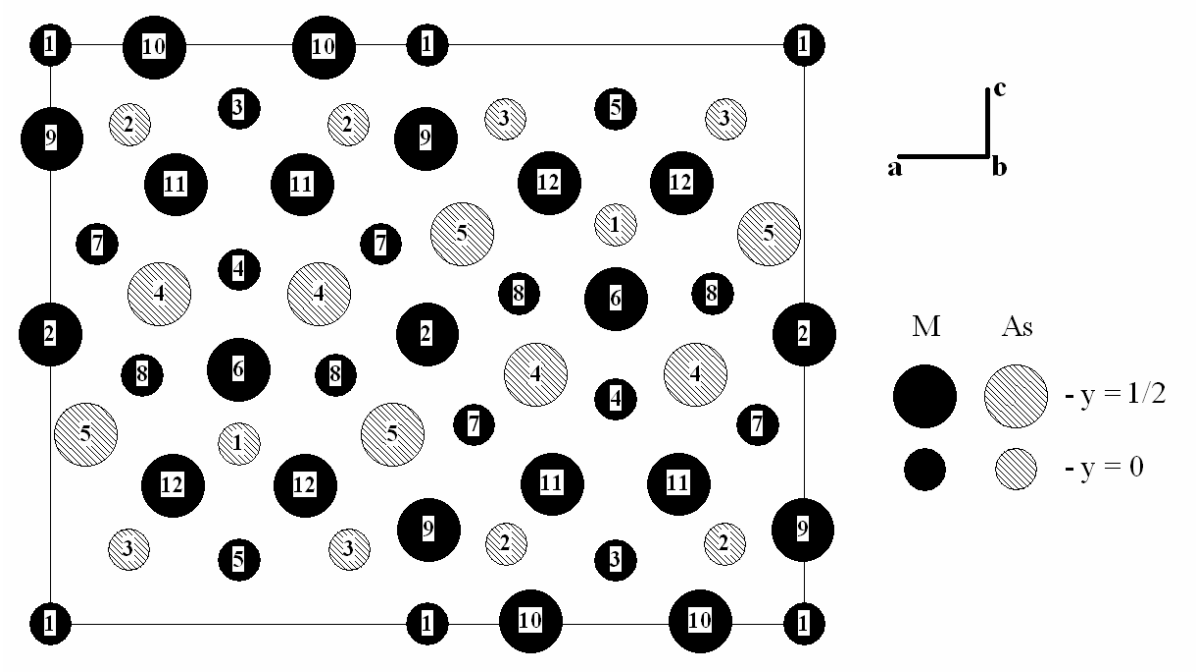


**Fig.D.1. The unit cell of the $Nb_2P$ compound - view in [$0\bar{1}0$]) direction. The numbers describe the atoms on the given atom position (see Table D.1).**

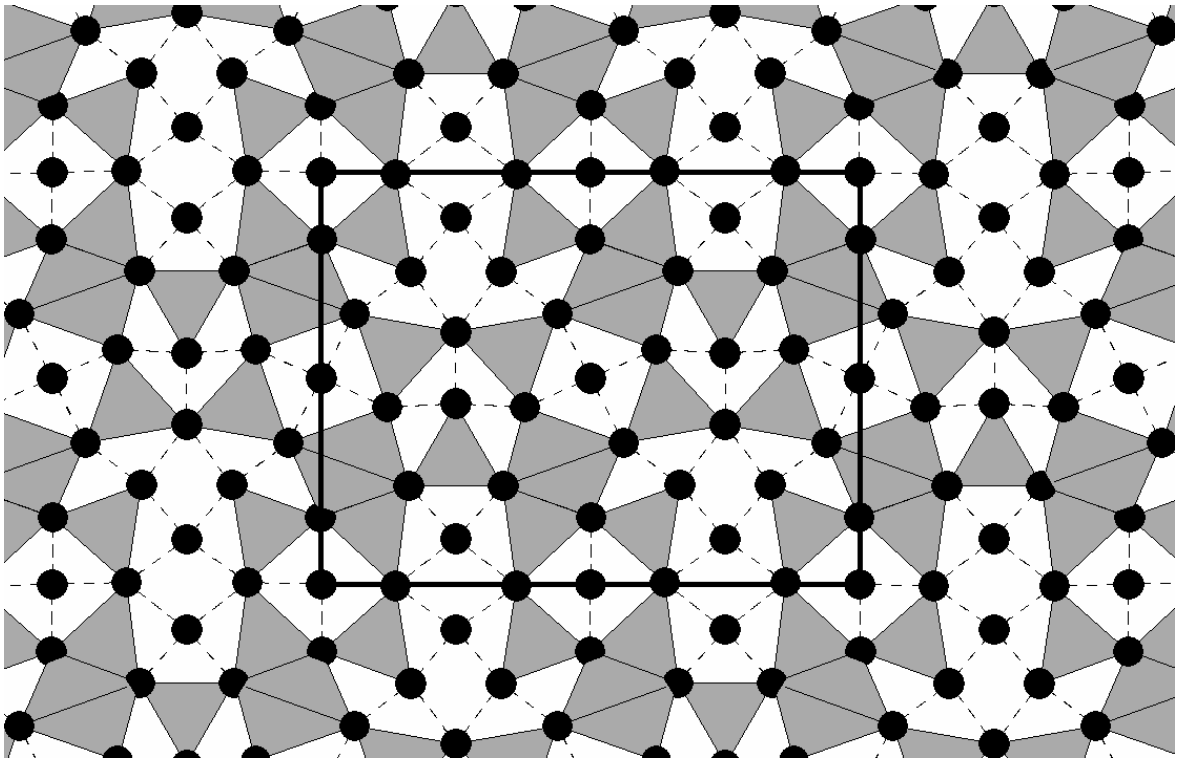

**Fig.D.2. The arrangement of the trigonal prisms in the $Nb_2P$ compound – view in [$00\bar{1}$] direction**

## D.2. Crystal structure of $Zr_2P$

$Hf_{3+x}Nb_{1-x}As_2$ phase (see chapter 4.1.1.3) is isostructural with $Zr_2P$ compound reported by Ahlzén and Rundqvist [115]. The reported data for $Zr_2P$ data are given in Table D.2 and the structure is depicted in Fig. D.3. The arrangement of the trigonal prisms around arsenic atoms found also in this structure is shown in Fig. D.4.

**Table D.2. The crystal structure data for the $Zr_2P$ compound [115]**

| Formula | | $Zr_2P$ | | |
|---|---|---|---|---|
| Structure type | | $Zr_2P$ | | |
| Pearson symbol | | *oC*108 | | |
| Space group | | *Cmmm* (no. 65) | | |
| Lattice parameters [Å] | a | 29.5099(8) | | |
| | b | 19.0634(7) | | |
| | c | 3.6076(1) | | |
| Atomic position | Wyckoff number | Coordinates | | |
| | | x | y | z |
| Zr1 | 4*e* | 1/4 | 1/4 | 0 |
| Zr2 | 4*g* | 0.22087(2) | 0 | 0 |
| Zr3 | 4*h* | 0.05691(2) | 0 | 1/2 |
| Zr4 | 4*h* | 0.30738(2) | 0 | 1/2 |
| Zr5 | 4*h* | 0.44754(2) | 0 | 1/2 |
| Zr6 | 4*i* | 0 | 0.10833(2) | 0 |
| Zr7 | 4*i* | 0 | 0.38473(2) | 0 |
| Zr8 | 4*j* | 0 | 0.25038(2) | 1/2 |
| Zr9 | 8*p* | 0.08322(1) | 0.24857(2) | 0 |
| Zr10 | 8*p* | 0.12141(1) | 0.08971(2) | 0 |
| Zr11 | 8*p* | 0.38067(1) | 0.08127(2) | 0 |
| Zr12 | 8*q* | 0.21574(1) | 0.12946(2) | 1/2 |
| Zr13 | 8*q* | 0.32936(1) | 0.18928(2) | 1/2 |
| P1 | 4*h* | 0.15538(4) | 0 | 1/2 |
| P2 | 8*p* | 0.16715(3) | 0.20543(5) | 0 |
| P3 | 8*p* | 0.28471(3) | 0.10673(4) | 0 |
| P4 | 8*q* | 0.06324(3) | 0.14524(5) | 1/2 |
| P5 | 8*q* | 0.06853(3) | 0.35093(5) | 1/2 |

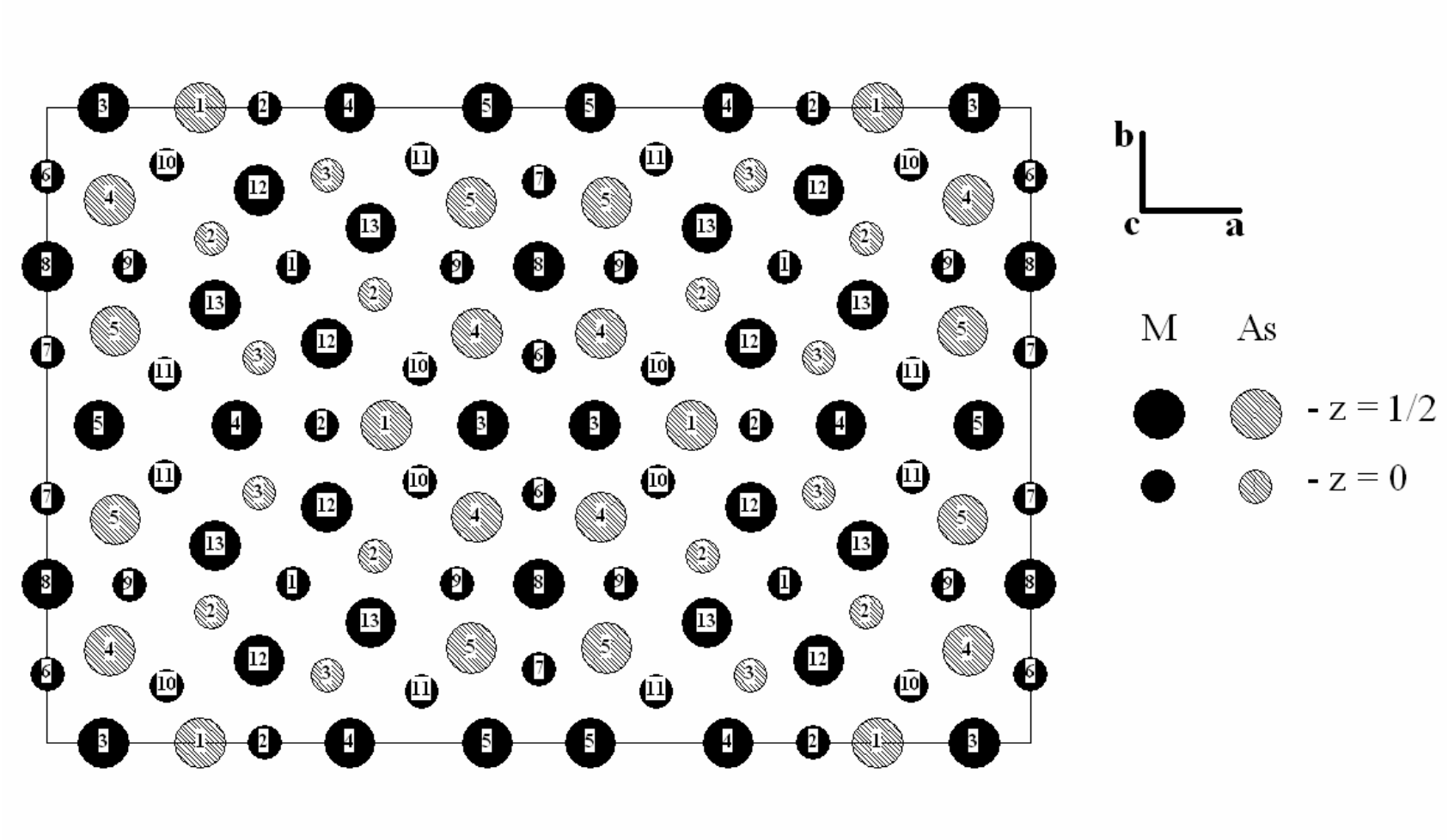


**Fig.D.3. The unit cell of the $Zr_2P$ compound - view in [00$\bar{1}$]) direction. The numbers describe the atoms on the given atom position (see Table D.2).**

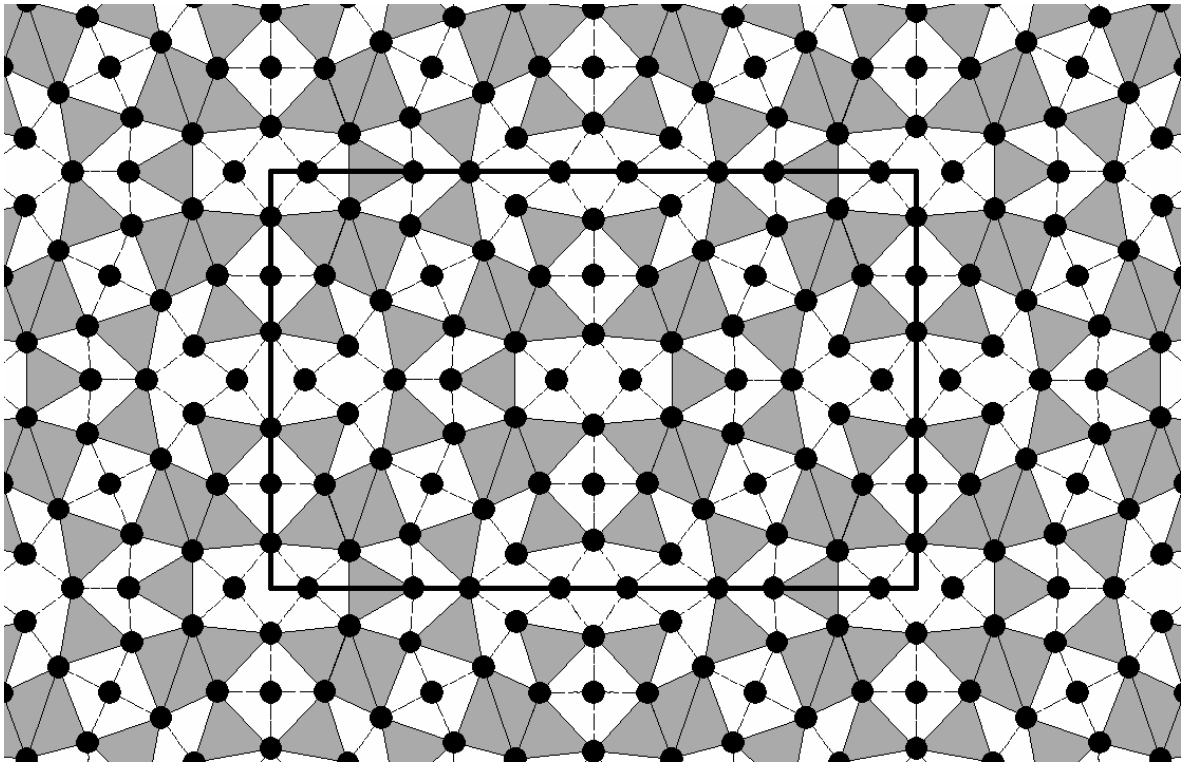

**Fig.D.4. The arrangement of the trigonal prisms in the $Zr_2P$ compound – view in [00$\bar{1}$] direction**

### D.3. Crystal structure of $Hf_{0.97}V_{1.03}As$

$Hf_{1+x}Nb_{1-x}As$ (see chapter 4.1.1.3) is isostructural with $Co_2Si$, similar to other ternary arsenides of the early transition metals [22]. The structure data for $Hf_{0.97}V_{1.03}As$ reported by Derakhshan et al. are given in Table D.3 and the structure is depicted in Fig. D.5. Also in this compound the trigonal prisms around arsenic atoms are found and their arrangement is shown shown in Fig. D.6

**Table D.3. The crystal structure data for the $Hf_{0.97}V_{1.03}As$ compound [22]**

| Formula | | $Hf_{0.97}V_{1.03}As$ | | |
|---|---|---|---|---|
| Structure type | | $Co_2Si$ | | |
| Pearson symbol | | *oP*12 | | |
| Space group | | *Pnma* (no. 62) | | |
| Lattice parameters [Å] | a | 6.741(2) | | |
| | b | 3.5888(9) | | |
| | c | 8.073(2) | | |
| Atomic position | Wyckoff number | Coordinates | | |
| | | x | y | z |
| M1 | 4*c* | 0.4564(1) | 1/4 | 0.6670(1) |
| M2 | 4*c* | 0.3720(5) | 1/4 | 0.0578(4) |
| As1 | 4*c* | 0.2428(3) | 1/4 | 0.3607(3) |

.

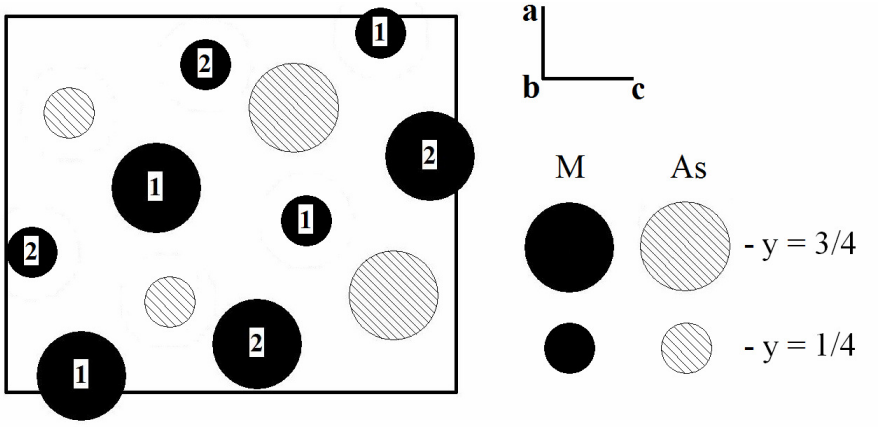


**Fig.D.5. Unit cell of $Hf_{0.97}V_{1.03}As$ crystal - view in [0$\bar{1}$0]) direction. The numbers describe the atoms on the given atom position (see Table D.3).**

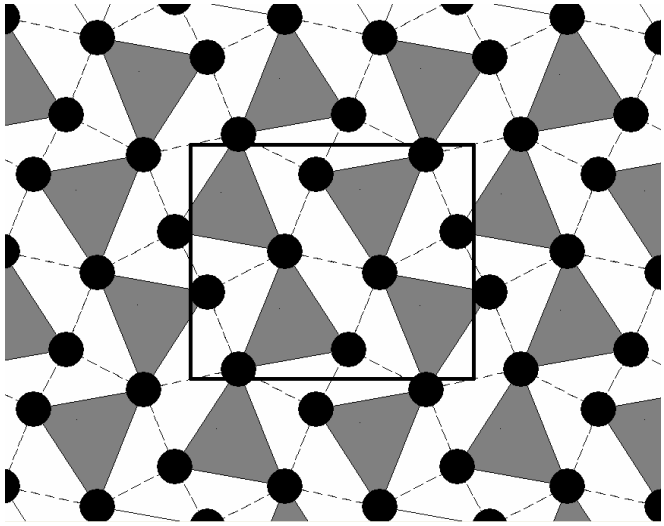

**Fig.D.6. Structure of $Hf_{0.97}V_{1.03}As$ shown as an arrangement of the trigonal prisms – view in $[0\bar{1}0]$ direction**

## D.4. Crystal structure of $Zr_{6.45}Nb_{4.55}P_4$

A single crystal XRD measurement of the phase showed that it is isostructural with $Zr_{6.45}Nb_{4.55}P_4$ compound reported by Marking and Franzen [99]. The reported structure data for this phosphide is given in Table D.4. It must be noted that the description of the unit cell in the paper is not consistent with the notation used in chapter 4.1.1.5 of this work. The first reason is that the authors designated the largest lattice parameter as *a* and the shortest as *c* – contrary to the notation used in ref. [117]. The second reason is the designation of the metal sites with the descending niobium occupation in ref. [99] ($y_{Nb}^{M1} = 1$, $y_{Nb}^{M2} = 0.42$, $y_{Nb}^{M3} = 0.06$). Thus the metal sites M2, M4 and M5 in ref. [99] (and in Table D.4), correspond with the sites M5, M2 and M4 in this work, respectively.

**Table D.4. The reported crystal structure data for the $Zr_{6.45}Nb_{4.55}P_4$ compound [99]**

| Formula | | $Zr_{6.45}Nb_{4.55}P_4$ | | |
|---|---|---|---|---|
| Structure type | | $Zr_{6.45}Nb_{4.55}P_4$ | | |
| Pearson symbol | | *oI*30 | | |
| Space group | | *Immm* (no. 71) | | |
| Lattice parameters [Å] | a | 15.917(1) | | |
| | b | 9.5684(9) | | |
| | c | 3.5892(3) | | |
| Atomic position | Wyckoff number | Coordinates | | |
| | | x | y | z |
| M1 | 8*l* | 0.29200(2) | 0.16228(4) | 0 |
| M2 | 2*a* | 0 | 0 | 0 |
| M3 | 4*j* | 0.90161(4) | 1/2 | 0 |
| M4 | 4*j* | 0.34113(4) | 1/2 | 0 |
| M5 | 4*h* | 0 | 0.72960(6) | 0 |
| P | 8*l* | 0.12147(7) | 0.2053(1) | 0 |

## Appendix E – Site volumes and Pauling bond orders of the metal sites in the selected structures

The following tables contain information about the coordination sphere (the distance to the next neighbour), the Dirichlet domain (the edge number and the area of the created polygon) and the order of the bond between these two atoms (calculated after Pauling [98]) for the metal sites. The interatomic distances are taken from the experimental measurements (single crystal or Rietveld refinement). The volumes of the Dirichlet domains (interpreted as site volumes) were calculated with program *DIDO95*(see chapter 3.2.1). The values of *D(1)* (single bond distance) needed for Pauling bond order calculation are a sum of the atom radii of the bonded atoms. The atomic radii which were used for the calculation are:

- $r_{Hf}$ = 1.44 Å
- $r_{Nb}$ = 1.34 Å
- $r_{As}$ = 1.21 Å
- $r_{Ga}$ = 1.25 Å

The atom radius of the site with the mixed occupation is assumed to change linearly with the site fraction (i.e. $r = y_{Nb}*r_{Nb}+y_{Hf}*r_{Hf}$, where $y_{Nb}+y_{Hf} = 1$).

## E.1. Sample S20, $(Hf,Nb)_5As_3$ phase

| Central atom | Neighbour atom | Distance [Å] | D(1) [Å] | Pauling bond order | Created polygon of the Dirichlet domain | Polygon's area [Å$^2$] |
|---|---|---|---|---|---|---|
| M1<br>$y_{Nb} = 0.47$<br>r = 1.393 | As1 | 2.60 | 2.60 | 1.008 | 5-gon | 5.07 |
| | As6 | 2.66 | 2.60 | 0.791 | 6-gon | 4.37 |
| | As6 | 2.66 | 2.60 | 0.791 | 6-gon | 4.37 |
| | As5 | 2.68 | 2.60 | 0.736 | 7-gon | 4.27 |
| | As5 | 2.68 | 2.60 | 0.736 | 7-gon | 4.27 |
| | Nb6 | 2.89 | 2.76 | 0.603 | 6-gon | 2.88 |
| | Nb6 | 2.89 | 2.76 | 0.603 | 6-gon | 2.88 |
| | Nb4 | 3.21 | 2.76 | 0.177 | 4-gon | 1.24 |
| | Nb10 | 3.32 | 2.81 | 0.139 | 6-gon | 2.07 |
| | Nb10 | 3.32 | 2.81 | 0.139 | 6-gon | 2.07 |
| | Nb2 | 3.41 | 2.82 | 0.102 | 4-gon | 0.97 |
| | Nb3 | 3.47 | 2.80 | 0.078 | 3-gon | 0.42 |
| | Nb10 | 3.57 | 2.81 | 0.053 | 4-gon | 0.83 |
| | Nb1 | 3.59 | 2.79 | 0.046 | 4-gon | 0.60 |
| | Nb1 | 3.59 | 2.79 | 0.046 | 4-gon | 0.60 |
| Sum of Pauling bond orders (i.e. electron population on the crystal site): 6.047 | | | | | | |
| Volume of the Dirichlet domain: 17.62 Å$^3$ | | | | | | |

| Central atom | Neighbour atom | Distance [Å] | D(1) [Å] | Pauling bond order | Created polygon of the Dirichlet domain | Polygon's area [Å$^2$] |
|---|---|---|---|---|---|---|
| M2<br>$y_{Nb} = 0.17$<br>r = 1.423 | As6 | 2.70 | 2.63 | 0.761 | 6-gon | 3.95 |
| | As6 | 2.70 | 2.63 | 0.761 | 6-gon | 3.95 |
| | As4 | 2.75 | 2.63 | 0.643 | 6-gon | 4.65 |
| | As4 | 2.75 | 2.63 | 0.643 | 6-gon | 4.65 |
| | Nb8 | 2.88 | 2.77 | 0.663 | 6-gon | 3.47 |
| | Nb8 | 2.88 | 2.77 | 0.663 | 6-gon | 3.47 |
| | As2 | 3.06 | 2.63 | 0.192 | 4-gon | 2.36 |
| | Nb6 | 3.15 | 2.79 | 0.247 | 6-gon | 2.33 |
| | Nb6 | 3.15 | 2.79 | 0.247 | 6-gon | 2.33 |
| | Nb7 | 3.38 | 2.81 | 0.110 | 6-gon | 1.73 |
| | Nb7 | 3.38 | 2.81 | 0.110 | 6-gon | 1.73 |
| | Nb1 | 3.41 | 2.82 | 0.102 | 4-gon | 0.97 |
| | Nb10 | 3.52 | 2.84 | 0.071 | 4-gon | 0.79 |
| | Nb2 | 3.59 | 2.85 | 0.058 | 5-gon | 0.53 |
| | Nb2 | 3.59 | 2.85 | 0.058 | 5-gon | 0.53 |
| | Nb5 | 3.72 | 2.86 | 0.037 | 4-gon | 0.40 |
| Sum of Pauling bond orders (i.e. electron population on the crystal site): 5.369 | | | | | | |
| Volume of the Dirichlet domain: 18.66 Å$^3$ | | | | | | |

| Central atom | Neighbour atom | Distance [Å] | D(1) [Å] | Pauling bond order | Created polygon of the Dirichlet domain | Polygon's area [Å$^2$] |
|---|---|---|---|---|---|---|
| M3<br>$y_{Nb}$ = 0.32<br>r = 1.408 | As1 | 2.62 | 2.62 | 0.977 | 6-gon | 5.10 |
| | As5 | 2.74 | 2.62 | 0.636 | 7-gon | 4.84 |
| | As5 | 2.74 | 2.62 | 0.636 | 7-gon | 4.84 |
| | As3 | 2.81 | 2.62 | 0.471 | 4-gon | 3.39 |
| | As2 | 2.85 | 2.62 | 0.409 | 5-gon | 3.33 |
| | Nb7 | 3.03 | 2.79 | 0.406 | 6-gon | 3.02 |
| | Nb7 | 3.03 | 2.79 | 0.406 | 6-gon | 3.02 |
| | Nb5 | 3.31 | 2.85 | 0.167 | 6-gon | 2.06 |
| | Nb5 | 3.31 | 2.85 | 0.167 | 6-gon | 2.06 |
| | Nb9 | 3.39 | 2.82 | 0.114 | 5-gon | 1.74 |
| | Nb9 | 3.39 | 2.82 | 0.114 | 5-gon | 1.74 |
| | Nb1 | 3.47 | 2.80 | 0.078 | 3-gon | 0.42 |
| | Nb3 | 3.59 | 2.82 | 0.051 | 4-gon | 1.44 |
| | Nb3 | 3.59 | 2.82 | 0.051 | 4-gon | 1.44 |
| | Nb4 | 3.67 | 2.77 | 0.032 | 4-gon | 0.53 |
| Sum of Pauling bond orders (i.e. electron population on the crystal site): 4.717 | | | | | | |
| Volume of the Dirichlet domain: 19.39 Å$^3$ | | | | | | |

| Central atom | Neighbour atom | Distance [Å] | D(1) [Å] | Pauling bond order | Created polygon of the Dirichlet domain | Polygon's area [Å$^2$] |
|---|---|---|---|---|---|---|
| M4<br>$y_{Nb}$ = 0.74<br>r = 1.366 | As4 | 2.59 | 2.58 | 0.940 | 5-gon | 4.91 |
| | As5 | 2.64 | 2.58 | 0.782 | 6-gon | 4.21 |
| | As5 | 2.64 | 2.58 | 0.782 | 6-gon | 4.21 |
| | As3 | 2.72 | 2.58 | 0.575 | 7-gon | 4.27 |
| | As3 | 2.72 | 2.58 | 0.575 | 7-gon | 4.27 |
| | Nb6 | 2.85 | 2.73 | 0.633 | 6-gon | 3.05 |
| | Nb6 | 2.85 | 2.73 | 0.633 | 6-gon | 3.05 |
| | Nb1 | 3.21 | 2.76 | 0.177 | 4-gon | 1.24 |
| | Nb5 | 3.25 | 2.81 | 0.183 | 6-gon | 2.14 |
| | Nb5 | 3.25 | 2.81 | 0.183 | 6-gon | 2.14 |
| | Nb5 | 3.42 | 2.81 | 0.096 | 4-gon | 0.97 |
| | Nb7 | 3.43 | 2.75 | 0.074 | 3-gon | 0.49 |
| | Nb4 | 3.59 | 2.73 | 0.037 | 4-gon | 0.57 |
| | Nb4 | 3.59 | 2.73 | 0.037 | 4-gon | 0.57 |
| | Nb3 | 3.67 | 2.77 | 0.032 | 4-gon | 0.53 |
| Sum of Pauling bond orders (i.e. electron population on the crystal site): 5.744 | | | | | | |
| Volume of the Dirichlet domain: 17.41 Å$^3$ | | | | | | |

| Central atom | Neighbour atom | Distance [Å] | D(1) [Å] | Pauling bond order | Created polygon of the Dirichlet domain | Polygon's area [Å$^2$] |
|---|---|---|---|---|---|---|
| M5<br>$y_{Nb}$ = 0.00<br>r = 1.440 | As3 | 2.65 | 2.65 | 0.996 | 7-gon | 4.55 |
| | As3 | 2.65 | 2.65 | 0.996 | 7-gon | 4.55 |
| | As4 | 2.67 | 2.65 | 0.912 | 7-gon | 4.77 |
| | As4 | 2.67 | 2.65 | 0.912 | 7-gon | 4.77 |
| | As5 | 2.84 | 2.65 | 0.488 | 4-gon | 3.74 |
| | Nb6 | 3.20 | 2.80 | 0.219 | 5-gon | 2.06 |
| | Nb6 | 3.20 | 2.80 | 0.219 | 5-gon | 2.06 |
| | Nb4 | 3.25 | 2.81 | 0.183 | 6-gon | 2.14 |
| | Nb4 | 3.25 | 2.81 | 0.183 | 6-gon | 2.14 |
| | Nb3 | 3.31 | 2.85 | 0.167 | 6-gon | 2.06 |
| | Nb3 | 3.31 | 2.85 | 0.167 | 6-gon | 2.06 |
| | Nb4 | 3.42 | 2.81 | 0.096 | 4-gon | 0.97 |
| | Nb7 | 3.53 | 2.82 | 0.066 | 4-gon | 0.76 |
| | Nb5 | 3.59 | 2.88 | 0.066 | 4-gon | 0.64 |
| | Nb5 | 3.59 | 2.88 | 0.066 | 4-gon | 0.64 |
| | Nb2 | 3.72 | 2.86 | 0.037 | 4-gon | 0.40 |
| Sum of Pauling bond orders (i.e. electron population on the crystal site): 5.773 | | | | | | |
| Volume of the Dirichlet domain: 18.87 Å$^3$ | | | | | | |

| Central atom | Neighbour atom | Distance [Å] | D(1) [Å] | Pauling bond order | Created polygon of the Dirichlet domain | Polygon's area [Å$^2$] |
|---|---|---|---|---|---|---|
| M6<br>$y_{Nb}$ = 0.76<br>r = 1.364 | As4 | 2.66 | 2.57 | 0.722 | 5-gon | 4.01 |
| | As5 | 2.69 | 2.57 | 0.636 | 4-gon | 2.82 |
| | As6 | 2.76 | 2.57 | 0.486 | 4-gon | 3.08 |
| | As3 | 2.77 | 2.57 | 0.464 | 5-gon | 3.07 |
| | Nb4 | 2.85 | 2.73 | 0.633 | 6-gon | 3.05 |
| | Nb4 | 2.85 | 2.73 | 0.633 | 6-gon | 3.05 |
| | Nb1 | 2.89 | 2.76 | 0.603 | 6-gon | 2.88 |
| | Nb1 | 2.89 | 2.76 | 0.603 | 6-gon | 2.88 |
| | Nb2 | 3.15 | 2.79 | 0.247 | 6-gon | 2.33 |
| | Nb2 | 3.15 | 2.79 | 0.247 | 6-gon | 2.33 |
| | Nb5 | 3.20 | 2.80 | 0.219 | 5-gon | 2.06 |
| | Nb5 | 3.20 | 2.80 | 0.219 | 5-gon | 2.06 |
| | Nb6 | 3.59 | 2.73 | 0.037 | 4-gon | 1.19 |
| | Nb6 | 3.59 | 2.73 | 0.037 | 4-gon | 1.19 |
| Sum of Pauling bond orders (i.e. electron population on the crystal site): 5.785 | | | | | | |
| Volume of the Dirichlet domain: 17.62 Å$^3$ | | | | | | |

| Central atom | Neighbour atom | Distance [Å] | D(1) [Å] | Pauling bond order | Created polygon of the Dirichlet domain | Polygon's area [Å$^2$] |
|---|---|---|---|---|---|---|
| M7<br>$y_{Nb}$ = 0.58<br>r = 1.382 | As4 | 2.62 | 2.59 | 0.891 | 5-gon | 5.17 |
| | As2 | 2.66 | 2.59 | 0.785 | 6-gon | 4.45 |
| | As2 | 2.66 | 2.59 | 0.785 | 6-gon | 4.45 |
| | As3 | 2.69 | 2.59 | 0.694 | 7-gon | 4.65 |
| | As3 | 2.69 | 2.59 | 0.694 | 7-gon | 4.65 |
| | Nb3 | 3.03 | 2.79 | 0.406 | 6-gon | 3.02 |
| | Nb3 | 3.03 | 2.79 | 0.406 | 6-gon | 3.02 |
| | Nb8 | 3.24 | 2.73 | 0.142 | 4-gon | 1.56 |
| | Nb2 | 3.38 | 2.81 | 0.110 | 6-gon | 1.73 |
| | Nb2 | 3.38 | 2.81 | 0.110 | 6-gon | 1.73 |
| | Nb4 | 3.43 | 2.75 | 0.074 | 3-gon | 0.49 |
| | Nb5 | 3.53 | 2.82 | 0.066 | 4-gon | 0.76 |
| | Nb9 | 3.56 | 2.80 | 0.055 | 4-gon | 0.76 |
| | Nb7 | 3.59 | 2.76 | 0.042 | 4-gon | 0.66 |
| | Nb7 | 3.59 | 2.76 | 0.042 | 4-gon | 0.66 |
| Sum of Pauling bond orders (i.e. electron population on the crystal site): 5.303 | | | | | | |
| Volume of the Dirichlet domain: 18.18 Å$^3$ | | | | | | |

| Central atom | Neighbour atom | Distance [Å] | D(1) [Å] | Pauling bond order | Created polygon of the Dirichlet domain | Polygon's area [Å$^2$] |
|---|---|---|---|---|---|---|
| M8<br>$y_{Nb}$ = 0.92<br>r = 1.348 | As1 | 2.64 | 2.56 | 0.744 | 5-gon | 3.91 |
| | As2 | 2.64 | 2.56 | 0.722 | 6-gon | 4.13 |
| | As2 | 2.64 | 2.56 | 0.722 | 6-gon | 4.13 |
| | As6 | 2.75 | 2.56 | 0.479 | 5-gon | 3.27 |
| | Nb2 | 2.88 | 2.77 | 0.663 | 6-gon | 3.47 |
| | Nb2 | 2.88 | 2.77 | 0.663 | 6-gon | 3.47 |
| | Nb9 | 3.04 | 2.76 | 0.352 | 6-gon | 2.81 |
| | Nb9 | 3.04 | 2.76 | 0.352 | 6-gon | 2.81 |
| | Nb10 | 3.20 | 2.76 | 0.184 | 5-gon | 2.16 |
| | Nb10 | 3.20 | 2.76 | 0.184 | 5-gon | 2.16 |
| | Nb7 | 3.24 | 2.73 | 0.142 | 4-gon | 1.56 |
| | Nb9 | 3.43 | 2.76 | 0.079 | 4-gon | 1.03 |
| | Nb8 | 3.59 | 2.70 | 0.032 | 4-gon | 0.85 |
| | Nb8 | 3.59 | 2.70 | 0.032 | 4-gon | 0.85 |
| Sum of Pauling bond orders (i.e. electron population on the crystal site): 5.350 | | | | | | |
| Volume of the Dirichlet domain: 17.78 Å$^3$ | | | | | | |

| Central atom | Neighbour atom | Distance [Å] | D(1) [Å] | Pauling bond order | Created polygon of the Dirichlet domain | Polygon's area [Å$^2$] |
|---|---|---|---|---|---|---|
| M9<br>$y_{Nb}$ = 0.24<br>r = 1.416 | As2 | 2.70 | 2.63 | 0.764 | 7-gon | 4.53 |
| | As2 | 2.70 | 2.63 | 0.764 | 7-gon | 4.53 |
| | As1 | 2.70 | 2.63 | 0.741 | 7-gon | 4.61 |
| | As1 | 2.70 | 2.63 | 0.741 | 7-gon | 4.61 |
| | As2 | 2.91 | 2.63 | 0.340 | 4-gon | 2.96 |
| | Nb8 | 3.04 | 2.76 | 0.352 | 6-gon | 2.81 |
| | Nb8 | 3.04 | 2.76 | 0.352 | 6-gon | 2.81 |
| | Nb9 | 3.25 | 2.83 | 0.205 | 6-gon | 2.26 |
| | Nb9 | 3.25 | 2.83 | 0.205 | 6-gon | 2.26 |
| | Nb3 | 3.39 | 2.82 | 0.114 | 5-gon | 1.74 |
| | Nb3 | 3.39 | 2.82 | 0.114 | 5-gon | 1.74 |
| | Nb8 | 3.43 | 2.76 | 0.079 | 4-gon | 1.03 |
| | Nb7 | 3.56 | 2.80 | 0.055 | 4-gon | 0.76 |
| | Nb9 | 3.59 | 2.83 | 0.055 | 4-gon | 0.62 |
| | Nb9 | 3.59 | 2.83 | 0.055 | 4-gon | 0.62 |
| | Nb10 | 3.69 | 2.83 | 0.036 | 4-gon | 0.44 |
| Sum of Pauling bond orders (i.e. electron population on the crystal site): 4.973 | | | | | | |
| Volume of the Dirichlet domain: 18.96 Å$^3$ | | | | | | |

| Central atom | Neighbour atom | Distance [Å] | D(1) [Å] | Pauling bond order | Created polygon of the Dirichlet domain | Polygon's area [Å$^2$] |
|---|---|---|---|---|---|---|
| M10<br>$y_{Nb}$ = 0.27<br>r = 1.413 | As1 | 2.74 | 2.62 | 0.646 | 7-gon | 4.62 |
| | As1 | 2.74 | 2.62 | 0.646 | 7-gon | 4.62 |
| | As6 | 2.75 | 2.62 | 0.626 | 7-gon | 4.29 |
| | As6 | 2.75 | 2.62 | 0.626 | 7-gon | 4.29 |
| | As6 | 2.98 | 2.62 | 0.259 | 4-gon | 3.15 |
| | Nb10 | 3.16 | 2.83 | 0.275 | 6-gon | 2.96 |
| | Nb10 | 3.16 | 2.83 | 0.275 | 6-gon | 2.96 |
| | Nb8 | 3.20 | 2.76 | 0.184 | 5-gon | 2.16 |
| | Nb8 | 3.20 | 2.76 | 0.184 | 5-gon | 2.16 |
| | Nb1 | 3.32 | 2.81 | 0.139 | 6-gon | 2.07 |
| | Nb1 | 3.32 | 2.81 | 0.139 | 6-gon | 2.07 |
| | Nb2 | 3.52 | 2.84 | 0.071 | 4-gon | 0.79 |
| | Nb1 | 3.57 | 2.81 | 0.053 | 4-gon | 0.83 |
| | Nb10 | 3.59 | 2.83 | 0.053 | 4-gon | 0.83 |
| | Nb10 | 3.59 | 2.83 | 0.053 | 4-gon | 0.83 |
| | Nb9 | 3.69 | 2.83 | 0.036 | 4-gon | 0.44 |
| Sum of Pauling bond orders (i.e. electron population on the crystal site): 4.267 | | | | | | |
| Volume of the Dirichlet domain: 19.66 Å$^3$ | | | | | | |

## E.2. Sample S23, $(Hf,Nb)_5As_3$ phase

| Central atom | Neighbour atom | Distance [Å] | D(1) [Å] | Pauling bond order | Created polygon of the Dirichlet domain | Polygon's area [Å$^2$] |
|---|---|---|---|---|---|---|
| M1<br>$y_{Nb} = 0.16$<br>r = 1.424 | As1 | 2.67 | 2.63 | 0.881 | 5-gon | 5.14 |
| | As6 | 2.67 | 2.63 | 0.868 | 6-gon | 4.51 |
| | As6 | 2.67 | 2.63 | 0.868 | 6-gon | 4.51 |
| | As5 | 2.80 | 2.63 | 0.533 | 7-gon | 4.27 |
| | As5 | 2.80 | 2.63 | 0.533 | 7-gon | 4.27 |
| | Nb6 | 2.95 | 2.80 | 0.571 | 6-gon | 3.03 |
| | Nb6 | 2.95 | 2.80 | 0.571 | 6-gon | 3.03 |
| | Nb10 | 3.33 | 2.85 | 0.155 | 6-gon | 2.25 |
| | Nb10 | 3.33 | 2.85 | 0.155 | 6-gon | 2.25 |
| | Nb4 | 3.37 | 2.84 | 0.131 | 4-gon | 1.11 |
| | Nb2 | 3.42 | 2.86 | 0.119 | 4-gon | 1.05 |
| | Nb3 | 3.53 | 2.86 | 0.079 | 3-gon | 0.42 |
| | Nb10 | 3.57 | 2.85 | 0.063 | 4-gon | 0.89 |
| | Nb1 | 3.62 | 2.85 | 0.051 | 4-gon | 0.75 |
| | Nb1 | 3.62 | 2.85 | 0.051 | 4-gon | 0.75 |
| Sum of Pauling bond orders (i.e. electron population on the crystal site): 5.629 | | | | | | |
| Volume of the Dirichlet domain: 18.65 Å$^3$ | | | | | | |

| Central atom | Neighbour atom | Distance [Å] | D(1) [Å] | Pauling bond order | Created polygon of the Dirichlet domain | Polygon's area [Å$^2$] |
|---|---|---|---|---|---|---|
| M2<br>$y_{Nb} = 0.00$<br>r = 1.440 | As6 | 2.76 | 2.65 | 0.666 | 6-gon | 3.95 |
| | As6 | 2.76 | 2.65 | 0.666 | 6-gon | 3.95 |
| | As4 | 2.77 | 2.65 | 0.626 | 6-gon | 4.74 |
| | As4 | 2.77 | 2.65 | 0.626 | 6-gon | 4.74 |
| | Nb8 | 2.96 | 2.81 | 0.560 | 6-gon | 3.44 |
| | Nb8 | 2.96 | 2.81 | 0.560 | 6-gon | 3.44 |
| | As2 | 3.09 | 2.65 | 0.186 | 4-gon | 2.56 |
| | Nb6 | 3.14 | 2.82 | 0.286 | 6-gon | 2.52 |
| | Nb6 | 3.14 | 2.82 | 0.286 | 6-gon | 2.52 |
| | Nb1 | 3.42 | 2.86 | 0.119 | 4-gon | 1.05 |
| | Nb7 | 3.44 | 2.88 | 0.116 | 6-gon | 1.75 |
| | Nb7 | 3.44 | 2.88 | 0.116 | 6-gon | 1.75 |
| | Nb10 | 3.59 | 2.86 | 0.063 | 4-gon | 0.75 |
| | Nb2 | 3.62 | 2.88 | 0.058 | 5-gon | 0.63 |
| | Nb2 | 3.62 | 2.88 | 0.058 | 5-gon | 0.63 |
| | Nb5 | 3.75 | 2.88 | 0.035 | 4-gon | 0.39 |
| Sum of Pauling bond orders (i.e. electron population on the crystal site): 5.027 | | | | | | |
| Volume of the Dirichlet domain: 19.43 Å$^3$ | | | | | | |

| Central atom | Neighbour atom | Distance [Å] | D(1) [Å] | Pauling bond order | Created polygon of the Dirichlet domain | Polygon's area [Å$^2$] |
|---|---|---|---|---|---|---|
| M3<br>$y_{Nb}$ = 0.00<br>r = 1.44 | As1 | 2.63 | 2.65 | 1.080 | 6-gon | 5.50 |
| | As5 | 2.72 | 2.65 | 0.767 | 7-gon | 5.09 |
| | As5 | 2.72 | 2.65 | 0.767 | 7-gon | 5.09 |
| | As3 | 2.87 | 2.65 | 0.427 | 4-gon | 3.42 |
| | As2 | 2.97 | 2.65 | 0.299 | 5-gon | 3.28 |
| | Nb7 | 3.10 | 2.88 | 0.432 | 6-gon | 3.10 |
| | Nb7 | 3.10 | 2.88 | 0.432 | 6-gon | 3.10 |
| | Nb5 | 3.33 | 2.88 | 0.180 | 6-gon | 2.11 |
| | Nb5 | 3.33 | 2.88 | 0.180 | 6-gon | 2.11 |
| | Nb9 | 3.49 | 2.88 | 0.095 | 5-gon | 1.66 |
| | Nb9 | 3.49 | 2.88 | 0.095 | 5-gon | 1.66 |
| | Nb1 | 3.53 | 2.86 | 0.079 | 3-gon | 0.42 |
| | Nb3 | 3.62 | 2.88 | 0.058 | 4-gon | 1.52 |
| | Nb3 | 3.62 | 2.88 | 0.058 | 4-gon | 1.52 |
| | Nb4 | 3.72 | 2.86 | 0.037 | 4-gon | 0.48 |
| Sum of Pauling bond orders (i.e. electron population on the crystal site): 4.985 | | | | | | |
| Volume of the Dirichlet domain: 20.13 Å$^3$ | | | | | | |

| Central atom | Neighbour atom | Distance [Å] | D(1) [Å] | Pauling bond order | Created polygon of the Dirichlet domain | Polygon's area [Å$^2$] |
|---|---|---|---|---|---|---|
| M4<br>$y_{Nb}$ = 0.20<br>r = 1.420 | As4 | 2.59 | 2.63 | 1.170 | 5-gon | 5.13 |
| | As5 | 2.70 | 2.63 | 0.767 | 6-gon | 4.34 |
| | As5 | 2.70 | 2.63 | 0.767 | 6-gon | 4.34 |
| | As3 | 2.71 | 2.63 | 0.741 | 7-gon | 4.52 |
| | As3 | 2.71 | 2.63 | 0.741 | 7-gon | 4.52 |
| | Nb6 | 2.93 | 2.80 | 0.593 | 6-gon | 3.05 |
| | Nb6 | 2.93 | 2.80 | 0.593 | 6-gon | 3.05 |
| | Nb5 | 3.27 | 2.86 | 0.206 | 6-gon | 2.14 |
| | Nb5 | 3.27 | 2.86 | 0.206 | 6-gon | 2.14 |
| | Nb1 | 3.37 | 2.84 | 0.131 | 4-gon | 1.11 |
| | Nb7 | 3.40 | 2.86 | 0.125 | 3-gon | 0.64 |
| | Nb5 | 3.46 | 2.86 | 0.099 | 4-gon | 0.93 |
| | Nb4 | 3.62 | 2.84 | 0.050 | 4-gon | 0.60 |
| | Nb4 | 3.62 | 2.84 | 0.050 | 4-gon | 0.60 |
| | Nb3 | 3.72 | 2.86 | 0.037 | 4-gon | 0.48 |
| Sum of Pauling bond orders (i.e. electron population on the crystal site): 6.278 | | | | | | |
| Volume of the Dirichlet domain: 18.06 Å$^3$ | | | | | | |

| Central atom | Neighbour atom | Distance [Å] | D(1) [Å] | Pauling bond order | Created polygon of the Dirichlet domain | Polygon's area [Å$^2$] |
|---|---|---|---|---|---|---|
| M5<br>$y_{Nb}$ = 0.00<br>r = 1.44 | As3 | 2.67 | 2.65 | 0.916 | 7-gon | 4.67 |
| | As3 | 2.67 | 2.65 | 0.916 | 7-gon | 4.67 |
| | As4 | 2.69 | 2.65 | 0.848 | 7-gon | 4.85 |
| | As4 | 2.69 | 2.65 | 0.848 | 7-gon | 4.85 |
| | As5 | 2.81 | 2.65 | 0.539 | 4-gon | 3.96 |
| | Nb6 | 3.25 | 2.82 | 0.191 | 5-gon | 2.03 |
| | Nb6 | 3.25 | 2.82 | 0.191 | 5-gon | 2.03 |
| | Nb4 | 3.27 | 2.86 | 0.206 | 6-gon | 2.14 |
| | Nb4 | 3.27 | 2.86 | 0.206 | 6-gon | 2.14 |
| | Nb3 | 3.33 | 2.88 | 0.180 | 6-gon | 2.11 |
| | Nb3 | 3.33 | 2.88 | 0.180 | 6-gon | 2.11 |
| | Nb4 | 3.46 | 2.86 | 0.099 | 4-gon | 0.93 |
| | Nb7 | 3.59 | 2.88 | 0.065 | 4-gon | 0.76 |
| | Nb5 | 3.62 | 2.88 | 0.058 | 4-gon | 0.65 |
| | Nb5 | 3.62 | 2.88 | 0.058 | 4-gon | 0.65 |
| | Nb2 | 3.75 | 2.88 | 0.035 | 4-gon | 0.39 |
| Sum of Pauling bond orders (i.e. electron population on the crystal site): 5.533 | | | | | | |
| Volume of the Dirichlet domain: 19.27 Å$^3$ | | | | | | |

| Central atom | Neighbour atom | Distance [Å] | D(1) [Å] | Pauling bond order | Created polygon of the Dirichlet domain | Polygon's area [Å$^2$] |
|---|---|---|---|---|---|---|
| M6<br>$y_{Nb}$ = 0.63<br>r = 1.377 | As4 | 2.67 | 2.59 | 0.741 | 5-gon | 4.11 |
| | As5 | 2.78 | 2.59 | 0.473 | 4-gon | 2.93 |
| | As3 | 2.79 | 2.59 | 0.455 | 5-gon | 3.22 |
| | As6 | 2.83 | 2.59 | 0.400 | 4-gon | 3.01 |
| | Nb4 | 2.93 | 2.80 | 0.593 | 6-gon | 3.05 |
| | Nb4 | 2.93 | 2.80 | 0.593 | 6-gon | 3.05 |
| | Nb1 | 2.95 | 2.80 | 0.571 | 6-gon | 3.03 |
| | Nb1 | 2.95 | 2.80 | 0.571 | 6-gon | 3.03 |
| | Nb2 | 3.14 | 2.82 | 0.286 | 6-gon | 2.52 |
| | Nb2 | 3.14 | 2.82 | 0.286 | 6-gon | 2.52 |
| | Nb5 | 3.25 | 2.82 | 0.191 | 5-gon | 2.03 |
| | Nb5 | 3.25 | 2.82 | 0.191 | 5-gon | 2.03 |
| | Nb6 | 3.62 | 2.75 | 0.036 | 4-gon | 1.30 |
| | Nb6 | 3.62 | 2.75 | 0.036 | 4-gon | 1.30 |
| Sum of Pauling bond orders (i.e. electron population on the crystal site): 5.423 | | | | | | |
| Volume of the Dirichlet domain: 18.46 Å$^3$ | | | | | | |

| Central atom | Neighbour atom | Distance [Å] | D(1) [Å] | Pauling bond order | Created polygon of the Dirichlet domain | Polygon's area [Å$^2$] |
|---|---|---|---|---|---|---|
| M7<br>$y_{Nb}$ = 0.02<br>r = 1.438 | As4 | 2.67 | 2.65 | 0.937 | 5-gon | 5.34 |
| | As2 | 2.67 | 2.65 | 0.912 | 6-gon | 4.75 |
| | As2 | 2.67 | 2.65 | 0.912 | 6-gon | 4.75 |
| | As3 | 2.75 | 2.65 | 0.687 | 7-gon | 4.69 |
| | As3 | 2.75 | 2.65 | 0.687 | 7-gon | 4.69 |
| | Nb3 | 3.10 | 2.88 | 0.432 | 6-gon | 3.10 |
| | Nb3 | 3.10 | 2.88 | 0.432 | 6-gon | 3.10 |
| | Nb8 | 3.35 | 2.80 | 0.125 | 4-gon | 1.42 |
| | Nb4 | 3.40 | 2.86 | 0.125 | 3-gon | 0.64 |
| | Nb2 | 3.44 | 2.88 | 0.116 | 6-gon | 1.75 |
| | Nb2 | 3.44 | 2.88 | 0.116 | 6-gon | 1.75 |
| | Nb5 | 3.59 | 2.88 | 0.065 | 4-gon | 0.76 |
| | Nb9 | 3.61 | 2.87 | 0.060 | 4-gon | 0.81 |
| | Nb7 | 3.62 | 2.88 | 0.057 | 4-gon | 0.76 |
| | Nb7 | 3.62 | 2.88 | 0.057 | 4-gon | 0.76 |
| Sum of Pauling bond orders (i.e. electron population on the crystal site): 5.718 | | | | | | |
| Volume of the Dirichlet domain: 19.11 Å$^3$ | | | | | | |

| Central atom | Neighbour atom | Distance [Å] | D(1) [Å] | Pauling bond order | Created polygon of the Dirichlet domain | Polygon's area [Å$^2$] |
|---|---|---|---|---|---|---|
| M8<br>$y_{Nb}$ = 0.75<br>r = 1.365 | As1 | 2.64 | 2.58 | 0.770 | 4-gon | 4.01 |
| | As2 | 2.69 | 2.58 | 0.646 | 6-gon | 4.23 |
| | As2 | 2.69 | 2.58 | 0.646 | 6-gon | 4.23 |
| | As6 | 2.77 | 2.58 | 0.470 | 4-gon | 3.40 |
| | Nb2 | 2.96 | 2.81 | 0.560 | 6-gon | 3.44 |
| | Nb2 | 2.96 | 2.81 | 0.560 | 6-gon | 3.44 |
| | Nb9 | 3.05 | 2.80 | 0.380 | 6-gon | 2.92 |
| | Nb9 | 3.05 | 2.80 | 0.380 | 6-gon | 2.92 |
| | Nb10 | 3.21 | 2.79 | 0.202 | 6-gon | 2.30 |
| | Nb10 | 3.21 | 2.79 | 0.202 | 6-gon | 2.30 |
| | Nb7 | 3.35 | 2.80 | 0.125 | 4-gon | 1.42 |
| | Nb9 | 3.46 | 2.80 | 0.081 | 4-gon | 1.09 |
| | Nb8 | 3.62 | 2.73 | 0.033 | 4-gon | 0.92 |
| | Nb8 | 3.62 | 2.73 | 0.033 | 4-gon | 0.92 |
| Sum of Pauling bond orders (i.e. electron population on the crystal site): 5.087 | | | | | | |
| Volume of the Dirichlet domain: 18.47 Å$^3$ | | | | | | |

| Central atom | Neighbour atom | Distance [Å] | D(1) [Å] | Pauling bond order | Created polygon of the Dirichlet domain | Polygon's area [Å$^2$] |
|---|---|---|---|---|---|---|
| M9<br>$y_{Nb}$ = 0.04<br>r = 1.436 | As1 | 2.74 | 2.65 | 0.697 | 7-gon | 4.71 |
| | As1 | 2.74 | 2.65 | 0.697 | 7-gon | 4.71 |
| | As2 | 2.74 | 2.65 | 0.687 | 7-gon | 4.61 |
| | As2 | 2.74 | 2.65 | 0.687 | 7-gon | 4.61 |
| | As2 | 2.96 | 2.65 | 0.299 | 4-gon | 2.89 |
| | Nb8 | 3.05 | 2.80 | 0.380 | 6-gon | 2.92 |
| | Nb8 | 3.05 | 2.80 | 0.380 | 6-gon | 2.92 |
| | Nb9 | 3.24 | 2.87 | 0.242 | 6-gon | 2.47 |
| | Nb9 | 3.24 | 2.87 | 0.242 | 6-gon | 2.47 |
| | Nb8 | 3.46 | 2.80 | 0.081 | 4-gon | 1.09 |
| | Nb3 | 3.49 | 2.88 | 0.095 | 5-gon | 1.66 |
| | Nb3 | 3.49 | 2.88 | 0.095 | 5-gon | 1.66 |
| | Nb7 | 3.61 | 2.87 | 0.060 | 4-gon | 0.81 |
| | Nb9 | 3.62 | 2.87 | 0.056 | 4-gon | 0.66 |
| | Nb9 | 3.62 | 2.87 | 0.056 | 4-gon | 0.66 |
| | Nb10 | 3.75 | 2.86 | 0.033 | 4-gon | 0.42 |
| Sum of Pauling bond orders (i.e. electron population on the crystal site): 4.787 | | | | | | |
| Volume of the Dirichlet domain: 19.67 Å$^3$ | | | | | | |

| Central atom | Neighbour atom | Distance [Å] | D(1) [Å] | Pauling bond order | Created polygon of the Dirichlet domain | Polygon's area [Å$^2$] |
|---|---|---|---|---|---|---|
| M10<br>$y_{Nb}$ = 0.16<br>r = 1.424 | As6 | 2.75 | 2.63 | 0.646 | 6-gon | 4.46 |
| | As6 | 2.75 | 2.63 | 0.646 | 6-gon | 4.46 |
| | As1 | 2.79 | 2.63 | 0.558 | 6-gon | 4.61 |
| | As1 | 2.79 | 2.63 | 0.558 | 6-gon | 4.61 |
| | As6 | 3.02 | 2.63 | 0.228 | 4-gon | 3.16 |
| | Nb8 | 3.21 | 2.79 | 0.202 | 6-gon | 2.30 |
| | Nb8 | 3.21 | 2.79 | 0.202 | 6-gon | 2.30 |
| | Nb10 | 3.24 | 2.85 | 0.222 | 6-gon | 2.84 |
| | Nb10 | 3.24 | 2.85 | 0.222 | 6-gon | 2.84 |
| | Nb1 | 3.33 | 2.85 | 0.155 | 6-gon | 2.25 |
| | Nb1 | 3.33 | 2.85 | 0.155 | 6-gon | 2.25 |
| | Nb1 | 3.57 | 2.85 | 0.063 | 4-gon | 0.89 |
| | Nb2 | 3.59 | 2.86 | 0.063 | 4-gon | 0.75 |
| | Nb10 | 3.62 | 2.85 | 0.051 | 5-gon | 0.88 |
| | Nb10 | 3.62 | 2.85 | 0.051 | 5-gon | 0.88 |
| | Nb9 | 3.75 | 2.86 | 0.033 | 4-gon | 0.42 |
| Sum of Pauling bond orders (i.e. electron population on the crystal site): 4.054 | | | | | | |
| Volume of the Dirichlet domain: 20.29 Å$^3$ | | | | | | |

## E.3. Sample S45, $Hf_{4-x}Nb_{3+x}As_3$ phase

| Central atom | Neighbour atom | Distance [Å] | D(1) [Å] | Pauling bond order | Created polygon of the Dirichlet domain | Polygon's area [Å$^2$] |
|---|---|---|---|---|---|---|
| M1<br>$y_{Nb}$ = 0.83<br>r = 1.357 | As2 | 2.63 | 2.57 | 0.773 | 6-gon | 4.22 |
| | As2 | 2.63 | 2.57 | 0.773 | 6-gon | 4.22 |
| | As3 | 2.67 | 2.57 | 0.666 | 5-gon | 3.99 |
| | As1 | 2.75 | 2.57 | 0.499 | 5-gon | 3.17 |
| | Nb4 | 2.84 | 2.72 | 0.619 | 6-gon | 3.19 |
| | Nb4 | 2.84 | 2.72 | 0.619 | 6-gon | 3.19 |
| | Nb7 | 3.01 | 2.80 | 0.438 | 6-gon | 3.33 |
| | Nb7 | 3.01 | 2.80 | 0.438 | 6-gon | 3.33 |
| | Nb6 | 3.24 | 2.80 | 0.185 | 5-gon | 2.12 |
| | Nb6 | 3.24 | 2.80 | 0.185 | 5-gon | 2.12 |
| | Nb3 | 3.39 | 2.80 | 0.102 | 4-gon | 1.02 |
| | Nb7 | 3.45 | 2.80 | 0.081 | 4-gon | 1.19 |
| | Nb1 | 3.59 | 2.71 | 0.035 | 4-gon | 0.85 |
| | Nb1 | 3.59 | 2.71 | 0.035 | 4-gon | 0.85 |
| Sum of Pauling bond orders (i.e. electron population on the crystal site): 5.450 | | | | | | |
| Volume of the Dirichlet domain: 17.86 Å$^3$ | | | | | | |

| Central atom | Neighbour atom | Distance [Å] | D(1) [Å] | Pauling bond order | Created polygon of the Dirichlet domain | Polygon's area [Å$^2$] |
|---|---|---|---|---|---|---|
| M2<br>$y_{Nb}$ = 0.72<br>r = 1.368 | As3 | 2.62 | 2.58 | 0.854 | 6-gon | 4.37 |
| | As3 | 2.62 | 2.58 | 0.854 | 6-gon | 4.37 |
| | As1 | 2.68 | 2.58 | 0.666 | 4-gon | 3.88 |
| | Nb5 | 2.87 | 2.73 | 0.603 | 6-gon | 3.67 |
| | Nb5 | 2.87 | 2.73 | 0.603 | 6-gon | 3.67 |
| | Nb6 | 3.10 | 2.81 | 0.321 | 6-gon | 2.91 |
| | Nb6 | 3.10 | 2.81 | 0.321 | 6-gon | 2.91 |
| | Nb4 | 3.16 | 2.73 | 0.191 | 4-gon | 2.43 |
| | Nb3 | 3.17 | 2.81 | 0.245 | 6-gon | 2.87 |
| | Nb3 | 3.17 | 2.81 | 0.245 | 6-gon | 2.87 |
| | Nb6 | 3.43 | 2.81 | 0.092 | 4-gon | 1.20 |
| | Nb7 | 3.49 | 2.81 | 0.074 | 4-gon | 0.89 |
| | Nb2 | 3.59 | 2.74 | 0.038 | 4-gon | 0.87 |
| | Nb2 | 3.59 | 2.74 | 0.038 | 4-gon | 0.87 |
| Sum of Pauling bond orders (i.e. electron population on the crystal site): 5.146 | | | | | | |
| Volume of the Dirichlet domain: 18.63 Å$^3$ | | | | | | |

| Central atom | Neighbour atom | Distance [Å] | D(1) [Å] | Pauling bond order | Created polygon of the Dirichlet domain | Polygon's area [Å$^2$] |
|---|---|---|---|---|---|---|
| M3 $y_{Nb}$ = 0.00 r = 1.440 | As1 | 2.73 | 2.65 | 0.733 | 6-gon | 4.16 |
| | As1 | 2.73 | 2.65 | 0.733 | 6-gon | 4.16 |
| | As2 | 2.80 | 2.65 | 0.569 | 6-gon | 3.96 |
| | As2 | 2.80 | 2.65 | 0.569 | 6-gon | 3.96 |
| | Nb4 | 3.10 | 2.80 | 0.320 | 6-gon | 3.08 |
| | Nb4 | 3.10 | 2.80 | 0.320 | 6-gon | 3.08 |
| | Nb5 | 3.16 | 2.81 | 0.254 | 6-gon | 2.44 |
| | Nb5 | 3.16 | 2.81 | 0.254 | 6-gon | 2.44 |
| | Nb2 | 3.17 | 2.81 | 0.245 | 6-gon | 2.87 |
| | Nb2 | 3.17 | 2.81 | 0.245 | 6-gon | 2.87 |
| | Nb4 | 3.31 | 2.80 | 0.139 | 4-gon | 1.21 |
| | Nb1 | 3.39 | 2.80 | 0.102 | 4-gon | 1.02 |
| | Nb3 | 3.59 | 2.88 | 0.066 | 5-gon | 0.78 |
| | Nb3 | 3.59 | 2.88 | 0.066 | 5-gon | 0.78 |
| | Nb5 | 3.62 | 2.81 | 0.045 | 4-gon | 1.10 |
| | Nb6 | 3.74 | 2.88 | 0.036 | 4-gon | 0.41 |
| | Nb7 | 3.81 | 2.88 | 0.028 | 4-gon | 0.35 |
| Sum of Pauling bond orders (i.e. electron population on the crystal site): 4.724 | | | | | | |
| Volume of the Dirichlet domain: 19.59 Å$^3$ | | | | | | |

| Central atom | Neighbour atom | Distance [Å] | D(1) [Å] | Pauling bond order | Created polygon of the Dirichlet domain | Polygon's area [Å$^2$] |
|---|---|---|---|---|---|---|
| M4 $y_{Nb}$ = 0.81 r = 1.359 | As1 | 2.62 | 2.57 | 0.832 | 6-gon | 3.95 |
| | As1 | 2.62 | 2.57 | 0.832 | 6-gon | 3.95 |
| | As2 | 2.77 | 2.57 | 0.470 | 4-gon | 2.96 |
| | Nb1 | 2.84 | 2.72 | 0.619 | 6-gon | 3.19 |
| | Nb1 | 2.84 | 2.72 | 0.619 | 6-gon | 3.19 |
| | Nb5 | 2.87 | 2.73 | 0.569 | 6-gon | 3.64 |
| | Nb5 | 2.87 | 2.73 | 0.569 | 6-gon | 3.64 |
| | Nb3 | 3.10 | 2.80 | 0.320 | 6-gon | 3.08 |
| | Nb3 | 3.10 | 2.80 | 0.320 | 6-gon | 3.08 |
| | Nb2 | 3.16 | 2.73 | 0.191 | 4-gon | 2.43 |
| | Nb3 | 3.31 | 2.80 | 0.139 | 4-gon | 1.21 |
| | Nb6 | 3.46 | 2.80 | 0.081 | 4-gon | 0.91 |
| | Nb4 | 3.59 | 2.72 | 0.036 | 4-gon | 0.61 |
| | Nb4 | 3.59 | 2.72 | 0.036 | 4-gon | 0.61 |
| Sum of Pauling bond orders (i.e. electron population on the crystal site): 5.629 | | | | | | |
| Volume of the Dirichlet domain: 17.69 Å$^3$ | | | | | | |

| Central atom | Neighbour atom | Distance [Å] | D(1) [Å] | Pauling bond order | Created polygon of the Dirichlet domain | Polygon's area [Å$^2$] |
|---|---|---|---|---|---|---|
| M5 $y_{Nb} = 0.74$ r = 1.366 | As2 | 2.71 | 2.58 | 0.589 | 4-gon | 3.96 |
| | As3 | 2.77 | 2.58 | 0.477 | 4-gon | 3.13 |
| | As1 | 2.85 | 2.58 | 0.347 | 4-gon | 2.74 |
| | Nb2 | 2.87 | 2.73 | 0.603 | 6-gon | 3.67 |
| | Nb2 | 2.87 | 2.73 | 0.603 | 6-gon | 3.67 |
| | Nb4 | 2.87 | 2.73 | 0.569 | 6-gon | 3.64 |
| | Nb4 | 2.87 | 2.73 | 0.569 | 6-gon | 3.64 |
| | Nb3 | 3.16 | 2.81 | 0.254 | 6-gon | 2.44 |
| | Nb3 | 3.16 | 2.81 | 0.254 | 6-gon | 2.44 |
| | Nb7 | 3.19 | 2.81 | 0.233 | 6-gon | 2.41 |
| | Nb7 | 3.19 | 2.81 | 0.233 | 6-gon | 2.41 |
| | Nb5 | 3.59 | 2.73 | 0.038 | 4-gon | 1.22 |
| | Nb5 | 3.59 | 2.73 | 0.038 | 4-gon | 1.22 |
| | Nb3 | 3.62 | 2.81 | 0.045 | 4-gon | 1.10 |
| Sum of Pauling bond orders (i.e. electron population on the crystal site): 4.848 | | | | | | |
| Volume of the Dirichlet domain: 18.78 Å$^3$ | | | | | | |

| Central atom | Neighbour atom | Distance [Å] | D(1) [Å] | Pauling bond order | Created polygon of the Dirichlet domain | Polygon's area [Å$^2$] |
|---|---|---|---|---|---|---|
| M6 $y_{Nb} = 0.00$ r = 1.44 | As3 | 2.76 | 2.65 | 0.658 | 7-gon | 4.50 |
| | As3 | 2.76 | 2.65 | 0.658 | 7-gon | 4.50 |
| | As1 | 2.77 | 2.65 | 0.638 | 7-gon | 4.10 |
| | As1 | 2.77 | 2.65 | 0.638 | 7-gon | 4.10 |
| | As3 | 3.10 | 2.65 | 0.177 | 4-gon | 2.62 |
| | Nb2 | 3.10 | 2.81 | 0.321 | 6-gon | 2.91 |
| | Nb2 | 3.10 | 2.81 | 0.321 | 6-gon | 2.91 |
| | Nb1 | 3.24 | 2.80 | 0.185 | 5-gon | 2.12 |
| | Nb1 | 3.24 | 2.80 | 0.185 | 5-gon | 2.12 |
| | Nb6 | 3.37 | 2.88 | 0.155 | 6-gon | 2.35 |
| | Nb6 | 3.37 | 2.88 | 0.155 | 6-gon | 2.35 |
| | Nb2 | 3.43 | 2.81 | 0.092 | 4-gon | 1.20 |
| | Nb4 | 3.46 | 2.80 | 0.081 | 4-gon | 0.91 |
| | Nb6 | 3.59 | 2.88 | 0.066 | 4-gon | 0.89 |
| | Nb6 | 3.59 | 2.88 | 0.066 | 4-gon | 0.89 |
| | Nb3 | 3.74 | 2.88 | 0.036 | 4-gon | 0.41 |
| | Nb7 | 3.83 | 2.88 | 0.027 | 4-gon | 0.33 |
| Sum of Pauling bond orders (i.e. electron population on the crystal site): 4.463 | | | | | | |
| Volume of the Dirichlet domain: 19.94 Å$^3$ | | | | | | |

| Central atom | Neighbour atom | Distance [Å] | D(1) [Å] | Pauling bond order | Created polygon of the Dirichlet domain | Polygon's area [Å$^2$] |
|---|---|---|---|---|---|---|
| M7<br>$y_{Nb}$ = 0.00<br>r = 1.44 | As2 | 2.75 | 2.65 | 0.692 | 6-gon | 4.62 |
| | As2 | 2.75 | 2.65 | 0.692 | 6-gon | 4.62 |
| | As3 | 2.83 | 2.65 | 0.494 | 6-gon | 3.82 |
| | As3 | 2.83 | 2.65 | 0.494 | 6-gon | 3.82 |
| | Nb1 | 3.01 | 2.80 | 0.438 | 6-gon | 3.33 |
| | Nb1 | 3.01 | 2.80 | 0.438 | 6-gon | 3.33 |
| | As2 | 3.10 | 2.65 | 0.175 | 4-gon | 2.67 |
| | Nb5 | 3.19 | 2.81 | 0.233 | 6-gon | 2.41 |
| | Nb5 | 3.19 | 2.81 | 0.233 | 6-gon | 2.41 |
| | Nb1 | 3.45 | 2.80 | 0.081 | 4-gon | 1.19 |
| | Nb2 | 3.49 | 2.81 | 0.074 | 4-gon | 0.89 |
| | Nb7 | 3.50 | 2.88 | 0.093 | 6-gon | 1.88 |
| | Nb7 | 3.50 | 2.88 | 0.093 | 6-gon | 1.88 |
| | Nb7 | 3.59 | 2.88 | 0.066 | 5-gon | 0.91 |
| | Nb7 | 3.59 | 2.88 | 0.066 | 5-gon | 0.91 |
| | Nb3 | 3.81 | 2.88 | 0.028 | 4-gon | 0.35 |
| | Nb6 | 3.83 | 2.88 | 0.027 | 4-gon | 0.33 |
| Sum of Pauling bond orders (i.e. electron population on the crystal site): 4.416 | | | | | | |
| Volume of the Dirichlet domain: 20.04 Å$^3$ | | | | | | |

## E.4. Sample S43, $Hf_{7+x}Nb_{4-x}As_4$ phase

| Central atom | Neighbour atom | Distance [Å] | D(1) [Å] | Pauling bond order | Created polygon of the Dirichlet domain | Polygon's area [Å$^2$] |
|---|---|---|---|---|---|---|
| M1<br>$y_{Nb}$ = 0.68<br>r = 1.372 | As | 2.65 | 2.58 | 0.759 | 6-gon | 3.96 |
| | As | 2.65 | 2.58 | 0.759 | 6-gon | 3.96 |
| | As | 2.80 | 2.58 | 0.442 | 4-gon | 2.95 |
| | M1 | 2.87 | 2.74 | 0.629 | 6-gon | 3.19 |
| | M1 | 2.87 | 2.74 | 0.629 | 6-gon | 3.19 |
| | M3 | 2.96 | 2.78 | 0.501 | 6-gon | 3.50 |
| | M3 | 2.96 | 2.78 | 0.501 | 6-gon | 3.50 |
| | M1 | 3.00 | 2.74 | 0.377 | 4-gon | 3.27 |
| | M2 | 3.14 | 2.81 | 0.282 | 6-gon | 2.99 |
| | M2 | 3.14 | 2.81 | 0.282 | 6-gon | 2.99 |
| | M2 | 3.40 | 2.81 | 0.104 | 4-gon | 1.01 |
| | M4 | 3.42 | 2.81 | 0.095 | 4-gon | 1.01 |
| | M1 | 3.58 | 2.74 | 0.040 | 4-gon | 0.82 |
| | M1 | 3.58 | 2.74 | 0.040 | 4-gon | 0.82 |
| Sum of Pauling bond orders (i.e. electron population on the crystal site): 5.439 | | | | | | |
| Volume of the Dirichlet domain: 18.27 Å$^3$ | | | | | | |

| Central atom | Neighbour atom | Distance [Å] | D(1) [Å] | Pauling bond order | Created polygon of the Dirichlet domain | Polygon's area [Å$^2$] |
|---|---|---|---|---|---|---|
| M2<br>$y_{Nb}$ = 0.00<br>r = 1.44 | As | 2.75 | 2.65 | 0.692 | 6-gon | 4.62 |
| | As | 2.75 | 2.65 | 0.692 | 6-gon | 4.62 |
| | As | 2.83 | 2.65 | 0.494 | 6-gon | 3.82 |
| | As | 2.83 | 2.65 | 0.494 | 6-gon | 3.82 |
| | M1 | 3.01 | 2.80 | 0.438 | 6-gon | 3.33 |
| | M1 | 3.01 | 2.80 | 0.438 | 6-gon | 3.33 |
| | M1 | 3.10 | 2.65 | 0.175 | 4-gon | 2.67 |
| | M1 | 3.19 | 2.81 | 0.233 | 6-gon | 2.41 |
| | M5 | 3.19 | 2.81 | 0.233 | 6-gon | 2.41 |
| | M5 | 3.45 | 2.80 | 0.081 | 4-gon | 1.19 |
| | M1 | 3.49 | 2.81 | 0.074 | 4-gon | 0.89 |
| | M1 | 3.50 | 2.88 | 0.093 | 6-gon | 1.88 |
| | M2 | 3.50 | 2.88 | 0.093 | 6-gon | 1.88 |
| | M2 | 3.59 | 2.88 | 0.066 | 5-gon | 0.91 |
| | M4 | 3.59 | 2.88 | 0.066 | 5-gon | 0.91 |
| | M4 | 3.81 | 2.88 | 0.028 | 4-gon | 0.35 |
| | M3 | 3.83 | 2.88 | 0.027 | 4-gon | 0.33 |
| Sum of Pauling bond orders (i.e. electron population on the crystal site): 4.946 | | | | | | |
| Volume of the Dirichlet domain: 19.59 Å$^3$ | | | | | | |

| Central atom | Neighbour atom | Distance [Å] | D(1) [Å] | Pauling bond order | Created polygon of the Dirichlet domain | Polygon's area [Å$^2$] |
|---|---|---|---|---|---|---|
| M3<br>$y_{Nb}$ = 0.34<br>r = 1.406 | As | 2.85 | 2.62 | 0.404 | 4-gon | 2.93 |
| | As | 2.85 | 2.62 | 0.404 | 4-gon | 2.93 |
| | M1 | 2.96 | 2.78 | 0.501 | 6-gon | 3.50 |
| | M1 | 2.96 | 2.78 | 0.501 | 6-gon | 3.50 |
| | M1 | 2.96 | 2.78 | 0.501 | 6-gon | 3.50 |
| | M1 | 2.96 | 2.78 | 0.501 | 6-gon | 3.50 |
| | M3 | 3.11 | 2.81 | 0.321 | 4-gon | 3.60 |
| | M4 | 3.17 | 2.84 | 0.287 | 6-gon | 3.20 |
| | M4 | 3.17 | 2.84 | 0.287 | 6-gon | 3.20 |
| | M4 | 3.17 | 2.84 | 0.287 | 6-gon | 3.20 |
| | M4 | 3.17 | 2.84 | 0.287 | 6-gon | 3.20 |
| | M3 | 3.58 | 2.81 | 0.052 | 4-gon | 1.50 |
| | M3 | 3.58 | 2.81 | 0.052 | 4-gon | 1.50 |
| | M2 | 3.92 | 2.85 | 0.016 | 4-gon | 0.50 |
| Sum of Pauling bond orders (i.e. electron population on the crystal site): 4.404 | | | | | | |
| Volume of the Dirichlet domain: 20.43 Å$^3$ | | | | | | |

| Central atom | Neighbour atom | Distance [Å] | D(1) [Å] | Pauling bond order | Created polygon of the Dirichlet domain | Polygon's area [Å$^2$] |
|---|---|---|---|---|---|---|
| M4<br>$y_{Nb}$ = 0.03<br>r = 1.437 | As | 2.75 | 2.65 | 0.692 | 6-gon | 4.62 |
| | As | 2.75 | 2.65 | 0.692 | 6-gon | 4.62 |
| | As | 2.83 | 2.65 | 0.494 | 6-gon | 3.82 |
| | As | 2.83 | 2.65 | 0.494 | 6-gon | 3.82 |
| | M3 | 3.01 | 2.80 | 0.438 | 6-gon | 3.33 |
| | M3 | 3.01 | 2.80 | 0.438 | 6-gon | 3.33 |
| | M3 | 3.10 | 2.65 | 0.175 | 4-gon | 2.67 |
| | M3 | 3.19 | 2.81 | 0.233 | 6-gon | 2.41 |
| | M5 | 3.19 | 2.81 | 0.233 | 6-gon | 2.41 |
| | M5 | 3.45 | 2.80 | 0.081 | 4-gon | 1.19 |
| | M1 | 3.49 | 2.81 | 0.074 | 4-gon | 0.89 |
| | M1 | 3.50 | 2.88 | 0.093 | 6-gon | 1.88 |
| | M4 | 3.50 | 2.88 | 0.093 | 6-gon | 1.88 |
| | M4 | 3.59 | 2.88 | 0.066 | 5-gon | 0.91 |
| | M2 | 3.59 | 2.88 | 0.066 | 5-gon | 0.91 |
| | M2 | 3.81 | 2.88 | 0.028 | 4-gon | 0.35 |
| Sum of Pauling bond orders (i.e. electron population on the crystal site): 4.871 | | | | | | |
| Volume of the Dirichlet domain: 19.91 Å$^3$ | | | | | | |

| Central atom | Neighbour atom | Distance [Å] | D(1) [Å] | Pauling bond order | Created polygon of the Dirichlet domain | Polygon's area [Å$^2$] |
|---|---|---|---|---|---|---|
| M5<br>$y_{Nb}$ = 0.31<br>r = 1.409 | As | 2.77 | 2.62 | 0.571 | 5-gon | 3.78 |
| | As | 2.77 | 2.62 | 0.571 | 5-gon | 3.78 |
| | As | 2.77 | 2.62 | 0.571 | 5-gon | 3.78 |
| | As | 2.77 | 2.62 | 0.571 | 5-gon | 3.78 |
| | M2 | 3.14 | 2.85 | 0.325 | 6-gon | 2.69 |
| | M2 | 3.14 | 2.85 | 0.325 | 6-gon | 2.69 |
| | M2 | 3.14 | 2.85 | 0.325 | 6-gon | 2.69 |
| | M2 | 3.14 | 2.85 | 0.325 | 6-gon | 2.69 |
| | M4 | 3.25 | 2.85 | 0.215 | 5-gon | 2.30 |
| | M4 | 3.25 | 2.85 | 0.215 | 5-gon | 2.30 |
| | M4 | 3.25 | 2.85 | 0.215 | 5-gon | 2.30 |
| | M4 | 3.25 | 2.85 | 0.215 | 5-gon | 2.30 |
| | M5 | 3.58 | 2.82 | 0.053 | 4-gon | 2.04 |
| | M5 | 3.58 | 2.82 | 0.053 | 4-gon | 2.04 |
| | As | 2.77 | 2.62 | 0.571 | 5-gon | 3.78 |
| | As | 2.77 | 2.62 | 0.571 | 5-gon | 3.78 |
| | As | 2.77 | 2.62 | 0.571 | 5-gon | 3.78 |
| Sum of Pauling bond orders (i.e. electron population on the crystal site): 4.549 | | | | | | |
| Volume of the Dirichlet domain: 20.01 Å$^3$ | | | | | | |

## E.5. Sample S43, $Hf_{3+x}Nb_{3-x}As_2$ phase

| Central atom | Neighbour atom | Distance [Å] | D(1) [Å] | Pauling bond order | Created polygon of the Dirichlet domain | Polygon's area [Å$^2$] |
|---|---|---|---|---|---|---|
| M1 $y_{Nb} = 0.49$ r = 1.391 | As | 2.77 | 2.60 | 0.527 | 4-gon | 3.869 |
| | As | 2.88 | 2.60 | 0.338 | 4-gon | 2.872 |
| | M2 | 2.88 | 2.76 | 0.629 | 6-gon | 3.842 |
| | M2 | 2.88 | 2.76 | 0.629 | 6-gon | 3.842 |
| | M1 | 2.96 | 2.78 | 0.503 | 6-gon | 3.956 |
| | M1 | 2.96 | 2.78 | 0.503 | 6-gon | 3.956 |
| | M2 | 3.15 | 2.76 | 0.219 | 4-gon | 2.609 |
| | M3 | 3.16 | 2.82 | 0.279 | 6-gon | 3.121 |
| | M3 | 3.16 | 2.82 | 0.279 | 6-gon | 3.121 |
| | M3 | 3.27 | 2.82 | 0.182 | 6-gon | 2.216 |
| | M3 | 3.27 | 2.82 | 0.182 | 6-gon | 2.216 |
| | M1 | 3.58 | 2.78 | 0.046 | 4-gon | 1.413 |
| | M1 | 3.58 | 2.78 | 0.046 | 4-gon | 1.413 |
| | M3 | 3.72 | 2.82 | 0.033 | 4-gon | 0.914 |
| Sum of Pauling bond orders (i.e. electron population on the crystal site): 4.393 | | | | | | |
| Volume of the Dirichlet domain: 20.08 Å$^3$ | | | | | | |

| Central atom | Neighbour atom | Distance [Å] | D(1) [Å] | Pauling bond order | Created polygon of the Dirichlet domain | Polygon's area [Å$^2$] |
|---|---|---|---|---|---|---|
| M2 $y_{Nb} = 0.75$ r = 1.365 | As | 2.67 | 2.58 | 0.697 | 6-gon | 3.917 |
| | As | 2.67 | 2.58 | 0.697 | 6-gon | 3.917 |
| | As | 2.77 | 2.58 | 0.471 | 4-gon | 3.046 |
| | M1 | 2.88 | 2.76 | 0.629 | 6-gon | 3.842 |
| | M1 | 2.88 | 2.76 | 0.629 | 6-gon | 3.842 |
| | M2 | 2.88 | 2.73 | 0.562 | 6-gon | 3.139 |
| | M2 | 2.88 | 2.73 | 0.562 | 6-gon | 3.139 |
| | M3 | 3.12 | 2.80 | 0.296 | 6-gon | 3.084 |
| | M3 | 3.12 | 2.80 | 0.296 | 6-gon | 3.084 |
| | M1 | 3.15 | 2.76 | 0.219 | 4-gon | 2.609 |
| | M3 | 3.43 | 2.80 | 0.089 | 4-gon | 1.05 |
| | M3 | 3.45 | 2.80 | 0.083 | 4-gon | 0.925 |
| | M2 | 3.58 | 2.73 | 0.038 | 4-gon | 0.73 |
| | M2 | 3.58 | 2.73 | 0.038 | 4-gon | 0.73 |
| Sum of Pauling bond orders (i.e. electron population on the crystal site): 5.307 | | | | | | |
| Volume of the Dirichlet domain: 18.17 Å$^3$ | | | | | | |

| Central atom | Neighbour atom | Distance [Å] | D(1) [Å] | Pauling bond order | Created polygon of the Dirichlet domain | Polygon's area [Å$^2$] |
|---|---|---|---|---|---|---|
| M3<br>$y_{Nb}$ = 0.07<br>r = 1.433 | As | 2.74 | 2.64 | 0.692 | 6-gon | 4.371 |
| | As | 2.74 | 2.64 | 0.692 | 6-gon | 4.371 |
| | As | 2.77 | 2.64 | 0.614 | 6-gon | 4.21 |
| | As | 2.77 | 2.64 | 0.614 | 6-gon | 4.21 |
| | M2 | 3.12 | 2.80 | 0.296 | 6-gon | 3.084 |
| | M2 | 3.12 | 2.80 | 0.296 | 6-gon | 3.084 |
| | M1 | 3.16 | 2.82 | 0.279 | 6-gon | 3.121 |
| | M1 | 3.16 | 2.82 | 0.279 | 6-gon | 3.121 |
| | M1 | 3.27 | 2.82 | 0.182 | 6-gon | 2.216 |
| | M1 | 3.27 | 2.82 | 0.182 | 6-gon | 2.216 |
| | M2 | 3.43 | 2.80 | 0.089 | 4-gon | 1.05 |
| | M2 | 3.45 | 2.80 | 0.083 | 4-gon | 0.925 |
| | M3 | 3.58 | 2.87 | 0.064 | 5-gon | 0.777 |
| | M3 | 3.58 | 2.87 | 0.064 | 5-gon | 0.777 |
| | M1 | 3.72 | 2.82 | 0.033 | 4-gon | 0.914 |
| | M3 | 3.79 | 2.87 | 0.029 | 4-gon | 0.389 |
| | M3 | 3.79 | 2.87 | 0.029 | 4-gon | 0.389 |
| Sum of Pauling bond orders (i.e. electron population on the crystal site): 4.517 | | | | | | |
| Volume of the Dirichlet domain: 19.90 Å$^3$ | | | | | | |

## E.6. Sample S42, $Hf_{2+x}Nb_{1-x}As$ phase

| Central atom | Neighbour atom | Distance [Å] | D(1) [Å] | Pauling bond order | Created polygon of the Dirichlet domain | Polygon's area [Å$^2$] |
|---|---|---|---|---|---|---|
| M1<br>$y_{Nb}$ = 0.22<br>r = 1.418 | As | 2.74 | 2.63 | 0.648 | 5-gon | 3.89 |
| | As | 2.79 | 2.63 | 0.531 | 5-gon | 4.03 |
| | Nb1 | 2.90 | 2.84 | 0.794 | 6-gon | 4.78 |
| | Nb3 | 2.98 | 2.82 | 0.541 | 6-gon | 3.54 |
| | Nb3 | 3.14 | 2.82 | 0.288 | 6-gon | 3.23 |
| | Nb3 | 3.24 | 2.82 | 0.197 | 5-gon | 2.54 |
| | Nb2 | 3.25 | 2.85 | 0.212 | 6-gon | 2.84 |
| | Nb2 | 3.29 | 2.85 | 0.184 | 5-gon | 2.10 |
| | Nb3 | 3.31 | 2.82 | 0.151 | 5-gon | 2.19 |
| | Nb1 | 3.38 | 2.84 | 0.126 | 5-gon | 2.57 |
| | Nb1 | 3.38 | 2.84 | 0.126 | 5-gon | 2.57 |
| | Nb1 | 3.38 | 2.84 | 0.126 | 5-gon | 2.00 |
| | Nb1 | 3.38 | 2.84 | 0.126 | 5-gon | 2.00 |
| | Nb3 | 3.38 | 2.82 | 0.114 | 5-gon | 2.02 |
| Sum of Pauling bond orders (i.e. electron population on the crystal site): 4.165 | | | | | | |
| Volume of the Dirichlet domain: 21.00 Å$^3$ | | | | | | |

| Central atom | Neighbour atom | Distance [Å] | D(1) [Å] | Pauling bond order | Created polygon of the Dirichlet domain | Polygon's area [Å$^2$] |
|---|---|---|---|---|---|---|
| M2<br>$y_{Nb}$ = 0.10<br>r = 1.430 | As | 2.70 | 2.64 | 0.782 | 6-gon | 4.63 |
| | As | 2.72 | 2.64 | 0.750 | 6-gon | 4.46 |
| | As | 2.72 | 2.64 | 0.750 | 7-gon | 4.42 |
| | As | 2.80 | 2.64 | 0.541 | 4-gon | 3.63 |
| | Nb3 | 2.99 | 2.83 | 0.535 | 6-gon | 3.67 |
| | Nb3 | 3.08 | 2.83 | 0.380 | 5-gon | 2.74 |
| | Nb2 | 3.11 | 2.86 | 0.388 | 6-gon | 2.51 |
| | Nb3 | 3.19 | 2.83 | 0.254 | 5-gon | 2.12 |
| | Nb2 | 3.22 | 2.86 | 0.255 | 6-gon | 2.16 |
| | Nb2 | 3.22 | 2.86 | 0.255 | 6-gon | 2.16 |
| | Nb1 | 3.25 | 2.85 | 0.212 | 6-gon | 2.84 |
| | Nb1 | 3.29 | 2.85 | 0.184 | 5-gon | 2.10 |
| | Nb2 | 3.73 | 2.86 | 0.035 | 4-gon | 0.46 |
| | Nb2 | 3.73 | 2.86 | 0.035 | 4-gon | 0.46 |
| | Nb3 | 3.93 | 2.83 | 0.015 | 4-gon | 0.36 |
| Sum of Pauling bond orders (i.e. electron population on the crystal site): 5.371 | | | | | | |
| Volume of the Dirichlet domain: 19.30 Å$^3$ | | | | | | |

| Central atom | Neighbour atom | Distance [Å] | D(1) [Å] | Pauling bond order | Created polygon of the Dirichlet domain | Polygon's area [Å$^2$] |
|---|---|---|---|---|---|---|
| M3<br>$y_{Nb}$ = 0.41<br>r = 1.399 | As | 2.70 | 2.61 | 0.694 | 5-gon | 4.04 |
| | As | 2.79 | 2.61 | 0.492 | 5-gon | 3.58 |
| | As | 2.85 | 2.61 | 0.401 | 5-gon | 3.20 |
| | Nb1 | 2.98 | 2.82 | 0.541 | 6-gon | 3.54 |
| | Nb2 | 2.99 | 2.83 | 0.535 | 6-gon | 3.67 |
| | Nb3 | 3.04 | 2.80 | 0.401 | 6-gon | 2.88 |
| | Nb2 | 3.08 | 2.83 | 0.380 | 5-gon | 2.74 |
| | Nb1 | 3.14 | 2.82 | 0.288 | 6-gon | 3.23 |
| | Nb2 | 3.19 | 2.83 | 0.254 | 5-gon | 2.12 |
| | Nb3 | 3.23 | 2.80 | 0.192 | 4-gon | 2.70 |
| | Nb1 | 3.24 | 2.82 | 0.197 | 5-gon | 2.54 |
| | Nb1 | 3.31 | 2.82 | 0.151 | 5-gon | 2.19 |
| | Nb1 | 3.38 | 2.82 | 0.114 | 5-gon | 2.02 |
| | Nb2 | 3.93 | 2.83 | 0.015 | 4-gon | 0.36 |
| Sum of Pauling bond orders (i.e. electron population on the crystal site): 4.656 | | | | | | |
| Volume of the Dirichlet domain: 19.68 Å$^3$ | | | | | | |

## E.7. Sample G5, $Hf_{1-x}Nb_xGa$ phase

| Central atom | Neighbour atom | Distance [Å] | D(1) [Å] | Pauling bond order | Created polygon of the Dirichlet domain | Polygon's area [Å$^2$] |
|---|---|---|---|---|---|---|
| M1<br>$y_{Nb}$ = 0.89<br>r = 1.351 | Hf1 | 2.74 | 2.70 | 0.881 | 6-gon | 3.21 |
| | Hf1 | 2.74 | 2.70 | 0.881 | 6-gon | 3.21 |
| | Ga3 | 2.75 | 2.60 | 0.567 | 6-gon | 3.80 |
| | Ga3 | 2.75 | 2.60 | 0.567 | 6-gon | 3.80 |
| | Ga2 | 2.80 | 2.60 | 0.462 | 5-gon | 3.42 |
| | Ga2 | 2.80 | 2.60 | 0.462 | 5-gon | 3.42 |
| | Ga2 | 2.84 | 2.60 | 0.395 | 6-gon | 3.37 |
| | Ga2 | 2.84 | 2.60 | 0.395 | 6-gon | 3.37 |
| | Hf3 | 3.16 | 2.76 | 0.214 | 5-gon | 1.90 |
| | Hf3 | 3.16 | 2.76 | 0.214 | 5-gon | 1.90 |
| | Hf2 | 3.31 | 2.75 | 0.117 | 4-gon | 1.35 |
| | Hf2 | 3.31 | 2.75 | 0.117 | 4-gon | 1.35 |
| | Hf3 | 3.54 | 2.76 | 0.050 | 4-gon | 0.74 |
| | Hf3 | 3.54 | 2.76 | 0.050 | 4-gon | 0.74 |
| Sum of Pauling bond orders (i.e. electron population on the crystal site): 5.373 | | | | | | |
| Volume of the Dirichlet domain: 17.16 Å$^3$ | | | | | | |

| Central atom | Neighbour atom | Distance [Å] | D(1) [Å] | Pauling bond order | Created polygon of the Dirichlet domain | Polygon's area [Å$^2$] |
|---|---|---|---|---|---|---|
| M2<br>$y_{Nb}$ = 0.40<br>r = 1.400 | Ga1 | 2.76 | 2.65 | 0.666 | 7-gon | 3.75 |
| | Ga1 | 2.76 | 2.65 | 0.666 | 7-gon | 3.75 |
| | Ga2 | 2.76 | 2.65 | 0.651 | 9-gon | 4.76 |
| | Ga3 | 2.84 | 2.65 | 0.486 | 7-gon | 3.26 |
| | Ga3 | 2.84 | 2.65 | 0.482 | 7-gon | 2.99 |
| | Ga3 | 2.87 | 2.65 | 0.435 | 6-gon | 3.55 |
| | Ga3 | 2.87 | 2.65 | 0.435 | 6-gon | 3.55 |
| | Ga1 | 2.90 | 2.65 | 0.377 | 5-gon | 2.72 |
| | Ga1 | 2.90 | 2.65 | 0.377 | 5-gon | 2.72 |
| | Hf1 | 3.31 | 2.75 | 0.117 | 4-gon | 1.35 |
| | Hf1 | 3.31 | 2.75 | 0.117 | 4-gon | 1.35 |
| | Hf3 | 3.53 | 2.81 | 0.063 | 3-gon | 0.77 |
| | Hf3 | 3.53 | 2.81 | 0.063 | 3-gon | 0.77 |
| | Hf2 | 3.59 | 2.80 | 0.048 | 4-gon | 0.57 |
| | Hf2 | 3.59 | 2.80 | 0.048 | 4-gon | 0.57 |
| Sum of Pauling bond orders (i.e. electron population on the crystal site): 5.031 | | | | | | |
| Volume of the Dirichlet domain: 17.80 Å$^3$ | | | | | | |

| Central atom | Neighbour atom | Distance [Å] | D(1) [Å] | Pauling bond order | Created polygon of the Dirichlet domain | Polygon's area [Å$^2$] |
|---|---|---|---|---|---|---|
| M3<br>$y_{Nb}$ = 0.29<br>r = 1.411 | Ga3 | 2.68 | 2.66 | 0.919 | 8-gon | 4.96 |
| | Ga1 | 2.80 | 2.66 | 0.596 | 7-gon | 4.02 |
| | Ga1 | 2.80 | 2.66 | 0.596 | 7-gon | 4.02 |
| | Ga2 | 2.83 | 2.66 | 0.533 | 7-gon | 3.70 |
| | Ga2 | 2.83 | 2.66 | 0.529 | 6-gon | 4.06 |
| | Ga2 | 2.98 | 2.66 | 0.296 | 7-gon | 3.49 |
| | Ga2 | 2.98 | 2.66 | 0.296 | 7-gon | 3.49 |
| | Hf1 | 3.16 | 2.76 | 0.214 | 5-gon | 1.90 |
| | Hf1 | 3.16 | 2.76 | 0.214 | 5-gon | 1.90 |
| | Hf3 | 3.35 | 2.82 | 0.130 | 4-gon | 1.50 |
| | Hf3 | 3.35 | 2.82 | 0.130 | 4-gon | 1.50 |
| | Hf2 | 3.53 | 2.81 | 0.063 | 3-gon | 0.77 |
| | Hf2 | 3.53 | 2.81 | 0.063 | 3-gon | 0.77 |
| | Hf1 | 3.54 | 2.76 | 0.050 | 4-gon | 0.74 |
| | Hf1 | 3.54 | 2.76 | 0.050 | 4-gon | 0.74 |
| Sum of Pauling bond orders (i.e. electron population on the crystal site): 4.679 | | | | | | |
| Volume of the Dirichlet domain: 18.66 Å$^3$ | | | | | | |

## Appendix F – Weighted amounts of the substrates, mass losses and calculated compositions of the prepared samples

### F.1. Samples in Hf-Nb-As system

A list of substrate and sample masses in Hf-Nb-As system is given below. Sample compositions were calculated by referring the sample mass loss (from pelletized to tempered stage) to the arsenic content.

| Sample name | Weighted amount [mg] | | | | Mass after [mg] | | | Calculated composition |
|---|---|---|---|---|---|---|---|---|
| | HfAs | NbAs | Hf | Nb | pelletizing | arc-melting | tempering | |
| S1 | 999.94 | 0.00 | 0.00 | 0.00 | 984.27 | 975.40 | 973.36 | $Hf_{0.510}Nb_{0.000}As_{0.490}$ |
| S2 | 739.59 | 0.00 | 260.54 | 0.00 | 988.26 | 982.83 | 981.03 | $Hf_{0.609}Nb_{0.000}As_{0.391}$ |
| S3 | 678.09 | 0.00 | 326.68 | 0.00 | 990.42 | 925.31 | 925.26 | $Hf_{0.716}Nb_{0.000}As_{0.284}$ |
| S4 | 634.97 | 0.00 | 365.37 | 0.00 | 987.76 | 967.48 | 967.46 | $Hf_{0.672}Nb_{0.000}As_{0.328}$ |
| S5 | 515.76 | 0.00 | 484.47 | 0.00 | 992.03 | 989.85 | 989.76 | $Hf_{0.704}Nb_{0.000}As_{0.296}$ |
| S6 | 321.29 | 0.00 | 678.83 | 0.00 | 989.80 | 989.19 | 989.03 | $Hf_{0.803}Nb_{0.000}As_{0.197}$ |
| S7 | 0.00 | 1000.11 | 0.00 | 0.00 | 975.43 | 896.89 | 893.26 | $Hf_{0.000}Nb_{0.544}As_{0.456}$ |
| S8 | 0.00 | 826.05 | 0.00 | 174.10 | 990.43 | 937.30 | 934.23 | $Hf_{0.000}Nb_{0.618}As_{0.382}$ |
| S9 | 0.00 | 783.33 | 0.00 | 216.93 | 975.60 | 924.73 | 922.55 | $Hf_{0.000}Nb_{0.635}As_{0.365}$ |
| S10 | 0.00 | 724.38 | 0.00 | 275.76 | 990.18 | 959.90 | 957.23 | $Hf_{0.000}Nb_{0.651}As_{0.349}$ |
| S11 | 0.00 | 657.66 | 0.00 | 342.36 | 989.54 | 967.94 | 965.40 | $Hf_{0.000}Nb_{0.678}As_{0.322}$ |
| S12 | 0.00 | 575.44 | 0.00 | 424.68 | 982.98 | 978.65 | 971.34 | $Hf_{0.000}Nb_{0.708}As_{0.292}$ |
| S13 | 0.00 | 376.00 | 0.00 | 624.18 | 985.71 | 983.88 | 981.97 | $Hf_{0.000}Nb_{0.803}As_{0.197}$ |
| S14 | 858.08 | 142.98 | 0.00 | 0.00 | 973.71 | 922.59 | 916.85 | $Hf_{0.439}Nb_{0.110}As_{0.451}$ |
| S15 | 693.63 | 306.42 | 0.00 | 0.00 | 986.31 | 913.45 | 910.47 | $Hf_{0.337}Nb_{0.225}As_{0.438}$ |
| S16 | 501.66 | 498.21 | 0.00 | 0.00 | 982.60 | 928.08 | 926.24 | $Hf_{0.216}Nb_{0.323}As_{0.461}$ |
| S17 | 274.15 | 725.92 | 0.00 | 0.00 | 987.76 | 889.04 | 887.31 | $Hf_{0.114}Nb_{0.455}As_{0.431}$ |
| S18 | 786.92 | 72.44 | 140.29 | 0.00 | 979.12 | 936.47 | 931.66 | $Hf_{0.540}Nb_{0.060}As_{0.401}$ |
| S19 | 613.44 | 235.19 | 151.59 | 0.00 | 972.47 | 932.36 | 929.62 | $Hf_{0.413}Nb_{0.176}As_{0.411}$ |
| S20 | 643.11 | 271.07 | 0.00 | 85.59 | 990.75 | 921.46 | 917.68 | $Hf_{0.307}Nb_{0.308}As_{0.385}$ |

| Sample name | Weighted amount [mg] | | | | Mass after [mg] | | | Calculated composition |
|---|---|---|---|---|---|---|---|---|
| | HfAs | NbAs | Hf | Nb | pelletizing | arc-melting | tempering | |
| S21 | 422.48 | 483.58 | 0.00 | 93.99 | 980.06 | 901.47 | 899.83 | $Hf_{0.183}Nb_{0.430}As_{0.386}$ |
| S22 | 155.71 | 740.56 | 0.00 | 103.64 | 989.52 | 910.88 | 908.27 | $Hf_{0.061}Nb_{0.547}As_{0.393}$ |
| S23 | 559.62 | 158.88 | 281.63 | 0.00 | 983.58 | 971.69 | 971.43 | $Hf_{0.491}Nb_{0.122}As_{0.387}$ |
| S24 | 348.10 | 345.79 | 306.14 | 0.00 | 905.28 | 895.28 | 892.71 | $Hf_{0.372}Nb_{0.234}As_{0.394}$ |
| S25 | 572.45 | 252.56 | 0.00 | 174.93 | 985.61 | 955.31 | 954.60 | $Hf_{0.250}Nb_{0.378}As_{0.372}$ |
| S26 | 316.92 | 489.78 | 0.00 | 193.65 | 980.57 | 934.37 | 931.03 | $Hf_{0.127}Nb_{0.512}As_{0.361}$ |
| S27 | 635.14 | 0.00 | 344.94 | 20.08 | 979.65 | 967.05 | 943.50 | $Hf_{0.667}Nb_{0.033}As_{0.300}$ |
| S28 | 528.34 | 79.69 | 391.87 | 0.00 | 990.17 | 986.83 | 985.69 | $Hf_{0.591}Nb_{0.065}As_{0.344}$ |
| S29 | 676.43 | 0.00 | 231.30 | 92.20 | 952.70 | 923.76 | 921.85 | $Hf_{0.551}Nb_{0.143}As_{0.306}$ |
| S30 | 312.70 | 260.53 | 426.32 | 0.00 | 991.59 | 987.94 | 984.29 | $Hf_{0.461}Nb_{0.197}As_{0.342}$ |
| S31 | 719.62 | 36.76 | 0.00 | 243.64 | 986.61 | 978.76 | 972.19 | $Hf_{0.331}Nb_{0.335}As_{0.334}$ |
| S32 | 0.00 | 566.41 | 344.03 | 89.55 | 991.25 | 933.54 | 930.24 | $Hf_{0.219}Nb_{0.490}As_{0.291}$ |
| S33 | 178.76 | 518.85 | 0.00 | 302.46 | 984.62 | 955.70 | 951.62 | $Hf_{0.067}Nb_{0.609}As_{0.324}$ |
| S34 | 0.00 | 537.61 | 416.49 | 45.90 | 969.95 | 957.85 | 956.99 | $Hf_{0.260}Nb_{0.402}As_{0.338}$ |
| S35 | 561.42 | 0.00 | 342.48 | 96.17 | 992.69 | 991.14 | 990.35 | $Hf_{0.562}Nb_{0.141}As_{0.296}$ |
| S36 | 615.55 | 0.00 | 174.26 | 210.78 | 989.32 | 987.40 | 980.09 | $Hf_{0.426}Nb_{0.286}As_{0.287}$ |
| S37 | 0.00 | 428.57 | 531.93 | 39.56 | 990.48 | 979.95 | 977.41 | $Hf_{0.358}Nb_{0.355}As_{0.286}$ |
| S38 | 0.00 | 451.73 | 448.22 | 100.04 | 991.87 | 981.82 | 979.58 | $Hf_{0.286}Nb_{0.426}As_{0.288}$ |
| S39 | 0.00 | 505.89 | 251.36 | 242.62 | 987.58 | 969.65 | 959.56 | $Hf_{0.146}Nb_{0.580}As_{0.274}$ |
| S40 | 439.88 | 0.00 | 495.79 | 64.45 | 980.56 | 972.06 | 970.65 | $Hf_{0.664}Nb_{0.103}As_{0.233}$ |
| S41 | 516.43 | 0.00 | 218.40 | 265.15 | 978.97 | 952.90 | 950.23 | $Hf_{0.419}Nb_{0.371}As_{0.210}$ |
| S42 | 375.42 | 0.00 | 440.73 | 183.56 | 990.37 | 989.97 | 989.45 | $Hf_{0.534}Nb_{0.268}As_{0.198}$ |
| S43 | 0.00 | 271.76 | 578.12 | 150.36 | 986.45 | 985.19 | 984.63 | $Hf_{0.402}Nb_{0.399}As_{0.198}$ |
| S44 | 0.00 | 291.90 | 465.72 | 242.33 | 971.32 | 970.22 | 968.86 | $Hf_{0.303}Nb_{0.499}As_{0.198}$ |
| S45 | 0.00 | 299.38 | 424.29 | 276.02 | 991.94 | 990.22 | 988.21 | $Hf_{0.269}Nb_{0.536}As_{0.196}$ |
| S46 | 268.60 | 0.00 | 567.50 | 164.17 | 964.65 | 961.29 | 960.07 | $Hf_{0.606}Nb_{0.255}As_{0.139}$ |
| S47 | 253.24 | 0.00 | 654.10 | 92.80 | 984.76 | 981.29 | 974.11 | $Hf_{0.716}Nb_{0.154}As_{0.130}$ |

### F.2. Samples in Hf-Nb-Ga system

A list of substrate and sample masses in Hf-Nb-Ga system is given below. Sample compositions were calculated by referring the sample mass loss (from substrate weighting to tempered stage, omitting the pelletizing step) to the gallium content.

| Sample name | Weighted amount [mg] | | | Mass after arc-melting [mg] | $Nb_3Ga$ added [mg] | Mass after [mg] | | Calculated Composition |
|---|---|---|---|---|---|---|---|---|
| | Hf | Nb | Ga | | | pelletizing | tempering | |
| G1 | 670.30 | 38.55 | 305.90 | 984.27 | 21.86 | 862.18 | 845.02 | $Hf_{0.447}Nb_{0.058}Ga_{0.495}$ |
| G2 | 617.66 | 80.24 | 316.69 | 988.26 | 8.71 | 965.25 | 936.78 | $Hf_{0.403}Nb_{0.104}Ga_{0.493}$ |
| G3 | 561.24 | 125.43 | 328.31 | 990.42 | 8.12 | 959.53 | 950.54 | $Hf_{0.349}Nb_{0.153}Ga_{0.498}$ |
| G4 | 500.35 | 173.49 | 340.89 | 987.76 | 21.01 | 955.83 | 943.84 | $Hf_{0.297}Nb_{0.205}Ga_{0.497}$ |
| G5 | 434.45 | 226.07 | 354.45 | 992.03 | 8.78 | 944.55 | 911.56 | $Hf_{0.253}Nb_{0.256}Ga_{0.491}$ |
| G6 | 362.84 | 283.36 | 369.17 | 989.80 | 34.66 | 941.24 | 920.4 | $Hf_{0.198}Nb_{0.308}Ga_{0.494}$ |
| G7 | 284.42 | 345.37 | 385.15 | 975.43 | 32.53 | 920.99 | 908.76 | $Hf_{0.148}Nb_{0.355}Ga_{0.497}$ |

## Appendix G - The structure data of the VASP Structures

As it was mentioned in the work, the aim of the DFT calculations was to find the ground state energy values which could be used for the thermodynamic modelling or could give some information on the phase stability. The ground state structures obtained by the structure relaxation were not of the primary interest and were only analysed in view of the credibility of the energy values (e.g. it was very useful to compare the relaxed structures of (Hf:Nb:Hf:Ge) and (Hf:Hf:Nb:Ge) endmembers of $Sm_5Ge_4$-type, see chapter 4.2.1). The structure relaxation was made by variation of the lattice parameters and by allowing the atoms to migrate according to the forces working on them. The lattice variation was performed with the constant volume constraint (i.e. the volume of the unit cell should not change during the relaxation). A series of calculation for different volumes was performed in order to find the optimal set. The atoms were "released" for the volume with minimal ground state energy and it's larger and smaller neighbours. The volumes were defined by the lattice parameters sets and have discrete values. Hence, the accuracy is taken as equal to the width of the step between the consecutive volumes.

### G.1. The elements

For the computation of the ground state energies of the elements, the lattice parameters were allowed to vary. Additionally, the atoms were allowed to migrate during the calculations for As and Ga structures (it was not necessary for Hf, Nb and Ge, as in theses structures the atoms occupy the special positions). The literature data are also given for the comparison [3]. In some cases, the difference between the calculated and the literature value exceeds 0.1 Å (the computed values are larger) but the relative difference is never greater than 2%

- Hf

| Element: Hf | | Structure type: Mg | | Space group: $P6_3/mmc$ (194) |
|---|---|---|---|---|
| Lattice parameters [Å] | | | | Cell volume [Å$^3$]: 45.05 |
| a = 3.20 | | c = 5.08 | | |
| Site | Mpl. | x | y | z |
| Hf | 2*c* | 1/3 | 2/3 | 1/4 |

Literature values:

Lattice parameters: a = 3.198, c = 5.061

- Nb

| Element: Nb | Structure type: W | | Space group: $Im\bar{3}m$ (229) | |
|---|---|---|---|---|
| Lattice parameters [Å] a = 3.31 | | | Cell volume [Å$^3$]: 36.26 | |
| Site | Mpl. | x | y | z |
| Nb | 2*a* | 0 | 0 | 0 |

Literature values:

Lattice parameters: a = 3.300

- As

| Element: As | Structure type: As | | Space group: $R\bar{3}m$ (166) | |
|---|---|---|---|---|
| Lattice parameters [Å] a = 3.82 | | c = 10.72 | Cell volume [Å$^3$]: 135.47 | |
| Site | Mpl. | x | y | z |
| As | 6*c* | 0 | 0 | 0.2271 |

Literature values:

Lattice parameters: a = 3.7598(1) , c = 10.5475(2)

Atom position: As – x = 0; y = 0; z = 0.2271

- Ge

| Element: Ge | Structure type: C | | Space group: $Fd\bar{3}m$ (227) | |
|---|---|---|---|---|
| Lattice parameters [Å] a = 5.76 | | | Cell volume [Å$^3$]: 191,10 | |
| Site | Mpl. | x | y | z |
| Ge | 8*a* | 0 | 0 | 0 |

Literature values:

Lattice parameters: a = 5.65692

- Ga

| Element: Ga | Structure type: Ga | | Space group: *Cmca* (64) | |
|---|---|---|---|---|
| Lattice parameters [Å] | | | Cell volume [Å$^3$]: | |
| a = 4.60 | b = 7.83 | c = 4.62 | 166.40 | |
| Site | Mpl. | x | y | z |
| Ga | 8*f* | 0 | 0.1561 | 0.0813 |

Literature values:

lattice parameters: a = 4.5199, b = 7.6603, c = 4.5259

Atom position: Ga – x = 0; y = 0.1549; z = 0.0810

### G.2. The binary structures in the Hf-As and Nb-As systems

The calculations of the binary structures (except $M_5As_3$ phases which did not converge within 4 weeks) were performed for the structure data taken from literature. The lattice parameters were not allowed to vary (except $Nb_2As$) and only the atoms could migrate. For $Nb_2As$ structure ($Nb_2P$–type), both the lattice parameters and the atom positions were varied. Below, the crystal structure data for the binary compounds for which the structure was not experimentally refined is given (compare Table 6 and 7 in chapter 2.2.2 and 2.2.3). The initial positions of the atoms were taken from the literature data for the structure type representative. The atom positions in the calculated structures of the compounds with the reported structure refinement agreed very well with the literature data of these.

- Phases in the Hf-As system

| Element: $Hf_3As_2$ | Structure type: $Hf_3P_2$ | | Space group: *Pnma* (62) | |
|---|---|---|---|---|
| Lattice parameters [Å] | | | Cell volume [Å$^3$]: | |
| a = 10.4362 | b = 3.6521 | c = 10.1465 | 386.724 | |
| Site | Mpl. | x | y | z |
| Hf1 | 4*c* | 0.0050 | 1/4 | 0.1259 |
| Hf2 | 4*c* | 0.3731 | 1/4 | 0.0681 |
| Hf3 | 4*c* | 0.2125 | 1/4 | 0.7934 |
| As1 | 4*c* | 0.3064 | 1/4 | 0.4984 |
| As2 | 4*c* | 0.4678 | 1/4 | 0.8233 |

| Element: $Hf_7As_4$ | Structure type: $Nb_7P_4$ | Space group: $C2/m$ (12) |
|---|---|---|

| Lattice parameters [Å] | | | | Cell volume [Å$^3$]: |
|---|---|---|---|---|
| a = 16.1150 | b = 3.5912 | c = 14.9283 | β = 104.24 | 837.388 |

| Site | Mpl. | x | y | z |
|---|---|---|---|---|
| Hf1 | 2*a* | 0 | 0 | 0 |
| Hf2 | 2*d* | 0 | 1/2 | 1/2 |
| Hf3 | 4*i* | 0.4297 | 0 | 0.8297 |
| Hf4 | 4*i* | 0.1976 | 0 | 0.3093 |
| Hf5 | 4*i* | 0.2070 | 0 | 0.7971 |
| Hf6 | 4*i* | 0.3365 | 0 | 0.0319 |
| Hf7 | 4*i* | 0.0014 | 0 | 0.6668 |
| Hf8 | 4*i* | 0.1793 | 0 | 0.5428 |
| As1 | 4*i* | 0.1767 | 0 | 0.1090 |
| As2 | 4*i* | 0.3731 | 0 | 0.5994 |
| As3 | 4*i* | 0.3717 | 0 | 0.3384 |
| As4 | 4*i* | 0.0630 | 0 | 0.8504 |

| Element: $Hf_2As$ | Structure type: $Ta_2P$ | Space group: *Pnnm* (58) |
|---|---|---|

| Lattice parameters [Å] | | | Cell volume [Å$^3$]: |
|---|---|---|---|
| a = 15.3606 | b = 12.4892 | c = 3.6498 | 700.183 |

| Site | Mpl. | x | y | z |
|---|---|---|---|---|
| Hf1 | 4*g* | 0.0815 | 0.1158 | 0 |
| Hf2 | 4*g* | 0.2948 | 0.1891 | 0 |
| Hf3 | 4*g* | 0.1048 | 0.5264 | 0 |
| Hf4 | 4*g* | 0.2426 | 0.9035 | 0 |
| Hf5 | 4*g* | 0.4768 | 0.8466 | 0 |
| Hf6 | 4*g* | 0.4253 | 0.4172 | 0 |
| As1 | 4*g* | 0.1515 | 0.3113 | 0 |
| As2 | 4*g* | 0.2875 | 0.5618 | 0 |
| As3 | 4*g* | 0.0855 | 0.7568 | 0 |

- Phases in the Nb-As system

| Element: $Nb_7As_4$ | Structure type: $Nb_7P_4$ | Space group: $C2/m$ (12) |
|---|---|---|

| Lattice parameters [Å] | | | | Cell volume [Å$^3$]: |
|---|---|---|---|---|
| a = 15.3716 | b = 3.5242 | c = 14.1920 | β = 104.74 | 743.516 |

| Site | Mpl. | x | y | z |
|---|---|---|---|---|
| Nb1 | 2*a* | 0 | 0 | 0 |
| Nb2 | 2*d* | 0 | 1/2 | 1/2 |
| Nb3 | 4*i* | 0.4306 | 0 | 0.8268 |
| Nb4 | 4*i* | 0.1949 | 0 | 0.3086 |
| Nb5 | 4*i* | 0.2118 | 0 | 0.7995 |
| Nb6 | 4*i* | 0.3348 | 0 | 0.0294 |
| Nb7 | 4*i* | 0.9994 | 0 | 0.6616 |
| Nb8 | 4*i* | 0.1800 | 0 | 0.5453 |
| As1 | 4*i* | 0.1728 | 0 | 0.1093 |
| As2 | 4*i* | 0.3702 | 0 | 0.5975 |
| As3 | 4*i* | 0.3713 | 0 | 0.3336 |
| As4 | 4*i* | 0.0638 | 0 | 0.8478 |

| Element: $Nb_2As$ | Structure type: $Nb_2P$ | Space group: *Pmma* (51) |
|---|---|---|

| Lattice parameters [Å] | | | Cell volume [Å$^3$]: |
|---|---|---|---|
| a = 18.582 | b = 3.520 | c = 14.242 | 931.549 |

| Site | Mpl. | x | y | z |
|---|---|---|---|---|
| Nb1 | 2*a* | 0 | 0 | 0 |
| Nb2 | 2*d* | 0 | 1/2 | 1/2 |
| Nb3 | 2*e* | 1/4 | 0 | 0.1098 |
| Nb4 | 2*e* | 1/4 | 0 | 0.3878 |
| Nb5 | 2*e* | 1/4 | 0 | 0.8898 |
| Nb6 | 2*f* | 1/4 | 1/2 | 0.5612 |
| Nb7 | 4*i* | 0.0616 | 0 | 0.3437 |
| Nb8 | 4*i* | 0.1216 | 0 | 0.5704 |
| Nb9 | 4*j* | 0.0016 | 1/2 | 0.1628 |
| Nb10 | 4*j* | 0.1375 | 1/2 | 0.0044 |
| Nb11 | 4*j* | 0.1661 | 1/2 | 0.2413 |
| Nb12 | 4*j* | 0.6621 | 1/2 | 0.2392 |
| As1 | 2*e* | 1/4 | 0 | 0.6891 |
| As2 | 4*i* | 0.1049 | 0 | 0.1378 |
| As3 | 4*i* | 0.6037 | 0 | 0.1282 |
| As4 | 4*j* | 0.1442 | 1/2 | 0.4304 |
| As5 | 4*j* | 0.5463 | 1/2 | 0.3275 |

### G.3. The ground state structures of the phases with $M_3As$ composition

The ground state energies for the binary arsenides with $M_3As$ composition were calculated for the $Ta_3As$, $Ti_3P$ and $Hf_{3+x}Nb_{3-x}As_2$ structure types. The lattice parameters and the atom positions were allowed to vary. The structure data of (Hf:Hf:Hf:Hf:Hf:Hf:As) ($Ta_3As$ type) and (Nb:Nb:Nb:As) ($Ti_3P$ type) end members can be compared with the literature data for binary $Hf_3As$ and $Nb_3As$ phases (Appendix A.7) – the lattice parameter differences do not exceed 1%.

- $Ta_3As$ structure type

| Compound | | | (Hf:Hf:Hf:Hf:Hf:Hf:As) | (Nb:Nb:Nb:Nb:Nb:Nb:As) |
|---|---|---|---|---|
| Lattice parameters [Å] | a | | 15.4727 | 14.7370 |
| | b | | 5.4146 | 5.2030 |
| | c | | 15.4112 | 14.6102 |
| | β | | 90.010 | 90.000 |
| Cell volume [$Å^3$] | | | 1291.11 | 1120.26 |
| Atom positions | M1 | x | 0.7393 | 0.7450 |
| | | y | 0.7906 | 0.7615 |
| | | z | 0.4053 | 0.4111 |
| | M2 | x | 0.1552 | 0.1601 |
| | | y | 0.7252 | 0.7414 |
| | | z | 0.5108 | 0.5065 |
| | M3 | x | 0.9421 | 0.9363 |
| | | y | 0.4808 | 0.4849 |
| | | z | 0.1667 | 0.1672 |
| | M4 | x | 0.0829 | 0.0767 |
| | | y | 0.9608 | 0.9888 |
| | | z | 0.6917 | 0.6796 |
| | M5 | x | 0.7336 | 0.7401 |
| | | y | 0.2644 | 0.2322 |
| | | z | 0.3012 | 0.2960 |
| | M6 | x | 0.9504 | 0.9519 |
| | | y | 0.7529 | 0.7540 |
| | | z | 0.4833 | 0.4903 |
| | As1 | x | 0.9155 | 0.9035 |
| | | y | 0.9786 | 0.9862 |
| | | z | 0.1282 | 0.1371 |
| | As2 | x | 0.1221 | 0.1171 |
| | | y | 0.4566 | 0.4861 |
| | | z | 0.6672 | 0.6609 |

- $Ti_3P$ structure type

| Compound | | | (Hf:Hf:Hf:As) | (Nb:Nb:Nb:As) |
|---|---|---|---|---|
| Lattice parameters [Å] | a | | 10.850 | 10.355 |
| | c | | 5.480 | 5.230 |
| Cell volume [Å$^3$] | | | 645.17 | 560.84 |
| Atom positions | M1 | x | 0.4169 | 0.4159 |
| | | y | 0.8937 | 0.9061 |
| | | z | 0.9692 | 0.9778 |
| | M2 | x | 0.3582 | 0.3506 |
| | | y | 0.5263 | 0.5111 |
| | | z | 0.7846 | 0.7693 |
| | M3 | x | 0.3180 | 0.3058 |
| | | y | 0.7844 | 0.7860 |
| | | z | 0.4937 | 0.4908 |
| | As1 | x | 0.2953 | 0.2936 |
| | | y | 0.5400 | 0.5212 |
| | | z | 0.2871 | 0.2702 |

- $Hf_{3+x}Nb_{3-x}As_2$ structure type

| Compound | | | (Hf:Hf:Hf:As) | (Nb:Nb:Nb:As) |
|---|---|---|---|---|
| Lattice parameters [Å] | a | | 7.334 | 6.995 |
| | b | | 3.680 | 3.510 |
| | c | | 11.949 | 11.397 |
| Cell volume [Å$^3$] | | | 322.50 | 279.84 |
| Atom positions | M1 | x | 0.0397 | 0.0569 |
| | | y | 1/4 | 1/4 |
| | | z | 0.5985 | 0.5963 |
| | M2 | x | 0.1647 | 0.1551 |
| | | y | 1/4 | 1/4 |
| | | z | 0.0110 | 0.0223 |
| | M3 | x | 0.2829 | 0.2602 |
| | | y | 1/4 | 1/4 |
| | | z | 0.3017 | 0.3069 |
| | As1 | x | 0.4225 | 0.4437 |
| | | y | 1/4 | 1/4 |
| | | z | 0.6764 | 0.6809 |

## G.4. The ground state structures of the $M_5Ge_4$ end members.

Below, the structure data of the end members of $M_5Ge_4$ phase ($Sm_5Ge_4$ structure type) calculated with the relaxed lattice parameter and atom positions are given. The calculation of the niobium monosubstituted end members for which the atoms were fixed on the positions of binary $Hf_5Ge_4$ resulted in the same lattice parameters. The atom positions of the (Hf:Hf:Nb:Ge) end member can be distinguished from the other ones. A translation of the cell origin by a vector [0.5 0.5 0] for this end member, however, results in the identical structure with the (Hf:Nb:Hf:Ge) end member.

| Compound | | | (Hf:Hf:Hf:Ge) | (Nb:Hf:Hf:Ge) | (Hf:Nb:Hf:Ge) | (Hf:Hf:Nb:Ge) |
|---|---|---|---|---|---|---|
| Lattice parameters [Å] | | a | 7.092 | 6.973 | 6.907 | 6.906 |
| | | b | 13.520 | 13.506 | 13.338 | 13.332 |
| | | c | 7.166 | 7.082 | 7.024 | 7.029 |
| Cell volume [Å$^3$] | | | 687.1 | 666.9 | 647.1 | 647.1 |
| Atom positions | Hf1 | x | 0.1811 | 0.1762 | 0.1695 | 0.3296 |
| | | y | 1/4 | 1/4 | 1/4 | 1/4 |
| | | z | 0.0020 | 0.9970 | 0.9939 | 0.0058 |
| | Hf2 | x | 0.1456 | 0.1508 | 0.1581 | 0.0126 |
| | | y | 0.6242 | 0.6247 | 0.6229 | 0.5930 |
| | | z | 0.1670 | 0.1695 | 0.1715 | 0.1734 |
| | Hf3 | x | 0.0142 | 0.0164 | 0.0124 | 0.1572 |
| | | y | 0.0946 | 0.0951 | 0.0929 | 0.1230 |
| | | z | 0.3231 | 0.3230 | 0.3265 | 0.3286 |
| | Ge1 | x | 0.0527 | 0.0473 | 0.0450 | 0.1907 |
| | | y | 1/4 | 1/4 | 1/4 | 1/4 |
| | | z | 0.6116 | 0.6076 | 0.6151 | 0.6456 |
| | Ge2 | x | 0.3215 | 0.3179 | 0.3087 | 0.4545 |
| | | y | 1/4 | 1/4 | 1/4 | 1/4 |
| | | z | 0.3530 | 0.3501 | 0.3545 | 0.3851 |
| | Ge3 | x | 0.3033 | 0.3076 | 0.3165 | 0.1838 |
| | | y | 0.5406 | 0.5403 | 0.5386 | 0.5383 |
| | | z | 0.4652 | 0.4687 | 0.4648 | 0.5356 |

| Compound | | | (Nb:Nb:Hf:Ge) | (Nb:Hf:Nb:Ge) | (Hf:Nb:Nb:Ge) | (Nb:Nb:Nb:Ge) |
|---|---|---|---|---|---|---|
| Lattice parameters [Å] | a | | 6.816 | 6.876 | 6.859 | 6.754 |
| | b | | 13.230 | 13.441 | 13.254 | 13.197 |
| | c | | 6.960 | 6.948 | 6.904 | 6.829 |
| Cell volume [Å$^3$] | | | 627.7 | 642.2 | 627.7 | 608.7 |
| Atom positions | Hf1 | x | 0.1663 | 0.1803 | 0.1780 | 0.1719 |
| | | y | 1/4 | 1/4 | 1/4 | 1/4 |
| | | z | 0.9939 | 0.9953 | 0.9940 | 0.9926 |
| | Hf2 | x | 0.1583 | 0.1466 | 0.1478 | 0.1537 |
| | | y | 0.6242 | 0.6239 | 06229 | 0.6243 |
| | | z | 0.1653 | 0.1665 | 0.1716 | 0.1644 |
| | Hf3 | x | 0.0128 | 0.0272 | 0.0224 | 0.0192 |
| | | y | 0.0907 | 0.0908 | 0.0922 | 0.0862 |
| | | z | 0.3254 | 0.3233 | 0.3251 | 0.3258 |
| | Ge1 | x | 0.0395 | 0.0508 | 0.0546 | 0.0462 |
| | | y | 1/4 | 1/4 | 1/4 | 1/4 |
| | | z | 0.6112 | 0.6001 | 0.6090 | 0.6042 |
| | Ge2 | x | 0.3094 | 0.3263 | 0.3180 | 0.3198 |
| | | y | 1/4 | 1/4 | 1/4 | 1/4 |
| | | z | 0.3477 | 0.3417 | 0.3495 | 0.3393 |
| | Ge3 | x | 0.3158 | 0.3004 | 0.3080 | 0.3109 |
| | | y | 0.5405 | 0.5422 | 0.5373 | 0.5412 |
| | | z | 0.4619 | 0.4737 | 0.4660 | 0.4654 |

## G.5. The ground state structures of the MGa end members.

Below, the structure data of the end members of MGa phase (ThTl structure type) calculated with the relaxed lattice parameter and atom positions are given. The calculation of the niobium monosubstituted end members for which the atoms were fixed on the positions of binary HfGa resulted in the same lattice parameters.

| Compound | | | (Hf:Hf:Hf:Ga) | (Nb:Hf:Hf:Ga) | (Hf:Nb:Hf:Ga) | (Hf:Hf:Nb:Ga) |
|---|---|---|---|---|---|---|
| Lattice parameters [Å] | a | | 9.210 | 9.181 | 9.208 | 9.120 |
| | b | | 8.544 | 8.465 | 8.345 | 8.400 |
| | c | | 5.663 | 5.507 | 5.617 | 5.624 |
| Cell volume [Å$^3$] | | | 445.6 | 428.0 | 431.6 | 430.9 |
| Atom Positions | Hf1 | x | 0.1112 | 0.1120 | 0.1127 | 0.1060 |
| | | y | 1/4 | 1/4 | 1/4 | 1/4 |
| | | z | 0 | 0 | 0 | 0 |
| | Hf2 | x | 0.6173 | 0.6216 | 0.6218 | 0.6170 |
| | | y | 0.5268 | 0.5309 | 0.5237 | 0.5330 |
| | | z | 1/4 | 1/4 | 1/4 | 1/4 |
| | Hf3 | x | 0.1920 | 0.1804 | 0.1888 | 0.1849 |
| | | y | 0.6349 | 0.6336 | 0.6337 | 0.6351 |
| | | z | 1/4 | 1/4 | 1/4 | 1/4 |
| | Ga1 | x | 0.5665 | 0.5738 | 0.5670 | 0.5793 |
| | | y | 1/4 | 1/4 | 1/4 | 1/4 |
| | | z | 0 | 0 | 0 | 0 |
| | Ga2 | x | 0.0869 | 0.0805 | 0.0874 | 0.0870 |
| | | y | 0.9505 | 0.9542 | 0.9512 | 0.9523 |
| | | z | 1/4 | 1/4 | 1/4 | 1/4 |
| | Ga3 | x | 0.6505 | 0.6516 | 0.6477 | 0.6519 |
| | | y | 0.8671 | 0.8686 | 0.8652 | 0.8706 |
| | | z | 1/4 | 1/4 | 1/4 | 1/4 |

| Compound | | | (Nb:Nb:Hf:Ga) | (Nb:Hf:Nb:Ga) | (Hf:Nb:Nb:Ga) | (Nb:Nb:Nb:Ga) |
|---|---|---|---|---|---|---|
| Lattice parameters [Å] | a | | 9.132 | 9.072 | 9.109 | 9.058 |
| | b | | 8.312 | 8.368 | 8.215 | 8.156 |
| | c | | 5.453 | 5.472 | 5.561 | 5.405 |
| Cell volume [$Å^3$] | | | 413.9 | 415.4 | 416.1 | 399.3 |
| Atom positions | Hf1 | x | 0.1152 | 0.1096 | 0.1091 | 0.1176 |
| | | y | 1/4 | 1/4 | 1/4 | 1/4 |
| | | z | 0 | 0 | 0 | 0 |
| | Hf2 | x | 0.6263 | 0.6219 | 0.6228 | 0.6340 |
| | | y | 0.5262 | 0.5362 | 0.5284 | 0.5279 |
| | | z | 1/4 | 1/4 | 1/4 | 1/4 |
| | Hf3 | x | 0.1814 | 0.1796 | 0.1827 | 0.1785 |
| | | y | 0.6312 | 0.6292 | 0.6332 | 0.6328 |
| | | z | 1/4 | 1/4 | 1/4 | 1/4 |
| | Ga1 | x | 0.5712 | 0.5834 | 0.5773 | 0.5778 |
| | | y | 1/4 | 1/4 | 1/4 | 1/4 |
| | | z | 0 | 0 | 0 | 0 |
| | Ga2 | x | 0.0812 | 0.0805 | 0.0890 | 0.0777 |
| | | y | 0.9519 | 0.9520 | 0.9511 | 0.9500 |
| | | z | 1/4 | 1/4 | 1/4 | 1/4 |
| | Ga3 | x | 0.6472 | 0.6517 | 0.6476 | 0.6444 |
| | | y | 0.8656 | 0.8706 | 0.8687 | 0.8736 |
| | | z | 1/4 | 1/4 | 1/4 | 1/4 |

# CURRICULUM VITAE

**Personal data:**

Name: Piotr Warczok

Date of birth : 20th of July, 1979

Place of Birth: Zabrze (woj. Śląskie, Poland)

Nationality: Polish

Marital status: Married

**Education:**

| | |
|---|---|
| 1986 – 1994 | Primary school: Szkoła Podstawowa nr 41, Gliwice (woj. Śląskie, Poland) |
| 1994 – 1998 | High school: Liceum Ogólnokształcące nr 2, Gliwice |
| June 1998 | A-level (Świadectwo dojrzałości) graduation |
| 1998 – 2003 | University of Mining and Metallurgy (AGH-UST), Faculty of Non-ferrous Metals, Master studies, course of study: Metallurgy |
| Winter 2001 | One-semester stay at the University of Vienna, Faculty of Chemistry within the Erasmus programme |
| October 2003 | Master of Engineering (Magister inżynier) graduation |
| 2004-2008 | University o Vienna, Faculty of Chemistry, Ph.D. studies, course of study: Chemistry |

**Professional Career:**

| | |
|---|---|
| 2004-2008 | Assistant at the Institute of Inorganic Chemistry, University of Vienna |
| 2008-present | Assistant at the Institute of Materials Science and Technology, Technical University of Vienna |